Inaugural dissertation

for

obtaining the doctoral degree

of the

Combined Faculty of Mathematics, Engineering and Natural Sciences

of the

Ruprecht – Karls – University

Heidelberg

Presented by

Dr. med. Timo Albert Nees

Born in: Karlsruhe, Germany

Oral examination: 21.03.2024

The molecular mechanism and physiological role of silent nociceptor activation

Referees: Prof. Dr. Marc Freichel
Prof. Dr. Stefan G. Lechner

TABLE OF CONTENTS

SUMMARY

Mechanically silent nociceptors, or mechanically insensitive afferents, do not typically respond to noxious mechanical stimuli. However, they become sensitized during inflammatory conditions. Despite their significant presence among joint-innervating nociceptive fibers and their abundance in organs such as the colon, bladder, and skin, the physiological role and molecular mechanism underpinning their activation have remained elusive since their discovery over thirty years ago.

In this doctoral thesis, it was elucidated that silent nociceptors constitute up to forty percent of all nociceptive afferents innervating the mouse knee joint. Notably, the infrapatellar fat pad exhibits particularly dense innervation by these afferents. Through RNA-sequencing and quantitative RT-PCR, data revealed that nerve growth factor-associated inflammation, as seen in conditions like osteoarthritis, selectively enhances the expression of the transmembrane protein TMEM100 within silent nociceptors. Electrophysiological analyses employing the mechano-clamp technique verified that TMEM100 overexpression is indispensable for the activation of these nociceptors. Significantly, TMEM100-deficient mice did not manifest secondary mechanical hypersensitivity in a model of knee joint monoarthritis. This secondary hypersensitivity represents pain that radiates beyond the immediate inflammation site and is intricately linked with the progression from acute to chronic pain. Supporting this notion, in experiments where TMEM100 was overexpressed in articular afferents without any inflammatory stimulus, mechanical hypersensitivity was observed in distant skin regions without inducing local knee joint pain.

Consequently, these findings postulate that in the context of inflammatory knee joint pain, primary and secondary hypersensitivities are mediated by distinct primary sensory afferent subpopulations. The functionally obscure mechanically silent nociceptors predominantly mediate secondary hyperalgesia, with TMEM100 emerging as a pivotal regulatory protein in this activation cascade.

ZUSAMMENFASSUNG

Mechanisch stumme Nozizeptoren sind somatosensorische Afferenzen, die unter physiologischen Bedingungen nicht auf schmerzhafte mechanische Reize reagieren. Im Rahmen von Entzündungsreaktionen werden die stummen Nozizeptoren jedoch aktiviert. Die physiologische Rolle und der molekulare Aktivierungsmechanismus dieser einzigartigen Nozizeptorsubpopulation blieb seit der Erstbeschreibung vor mehr als 30 Jahren rätselhaft, obwohl die stummen Nozizeptoren einen großen Anteil an den gelenkinnervierenden Schmerzfasern ausmachen und auch in anderen Organen wie Haut, Blase und Kolon vorhanden sind.

In der vorliegenden Doktorarbeit wurde am Mausmodell gezeigt, dass stumme Nozizeptoren bis zu vierzig Prozent aller nozizeptiven Gelenkafferenzen ausmachen können und der Hoffa-Fettkörper besonders dicht innerviert ist. Mithilfe von RNA-Sequenzierung und quantitativer RT-PCR wurde demonstriert, dass Nerve Growth Factor abhängige Entzündungsreaktionen (zum Beispiel aktivierte Arthrose) zu einer selektiven Überexpression des Transmembranproteins TMEM100 in stummen Nozizeptoren führen. Die in der Folge durchgeführten elektrophysiologischen Untersuchungen (mechano-clamp technique) bestätigen, dass die Überexpression von TMEM100 sowohl erforderlich als auch ausreichend ist, um stumme Nozizeptoren zu aktivieren. Darüber hinaus konnte gezeigt werden, dass TMEM100-Knockout Mäuse in einem Modell für Kniegelenksarthritis keine sekundäre mechanische Hyperalgesie entwickeln – das heißt sie entwickeln keine Schmerzüberempfindlichkeit, die über den primären Entzündungsherd hinausgeht und mit der Entwicklung von chronischen Schmerzen zusammenhängt. Dementsprechend reicht die alleinige Überexpression von TMEM100 in Gelenkafferenzen in Abwesenheit einer Entzündung aus, um eine mechanische Überempfindlichkeit in entfernten Hautregionen auszulösen, ohne primäre Kniegelenksschmerzen zu verursachen.

Diese Ergebnisse legen nahe, dass primäre und sekundäre Hyperalgesie im Rahmen von entzündlichen Kniegelenksschmerzen durch separate Subpopulationen von primären sensorischen Afferenzen vermittelt werden. Die physiologische Rolle der bislang rätselhaften stummen Nozizeptoren liegt dabei in der Vermittlung von sekundärer Hyperalgesie, wobei TMEM100 als entscheidendes, regulatorisches Schlüsselprotein des Aktivierungsprozesses identifiziert werden konnte.

LIST OF ABBREVIATIONS

AAV	Adeno-associated virus
AITC	Allylisothiocyanate
AM	A-fiber mechanonociceptor
A-MC	A-fiber mechanocold nociceptor
A-MH	A-fiber mechanoheat nociceptor
A-MHC	A-fiber mechanoheatcold nociceptor
AMPA	α-Amino-3-hydroxy-5-methyl-4-isoxazolepropionic acid
ANOVA	Analysis of variance
ASIC	Acid-sensing ion channel
ATP	Adenosine triphosphate
BDKRB2	Bradykinin receptor beta 2
BDNF	Brain-derived neurotrophic factor
BSA	Bovine serum albumin
cAMP	cyclic adenosine monophosphate
CFA	Complete Freund's Adjuvant
CGRP	Calcitonin gene-related peptide
CHRNA3	cholinergic receptor nicotinic alpha 3 subunit
Cl^-	Chloride
CL	Cruciate ligament
CM	C-fiber mechanonociceptor
C-MC	C-fiber mechanocold nociceptor
C-MH	C-fiber mechanoheat nociceptor
C-MHC	C-fiber mechanoheatcold nociceptor
C-MiHi	C-fiber Mechano-insensitive, Heat-insensitive nociceptor

CNS	Central nervous system
DAPI	4,6-diamidino-2-phenylindole
DNA	Deoxyribonucleic acid
dpi	Days post-injection
DRG	Dorsal root ganglia
EDTA	Ethylenediaminetetraacetic acid
EGFP	Enhanced green fluorescent protein
FP	Hoffa's fat pad
GABA	γ-Aminobutyric acid
GDNF	Glial cell-line derived neurotrophic factor
GPCR	G protein-coupled receptor
i.a.	Intraarticular
IB4	Isolectin B4
K^+	Potassium ion
KCNK	Potassium two pore domain channel subfamily K
KO	Knock-out
LJC	Lateral joint capsule
LM	Lateral meniscus
LTMR	Low-threshold mechanoreceptor
MA	Mechanically activated current
MIA	Mechanically insensitive afferent
MJC	Medial joint capsule
MM	Medial meniscus
Mrgpr	Mas-related G protein-coupled receptor
mRNA	Messenger ribonucleic acid
NDS	Normal donkey serum

NGF	Nerve growth factor
NMDA	N-Methyl-D-Aspartate
NPY2R	Neuropeptide Y receptor type 2
PBS	Phosphate-buffered saline
PBST	Phosphate-buffered saline with Triton X-100
PBS-Tw	Phosphate-buffered saline with Tween®
PGE2	Prostaglandin E2
PKA	Protein kinase A
PKC	Protein kinase C
PLC	Phospholipase C
RT	Room temperature
RT-qPCR	Reverse transcription quantitative real-time polymerase chain reaction
SEM	Standard error of the mean
TMEM100	Transmembrane protein 100
TMEM100KO	Transmembrane protein 100 knock-out
TrkA	Tropomyosin receptor kinase A
TRP	Transient receptor potential
vF	von Frey
WDL	Withdrawal latency
WDT	Withdrawal threshold
WT	Wildtype

LIST OF FIGURES

LIST OF TABLES

1. INTRODUCTION

Pain is an unpleasant personal experience with a sensory and emotional component that involves biological, psychological and social factors. From one perspective, pain serves a crucial physiological function by effectively deterring severe injuries. On the flip side, it has the potential to manifest as a debilitating ailment, significantly impacting individuals' lives. The twofold nature of pain, acting as both a vital physiological alert and a distressing pathological state, has captivated medical professionals and researchers for generations, revealing fundamental insights into the structure and operation of the somatosensory system. Despite significant progress in the understanding, treatment and management of pain over the past century, the resulting therapeutic effects often remain unsatisfactory, and fundamental mechanisms behind pain are still not fully understood. Thus, untangling pain pathways including a systematic characterization of different nociceptor subpopulations plays a pivotal role in the development of novel therapeutic strategies to conquer pain.

One relatively large population of nociceptors that has remained enigmatic since its initial description in 1988 (Schaible and Schmidt 1988) is that of silent nociceptors. Silent nociceptors only become sensitized during inflammatory processes but remain inactive under physiological conditions. Given the significant presence of silent nociceptors in visceral organs and deep somatic tissue it has been hypothesized that un-silencing of silent nociceptors during inflammation considerably amplifies nociceptive signaling to the spinal cord. This, in turn, is believed to enhance central pain processing, ultimately leading to increased pain sensitivity. As targeting this distinct subpopulation of nociceptors could offer an innovative strategy for addressing inflammatory pain conditions, the content of this manuscript centers around elucidating the physiological role and activation mechanism of silent nociceptors.

1.1 The somatosensory system and pain pathway

To gain insight into the processes underlying pain and the activation of silent nociceptors, it is imperative to develop a foundational understanding of the somatosensory nervous system, which includes a thorough comprehension of the pain pathway (**Figure 1**). The somatosensory system comprises peripheral receptors and neural pathways that enable the nervous system to detect and subsequently process information related to tactile sensations (mechanoception), painful stimuli (nociception), temperature perception (thermoception), as well as awareness of bodily position and movement (proprioception). Thus, the somatosensory system primarily governs the perception of both external (exteroception) and internal (interoception) stimuli, as well as proprioceptive feedback. The initial step in perceiving any somatosensory modality requires the activation of primary sensory neurons located within the dorsal root ganglia (DRG). These primary sensory neurons are afferent pseudounipolar neurons, signifying that they possess a single axon that bifurcates into both a peripheral and central branch. The peripheral branch, known as the primary afferent, innervates peripheral target tissues, where it detects sensory stimuli and converts them into electrical signals. Meanwhile, the central branch forms synaptic connections with second-order neurons within the spinal cord, thereby transmitting the sensory information to the central nervous system. Depending on the sensory information (e.g., pain, light touch stimuli), different primary afferents originating from distinct sensory neurons become activated in the DRG, which house numerous subpopulations of primary sensory neurons. Consequently, the central branches of these primary sensory neurons target spinal second-order neurons located in the dorsal horn of the spinal cord, characterized by its unique laminar organization in the gray matter. Hence, subsets of incoming primary afferents specifically target spinal neurons within particular layers of the spinal cord depending on the type of sensory information they carry. Within the spinal cord, the second-order neuron is subject to modulation by a complex network of inhibitory and excitatory interneurons as well as supraspinally-derived signals, thereby regulating the sensory input before these second-order neurons relay this information via different neuronal pathways to higher brain centers, ultimately reaching the somatosensory cortex (Braz et al. 2014; Lechner 2017; Todd 2010). The neuronal pathway through which sensory information travels to

the somatosensory cortex, including distinct connections along the neuroaxis, varies depending on the type of sensory input.

As this thesis primarily focuses on exploring the peripheral aspects of the somatosensory nervous system, specifically nociceptors, the descriptions of different neuronal pathways within the central nervous system (CNS) will be concise and limited to the pain pathway and the transmission of innocuous tactile information. In brief, within the pain pathway, the cell bodies of second-order neurons responsible for relaying nociceptive information are primarily located in laminae I and III-IV of the dorsal horn. These neurons project their axons, which cross over in the ventral commissure, from the spinal cord to the thalamus, brainstem, and pons via the anterolateral tract system including the spinothalamic, spinoreticulothalamic, and spinoparabrachial tracts, respectively (Basbaum et al. 2009). While spinothalamic projections are believed to play a pivotal role in the sensory-discriminative component of pain perception, spinoreticulothalamic projections are implicated in the secondary, more diffusely localized pain sensation. The neural connections between the spinal cord and the parabrachial regions of the dorsolateral pons are thought to contribute significantly to the aversive aspects of pain experience. Ultimately, nociceptive information is transmitted to cortical regions, encompassing the somatosensory and insula cortex, as well as the anterior cingulate gyrus. Moreover, descending pain-modulating fiber tracts originating from the periaqueductal gray and rostral ventral medulla are instrumental in influencing the pain processing network at the spinal level (Basbaum et al. 2009)

In contrast, innocuous tactile information is transmitted by postsynaptic dorsal column and spinocervical tract neurons. The projections of these neurons ascend through the dorsal columns and dorsolateral white matter of the spinal cord, respectively. It is worth noting that these neurons have their cell bodies located in laminae III–V (Abraira and Ginty 2013).

In the forthcoming sections, a comprehensive overview will be presented on how diverse sensory modalities are detected and encoded by various types of sensory neurons, along with an exploration of the involvement of transduction molecules in these processes. This exploration is crucial for gaining a better understanding of the

connection between mechanosensation and pain, as well as for delving into the investigation of silent nociceptors.

1.1.1 Primary sensory neurons

Within the exteroceptive somatosensory system, primary sensory afferents can be categorized into three major fiber types based on their diameter, degree of myelination, and conduction velocity. These include:

1) Myelinated large-diameter Aβ-fibers.
2) Thinly myelinated medium-diameter Aδ-fiber
3) Unmyelinated small-diameter C-fibers.

Aβ-afferents, with their insulating myelin sheaths, exhibit the highest conduction velocity, typically ranging from approximately 30 to 100 m/s in humans and 10 to 20 m/s in mice. In contrast, C-fibers conduct signals at a considerably slower rate, approximately 0.2 to 2 m/s, while Aδ-fibers fall in between, with conduction velocities of approximately 5 to 30 m/s.

In addition to categorizing primary sensory afferents based on their conduction velocity, primary sensory neurons can also be classified according to their physiological role, broadly distinguishing between three major groups. Depending on the sensory stimuli detected by primary sensory neurons, they can be categorized as proprioceptors, low-threshold mechanoreceptors (LTMRs) and nociceptors.

Proprioceptors are mechanosensory neurons distributed throughout the body, primarily situated within tissues such as muscles, tendons, and joints. Their function is to perceive and monitor body position and movement (Tuthill and Azim 2018). Since proprioception was not a subject of investigation in this thesis, proprioceptors will not be further discussed.

LTMRs constitute a diverse group of primary somatosensory neurons tasked with sensing various tactile stimuli. These neurons play a pivotal role in perceiving innocuous mechanical stimuli, and they are found in both glabrous and hairy skin. LTMRs extend their nerve fibers to specialized structures called end-organs located

within the skin. In brief, LTMRs can be further categorized based on their conduction velocity (Aβ-, Aδ-, C-LTMR) and adaptation properties, which refer to their firing patterns in response to sustained mechanical stimulation, ranging from slow adaptation (SA) to rapid adaptation (RA). Additionally, distinctions among LTMRs can be made based on their preferred stimuli or tuning properties, such as their responsiveness to indentation, stretching, vibration, or movement of the skin, as well as their associations with specific cutaneous end organs, like Merkel cells, Ruffini corpuscles, Pacinian corpuscles, and Meissner corpuscle (Abraira and Ginty 2013; Lechner 2017). Since noxious mechanical stimuli inevitably also activate LTMRs, mechanosensation and pain are interconnected. Thus, painful stimuli, particularly those of a mechanical nature, activate a wide range of functionally distinct sensory afferent subtypes, leading to the generation of a multitude of sensory information that is simultaneously transmitted to the spinal cord (Lechner 2017). Consequently, there is a vigorous debate surrounding whether various pain types arise from the processing and integration of numerous sensory inputs (known as the pattern theory) or from neural activity in specific subtypes of sensory afferents that are exceptionally responsive to particular types of stimuli (referred to as the labeled lines theory) (Ma 2010; Prescott et al. 2014).

The final significant group of primary sensory neurons comprises the nociceptors, which are peripheral sensory neurons responsible for detecting and encoding painful stimuli. As nociception is a critical aspect of this thesis, the following section will offer an in-depth exploration of nociceptors.

1.1.1.1 Nociceptors

Nociceptors can be defined as sensory receptors within the peripheral somatosensory nervous system that possess a high activation threshold and have the ability to transduce and encode painful stimuli. Nociceptive afferents innervate both glabrous and hairy skin, as well as visceral organs and deep somatic tissues, including joint structures like tendons, subchondral bone, and muscles. They terminate as free nerve endings within the innervated tissue and have the capacity to detect and transduce potentially harmful stimuli into electrical signals (Abraira and Ginty 2013; Dubin and Patapoutian 2010). Consequently, painful stimuli at the peripheral terminal are converted into inward depolarizing currents. These currents generate graded

receptor potentials at the primary nerve ending level. When these depolarizations reach a sufficient magnitude, they initiate a sequence of action potentials along the axon, with the frequency directly proportional to the stimulus intensity (Woolf and Ma 2007). The specificity of nociceptors in detecting and responding to noxious stimuli is established through the expression of ion channels with high activation thresholds. These channels selectively respond to particular aspects of the mechanical, thermal, and chemical environment (Ramsey et al. 2006). This high threshold sets nociceptors apart from sensory neurons that respond to non-painful stimuli (LTMRs) by utilizing transduction channels with lower activation thresholds. In general, nociceptors can be triggered by a diverse array of stimuli, encompassing noxious temperature extremes (heat and cold), painful cutaneous pressure, deviations in pH levels, distension of hollow organs, mechanical stresses on joints, instances of inflammation, and occurrences of ischemic events (Gold and Gebhart 2010). Nociceptors can be categorized into two main groups according to their conduction velocities: unmyelinated C-fiber nociceptors and myelinated A-fiber nociceptors (Dubin and Patapoutian 2010; Lewin and Moshourab 2004). It is believed that differences in conduction velocities between A- and C-fiber nociceptors result in an initial "sharp" and well-localized first pain sensation mediated by A-fiber nociceptors, which is subsequently followed by a "deeper," poorly localized pain experience mediated by C-fibers (Basbaum et al. 2009). Within these groups, there exist several subpopulations, each finely attuned to detect various forms of noxious physical and chemical stimuli. However, the majority of all nociceptors responds to painful mechanical stimuli. Nociceptors that exclusively respond to mechanical stimuli are termed C-fiber mechanonociceptors (C-Ms) or A-fiber mechanonociceptors (AMs), depending on their fiber type. Nociceptors that are additionally activated by noxious thermal stimuli are referred to as polymodal C-fiber or polymodal A-fiber nociceptors. Subclassification can be based on their responsiveness to noxious cold and/or heat (Lechner 2017).

Regarding A-fiber nociceptors, the majority of them can be categorized as Aδ-fibers, characterized by a thin myelin sheath and conduction velocities within the Aδ range. A smaller proportion of A-fiber nociceptors exhibit conduction velocities in the Aβ range. Most A-fiber nociceptors are AMs, responding exclusively to noxious mechanical stimuli. However, polymodal A-fiber nociceptors with additional sensitivity to noxious heat, cold, or both have also been identified. These are respectively termed A-MH, A-MC, and A-MHC nociceptors. For example, the percentage of AMs that exhibit a

response to heat in rodents is relatively low, typically averaging around 20 % (Cain et al. 2001; Caterina et al. 2000; Djouhri and Lawson 2004; Lewin and Moshourab 2004).

As reviewed by Lewin and Moshourab, the largest group of nociceptors comprises C-fiber nociceptors, characterized by their slow conduction velocities (< 1.3 m/s) due to the absence of a myelin sheath (Lewin and Moshourab 2004). Early investigations systematically analyzed C-fiber receptors using a wide range of stimuli, including intense thermal and mechanical inputs. These studies revealed that the majority of C-fiber nociceptors, spanning various species such as cats, rats, and monkeys, exhibit polymodal characteristics, responding to both noxious mechanical and thermal stimulation (Bessou and Perl 1969; Birder and Perl 1994; Iggo 1960; Lynn and Carpenter 1982; Perl 1968). Furthermore, it was observed that these C-fiber nociceptors can be activated or sensitized to thermal stimuli by various substances known to induce pain, such as bradykinin, capsaicin, and prostaglandin (Dubin and Patapoutian 2010; Lewin and Moshourab 2004). However, a substantial proportion of C-fiber nociceptors exclusively respond to noxious mechanical stimuli but not to painful thermal input (Handwerker et al. 1991). Recognizing the distinctive responsiveness of C-fiber nociceptors to potentially harmful thermal and/or mechanical stimuli, Handwerker and colleagues proposed a simple classification scheme that categorizes polymodal C-fiber nociceptors into the following subpopulations: C-mechanoheat (C-MH), C-mechanocold (C-MC), or C-mechanoheatcold (C-MHC). Neurons that do not respond to noxious thermal stimuli were classified as C-mechanonociceptors (C-M) (Fleischer et al. 1983; Handwerker et al. 1987; Handwerker et al. 1991; Kress et al. 1992; Lewin and Mendell 1994). Nociceptors of the C-MH type make up the largest subpopulation of nociceptive C-fiber. Furthermore, it is worth noting that a significant subgroup of C-fiber nociceptors is referred to as mechanically insensitive afferents (MIAs). MIAs exhibit minimal or no sensitivity to mechanical stimuli under normal physiological conditions but become sensitized to such stimuli during inflammation. At times, MIAs are described as "silent" or "sleeping" nociceptors (Feng and Gebhart 2011; Häbler et al. 1990; McMahon and Koltzenburg 1990; Meyer et al. 1991; Prato et al. 2017; Schaible and Schmidt 1988). As MIAs are the primary focus of investigation in this thesis, a dedicated section highlighting MIAs will follow (see 1.1.1.2 Silent nociceptors). Lastly, it is noteworthy that C-fibers unresponsive to both mechanical and heat stimuli have been identified and characterized in humans. These fibers have been

categorized within the previously mentioned classification scheme as C-Mechano insensitive, heat-insensitive (C-MiHi) (Schmidt et al. 1995; Weidner et al. 1999)

Within the domain of nociceptor classification, C-fiber nociceptors manifest differences not only in their responsiveness to diverse painful sensory stimuli but also in their categorization based on neurochemical properties and trophic requirements (Snider and McMahon 1998). Following sensory neurogenesis, precursor nociceptors undergo differentiation, giving rise to two principal classes of C-fiber nociceptors: "peptidergic" and "non-peptidergic" C-fiber nociceptors. These classes are demarcated by their distinctive expression patterns of neuropeptides and neurotrophin receptors. Peptidergic C-fiber nociceptors are characterized by their expression of the nociceptive peptides calcitonin gene-related peptide (CGRP) and substance P, as well as the presence of the nerve growth factor (NGF) receptor Tropomyosin receptor kinase A (TrkA). During embryonic development, peptidergic nociceptors rely on NGF for their survival (Bennett et al. 1998; Golden et al. 2010). Conversely, the second major class of C-fiber nociceptors, termed "non-peptidergic" nociceptors, exhibit a transition in receptor expression during their development. These nociceptors downregulate TrkA receptor expression and, notably, upregulate the receptor tyrosine kinase c-RET, rendering them responsive to glial cell line-derived neurotrophic factor (GDNF). This transition from NGF to GDNF dependence occurs early in postnatal life (Molliver et al. 1997). Moreover, a significant proportion of c-RET-positive "non-peptidergic" C-fiber nociceptors display an affinity for Isolectin B4 (IB4) from *Bandeiraea simplicifolia* (Molliver, 1997). Additionally, they express both G protein-coupled receptors (GPCRs) from the Mas-related gene (Mrg) family and purinergic receptor subtypes $P2X_3$ (Basbaum et al. 2009; Dong et al. 2001). Within the realm of nociception, it is postulated that these two distinct groups of nociceptors assume disparate functional roles, underpinned by their distinct anatomical organizations. Specifically, peptidergic afferents are noted for their innervation of the basal layers of the epidermis, with their projections extending to the outermost laminae of the dorsal horn (laminae I and outer lamina II). In contrast, non-peptidergic fibers exhibit a propensity for termination within the more superficial epidermal layers, primarily targeting the inner lamina II of the dorsal horn of the spinal cord (Abraira and Ginty 2013; Braz et al. 2014).

Elucidating the intricacies of transduction processes and delineating the unique roles played by various nociceptor subtypes in pain signaling constitute subjects of

rigorous investigation within the scientific community. The underlying cellular and molecular mechanisms responsible for cold and heat pain are reasonably well comprehended. The transient receptor potential cation channel subfamily V (vanilloid) member 1 (TRPV1) is a nonselective cation channel that has been demonstrated to serve as a transducer for noxious heat and is prevalent among heat-sensitive nociceptors, as established by Caterina and colleagues (Caterina et al. 1997). TRPV1 exhibits an activation threshold of approximately 43 °C and is also responsive to the agonist capsaicin, the pungent agent from chili peppers, and protons. Genetic studies in mice have revealed that the deletion of the TRPV1 channels leads to complete insensitivity to capsaicin, reduced thermal hyperalgesia during CFA-induced inflammation and impaired responses only to noxious heat at very high temperatures (Caterina et al. 2000). Ablation of TRPV1-expressing DRG neurons using intrathecal injections of high-dose capsaicin or Resiniferatoxin (Cavanaugh et al. 2009; Mishra and Hoon 2010) as well as silencing with the selective uptake of the voltage-gated sodium channel blocker QX-314 (Brenneis et al. 2013), resulted in a nearly complete loss of sensitivity to noxious heat in rodents. Similarly, the diphtheria toxin induced ablation of nociceptors expressing both the neuropeptide CGRP and TrkA, a group encompassing the majority of TRPV1-expressing neurons, resulted in a significant loss of sensitivity to heat-induced pain (McCoy et al. 2013). Hence, this substantial evidence supports the essential role of TRPV1 in the detection of noxious heat and underscores why TRPV1-expressing fibers are widely accepted as cellular sensors for heat pain. Nevertheless, these results also suggest the existence of one or more additional heat sensors. Indeed, other members of the TRP channel family, including TRPV2, TRPV3, and TRPV4, are believed to contribute to the detection of potentially harmful temperatures in the warm (TRPV3 ~ 32–39 °C, TRPV4 ~ 27–34 °C) or very hot (TRPV2 > 50 °C) ranges (Lumpkin and Caterina 2007).

Similar results were obtained regarding cold sensitivity, in which the transient receptor potential cation channel subfamily M (melastatin) member 8 (TRPM8) plays an essential role. TRPM8 is responsive to menthol and is considered the primary sensor for environmental cold. In fact, mice lacking TRPM8 display insensitivity to innocuous cooling and manifest substantial behavioral impairments in response to cold stimuli ranging from 30°C to 10°C. This insensitivity is evident under both physiological conditions and in models of inflammation and nerve injury (Bautista et al. 2007; Dhaka et al. 2007). However, it is noteworthy that TRPM8-deficient mice exhibit unaltered

nocifensive behavior in response to subzero centigrade temperatures (Dhaka et al. 2007). This observation implies the potential involvement of other cold-sensing molecules in the detection of such extreme cold stimuli. Analogous to the role of TRPV1 in heat perception, the conditional ablation of TRPM8-expressing neurons in adult mice using of diphtheria toxin results in a more pronounced behavioral phenotype, characterized by an almost complete loss of sensitivity to cold-induced pain (Knowlton et al. 2013).

In addition to thermal stimuli, various environmental irritants and endogenous factors can stimulate peripheral sensory neurons, eliciting pain through a process known as chemo-nociception. In the context of acute pain induced by irritating substances, the transient receptor potential cation channel subfamily A (ankyrin) member 1 (TRPA1) has emerged as a pivotal channel due to its capacity to respond to pungent compounds (Bandell et al. 2004; Jordt et al. 2004). TRPA1 channels can be activated by allyl isothiocyanate (found in mustard oil), cinnamaldehyde (present in cinnamon), thiosulfinates like allicin (abundant in garlic), formaldehyde (commonly used to elicit chemical nociception responses in rodents), acrolein (used as a tear gas), and numerous other volatile irritants (Patapoutian et al. 2009). What is shared among all these substances capable of activating TRPA1 is their capacity to form adducts with thiol groups. Consequently, in this specific scenario, they lead to covalent modifications of cysteine residues within the amino-terminal cytoplasmic domain of TRPA1 (Bandell et al. 2004; Jordt et al. 2004; Macpherson et al. 2007). In animal models, genetic and pharmacological inhibition of TRPA1 has proven effective in significantly reducing chemically induced inflammatory hyperalgesia, encompassing both thermal and mechanical responses (McNamara et al. 2007; Petrus et al. 2007). Interestingly, TRPA1 and TRPV1 are co-expressed in a subset of dorsal root ganglia (DRG) and trigeminal neurons, representing polymodal C-fiber nociceptors (Jordt et al. 2004; Patapoutian et al. 2009; Salas et al. 2009; Weng et al. 2015). Given that TRPA1 can be directly activated by Ca^{2+} (Doerner et al. 2007; Zurborg et al. 2007) it has been posited that TRPA1 may function as an amplifier of other signals that elevate intracellular calcium levels, including those involving TRPV1. In alignment with these discoveries, Weng and colleagues recently identified the transmembrane protein 100 (TMEM100) as a potentiating modulator of the TRPA1-TRPV1 complex within DRG neurons. TMEM100 disrupts the interaction between TRPA1 and TRPV1, selectively

enhancing TRPA1 activity by alleviating its inhibition induced by TRPV1 (Weng et al. 2015).

In contrast to thermal and chemically-induced pain, deciphering the cellular and molecular foundations of mechanical pain proves significantly more challenging as concisely reviewed by Lechner (Lechner 2017). Hence, the specific ion channel responsible for transducing noxious mechanical stimuli remains elusive (Ranade et al. 2014). Furthermore, our comprehension of how discrete sensory afferent subtypes contribute to various forms of mechanical pain remains limited. Notably, some of the aforementioned investigations involving mice lacking TRPV1- or TRPM8-expressing fibers failed to identify changes in mechanically-induced pain responses (Cavanaugh et al. 2009; Knowlton et al. 2013; McCoy et al. 2013; Mishra and Hoon 2010). In fact, it has been demonstrated that the ablation of a subset of non-peptidergic polymodal C-fiber nociceptors, characterized by the expression of the Mas-related G-protein coupled receptor D (MRGPRD), only reduces sensitivity to painful mechanical stimuli induced by blunt von Frey filaments but does not impact heat pain thresholds (Cavanaugh et al. 2009; Rau et al. 2009). These findings collectively suggest that MRGPRD$^+$ sensory neurons, rather than TRPV1$^+$ or TRPM8$^+$ nociceptors, are indispensable for mechanical pain, despite all three subpopulations being responsive to mechanical stimulation. It is important to highlight that in all of these studies, pain sensitivity was evaluated several days after the specific cell populations were eliminated. This timeframe allows for potential compensatory adjustments in the pain pathways, which could influence the study outcomes. In line with this concern, a more rapid pharmacological approach, involving targeted axonal silencing of TRPV1-expressing fibers in mice, revealed deficits in both heat pain and mechanical pressure, indicating that TRPV1$^+$ sensory neurons also contribute to mechanical pain, in addition to heat pain.

Apart from the timing of behavioral assessment following nociceptor subpopulation silencing, the conflicting results may also be attributed to the different tests used to assess mechanical sensitivity. While Brenneis and colleagues employed the pinch test and pinprick stimuli, the other groups used punctate mechanical stimuli applied with von Frey filaments (Cavanaugh et al. 2009; Knowlton et al. 2013; Mishra and Hoon 2010). It is noteworthy that Brenneis only observed differences in pain evoked by pinching but not in responses to pinprick or light touch stimuli (Brenneis et al. 2013),

indicating that distinct submodalities of mechanical pain may be mediated by different subsets of nociceptors. Thus, another plausible interpretation for the divergence among the previously mentioned studies is that MRGPRD$^+$ nociceptors may be more effectively stimulated by von Frey filaments, whereas TRPV1-expressing sensory neurons might exhibit heightened sensitivity to pinch stimuli.

Recent findings from the Lechner lab emphasize the idea that different types of mechanical stimuli are detected by distinct subsets of nociceptors (Arcourt et al. 2017). Specifically, this study unveiled that pinprick stimuli are detected by a subset of nociceptors characterized by conduction velocities within the Aβ range and the presence of neuropeptide Y receptor type 2 (NPY2R). Intriguingly, these nociceptors display selective sensitivity to pinprick stimuli while showing no response to other forms of noxious mechanical stimuli. Significantly, the diphtheria toxin-induced ablation of NPY2R-expressing DRG neurons in mice had no discernible impact on heat-induced pain responses. However, it did result in significantly prolonged paw withdrawal latencies exclusively in response to pinprick stimuli, with no effect observed in response to von Frey stimuli. Moreover, it was demonstrated that selective activation of NPY2R-positive neurons induced abnormal pain behavior. Importantly, simultaneous activation of NPY2R-positive nociceptors and LTMRs was necessary to replicate pinprick-induced pain behavior (Arcourt et al. 2017). Thus, the study directly illustrates that the integration of multiple sensory inputs from functionally distinct afferent subtypes is essential for generating a specific submodality of mechanical pain. Consequently, it is possible that the loss of a single afferent subpopulation may alter the perception of a particular stimulus but may not necessarily alter the behavioral response evoked by that stimulus. In summary, the available evidence suggests that distinct nociceptor subtypes are necessary for detecting various forms of painful mechanical stimuli. Nonetheless, the specific ion channels responsible for converting these noxious mechanical stimuli into electrical signals remain unidentified.

In principle, all of the previously mentioned functionally distinct sensory afferents were identified through classical neurophysiological studies decades ago (Lewin and Moshourab 2004). The advent of novel techniques, such as single-cell RNA-sequencing, has allowed for the mapping of transcriptional profiles in these functionally categorized neurons (Zeisel et al. 2018; Zheng et al. 2019). Zeisel and colleagues used single-cell RNA sequencing to generate a comprehensive cell atlas of the mouse

nervous system and revealed previously unrecognized cell classes and types in various regions. On a molecular level, neurons of the peripheral nervous system (PNS) were distinguished from those in the CNS and gave rise to distinct sensory, sympathetic, and enteric subdivisions. Among the peripheral sensory neurons located within the DRG, cell types were categorized into three primary branches: peptidergic (comprising eight types: PSPEP1-8), non-peptidergic (comprising six types: PSNP1-6), and neurofilament (comprising three types: PSNF1-3). This observation suggests refinements to previous classifications (Li et al. 2016; Usoskin et al. 2015; Zeisel et al. 2018). Interestingly, when analyzing the transcriptional signature of peripheral sensory neurons in non-human primates, specific cell types appeared to be associated with chronic pain (Kupari et al. 2021). Additionally, profiling sensory ganglia in mice at a single-cell resolution revealed that all somatosensory neuronal subtypes undergo a similar transcriptional response to peripheral nerve injury, which both promotes axonal regeneration and transiently suppresses cell identity (Renthal et al. 2020). Despite recent advances in the classification of peripheral sensory neurons, achieving an unambiguous categorization of the cell types responsible for mediating noxious mechanical pain, including the transducers, remains elusive.

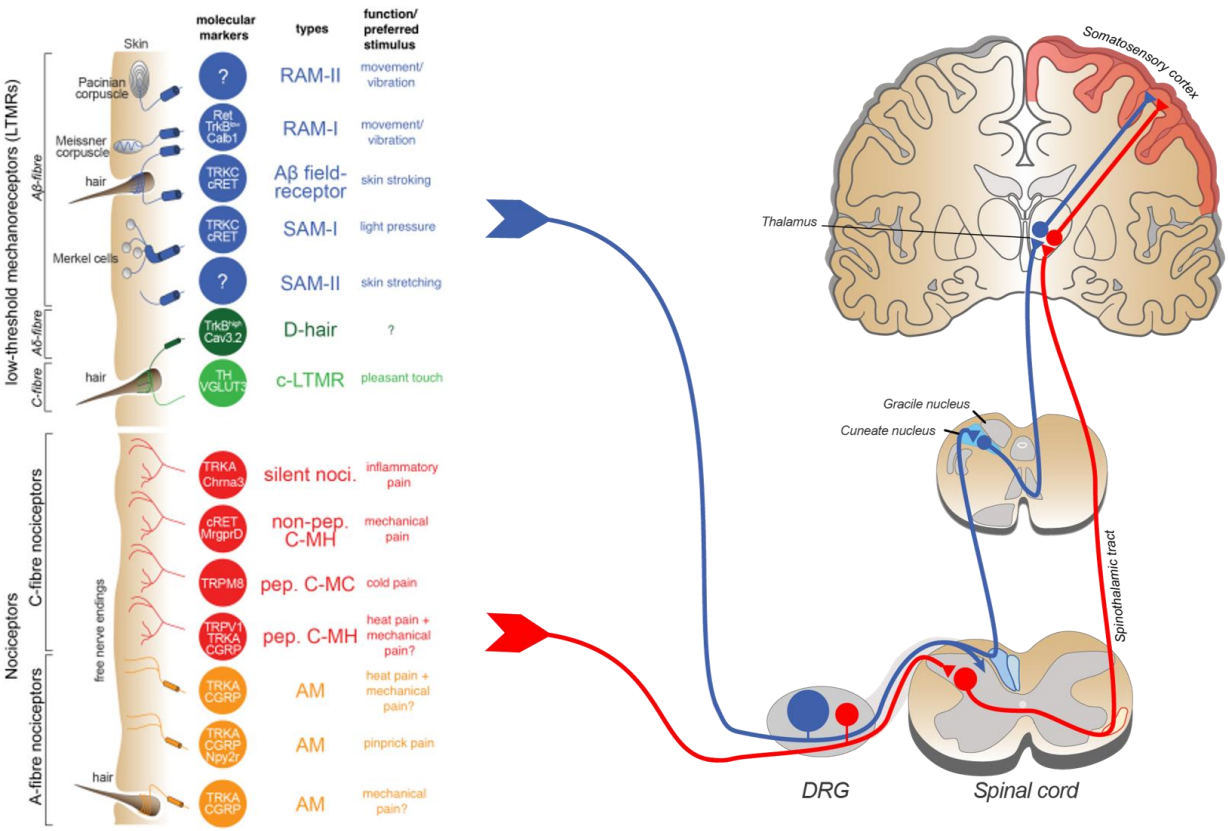

Figure 1 | Overview of the somatosensory system

Primary sensory neurons can be broadly categorized into low-threshold mechanoreceptors (LTMRs; highlighted at the top left in blue and green) and nociceptors (shown at the bottom left in red and orange). LTMRs target specialized structures within the skin, such as Pacinian and Meissner corpuscles or Merkel cells, and are activated by tactile stimuli (refer to the upper section labeled "function/preferred stimulus"). On the other hand, nociceptors possess free nerve endings that are adept at detecting various harmful stimuli (also referenced in the "function/preferred stimulus" section). Distinct molecular markers (indicated in the "molecular markers" column) differentiate primary afferent subtypes, each correlating to specific DRG neuron subtypes (outlined in the "types" column). The neuronal pathways through which sensory information travels to the somatosensory cortex differ depending on the type of the sensory input (LTMRs vs. nociceptors). Both pain (illustrated by the red line) and innocuous tactile information pathways (denoted by the blue line) originate from the cell bodies of primary afferents located in the pseudounipolar dorsal root ganglia (DRG). Primary nociceptors establish synapses with second-order neurons at the ipsilateral spinal cord level. The axons of these second-order nociceptive neurons cross the spinal cord to connect to the thalamus via the spinothalamic tract. From there, the nociceptive data is routed to the somatosensory cortex. In contrast, the central projections of LTMRs responsible for transmitting harmless tactile information journey along the ipsilateral dorsal column. These projections do not synapse or cross until they encounter their corresponding second-order neurons in the gracile and cuneate nuclei. Here, at the level of the dorsal medulla, tactile information crosses over to the contralateral side and is subsequently relayed in the thalamus. From there, the information is finally dispatched to the somatosensory cortex. Adapted from Lechner et al. 2017.

RAM-II and RAM-I: Rapidly-adapting mechanoreceptor types I and II; SAM-I and SAM-II: Slowly-adapting mechanoreceptor types I and II; D-hair: Aδ-fiber LTMR; C-LTMR: C-fiber LTMR; Noci.: Nociceptor; Non-pep. C-MH: Non-peptidergic C-fiber mechanoheat nociceptor; Pep. C-MC: Peptidergic C-fiber mechanocold nociceptor; Pep. C-MH: Peptidergic C-fiber mechanoheat nociceptor; AM: A-fiber mechanonociceptor;

TrkA, TrkB, TrkC: Tyrosine kinase receptors types A, B, and C; Calb1: Calbindin1; Cav3.2: Voltage-gated calcium channel alpha 1H subunit; VGLUT3: Vesicular glutamate transporter 3; MRGPRD: Mas-related G protein-coupled receptor type D; TRPM8: Transient receptor potential cation channel subfamily M member 8; TRPV1: transient receptor potential cation channel subfamily V (vanilloid) member 1 (TRPV1); CGRP: Calcitonin-gene related peptide; NPY2R: Neuropeptide Y receptor type 2.

1.1.1.2 Silent nociceptors

Silent nociceptors represent a heterogeneous group of nociceptive primary sensory neurons characterized by their insensitivity to specific sensory stimuli under physiological conditions and their ability to become activated during pathological conditions, such as inflammation and neuropathic pain. The term "silent nociceptor" is

inconsistently used for different subsets of primary sensory afferents with these properties. When authors use the term "silent nociceptors," most commonly, they are referring to afferents that are normally insensitive to mechanical stimuli but acquire mechanosensitivity during inflammation. However, silent neurons insensitive to cold stimuli (MacDonald et al. 2021) and to both mechanical and heat input (Schmidt et al. 1995; Weidner et al. 1999) have also been documented. Therefore, it is more appropriate to use specific terms that indicate insensitivity to distinct sensory stimuli, such as "silent cold-sensing nociceptors"(MacDonald et al. 2021) or mechanically insensitive afferents (MIAs). For example, recent findings have demonstrated that silent cold-sensing neurons can be classified as peptidergic A-fiber nociceptors based on their functional and molecular characteristics. These neurons significantly contribute to cold allodynia in various mouse models of neuropathic pain. These results imply that cold allodynia results from the sensitization of silent cold-sensing neurons, leading them to acquire increased sensitivity to cold (MacDonald et al. 2021).

In contrast, the relatively large subpopulation of MIAs consists of peptidergic C-fiber nociceptors, and their initial documentation dates back more than 30 years. However, the physiological role of this unique nociceptor subpopulation has remained enigmatic. Schaible and Schmidt were the first to report findings about MIAs from electrophysiological recordings of single-afferent units in the medial articular nerve innervating the knee joint of cats. They discovered sensory afferents that did not respond to local mechanical stimulation or to innocuous/noxious movements in a normal knee joint but displayed sensitivity to these stimuli after inducing experimental arthritis (Schaible and Schmidt 1988). Subsequently, MIAs were identified in several species and anatomical regions including the colorectum of mice and rats (Feng and Gebhart 2011; Sengupta and Gebhart 1994a), the urinary bladder of both rats and cats (Häbler et al. 1990; Sengupta and Gebhart 1994b), as well as the human skin (Schmidt et al. 1995). The widespread presence of MIAs in visceral organs, deep somatic tissues, and the skin suggests their pivotal physiological role and potential involvement in painful conditions such as arthritis, irritable bowel syndrome, and urocystitis. MIAs are estimated to comprise approximately 30 % of all C-fiber afferents in visceral organs and articular tissues, with a prevalence of around 15 – 20 % in human skin. However, their prevalence in mouse skin seems comparatively lower (Gebhart 1999; Michaelis et al. 1996). Given the substantial proportion of MIAs across various tissues it has been postulated that the activation of MIAs during inflammation significantly amplifies

nociceptive signaling to the spinal cord. This, in turn, is believed to enhance central pain processing, ultimately leading to increased pain sensitivity. Conversely, in a combined microneurographic and psychophysical study investigating the role of cutaneous human mechano-insensitive nociceptors, it was suggested that silent nociceptors may elicit secondary mechanical hyperalgesia (Sauerstein et al. 2018). Due to the absence of tools enabling unequivocal identification or selective genetic manipulation of MIAs, neither the mechanism behind the un-silencing of MIAs nor their precise role in pain signaling has been fully elucidated.

Recently, seminal research conducted by Prato and colleagues (Prato et al. 2017) has revealed that MIAs in visceral organs and deep somatic tissues of mice express the nicotinic acetylcholine receptor alpha-3 subunit (CHRNA3). This discovery has allowed for the straightforward identification of MIAs through the utilization of a reporter mouse line expressing enhanced green fluorescent protein (EGFP) in MIAs, facilitating a conclusive assessment of their distribution patterns and functional characteristics. Notably, CHRNA3$^+$ neurons were detected in all DRG segments along the neuroaxis, spanning from cervical (C1) to sacral (S1) regions. Furthermore, nearly all CHRNA3$^+$ neurons also co-expressed CGRP, although the prevalence of these mechanically insensitive peptidergic C-fiber nociceptors varied among different spinal levels. Specifically, CHRNA3$^+$ neurons constituted approximately 40 % of the CGRP$^+$ subpopulation in DRG at the thoracolumbar and lumbosacral levels, while in other DRG, CHRNA3$^+$ neurons were relatively rare, accounting for approximately 15 % of all CGRP$^+$ neurons. Significantly, this study confirmed that deep somatic tissues, including the knee joint and gastrocnemius muscle, as well as the urinary bladder and distal colon, are densely innervated by CHRNA3$^+$ neurons. Conversely, no MIAs were observed in the glabrous and hairy skin of mice. Of paramount significance, this study has unveiled that MIAs, typically unresponsive to noxious mechanical stimuli, acquire mechanosensitivity upon exposure to the inflammatory mediator NGF, with no concurrent impact on the mechanosensitivity of other nociceptor subtypes. NGF is known to activate several signaling pathways upon binding to its receptor TrkA, including the PLCγ pathway, the PI3-kinase pathway, and the Ras/Raf/MEK/ERK pathway. Employing a systematic pharmacological approach to selectively block these distinct pathways, it has been demonstrated that the NGF-induced acquisition of mechanosensitivity hinges on de-novo gene transcription. Notably, only inhibition of the ERK1/2 kinase using the transcription blocker actinomycin D was effective in

diminishing NGF-mediated mechanotransduction currents in MIAs. Furthermore, it was observed that pharmacological inhibition of the mechanotransduction channel PIEZO2, using the toxin GsMTx4, and interference RNA (siRNA)-mediated knockdown of PIEZO2 expression in MIAs, effectively prevented the NGF-induced un-silencing of MIAs.

In summary, this study established that MIAs acquire mechanosensitivity upon exposure to the inflammatory mediator NGF. It further elucidated that the mechanically gated ion channel PIEZO2 mediates the NGF-induced mechanosensitivity in this distinctive peptidergic C-fiber nociceptor subpopulation. Importantly, this process necessitates de-novo gene transcription, leading to the expression of as yet unidentified proteins. Consequently, the data strongly suggest that the NGF-induced un-silencing of CHRNA3^{+} nociceptors may significantly contribute to the development of mechanical hypersensitivity during inflammation (**Figure 2**).

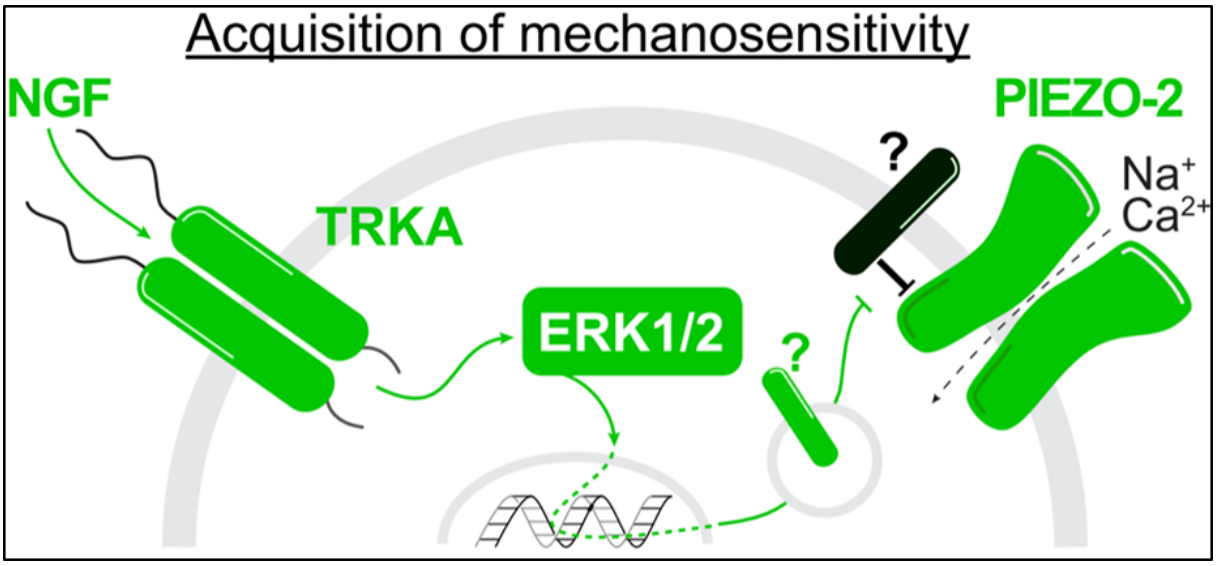

Figure 2 | Current concepts of silent nociceptor activation

According to current understanding, mechanically insensitive afferents (MIAs) gain mechanosensitivity when exposed to the inflammatory mediator, Nerve Growth Factor (NGF). This mechanosensitivity is mediated by the mechanically-gated ion channel, PIEZO2. The process requires de-novo gene transcription through the ERK1/2 kinase pathway, which leads to the expression of as-yet-unidentified proteins. Adapted from Prato et al. 2017.

1.2 Mechanotransduction

The operation of our tactile, nociceptive, and proprioceptive senses depends on the ability of primary sensory neurons to promptly detect and convert mechanical forces into electrical signals. However, this fundamental process continues to pose a mystery at the cellular and molecular levels. Virtually all sensory neurons (> 90 %) within the DRG are equipped with sensors enabling them to detect and convert mechanical stimuli into biochemical signals, a phenomenon known as mechanotransduction (Hu and Lewin 2006). The prevailing theory posits that mechanical forces acting upon sensory nerve endings directly initiate the opening of ion channels within the cell membrane, resulting in depolarization and excitation of the neuron. However, mechanotransduction in-vivo occurs exclusively at the sensory nerve endings. Therefore, when it comes to cutaneous sensory receptors, directly recording the mechanically gated receptor potential has proven to be challenging due to the small size and inaccessibility of the sensory nerve endings. To still investigate mechanotransduction, an alternative electrophysiological approach has been developed, enabling the recording of membrane currents with high resolution. This method is referred to as the whole-cell patch-clamp technique or the mechano-clamp technique. It involves the use of cultured DRG neurons, where mechanotransduction currents are elicited by mechanically stimulating the cell body with a piezo-electrically driven glass probe while conducting patch-clamp recordings in the whole-cell configuration with another pipette. This method has provided researchers with the opportunity to study the biophysical characteristics of currents that are activated by mechanical stimuli, known as MA currents, in DRG neurons (Coste et al. 2010; Drew et al. 2004; Drew et al. 2002; Hu and Lewin 2006; McCarter et al. 1999; Verkest et al. 2022). Numerous investigations have demonstrated that mechanically activated (MA) currents are facilitated by non-selective cation channels characterized by specific attributes, including a reversal potential in proximity to 0 mV, kinetics involving time-dependent inactivation, and current amplitudes that exhibit a direct correlation with the applied stimulus intensity (Delmas and Coste 2013; Hao and Delmas 2010; Rugiero et al. 2010). Three distinct types of mechanically activated (MA) currents, characterized by their respective inactivation time constants (τ_{inact}), have been identified: rapidly-adapting (RA, τ_{inac}< 10 ms), intermediately-adapting (IA, τ_{inac} < 30 ms), and slowly-adapting (SA, τ_{inac} > 30 ms) MA currents (Delmas and Coste 2013; Drew et al. 2002;

Hao and Delmas 2010; Hu and Lewin 2006). Various compounds have been documented to interfere with the MA currents detected in cultured DRG neurons. These compounds include gadolinium (Gd^{3+}), the inorganic dye ruthenium red, the fluorescent dye FM1-43, and the neurotoxin GsMTx4 (Hong et al. 2016).

Over the past two decades, numerous research groups have endeavored to pinpoint the ion channels accountable for mechanotransduction. Among the proposed candidates for transducing mechanical stimuli are members of the degenerin/epithelial Na^+ (DEG/ENaC) and KCNK channel families (potassium two pore domain channel subfamily K), as well as members of the TRP family (Basbaum et al. 2009). Studies conducted in Caenorhabditis elegans (C. elegans) have successfully pinpointed mechanotransducers in body touch neurons belonging to the DEG/ENaC family, specifically mec-4 and mec-10. Consequently, their mammalian counterparts, the acid-sensing ion channels (ASICs) ASIC1, ASIC2, and ASIC3, have been investigated for their mechanotransductive properties (Chalfie 2009; Waldmann and Lazdunski 1998). ASICs become active during tissue acidosis and have been found to be expressed in both low- and high-threshold mechanosensitive neurons. However, genetic studies in mice regarding the role of ASICs in mechanotransduction have produced inconsistent results. Mice lacking ASIC1 channels displayed normal behavioral responses to cutaneous touch (Page et al. 2004), whereas ASIC2-deficient mice showed significantly reduced sensitivity in rapidly adapting low-threshold mechanoreceptors (RA LTMR), indicating a role in normal touch sensation (Price et al. 2000). In contrast, ASIC3 knockout mice exhibited increased sensitivity in RA-LTMR but lower firing rates in A-fiber mechanonociceptors. An examination of mice lacking both ASIC2 and ASIC3 does not provide compelling evidence supporting the involvement of these channels in cutaneous mechanotransduction (Drew et al. 2004). In summary, the exact role of ASICs in mechanosensation is still under investigation and remains unresolved.

Three members of the KCNK channel family, specifically KCNK2, KCNK4, and KCNK18, have been suggested to be involved in mechanical transduction (Basbaum et al. 2009; Bautista et al. 2008; Dobler et al. 2007; Noël et al. 2009). KCNK2a and KCNK4 are expressed in a subset of C-fiber nociceptors and can be modulated by pressure, among other factors (Noël et al. 2009). On the other hand, KCNK18 is expressed in a subset of presumptive peptidergic C-fibers and low-threshold Aβ-mechanoreceptors (Bautista et al. 2008). However, to date, it remains unknown

whether these channels are directly responsive to mechanical stimulation, although the available data does not support KCNK channels as primary detectors of acute mechanical stimuli.

From the TRP family TRPA1 has been proposed to serve as mechanotransducer. The results obtained in mouse studies, however, are conflicting. Two studies found no relevant alterations in mechanical thresholds in TRPA1-deficient animals (Bautista et al. 2006; Petrus et al. 2007), whereas a third study reported significant deficits to suprathreshold punctuate mechanical stimuli (Kwan et al. 2006). A follow-up study by the same author found that TRPA1 modulated mechanotransduction in cutaneous sensory neurons showing that C and Aβ mechanosensitive fibers in TRPA1 knockout animals have altered responses to mechanical stimulation. Specifically, in TRPA1 knock-out mice, there is a decrease in firing rates of C-fiber nociceptors and SA-LTMRs in response to mechanical stimulation, while RA-LTMRs and D-hair LTMRs exhibit an increase in the number of action potentials fired (Kwan et al. 2009). A more recent study noted that the suppression of TRPA1 resulted in a reduction in the amplitudes of SA-currents within small-diameter IB4-negative nociceptors, although its expression in heterologous cells did not prove adequate for mediating mechanically activated currents (Vilceanu and Stucky 2010). It remains unclear whether and how these distinct physiological effects translate to a behavioral level, although some reports indicate that TRPA1 inhibition suppresses CFA-induced mechanical sensitization of cutaneous C-fiber nociceptors and alleviates mechanical hyperalgesia (Lennertz et al. 2012). Collectively, these findings suggest that TRPA1 does not seem to act as the principal sensor for acute mechanical stimuli but may instead regulate the excitability of mechanosensitive afferents.

Moreover, TRPC3 (member 3 of the transient receptor potential cation channel subfamily C (canonical)) may play a role in mechanotransduction. Consequently, the ablation of the TRPC3 channel led to a change in the inactivation pattern of MA currents in small-diameter DRG neurons, shifting from rapidly RA to IA responses. Furthermore, in the same research, mice with both TRPC3 and TRPC6 knocked out displayed impairments in detecting innocuous touch, which were linked to a decrease in RA responses and an increased number of neurons that did not respond to the stimulus (Quick et al. 2012).

Recently, in a transmembrane protein 150c (TMEM150c) knock-out mouse model it was found that the population of DRG neurons exhibiting SA-currents was reduced. This alteration was associated with deficits in coordinated movement and the presentation of an abnormal gait in the affected mice. Furthermore, the introduction of TMEM150c into HEK293 and F11 cells demonstrated the ability to confer mechanosensitivity to these cells (Hong et al. 2016). Nevertheless, a subsequent study cast doubt on these results, underlining the significance of selecting heterologous cells without pre-existing endogenous MA currents for mechanotransduction studies (Dubin et al. 2017).

To date PIEZO1 and PIEZO2 stand as the sole recognized mammalian ion channels that, when individually expressed, possess the capability to mediate MA currents across diverse cell types (Coste et al. 2010). PIEZO2 is prominently expressed in a majority of LTMRs. In mice where PIEZO2 has been conditionally disrupted, significant impairments in proprioception have been observed (Woo et al., 2015), indicating that PIEZO2 serves as the primary mechanotransducer for proprioception (Woo et al. 2015). Furthermore, mice lacking PIEZO2 experience a profound loss of touch perception, while the recognition of noxious mechanical stimuli remains unaltered (Coste et al., 2010; Ranade et al., 2014). In line with this, when examining cultured DRG neurons from mice lacking PIEZO2, Ranade and colleagues noted a specific decrease in RA-currents (approximately 75 %), while IA- and SA-currents, which are unique to nociceptors, remained unaffected (Ranade et al. 2014). Consequently, it appears that another as-yet-unidentified ion channel is responsible for the detection of noxious mechanical stimuli.

1.3 Pain

1.3.1 Terminology, epidemiology and clinical manifestation

The International Association for the Study of Pain (IASP) defines pain as *"an unpleasant sensory and emotional experience associated with, or resembling that associated with, actual or potential tissue damage"* (Raja et al. 2020). Pain is a unique experience for each individual, influenced by biological, psychological, and social factors. It is distinct from nociception, as the experience of pain cannot be solely attributed to sensory neuron activity. Individuals learn the concept of pain through life experiences, and their self-reported pain encounters should be respected. While pain often serves an adaptive purpose, it can have negative effects on well-being and functioning. Verbal expression is just one method of communicating pain. Thus, even when unable to communicate, both humans and animals can still undergo pain (Raja et al. 2020). The findings from the Global Burden of Disease Study in 2016 (GBD 2017) underscored the persistent and paramount role of pain and pain-related ailments as the primary drivers of disability and the overall disease burden on a global scale. Globally, the burden associated with chronic pain is on an upward trajectory. When examining years lived with disability, it becomes evident that low back and neck pain have consistently occupied the top positions as leading contributors to disability worldwide, with other chronic pain conditions also prominently featuring among the top 10 causes of disability (GBD 2017; Mills et al. 2019). The global prevalence of pain, after adjusting for age and sex, was found to be 27.5 %, although there were considerable disparities among countries, spanning a range from 9.9 % to 50.3 %. Notably, women, older individuals, and those residing in rural areas were significantly more prone to reporting pain (Zimmer et al. 2022). Furthermore, the economic impact of chronic pain is substantial, with an estimated annual cost ranging from 560 billion to 635 billion US dollar in the USA in 2010 (Gaskin and Richard 2012). Several underlying medical conditions contribute to the global severity of chronic pain. These conditions include osteo- and rheumatoid arthritis, diabetes, irritable bowel syndrome, fibromyalgia, chronic cystitis, pancreatitis, migraines, and pain associated with various forms of cancer (Chang et al. 2016; Denk et al. 2017; Goldberg and McGee 2011; Treede et al. 2015). Managing these chronic conditions poses significant challenges due to their potential connection to functional disorders. Moreover, the experience of pain is influenced by various factors, including the sensory innervation of the affected

tissue, which can vary based on the type and history of the injury, the presence of neural damage, as well as an individual's sex and genetic background (Gold and Gebhart 2010). Opioids and non-steroidal anti-inflammatory drugs (NSAIDs) continue to be the primary pillars of pharmacological pain management, despite the fact that these very analgesics have driven research and development efforts for novel painkillers due to their limited efficacy, tolerability, and associated adverse effects (Kissin 2010). Unfortunately, a majority of chronic pain patients still do not attain satisfactory pain relief through current therapeutic approaches, resulting in a reduced quality of life (Chang et al. 2016; Goldberg and McGee 2011; Mills et al. 2019). Hence, there is an ongoing demand for pain medications that are both safe and highly effective (Kissin 2010).

As demonstrated, pain can arise as a debilitating condition that severely affects people's lives. On the other hand, pain plays a crucial physiological role and effectively aids in preventing severe injuries. The dual role of pain, serving as both an essential physiological warning signal and an excruciating pathological condition, has not only captivated clinicians and researchers for centuries but has also unveiled principles regarding the organization and function of the somatosensory system. Physiological nociceptive pain emerges from actual or potential damage to non-neural tissue and results from the activation of nociceptors by noxious heat, cold, chemical or mechanical stimuli (IASP 2023). The development of pathological pain is more complex and does not necessarily require peripheral nociceptive stimulation. Regardless of nociceptor activation, pain is an uncomfortable and multi-faceted sensation that can manifest as stabbing, burning, throbbing, or prickling. Patients suffering from pain can present increased sensitivity to peripheral stimulation. Pain caused by a stimulus that does not normally induce pain is referred to as allodynia. Of note, allodynia may occur after various types of non-painful somatosensory stimuli applied to diverse tissues generating an unexpectedly painful response. Thus, allodynia entails a shift in the quality of a sensation, whether it is tactile, hot, cold or chemical. The original modality is typically non-painful, but the resulting response is painful indicating a loss of specificity of a sensory modality (IASP 2023). Allodynia is not solely, but it is frequently linked to sensory nerve damage, such as the kind observed in diabetic patients, those with peripheral neuropathies, and individuals experiencing postherpetic neuralgia (Sandkühler 2009).

In contrast to allodynia, the term hyperalgesia refers to an increased pain response elicited by a stimulus that typically induces pain. Thus, hyperalgesia indicates an increased perception of pain upon suprathreshold stimulation and is accurately employed for cases exhibiting an augmented pain response at a normal or increased threshold. Of note, in hyperalgesia the stimulus and the response occur in the same mode (pain), whereas in allodynia they occur in different modes. Similar to allodynia, hyperalgesia can manifest following various forms of somatosensory stimulation (e.g. mechanical, thermal, chemical) applied to different tissues and both, allodynia and hyperalgesia are clinical terms that do not directly imply a specific mechanism. Hyperalgesia can be further differentiated into primary and secondary hyperalgesia. Primary hyperalgesia means increased pain sensitivity at the site of tissue damage such as an inflamed area of the body caused by conditions like wounds, sunburns, or surgical incisions. In primary hyperalgesia, increased sensitivity to painful stimuli is limited to the region affected by inflammation or, in cases of mononeuropathies, within the innervation territory of a damaged nerve. Secondary hyperalgesia, in contrast, reflects pain hypersensitivity in undamaged skin adjacent or even more distant, from the injury site (Gebhart and Schmidt 2013). While primary hyperalgesia frequently subsides simultaneously with the initial source of pain, secondary hyperalgesia often endures even after the initial pain cause has been alleviated. Clinical data suggests that the extent and intensity of secondary pain hypersensitivity are correlated with the probability of chronic pain development (Richebé et al. 2018). Secondary pain hypersensitivity has been identified in various pain disorders and rodent pain models (Drake et al. 2016; Eitner et al. 2017; Hsieh et al. 2015; Martindale et al. 2007; Sandkühler 2009; Woolf 2011). The existing body of literature indicates that hyperalgesia, in general, emerges as a consequence of perturbations in the nociceptive system, involving peripheral or central sensitization, or both (IASP 2023). However, there is a consensus that the mechanisms underlying primary and secondary hyperalgesia are distinct. Primary hyperalgesia is ascribed to the sensitization of peripheral nociceptors at the site of injury, in addition to central sensitization. Conversely, secondary hyperalgesia is predominantly believed to arise from central sensitization, a process triggered and frequently sustained by enhanced afferent input.

In the context of nociceptive neurons and pain perception, sensitization refers to the increased responsiveness of nociceptive neurons to their regular input, as well as the recruitment of responses to inputs that normally fall below the activation threshold.

Thus, sensitization can encompass both a reduction in the activation threshold and an augmentation in suprathreshold responses. Spontaneous discharges and expansions in the size of the receptive field could also manifest. Of note, sensitization is originally a neurophysiological term that is applicable solely when a clear understanding of both the input and output of the studied neural system exists. Hence, in a clinical setting sensitization can be indirectly deduced, as seen in phenomena like hyperalgesia or allodynia. When nociceptive neurons in the central nervous system exhibit increased responsiveness to their normal or subthreshold afferent input, the term "central sensitization" is utilized. Central sensitization may involve augmented responses from central nociceptive neurons due to the malfunction of endogenous pain control systems, while peripheral neurons function normally. This results in functional changes solely within central neurons. When nociceptive neurons in the peripheral nervous system become sensitized, the term "peripheral sensitization" is applied.

1.3.2 Mechanisms of inflammatory pain and hypersensitivity

Inflammatory pain can be defined as the sensory perception of and emotional response to painful stimuli that arise in the context of an inflammatory or immune reaction. Inflammatory responses comprise a series of precisely coordinated physiological events initiated in response to injury or infection, with the goal of addressing and resolving the underlying pathology. This process is characterized by five hallmark symptoms: erythema (rubor), increased temperature (calor), edema (tumor), pain or enhanced sensory sensitivity (dolor), and compromised function (functio laesa). In physiological circumstances, inflammation serves as a vital protective mechanism crucial for facilitating wound healing. However, during instances of acute inflammation, inflammatory cellular and molecular factors can directly stimulate sensory neurons, resulting in the manifestation of pronounced pain (Vasko 2009).

In general, effective management of inflammation typically relieves inflammatory pain since nociceptor activation resolves when inflammatory processes subside. However, inflammatory mediators can reduce the thresholds for neuronal excitability and increase the sensitivity of nociceptor firing rates in acute and chronic states of inflammation, potentially leading to both peripheral and central sensitization (Kidd and

Urban 2001). In such sensitized conditions, pain perception can become abnormal, resulting in phenomena like allodynia and hyperalgesia, which are primary characteristics of inflammatory pain. These features, by themselves, lack specificity and do not help identify distinct underlying pathological processes. For instance, movement-related symptoms in osteoarthritis and touch-induced pain in herpetic neuralgia both manifest as mechanical allodynia, despite having distinct underlying mechanisms. This example highlights the limitations of current terminology (Kidd and Urban 2001) (Kidd, 2001). Therefore, in the context of inflammatory pain, the overarching term 'hypersensitivity' is frequently used to describe an increased sensitivity to usually non-painful (allodynia) or painful (hyperalgesia) stimuli.

1.3.2.1 Central sensitization

The processes underlying various types of pain hypersensitivity may involve the PNS, CNS or both. It is well established that central sensitization plays a pivotal role in the development of pain hypersensitivity (Latremoliere and Woolf 2009; Woolf 2011). Consequently, input from nociceptors in the periphery can trigger a prolonged yet reversible enhancement of the excitability and synaptic efficacy of neurons within central nociceptive pathways. This, in turn, results in hypersensitivity, including dynamic tactile allodynia, increased sensitivity to punctate or pressure stimuli, persistent after-sensations, as well as amplified temporal summation (Woolf 2011). Central sensitization was initially observed in a rat model involving localized thermal injury, where injury-induced hyperexcitability of the flexion reflex was partly attributed to changes in spinal cord activity (Woolf 1983). The precise mechanisms underlying central sensitization are multifaceted, intricate, and not comprehensively elucidated. Nevertheless, it is evident that dynamic changes within the spinal pain processing network, such as synaptic potentiation, disinhibition, and interactions between neurons and glial cells, play fundamental roles in this process. Additionally, these mechanisms may also be influenced by a disruption in the equilibrium between the ascending and descending nociceptive pathways, along with changes in higher brain regions responsible for processing pain (Latremoliere and Woolf 2009; Peirs and Seal 2016; Woolf 2011). In summary, central sensitization, independent of the exact underlying mechanism, results in increased nociceptive output of second-order neurons in the spinal cord involving pain pathways.

1.3.2.2 Peripheral sensitization

The mechanisms underpinning peripheral sensitization are initiated by processes that directly sensitize sensory nerve endings, thereby increasing the responsiveness of primary afferent nociceptors to natural stimuli. During tissue damage and inflammation, a complex interplay occurs among various cell types. This includes leukocytes, macrophages, mast cells, endothelial cells, platelets, and neurons, such as sympathetic efferents and primary sensory afferents. This orchestration results in the release of inflammatory mediators such as ATP, bradykinin, cytokines, glutamate, leukotrienes, NGF, prostaglandin E2 (PGE2) and neuropeptides including substance P and CGRP (Bhave and Gereau 2004; Woolf and Ma 2007). These inflammatory mediators, in turn, interact with a diverse array of receptors and ion channels expressed on the nociceptor membranes in the periphery. Subsequently, these interactions activate various intracellular signaling pathways, leading to an increased excitability of nociceptive nerve fibers (Basbaum et al. 2009). Thus, nociceptors undergo a transformation from solely detecting noxious stimuli to also perceiving innocuous inputs. As a result, even low-intensity stimuli can activate the nociceptive pathway and lead to the sensation of pain. Consequently, hypersensitivity to both thermal and mechanical stimuli are common clinical features of this inflammation-induced peripheral sensitization (Woolf and Ma 2007).

1.3.2.2.1 Thermal hypersensitivity

Regarding thermal hypersensitivity, it has been well-documented that several inflammatory mediators, including ATP, bradykinin, PGE2, and NGF, can sensitize TRPV1 channels, the main heat sensors (Bhave and Gereau 2004; Caterina et al. 2000; Cesare et al. 1999; Davis et al. 2000; Gold and Gebhart 2010). Genetic studies showing the absence of thermal hypersensitivity in TRPV1-deficient mice during inflammation clearly underscore the pivotal role of TRPV1 channels in the process by which inflammation induces increased sensitivity to heat (Caterina et al. 2000; Davis et al. 2000). Certain TRPV1 sensitizing inflammatory factors, such as extracellular protons and lipids, directly serve as positive allosteric modulators of the TRPV1 channel (Basbaum et al. 2009; Caterina et al. 1997). Meanwhile, others like ATP, bradykinin, and NGF bind to their respective receptors on primary afferent fibers, thereby indirectly influencing TRPV1 through the activation of downstream intracellular

signaling pathways (Basbaum et al. 2009). In both scenarios, these modulations significantly lower the thermal activation threshold of the TRPV1 channel and enhance responses at suprathreshold temperatures, which can be interpreted as biophysical manifestations of thermal hypersensitivity (Basbaum et al. 2009). Although the intracellular signaling pathways of TRPV1 sensitization have not been fully elucidated, it has become evident that pathways involving phospholipase C (PLC) through the activation of G protein-coupled receptors (GPCRs) and receptor tyrosine kinases play a significant role. At the subcellular level, there are multiple points of interaction between different pathways, often involving the activation of protein kinase A (PKA) and protein kinase C (PKC), as well as increases in intracellular Ca^{2+} levels. For example, these increases in Ca^{2+} levels can activate Ca^{2+}-calmodulin–dependent protein kinase II (CaMKII), thereby sensitizing TRPV1 (Basbaum et al. 2009; Gold and Gebhart 2010).

1.3.2.2.2 Mechanical hypersensitivity

In contrast to thermal hypersensitivity, the exact mechanisms driving mechanical hypersensitivity during inflammation-induced peripheral sensitization are not as well understood. Nonetheless, several fundamental processes have been identified as the underpinnings of mechanical hypersensitivity, which are succinctly delineated below. Interestingly, these processes frequently entail the activation of protein kinase A (PKA) and protein kinase C (PKC), akin to their involvement in thermal hypersensitivity. One notable mechanism described to enhance excitability to mechanical stimuli in DRG neurons during inflammatory pain involves posttranslational modifications of voltage-gated ion channels. Prompted by the release of inflammatory mediators, these posttranslational modifications have been observed in voltage-gated sodium, potassium, and calcium channels (Bhave and Gereau 2004). More precisely, it has been reported that PGE2-induced increases in sensory neuron excitability depend on the cyclic adenosine monophosphate (cAMP)-PKA mediated phosphorylation of voltage-gated sodium channels, which significantly affects the resting membrane potential and lowers the action potential threshold in nociceptors. This effect can occur either through an increase in sodium current amplitudes or the induction of a hyperpolarizing shift in their activation curve (England et al. 1996). Furthermore, the modification of voltage-gated potassium channels through PGE2 mediated post-translational changes involving the cAMP-PKA transduction cascade, can enhance

nociceptor excitability and spike firing by dampening delayed rectifier-like and after-hyperpolarization potassium currents (Evans et al. 1999). Moreover, the sensitization of nociceptors to mechanical stimuli may also involve the regulation of voltage-gated calcium channels by both endogenous reducing agents and phosphorylation mechanisms (Bhave and Gereau 2004). Specifically, PKC mediates the bradykinin-induced release of neuropeptides, such as substance P and CGRP, from rat sensory neurons at their sensory nerve terminals by modulating calcium currents, which aggravate inflammatory conditions (Barber and Vasko 1996; Bhave and Gereau 2004). Additionally, the control of low voltage-activated T-type calcium currents may intensify the excitability and repetitive firing in nociceptive fibers (Catterall 2000; Todorovic et al. 2001)

Another important mechanism proposed to underlie mechanical hypersensitivity during peripheral sensitization involves the modulation of mechanosensitive ion channels. Di Castro and colleagues discovered that the activation of two different inflammatory signaling pathways, namely the NGF and PKC pathways, significantly increased mechanotransduction in a substantial portion of nociceptors. PKC activation, both in vitro and in vivo, led to heightened mechanically activated membrane currents and increased sensitivity to mechanical stimulation in behavioral tests. As the influence of PKC activation was counteracted by tetanus toxin, which inhibits vesicle fusion with the cell membrane, these results suggest that the insertion of new mechanosensitive channels into the cell membrane contributes to sensitization. In contrast, NGF enhances MA currents through the transcription of new mechanotransduction channels or a protein that regulates them. Therefore, these findings revealed that the activation of both the PKC and NGF pathways enhances nociceptor responses to mechanical stimuli through distinct yet potentially synergistic mechanisms that target mechanosensitive ion channels (Di Castro et al. 2006). Furthermore, in rat DRG neurons, high-threshold mechanosensitive currents elicited by pressure stimuli were sensitized upon exposure to PGE2 through activation of the PKA pathway, whereas low-threshold currents remained unaffected (Cho et al. 2002). Lechner and Lewin discovered that allogenic agents simulating inflammatory conditions potentiate mechanotransduction currents in nociceptors from neonatal mice. Specifically, the inflammatory algogenic agents UTP and ATP enhance mechanically-gated RA currents in a subset of peptidergic C-fiber nociceptors, effectively reducing thresholds for mechanically induced action potential firing in these neurons. Employing a

pharmacological approach that selectively blocked different Gq-coupled P2Y nucleotide receptor subtypes, they demonstrated that the potentiation of RA currents in these nociceptors is most likely mediated by the $P2Y_2$ subtype. Furthermore, their study showed that UTP also increases action potential firing rates, exhibiting significant sensitization in response to mechanical stimuli within a specific subset of skin C-fiber nociceptors, as indicated by in vitro skin nerve recordings. In summary, these findings revealed that the inflammatory agent UTP induces peripheral sensitization in a subgroup of cutaneous C-fiber nociceptors through the amplification of mechanically activated RA-type currents, and that this effect is contingent upon the activation of the Gq-coupled $P2Y_2$ nucleotide receptor (Lechner and Lewin 2009). Additionally, data from the group led by Patapoutian support the growing evidence that heightened pain sensitivity to noxious mechanical stimuli at sites of inflammation results from peripheral sensitization of mechanotransduction in nociceptors (Dubin et al. 2012). They revealed that inflammatory signaling induced by bradykinin via PKA and PKC significantly enhances mechanosensitive currents in nociceptors mediated by PIEZO2. More precisely, in a heterologous cell expression system using HEK293T cells, activation of the bradykinin receptor beta 2 (BDKRB2) leads to an increase in the amplitude of PIEZO2 currents and a deceleration of their inactivation process. Additionally, the activity of PIEZO2 is enhanced by both PKA and PKC agonists. Consistent with these findings, the effects induced by BDKRB2 activation are reversed by inhibitors of PKA and PKC. Moreover, in a subset of small to medium-sized dorsal root ganglion (DRG) neurons, which are likely nociceptors based on their expression of RA-currents and TRPV1 channels, bradykinin significantly potentiates PIEZO2-dependent mechanically-activated currents through PKA and PKC signaling. Consequently, these data indicate that the sensitization of PIEZO2 by bradykinin via PKA and PKC may contribute to mechanical hyperalgesia (Dubin et al. 2012). In vivo, inflammation induced by CFA in the hindpaw or gastrocnemius muscle of mice elicited a significant augmentation of mechanical currents upon focal mechanical stimulation of sensory neurons innervating the paw skin or muscle, respectively. Intriguingly, these sensitized fibers comprise two discrete subpopulations of A-fiber type sensory neurons, discerned by their CGRP expression. In the case of hindpaw inflammation, $CGRP^+$ A-fibers projecting to the skin undergo sensitization, whereas muscle inflammation induces sensitization of $CGRP^-$ A-fibers. In both subtypes, mechanical sensitization manifests as an amplification of mechanically gated currents (Weyer et al. 2015).

Eventually, in the context of inflammation, the recruitment of nociceptors, particularly the sensitization of silent nociceptors, has been hypothesized as a potential mechanism contributing to the development of mechanical hypersensitivity. It is believed that un-silencing of silent nociceptors during inflammatory processes amplifies nociceptive input to the spinal cord, resulting in increased neuronal excitability and, consequently, mechanical hypersensitivity. As outlined previously (see 1.1.1.2 Silent nociceptors) mechanically insensitive afferents are abundantly present in deep somatic tissue and visceral organs. MIAs are capable of generating action potentials upon electrical stimulation. Yet, under typical physiological circumstances, they do not exhibit responsiveness to noxious mechanical stimuli and do not seem to play a role in pain signaling. Nonetheless, these typically mechanically insensitive sensory afferents acquire mechanosensitivity when exposed to inflammatory mediators (Feng and Gebhart 2011; Hirth et al. 2013; Prato et al. 2017; Schaible and Schmidt 1988). Indeed, in pioneering work by Schaible and Schmidt, it was found that MIAs innervating the cat knee joint exhibited afferent activity within the first hours after inducing experimental arthritis through the injection of kaolin. This activity was manifested through spontaneous discharges and responses to both innocuous and noxious movements of the knee joint. These results marked the first indication that silent nociceptors might be recruited during inflammation, thereby influencing the central processing of nociceptive discharges originating from inflamed tissue. Several subsequent reports have provided further support for the recruitment and sensitization of MIAs in inflammatory conditions. For instance, it was demonstrated that a significant portion of afferents that initially did not respond to mechanical stimulation of the feline urinary bladder through increases in intravesical pressure became sensitized at the onset of acute artificial inflammation induced by intraluminal injection of mustard or turpentine oil (Häbler et al. 1990). Similarly, in the colorectum of mice, MIAs constituted 23 % and 33 % in the pelvic and lumbar splanchnic nerves, respectively. Interestingly, 71 % of MIAs in the pelvic nerve acquired mechanosensitivity after localized exposure to an inflammatory mixture containing bradykinin, serotonin, histamine, and PGE2. In the splanchnic nerve, approximately a quarter of MIAs acquired mechanosensitivity during experimental bowel inflammation (Feng and Gebhart 2011). In a follow up study the same research group found that long-term sensitization of MIAs might contribute to persistent colorectal hypersensitivity in a model of zymosan-induced bowel inflammation (Feng and Gebhart 2011). In the hairy skin of monkeys (*Macaca*

fascicularis), 48 % of cutaneous Aδ-fibers (63 out of 130) and 30 % of C-fibers (22 out of 74) exhibited mechanical insensitivity. This insensitivity was characterized by exceedingly high mechanical thresholds or complete unresponsiveness to mechanical stimuli. Moreover, 63 % of Aδ-fiber MIAs and 56 % of C-fiber MIAs displayed responsiveness upon intradermal injection of an inflammatory soup containing mediators such as bradykinin, PGE, serotonin, and histamine, while remaining unresponsive to control saline injections. Notably, following the administration of the inflammatory soup, 3 out of 19 tested Aδ-fiber MIAs and 2 out of 9 tested C-fiber MIAs exhibited an augmented response to mechanical stimuli. This observation suggests that 16 % of Aδ-fiber MIAs and 22 % of C-fiber MIAs underwent sensitization, thereby acquiring mechanosensitivity in response to the inflammatory stimulus (Meyer et al. 1991). In human hairy skin, it has been documented that 24 % of cutaneous C-fibers exhibit insensitivity to both mechanical and thermal stimuli (C-M_iH_i). Among the entire tested C-M_iH_i population, 7 out of 22 units (32 %) exhibited excitability in response to topical exposure to mustard oil, while 4 out of 15 units (27 %) displayed increased sensitivity to heat and/or mechanical stimuli following mustard oil treatment. Following exposure to capsaicin, 2 out of the 15 C-M_iH_i units acquired mechanical sensitivity. In summary, after exposure to inflammatory irritants, a significant proportion of C-M_iH_i fibers, specifically 40 % (6/15), manifested heightened sensitivity to natural stimuli. Within this subset, 4 C-MiHi fibers (4/15, 27 %) acquired mechanical sensitivity.

In accordance with these findings, a recent study conducted an in-depth exploration of the neural mechanisms responsible for NGF-induced hypersensitivity, with a primary focus on functionally assessing neuronal excitability and investigating potential associations with the structural plasticity of cutaneous innervation (Hirth et al. 2013). It has been shown that intradermal administration of NGF in humans leads to enduring mechanical hypersensitivity, characterized by a delayed onset, peaking at 3 weeks, and persisting for at least 49 days following NGF injection (Rukwied et al. 2010). Similarly, in pigs, intradermal NGF injections were found to sensitize the axons of previously quiescent mechano-insensitive nociceptors within one week, although mechanical sensitization was not discernible at this early stage (Obreja et al. 2011). Building upon these observations, Hirth and colleagues investigated the effects of NGF administration three weeks after intradermal injections in both pig and human subjects. In the porcine model, they found that following NGF treatment, there was a notable augmentation in the fraction of mechanosensitive C-fiber nociceptors within the treated

cutaneous regions, escalating from 45.1 % in the control group to 71 %. Additionally, the median mechanical thresholds of these nociceptors exhibited a substantial reduction, while their mechanical receptive fields expanded significantly. Importantly, the proportion of sensitized MIAs significantly increased following NGF treatment. Specifically, three weeks after NGF application, 14 % of MIAs exhibited sensitization and responded to noxious mechanical stimuli. This represented a substantial sevenfold increase compared to the 2.2 % sensitized MIAs observed in control animals. Consistent with these findings, extracellular single-fiber recordings revealed that NGF application led to an increase in conduction velocity and a reduction in both activity-dependent slowing and propagation failure in MIAs. The acquisition of mechanosensitivity in MIAs within the porcine model parallels the onset of mechanical hypersensitivity observed in humans. Analysis of skin biopsies from both porcine and human subjects treated with NGF in the affected regions revealed that NGF did not induce alterations in intraepidermal nerve fiber densities. This observation suggests that the hyperalgesia induced by NGF is unlikely to be attributed to structural changes but rather may be attributed to the activation of previously quiescent nociceptors (Hirth et al. 2013). Increasing evidence substantiates the essential role of NGF in the sensitization of MIAs, as indicated by findings presented by Prato and colleagues (Prato et al. 2017). Their research demonstrated that the acquisition of mechanosensitivity in MIAs is contingent upon NGF, with no concurrent impact on the mechanosensitivity of other nociceptor subtypes. Incubation of mouse MIAs with NGF for 24 hours effectively sensitized MIAs to mechanical stimuli, whereas incubation with an inflammatory mixture containing bradykinin, PGE2, histamine, and serotonin did not produce the same effect. Additionally, they elucidated the downstream signaling pathway through which NGF sensitizes MIAs. Their findings revealed that the acquisition of mechanosensitivity hinges on ERK1/2 kinase-mediated de-novo gene transcription, leading to the synthesis of an as-yet-unidentified protein. Moreover, PIEZO2 was identified as the mechanotransduction channel responsible for conferring mechanosensitivity to MIAs (see 1.1.1.2 Silent nociceptors).

In summary, these studies collectively suggest that the activation of silent nociceptors plays a pivotal role in the emergence of mechanical hypersensitivity during inflammation. Furthermore, they underscore the indispensable role of NGF as a mediator in the context of inflammatory pain and the sensitization of MIAs.

1.3.2.3 Nerve Growth Factor: mediator of pain hypersensitivity

NGF is a neurotrophin that plays a fundamental role in growth, development, maintenance, and survival of neurons. It was initially discovered in the 1950s as a neurotrophic factor that promotes neuronal growth during the development of chick embryos (Levi-Montalcini and Hamburger 1951). Over the past few decades, it has become evident that NGF serves dual functions, distinct in developmental and mature contexts. During development NGF is secreted by target tissues and binds to its high-affinity receptors TrkA expressed on neuronal cell surfaces triggering neuronal survival, sprouting and growth.

In adulthood, however, NGF is an important pain mediator (Denk et al. 2017; Schmelz et al. 2019). The proper function of nociceptors relies on NGF signaling, as mutations in either the NGF or TrkA gene result in congenital loss of pain sensation (Davidson et al. 2012; Einarsdottir et al. 2004). Essentially, nociceptive sensory neurons overwhelmingly depend on NGF for their survival during the developmental phase. In rodents, this dependency undergoes a notable shift, typically manifesting around 1-2 weeks postnatally. During this period, approximately 50 % of sensory neurons undergo a transition characterized by the downregulation of TrkA receptor expression and the concomitant upregulation of receptors specific to GDNF (Denk et al. 2017). Nevertheless, a significant portion of mature sensory neurons still maintains TrkA expression. In fact, it has been shown that 40 % of adult rat DRG neurons are TrkA-positive, primarily consisting of peptidergic C-fibers that innervate a wide range of peripheral tissues, including the skin, muscles, bones, and viscera (Averill et al. 1995; Schmelz et al. 2019) These findings align with studies that have examined TrkA expression in human DRG neurons (Rostock et al. 2018).

Meanwhile, a substantial body of literature provides strong support for the significant role of NGF in pain signaling. For instances, increases in NGF levels in naive rodents induced through exogenous administration, overexpression, or inhibition of endogenous degradation (Andreev et al. 1995; Davis et al. 1993; Lewin et al. 1993; Osikowicz et al. 2013) lead to mechanical and thermal hypersensitivity. Likewise, intradermal or intramuscular NGF administration in humans results in mechanical hypersensitivity (Dyck et al. 1997; Svensson et al. 2003). In line with this, elevated NGF levels have been observed in several animal models of pain, including

experimental low-back and osteoarthritis pain (Miller et al. 2020; Orita et al. 2011; Shi et al. 2018). Vice versa, inhibition of NGF signaling, either by using NGF antibodies or blocking the NGF receptor TrkA, effectively alleviated pain in various animal models of pain. These models included bone cancer and skeletal fracture pain (Koewler et al. 2007; Sevcik et al. 2005), although the majority of models were inflammatory pain models such as autoimmune and inflammatory arthritis (Ashraf et al. 2016; Ishikawa et al. 2015; Iwakura et al. 2010; Koewler et al. 2007; LaBranche et al. 2017; Miyagi et al. 2017; Nwosu et al. 2016; Sevcik et al. 2005; Shelton et al. 2005; Xu et al. 2016). These collective observations underscore the potential role of NGF as a pivotal link between inflammation and pain.

While NGF seems to be expressed at low levels in physiological conditions, it becomes notably upregulated following peripheral injury, a condition often associated with inflammation. NGF is predominantly released by immune cells, specifically macrophages and mast cells, as an integral component of the inflammatory response (Barouch et al. 2001; Denk et al. 2017; Lewin et al. 1994; Woolf et al. 1996). Additionally, non-immune cells, including endothelial cells, chondrocytes, keratinocytes, pericytes, and synoviocytes, have also been documented as sources of NGF secretion (Chartier et al. 2017; Fujimoto et al. 2008; Hiltunen et al. 2001; Miller et al. 2017; Schmelz et al. 2019). As reviewed by Schmelz and colleagues it is well-established that inflammatory processes can give rise to both peripheral and central sensitization (Schmelz et al. 2019). NGF is believed to exert a significant role in acute peripheral sensitization through its direct interaction with TrkA receptors located on the peripheral terminals of nociceptors and the surface of inflammatory cells. Moreover, it exerts an indirect influence on central sensitization through its downstream effects on transcription processes. Upon binding of NGF to its TrkA receptor, it initiates receptor homodimerization and autophosphorylation, subsequently activating all three downstream second-messenger cascades of TrkA, which encompass the PI3-kinase, PLCγ, and Ras/Raf/MEK/ERK pathways (Denk et al. 2017).

The initiation of NGF/TrkA signaling in peripheral nociceptive endings induced by inflammation can lead to both short-term and long-term responses. In the short term, this cascade results in rapid local peripheral sensitization and nociceptor depolarization by augmenting the activity and/or expression of diverse ion channels and receptors at the nociceptor cell membrane (Schmelz et al. 2019). These include

ASICs 2 and 3, bradykinin receptors, voltage-gated ion channels, and TRPV1 (Ji et al. 2002; Lee et al. 2002; Lesser and Lo 1995; Mamet et al. 2002). For instance, it has been demonstrated that hindpaw inflammation induced by CFA, which triggers NGF/TrkA signaling, can enhance TRPV1 activity by upregulating the levels of TRPV1 protein in the peripheral terminals of C-fiber nociceptors, leading to the onset of thermal hypersensitivity within mere minutes after TrkA binding (Ji et al. 2002; Schmelz et al. 2019). In contrast, the long-term consequences involve transcriptional signaling and may take several days to become evident (Mantyh et al. 2011). Specifically, following internalization, the NGF/TrkA complex undergoes retrograde transport to the cell soma of nociceptors situated within the DRG. Within the nociceptor cell body, the NGF/TrkA complex initiates transcriptional processes, leading to heightened expression levels of pro-nociceptive peptides and neurotrophins, including substance P, CGRP, and BDNF, alongside nociceptor-specific sodium and calcium channels (Fjell et al. 1999; Michael et al. 1997; Park et al. 2010; Skoff and Adler 2006). Subsequently, originating from the DRG cell body, the newly synthesized pro-nociceptive mediators undergo translational modifications and reach both the peripheral and central terminals of the nociceptors. There, they ultimately facilitate peripheral and central sensitization (Denk et al. 2017; Schmelz et al. 2019).

Furthermore, NGF augments peripheral sensitization through its interaction with TrkA receptors located on inflammatory cells at the site of injury. The NGF/TrkA signaling cascade elicits the release of inflammatory mediators from these cells. These mediators, including histamine, serotonin, PGE2, and NGF itself, subsequently engage with their respective receptors situated at the peripheral terminals of nociceptors, thereby instigating sensitization processes (Horigome et al. 1993; Mantyh et al. 2011; Marshall et al. 1999; Schmelz et al. 2019).

Lastly, it is well-documented that NGF can induce structural plasticity in nociceptors, impacting both peripheral and central terminals, thereby contributing to heightened pain sensitivity. Specifically, numerous reports from various rodent models, including those of bone cancer and joint pain, have demonstrated that NGF promotes the sprouting of peripheral nociceptive afferents, leading to the development of pain hypersensitivity (Ghilardi et al. 2012; Jimenez-Andrade et al. 2011; Jimenez-Andrade and Mantyh 2012; Mantyh et al. 2010). Likewise, NGF-induced aberrant plasticity in

central nociceptor terminals has been substantiated and is associated with an increased sensitivity to pain (Lin et al. 2014; Romero et al. 2000; Schmelz et al. 2019).

In summary, there exists compelling evidence affirming the pronociceptive role of NGF in the context of inflammatory pain. Consequently, it is unsurprising that numerous experimental and clinical investigations have explored the analgesic potential of inhibiting NGF signaling, exemplified by the use of anti-NGF antibodies, in the management of inflammatory pain conditions (Denk et al. 2017; Schmelz et al. 2019). Significantly, multiple clinical trials have substantiated the remarkable effectiveness of anti-NGF therapies in mitigating mechanical pain hypersensitivity associated with chronic inflammatory diseases. Notably, antibodies targeting NGF and pharmacological agents impeding the activation or function of the TrkA receptor have been developed to address various chronic pain conditions (Chang et al. 2016; Schmelz et al. 2019). Remarkably, the anti-NGF drug Tanezumab demonstrated efficacy in patients afflicted with diverse chronic pain disorders, encompassing osteoarthritis, chronic low back pain, pancreatitis, interstitial cystitis, and metastatic bone cancer. However, despite encouraging initial outcomes, the Phase III trial of anti-NGF treatment was prematurely halted due to the emergence of dose-dependent rapidly progressive osteoarthritis in some treated patients, necessitating joint replacement surgeries (Chang et al. 2016; Schmelz et al. 2019).

In conclusion, it is widely recognized that NGF plays a pivotal role in the pathophysiology of inflammatory pain and that the inhibition of NGF signaling holds substantial analgesic potential for the management of painful inflammatory conditions. Despite considerable progress in understanding the molecular mechanisms underlying NGF-induced pain hypersensitivity during inflammatory states, the predominant contribution of peripheral versus central mechanisms to long-lasting mechanical hypersensitivity remains unresolved (Lewin et al. 2014). Recently, it was demonstrated that the sensitization of mechanically insensitive afferents relies on NGF, as MIAs acquire mechanosensitivity following in-vitro NGF treatment. However, the precise mechanism by which NGF activates MIAs and the extent to which this NGF-induced un-silencing translates to mechanical hypersensitivity in-vivo remain unclear. Given the substantial proportion and widespread distribution of silent nociceptors across various tissues, it is evident that the physiological role and the NGF-induced activation mechanism of MIAs warrant further investigation. Consequently, this situation offers a

unique opportunity to develop innovative pharmaceutical strategies for mitigating inflammatory pain.

1.4 Aim of the thesis

The overarching objective of this thesis was to investigate the physiological significance of MIAs and elucidate the mechanism driving the activation of this unique peptidergic C-fiber nociceptor subset.

To date, in-vitro research has established that MIAs acquire mechanosensitivity upon exposure to the inflammatory mediator NGF. This mechanosensitivity is conferred to MIAs by the mechanically-gated ion channel PIEZO2. Furthermore, it has been shown that this process of un-silencing necessitates de-novo gene transcription of an as-yet-unidentified protein (Prato et al. 2017). Nevertheless, the physiological role and significance of silent nociceptors in-vivo, as well as the mechanism governing their activation, remain enigmatic.

To tackle the primary aim of this thesis, my research incorporated several essential sub-objectives, building on the discoveries made by Prato and colleagues (Prato et al. 2017).

To begin with, MIAs underwent a systematic screening to identify potential target proteins implicated in NGF-induced sensitization of silent nociceptors. In parallel, an inflammatory knee pain model was established and comprehensively characterized to assess the physiological role of MIAs in-vivo.

Given that the screening identified the transmembrane protein TMEM100 as a potential missing link in the activation mechanism of MIAs during NGF-mediated inflammatory pain, a genetically engineered TMEM100 knockout mouse line was generated. This innovative mouse model paved the way for an in-depth analysis of TMEM100's pivotal role on molecular, cellular, and behavioral scales. Specifically, the conducted experiments sought to ascertain if TMEM100 is both indispensable and adequate for bestowing mechanosensitivity upon MIAs and to shed light on the protein's impact on inflammatory pain behavior.

2. MATERIALS AND METHODS

2.1 Materials

2.1.1 Equipment and instruments

Table 1 | Equipment and instruments for knee joint injections and tissue processing

Equipment/Instrument	Source
BD Micro-Fine™ Plus Insulin Syringes (8 mm X 30 G, 0.3 ml)	Becton, Dickinson and Company, Franklin Lakes, NJ, USA
Cryostat Leica CM1950	Leica, Wetzlar, Germany
Disposable scalpel (No. 11 pfm)	FEATHER Safety Razor Co. Ltd, Osaka, Japan
Dowel Spring Scissor (Moria MC26, 10 mm)	Fine Science Tools GmbH, Heidelberg, Germany
Dräger Vapor® 2000	Drägerwerk AG & Co. KGaA, Lübeck, Germany
Dumont #5CO Forceps	Fine Science Tools GmbH, Heidelberg, Germany
Fine Scissor (straight, length 9 cm, cutting edge 22 mm)	Fine Science Tools GmbH, Heidelberg, Germany
Steri 350	Fine Science Tools GmbH, Heidelberg, Germany
Vannas Spring Scissors (curved, cutting edge 3 mm)	Fine Science Tools GmbH, Heidelberg, Germany

Table 2 | Equipment and instruments used for behavioral testing

Equipment/Instrument	Source
Aesthesio® Precision Tactile Sensory Evaluators	DanMic Global, LLC, San Jose, CA, USA
CatWalk XT	Noldus, Wageningen, Netherlands
Framed testing surface	Ugo Basile Srl, Gemonio, VA, Italy
Hargreaves Apparatus	Ugo Basile Srl, Gemonio, VA, Italy
LABORAS	Metris B.V., Hoofddorp, Netherlands
Modular animal-enclosure	Ugo Basile Srl, Gemonio, VA, Italy
Stimulation base (Large platform and supporting columns)	Ugo Basile Srl, Gemonio, VA, Italy

Table 3 | Equipment and instruments for microscopy and imaging

Equipment/Instrument	Source
CoolLED pE-340^{fura}	CoolLED Ltd., Andover, United Kingdom
KL1500 electronic (light)	Carl Zeiss Microscopy GmbH, Jena, Germany
Leica L2	Leica, Wetzlar, Germany
Leica MZFLIII	Leica, Wetzlar, Germany
Leica SP8 confocal microscopy platform equipped with a Lasx 3.5. Laser	Leica, Wetzlar, Germany
Nikon DS-Qi2 camera	Nikon Corporation, Minato, Tokyo, Japan
Nikon Ni-E epifluorescence microscope	Nikon Corporation, Minato, Tokyo, Japan
ORCO-Flash4.0 camera	Hamamatsu Photonics K.K, Hamamatsu City, Japan
Zeiss Axio Observer A1	Carl Zeiss Microscopy GmbH, Jena, Germany

Table 4 | Equipment and instruments for cell cultures

Equipment/Instrument	Source
Cell culture incubator (BINDER)	BINDER GmbH, Tuttlongen, Germany
Cell culture incubator (Heraeus BBD6220)	Thermo Fisher Scientific, Waltham, MA, USA
Cell culture sterile hood (HERAsafeKS)	Thermo Fisher Scientific, Waltham, MA, USA
Centrifuge (Eppendorf Centrifuge 5424)	Eppendorf SE, Hamburg, Germany
Thermomixer compact	Eppendorf SE, Hamburg, Germany
Vortex Mixer (model 7-2020)	neoLab Migge Laborbedarf-Vertriebs GmbH, Heidelberg, Germany
Waterbath (Grant Sub Aqua Pro)	Grant Instruments Ltd., Cambridge, UK

Table 5 | Equipment and instruments for electrophysiology

Equipment/Instrument	Source
AC coupled differential amplifier (NeuroLog™ NL104 AC)	Digitimer Ltd., Welwyn Garden City, UK
EPC-10 amplifier	HEKA, Lambrecht, Germany
Force measurement device (FMS-LS)	Kleindiek Nanotechnik, Reutlingen, Germany
Microforge (CPM-2)	ALA Scientific Instruments, Inc., Farmingdale, NY, USA
Microprocessor pH meter (pH211)	Hanna Instruments, Woonsocket, RI, USA
Nanomotor© (MM3A-LS)	Kleindiek Nanotechnik, Reutlingen, Germany

Notch filter (NeuroLog™ NL125-6)	Digitimer Ltd., Welwyn Garden City, UK
Osmometer (Vapor Pressure Osmometer Vapro 5520)	Wescor, Langenfeld, germany
P-97 Flaming/Brown Micropipette Puller	Sutter Instruments, Novato, CA, USA
EcoVac Vakuumpumpe PowerLab SP4	Schuett-biotec GmbH, Göttingen, Germany ADInstruments, Dunedin, New Zealand
Valve Controlled Gravity Perfusion Systems (VC3-8xG)	ALA Scientific Instruments, Inc., Farmingdale, NY, USA

Table 6 | Equipment and instruments for RT-qPCR and RNA sequencing

Equipment/Instrument	Source
Thermal cycler (MJ Mini™ Gradient Thermal Cycler)	Bio-Rad Laboratories, Inc., Hercules, CA, USA
LightCycler 96	Roche, Basel, Switzerland
Illumina HiSeq 2000	Illumina, Inc., San Diego, CA, USA

2.1.2 Chemicals

Table 7 | Chemicals

Chemical/Solution/Enzyme	Source
Bovine serum albumin	Sigma-Aldrich Co., St. Louis, MO, USA
Braunol®	Braun Melsungen AG, Melsungen, Germany
Collagenase Type IV from Clostridium histolyticum (product number: C5138)	Sigma-Aldrich Co., St. Louis, MO, USA
Complete Freund's Adjuvant (product number: F5881)	Sigma-Aldrich Co., St. Louis, MO, USA
D(+)-Glucose	Carl Roth GmbH & Co. KG, Karlsruhe, Germany
D(+)-Saccharose (sucrose)	Carl Roth GmbH & Co. KG, Karlsruhe, Germany
DENARASE® (product number: 20804)	c-LEcta GmbH, Leipzig, Germany
Distilled water (ultra pure type 1 water)	Milli-Q®, Merck KGaA, Darmstadt, Germany
Disodium hydrogen phosphate (Na_2HPO_4)	Carl Roth GmbH & Co. KG, Karlsruhe, Germany
Dulbecco's Phosphate Buffered Saline (PBS)	Gibco™, Thermo Fisher Scientific, Waltham, MA, USA
Dulbecco's Phosphate Buffered Saline (PBS) without Ca^{2+} and Mg^{2+}	Gibco™, Thermo Fisher Scientific, Waltham, MA, USA
Dulbecco's Modified Eagle Medium (DMEM)	Gibco™, Thermo Fisher Scientific, Waltham, MA, USA
Dulbecco's Modified Eagle Medium/F12 (DMEM/F-12) (product number: 21331020)	Gibco™, Thermo Fisher Scientific, Waltham, MA, USA
Ethylenediaminetetraacetic acid (EDTA)	Carl Roth GmbH & Co. KG, Karlsruhe, Germany
Fast Blue (product number: 17740-1)	Polysciences Europe GmbH, Hirschberg an der Bergstraße, Germany
Fetal horse serum (product number: 26050088)	Gibco™, Thermo Fisher Scientific, Waltham, MA, USA
FluoProbes® FluoroGel	Interchim, Montluçon France
Glycine	Fisher Scientific GmbH, Schwerte, Germany
HEPES (4-(2-hydroxyethyl)-1-piperazineethanesulfonic acid)	Carl Roth GmbH & Co. KG, Karlsruhe, Germany
Isoflurane (Isoflurane Baxter)	Baxter International Inc., Deerfield, IL, USA
L-Glutamine (200 mM) (product number: 25030024)	Gibco™, Thermo Fisher Scientific, Waltham, MA, USA
Nerve Growth Factor (NGF; beta-NGF human, recombinant, expresses in E. coli) (product number: SRP3015)	Sigma-Aldrich Co., St. Louis, MO, USA
Ni-sepharose excel histidine-tagged protein purification resin (product number: 17371202)	Cytiva, Marlborough, MA, USA

Normal donkey serum	Sigma-Aldrich Co., St. Louis, MO, USA
pAdDeltaF6 (AAV helper plasmid) (product number:112867)	Addgene, Watertown, MA, USA
Penicillin-Streptomycin (10.000 U/ml) (product number: 15140122)	Gibco™, Thermo Fisher Scientific, Waltham, MA, USA
Polyethylenimine (Linear, MW 25000, Transfection Grade (PEI 25K™) (product number: 23966)	Polysciences Europe GmbH, Hirschberg an der Bergstraße, Germany
Poly-L-lysine solution (product number: P4707)	Sigma-Aldrich Co., St. Louis, MO, USA
pUCmini-iCAP-PHP.S (product number: 103006)	Addgene, Watertown, MA, USA
Ringer's solution	Braun Melsungen AG, Melsungen, Germany
RNase A (product number: 10109169001)	Roche, Basel, Switzerland
RNase Inhibitor (recombinant) (product number: 2313A)	Takara Bio Europe SAS, St-Germain-en-Laye, France
Sodium chloride (NaCl)	VWR, Belgium
Sodium dihydrogen phosphate (NaH_2PO_4)	Carl Roth GmbH & Co. KG, Karlsruhe, Germany
Sodium hydroxide solution 40 % (10 M, NaOH)	Carl Roth GmbH & Co. KG, Karlsruhe, Germany
Sterile saline solution (0.9 %)	Braun Melsungen AG, Melsungen, Germany
Tissue-Tek™ O.C.T. Compound;	Sakura Finetek Germany GmbH, Umkirch, Germay
Triton X-100	neoLab Migge Laborbedarf-Vertriebs GmbH, Heidelberg, Germany
Trypsin from bovine pancreas (product number T1005)	Sigma-Aldrich Co., St. Louis, MO, USA
Tween®	Carl Roth GmbH & Co. KG, Karlsruhe, Germany
Ethylene glycol-bis(β-aminoethyl ether)-N,N,N′,N′-tetraacetic acid (EGTA)	Sigma-Aldrich Co., St. Louis, MO, USA
Guanosine-5'-triphosphate (GTP) lithium type I (product number: G5884)	Sigma-Aldrich Co., St. Louis, MO, USA
Adenosine-5'-triphosphate (ATP) disodium salt (product number: A6419)	Sigma-Aldrich Co., St. Louis, MO, USA
Calbryte™ 590 AM (product number: 20700)	AAT Bioquest® Inc., Pleasanton. CA, USA
Dimethylsulfoxid (DMSO)	Sigma-Aldrich Co., St. Louis, MO, USA
Sodium Chloride (NaCl)	Sigma-Aldrich Co., St. Louis, MO, USA
BES-buffered saline (BBS) (2X)	Sigma-Aldrich Co., St. Louis, MO, USA
Imidazol	Merck KGaA, Darmstadt, Germany
Allylisothiocyanat (AITC) (Pestanal®, product number: 36682)	Sigma-Aldrich Co., St. Louis, MO, USA

2.1.3 Kits

Table 8 | Kits

Kit	Source
Power SYBR® Green Cells-to-CT™ (product number: 4402953)	Thermo Fisher Scientific, Waltham, MA, USA
FastStart Essential DNA Green Master (product number: 06402712001)	Roche, Basel, Switzerland
Amaxa™ 4D-Nucleofector™	Lonza Group, Basel, Switzerland
Nextera DNA Library Preparation Kit	Illumina, Inc., San Diego, CA, USA

2.1.4 Antibodies

Table 9 | Primary antibodies

Antibody	Source	Dilution/Concentration	Product number
Isolectin GS-IB4 from *Griffonia simplicifolia* Alexa Fluor™ 568 Conjugate	Invitrogen™/Thermo Fisher Scientific, Waltham, MA, USA	2.5 µg/ml	I21412
Isolectin GS-IB4 from *Griffonia simplicifolia* Alexa Fluor™ 647 Conjugate	Invitrogen™/Thermo Fisher Scientific, Waltham, MA, USA	2.5 µg/ml	I32450
Rat anti-GFP	Nacalai Tesque Inc., Kyoto, Japan	1:3000	04404-84
Rabbit anti-CGRP	ImmunoStar Inc., Hudson, WI, USA	1:200	24112
Rabbit anti-dsRed	Takara Bio Europe SAS, St-Germain-en-Laye, France	1:1000	632496

Table 10 | Secondary antibodies

Antibody	Source	Dilution	Product number
Donkey anti-Rat IgG (H+L) Highly Cross-Adsorbed Secondary Antibody, Alexa Fluor™ Plus 488	Invitrogen™/Thermo Fisher Scientific, Waltham, MA, USA	1:750	A48269
Donkey anti-Rabbit IgG (H+L) Highly Cross-Adsorbed Secondary Antibody, Alexa Fluor™ Plus 594	Invitrogen™/Thermo Fisher Scientific, Waltham, MA, USA	1:750	A32754

2.1.5 Buffer, media and solutions

Table 11 | Buffer, media and solutions

Reagent	Application
Primary DRG cell culture growth medium	Volume: 50 ml • 45.6 ml DMEM/F-12 • 500 µl L-Glutamine (2 µM) • 0.4 ml 30 % Glucose solution (8 mg/ml) • 1 ml Penicillin/Streptomycin (200 U/ml Penicillin / 200 µg/ml Streptomycin) • 2.5 ml fetal horse serum (5 %)
HEK293 cell culture growth medium	• DMEM • 10 % fetal bovine serum • 2 mM L-Glutamine • 100 U/mL Penicillin-Streptomycin
HEK293 cell transfection medium	• DMEM • 10 % calf serum • 4 mM L-Glutamine
BES Buffered Saline (2X)	• 50 mM HEPES • 280 mM NaCl • 1.5 mM Na_2HPO_4 • Adjust to pH 7.0
Lysis buffer (AAV-PHP.S production)	• PBS • 6 mM $MgCl_2$

	• 0.4 % Triton X-100 • 6µg/ml RNase A • 250U/µl DENARASE
Washing buffer (AAV-PHP.S production)	• PBS • 20 mM Imidazole • Adjust to pH 7.4
Elution buffer (AAV-PHP.S production)	• PBS • 500 mM Imidazole • Adjust to pH 7.4
Sucrose Solution (30 %)	• 300 g sucrose • 400 ml 0.2 M phosphate buffer • 400 ml ddH_20 • Stir until dissolved
Cell picking buffer (RT-qPCR and RNA sequencing)	Volume 50 1µL • 1µL recombinant RNase inhibitor • 49 µL PBS.
Intracellular buffer (ICB) (patch clamp recordings)	• 110 mM KCl • 10 mM NaCl • 1 mM MgCl2 • 1 mM EGTA • 10 mM HEPES • 2 mM GTP • 2 mM ATP • in sterile ddH_20 • Stir until dissolved • Adjusted to pH 7.3 with KOH, mOsm ~ 300 • Store at 4 °C until further use • Add before use: 2 mM GTP and 2 mM ATP
Extracellular buffer (ECB) (patch clamp recordings and calcium imaging)	• 140 mM NaCl • 4 mM KCl • 2 mM $CaCl_2$ • 1 mM $MgCl_2$ • 4 mM Glucose • 10 mM HEPES • In sterile ddH20 • Adjusted to pH 7.4 with NaOH, mOsm ~ 310 • Stir until dissolved
Synthetic interstitial fluid buffer (SIF).	• 108 mM NaCl • 3.5 mM KCl

	• 0.7 mM $MgSO_4$ • 26 mM $NaHCO_3$ • 1.7 mM NaH_2PO_4 • 1.5 mM $CaCl_2$ • 9.5 mM sodium gluconate • 5.5 mM glucose • 7.5 mM sucrose • In sterile ddH20 • Adjusted to a pH of 7.4 • Stir until dissolved t

2.1.6 Consumables

Table 12 | Consumables

Product	Source
12-well plates	Falcon®, Corning Inc, Corning, NY, USA
Borosilicate glass capillaries (product number: BF150-86-10)	Sutter Instruments, Novato, CA, USA
Cover Slips 24 x 40 mm	Carl Roth GmbH & Co. KG, Karlsruhe, Germany
Econo-Pac® Chromatography Column, 30 µm filter (product number: 7321010)	Bio-Rad Laboratories, Inc., Hercules, CA, USA
GG-12-Laminin coated coverslips (GG-12-Laminin, 12mm dia.#1 thick)	Neuvitro Corporation, Camas, WA, USA
LightCycler 480 Multiwell Plate 96	Roche, Basel, Switzerland
LightCycler 480 Sealing Foil	Roche, Basel, Switzerland
Microscope Slides SUPERFROST® PLUS	Thermo Fisher Scientific, Waltham, MA, USA
Micro-Touch® Nitra-Tex® Sterile, Powder-Free Examination Gloves	Ansell Limited, Australia
PCR tubes (0.2 ml)	Peqlab, VWR International, Radnor, PA, USA
Pipette tips	Sarstedt, Nümbrecht, Germany
Tissue-Tek® O.C.T™ compound	Sakura Finetek Germany GmbH, Staufen, Germany
Tubes (0.5 ml, 1 ml, 2.0 ml, 15 ml, 50 ml)	Sarstedt, Nümbrecht, Germany
Vivaspin 20 ultrafiltration unit (molecular weight cut-off 1,000,000)	Sartorius AG, Göttingen, Germany

2.1.7 Software

Table | 13: Software programs

Program	Software producer
Adobe Photoshop **C**S6	Adobe Systems Incorporated, San Jose, CA, USA
Adobe Illustrator 2022	Adobe Systems Incorporated, San Jose, CA, USA
EndNote X9 for Microsoft Windows	Thomson Reuters Corporation, NY, USA
GraphPad Prism 9	GraphPad Software Inc., La Jolla, CA, USA
ImageJ 1.53e; Java 1.8.0_172 [64-bit]	Public domain imaging software developed by Wayne Rasband, the National Institutes of Health, USA
ZEN 2 pro software	Carl Zeiss Microscopy GmbH, Jena, Germany
CatWalk XT software	Noldus, Wageningen, Netherlands
LABORAS software (version 2.6)	Metris B.V., Hoofddorp, Netherlands
LabChart (version 7.1)	ADInstruments, Dunedin, New Zealand
LightCycler® 96 (version 1.1)	Roche, Basel, Switzerland
Patchmaster© software (version 2.96)	HEKA, Lambrecht, Germany
Fitmaster© software (version 2.94)	HEKA, Lambrecht, Germany
Microsoft® Excel® (Microsoft Office Professional Plus 2016)	Microsoft Corporation, Redmond, WA, USA

2.2 Methods

2.2.1 Animal subjects

The experiments adhered to the European Communities Council Directive (EU and institutional guidelines), which included the ethical guidelines of the 'Protection of Animals Act.' They were conducted under the supervision of Animal Welfare Officers from Heidelberg University and were approved by the local governing body (Regierungspräsidium Karlsruhe, approval number G16/20). ARRIVE guidelines were followed and sample sizes were determined based on previous experience with G-power analyses.

CHRNA3-EGFP mice (Tg(Chrna3-EGFP)BZ135Gsat/Mmnc) were obtained from the Mutant Mouse Resource & Research Center and were backcrossed to a C57Bl/6J background. Conditional nociceptor TMEM100 knock-out (TMEM100KO) mice were created by crossing mice with a conditional TMEM100 allele (B6.Tmem100tm1.1Yjl) (Moon et al. 2010) with SNS-Cre mice C57BL/6-Tg(SCN10A-Cre)1Rkun/Uhg (Agarwal et al. 2004) (a gift from Rohini Kuner). To identify MIAs, these mice were further bred with CHRNA3-EGFP mice. Additionally, Tg(Npy2r-cre)SM19Gsat/Mmucd x B6;129S-Gt(ROSA)26Sortm32(CAG-COP4*H134R/EYFP)Hze/J (Npy2rCre;ChR2-EYFP) mice, in which Aδ-fiber nociceptors express EYFP (Arcourt et al. 2017), were used to identify different nociceptor subclasses for RT-qPCR experiments.

Animals were housed in the Interfaculty Biomedical Facility of Heidelberg University, following institutional guidelines, in a 12/12-hour light-dark cycle with an enriched housing environment. They had access to food and water ad libitum. Only adult (aged 8-15 weeks) male and female mice were used for all experiments. Behavioral experiments took place at the Interdisciplinary Neurobehavioral Core of Heidelberg University. Before starting behavioral experiments, mice with the same genetic background and age were randomly assigned to different experimental groups. To reduce bias, investigators were blinded to group identity, including treatment (CFA/Saline) and genotype (TMEM100KO/WT).

2.2.2 Inflammatory knee pain model

To induce inflammatory knee joint pain, the Complete Freund's Adjuvant (CFA)-induced knee joint monoarthritis model was used according to a previously described protocol (Krug et al. 2019). In brief, the animals were anesthetized in a transparent plexiglass chamber filled with 4 % isoflurane in 100 % O_2 at a flow rate of 1.0 L/min for 3 minutes. Throughout the procedure, anesthesia was maintained using a nosecone delivering a 1.5 % Isoflurane-O_2 mixture, while closely monitoring respiratory function. Adequate anesthesia was confirmed by the absence of the pedal reflex (toe pinch). Subsequently, ophthalmic ointment was applied to both eyes to prevent dryness, and the animals were placed in a supine position. Before the CFA injection, the left knee was shaved using an electrical facial hair trimmer, disinfected with a 7.5 % povidone-iodine scrub (Braunol®), and stabilized in a bent position by positioning the index finger

beneath the knee joint and the thumb above the anterior surface of the ankle joint. The patellar tendon, visible through the shaved skin, served as a visual landmark for the injection. To ensure precise intraarticular (i.a.) injection, the gap below the lower edge of the patella was identified by gently running a 30 G Insulin syringe horizontally along the knee. A horizontal dermal print line was left on the skin without piercing it to mark the injection level. The needle was then lifted vertically at the marked level and inserted at the midline through the patella tendon, perpendicular to the tibial axis. The needle was advanced approximately 2 - 2.5 mm without resistance to fully enter the knee joint. Then, 30µl of CFA (1µg/µl) or saline were injected into the joint cavity. After the injection, the injection site was again disinfected with a 7.5 % povidone-iodine scrub, and the knee was briefly massaged and mobilized to ensure equal distribution of CFA/saline. For recovery the animals were returned to their home cages and placed on a heating pad.

2.2.3 Retrograde labeling

To identify the sensory neurons innervating the knee joint, retrograde labeling was performed using the retrograde tracer Fast Blue (FB; Polysciences). For this purpose, the identical anesthesiological and surgical approach was employed as previously described (see 2.2.2 Inflammatory knee pain model). Using a 10 µl Hamilton syringe equipped with a 30 G needle, 2 µl of a 4 % FB solution (in saline) were injected i.a. into both knee joints. After a 7-day waiting period, during which Fast Blue (FB) retrogradely traveled to the DRG, animals underwent subsequent processing based on the following experiment. To quantify the knee-innervating neurons, animals were sacrificed for microscopy, following the procedures outlined in section 2.2.5 Tissue processing and immunohistochemistry. Additionally, for electrophysiological and qPCR experiments, the left knee underwent a subsequent injection of CFA (as previously described in 2.2.2 Inflammatory knee pain model). 3 days after CFA injections, at the time of peak pain, the animals were euthanized to obtain primary DRG cultures.

2.2.4 Behavioral testing

All behavioral tests were conducted on awake, unrestrained mice. Before behavioral testing, all animals underwent habituation to the respective test setups, which occurred at least three times over the course of three days (1x/d per setup) during the week prior to behavioral assessment. For the von Frey (vF) and Hargreaves' tests, the animals were habituated for 1 hour per setup, and an additional 30 to 60 minutes immediately before each test, with the experimenter present in the same room. Regarding the CatWalk XT test, habituation was considered complete when mice voluntarily crossed the runway three times without stopping, turning around, or changing direction, which typically took approximately 5 minutes per animal. On testing days, acclimatization to the CatWalk XT setup was not required. The behavioral assays were consistently performed in the same order (1. CatWalk XT, 2. vF, 3. Hargreaves) using the same rooms and test setups, conducted at the same time of day between 8 a.m. and 3 p.m.

Before knee injection, all behavioral tests were conducted to establish at least two baseline measurements on different days. Following the injections, behavior was assessed at 1, 2, 3, 5, and 7 days post-injection (dpi), and subsequently at weekly intervals (14 dpi) for a total observation period of 3 weeks (21 dpi).

2.2.4.1 Von Frey Test: mechanical sensitivity

Mechanical sensitivity was assessed using the von Frey test as previously described (Nees et al. 2016). In brief, animals were placed in transparent plastic chambers (Modular animal-enclosure; Ugo Basile Srl, Gemonio, Italy) on a 90 x 38 cm perforated metal shelf (Framed testing surface; Ugo Basile Srl, Gemonio, Italy), which was mounted on a stimulation base. To evaluate mechanical sensitivity, the plantar surface of the hind paws was perpendicularly stimulated with graded von Frey filaments (Aesthesio® Precision Tactile Sensory Evaluators) of varying forces, ranging from 0.07 to 1.4 grams, without any horizontal movement of the filaments during application. Each filament was applied five times to both the right and left hind paws, and the response rate to stimulation in percentage (positive response/number of applied stimuli) was used to express mechanical sensitivity. A positive response was defined as the withdrawal of the stimulated paw. To allow a brief recovery, animals were

given at least a one-minute break between stimulations of the same hind paw. Before knee injection, baseline withdrawal frequencies were determined by measuring the withdrawal response rates for all filaments on two different days. Following the injections, mechanical sensitivity was evaluated at 1, 2, 3, 5, and 7 dpi, and then at weekly intervals for a total observation period of 3 weeks (21 dpi).

The 50 % withdrawal threshold (WDT) in grams was determined by fitting the response rate versus von Frey force curves with a Boltzmann sigmoid equation, setting constant bottom and top constraints equal to 0 and 100, respectively.

2.2.4.2 Hargreaves' test: thermal sensitivity

Thermal sensitivity was evaluated using Hargreaves' method (Hargreaves et al. 1988) with the Plantar test (Hargreaves Apparatus; Ugo Basile Srl). To determine thermal sensitivity, the withdrawal latency (WDL) in seconds to an infrared (IR) heat beam stimulus applied to the plantar surface of the hindpaws was recorded. The IR intensity of the radiant heat source was adjusted to achieve baseline WDL between 5 and 7 seconds (IR intensity 50 %), and a predefined cut-off time of 15 seconds was set to prevent tissue damage. Each paw was assessed three times, and between trials for the same paw, animals were given at least a one-minute break. To avoid any order effect, the testing order of the paws was randomized. Baseline measurements and post-interventional assessments were conducted at the same time points as described for the von Frey test.

2.2.4.3 CatWalk XT: gait analysis

The CatWalk XT (version 10.6) gait analysis system (Noldus, Netherlands) was used to quantitatively assess locomotion. This system comprises a black corridor (1.3 m length) enclosed on a glass plate. Within the glass plate, a green LED light is internally reflected. When animals make contact with the glass plate, the light is refracted on the opposite side, resulting in illuminated and detectable areas of contact, such as paw prints. With the use of the Illuminated Footprints™ technology, videos capturing the illuminated areas (such as paw prints) can be recorded using a high-speed color camera (100 frames/s) positioned underneath the glass plate. The recorded data is automatically transferred to a computer running the CatWalk XT

software for subsequent gait analysis. Before testing, the animals were habituated to the setup as described earlier (see 2.2.4 Behavioral testing). On testing days, the walkway was set up according to the manufacturer's recommendations. Then, mice were placed on one end of the corridor of the walkway and were allowed to travel across it voluntarily without any external enforcement. For each mouse at each measurement time point, three compliant runs were recorded. A compliant run was defined as a mouse walking across the runway without stopping, turning around, or changing direction while meeting the specific pre-determined run criteria of a minimum run duration of 0.5 seconds and a maximum run duration of 12 seconds. Consistent detection settings were applied to all runs, including a camera gain of 16.99, green intensity threshold of 0.10, red ceiling light of 17.7, and green walkway light of 16.5.

Data analyses focused on the following gait parameters: stand time (in seconds), paw print area (in cm^2), and swing speed (in cm/s). To highlight pain-related changes in the gait cycle, including the stand and swing phase, run data for the left (LH) and right hind paw (RH) were displayed as a ratio (LH/RH). For each testing day, the ratios (LH/RH) from all three runs per animal were averaged to obtain the mean value, representing the overall result for that testing day.

2.2.4.4 Homecage monitoring

The Laboratory Animal Behaviour Observation, Registration, and Analysis System (LABORAS) serves as a monitoring tool utilized to observe and analyze voluntary animal behavior within their homecage environment. It incorporates a carbon fiber platform designed to detect distinct vibrations generated by the animal as it moves within its homecage. The platform is accompanied by a software (LABORAS software version 2.6), which translates these vibrations into various behavioral parameters, including locomotion, immobility, rearing, drinking, and grooming. These parameters were quantified as frequency counts. For the experiments, individual animals were placed in calibrated cages under standard housing conditions, with unrestricted access to food and water. Their activities were continuously monitored for 16-24 hours before and 3 or 18 days after an intraarticular knee joint injection with Saline/CFA or AAV-PHP.S-TMEM100-Ires-dsRed/AAV-PHP.S-dsRed, respectively.

2.2.5 Tissue processing and immunohistochemistry

2.2.5.1 DRG processing and immunohistochemistry

To quantify retrogradely labeled neurons, DRG were first dissected in ice-cooled PBS. They were then fixed with Zamboni's fixative for 1 hour at 4°C and subsequently incubated overnight in a 30 % sucrose solution at 4 °C. After this, the DRG were embedded in optimum cutting temperature compound (Tissue-Tek™ O.C.T. Compound; Sakura Finetek Germany GmbH), and 16 µm cryo-sections were obtained using a cryostat (Leica CM1950, Leica, Wetzlar, Germany). These sections were mounted onto slides (Microscope Slides SUPERFROST PLUS; Thermo Fisher Scientific, USA) and stored at -80 ˚C until used for immunohistochemistry. To this end, the sections were dried and then treated with 50 mM Glycine in PBS for 20 minutes and washed twice with 0.2 % Triton X-100 in PBS (0.2 % PBST). To block non-specific binding, the sections were incubated with a solution containing 10 % normal donkey serum (NDS) and 1 % bovine serum albumin (BSA) in 0.2 % PBST for 30 minutes. Subsequently, primary antibodies were applied to the sections and left to incubate overnight at 4 °C. The primary antibodies were diluted in a blocking solution comprising 10 % NDS and 1 % BSA in 0.2 % PBST. On the following day, the sections were washed four times for 15 minutes each with 0.2 % PBST, and then incubated with secondary antibodies for 1 hour at room temperature (RT). After additional washing steps with 0.2 % PBST, the sections were dried and coverslipped using FluoroGel (FluoProbes®, Interchim, France) for further analysis.

Immunostaining images were acquired using the Nikon DS-Qi2 camera attached to a Nikon Ni-E epifluorescence microscope. Consistent exposure times and suitable filter cubes were employed for all slides within a given experiment.

2.2.5.2 Knee processing and immunohistochemistry

Initially, the knees were dissected in cold PBS and fixed with Zamboni's fixative overnight. Subsequently, the knee joints were washed in purified water (Milli-Q, Merck KGaA, Darmstadt, Germany) three times for 30 minutes each. Following this, the samples were decalcified by immersing them in 10 % EDTA in PBS for 7-10 days, with PBS/EDTA being replaced every other day. The decalcification process was carried

out on a tube roller mixer at 4 °C. After decalcification, the samples were washed in PBS for three rounds of 10 minutes at RT and then cryoprotected in a 30 % sucrose solution at 4 °C for at least 24 hours. To prepare tissue sections, the samples were embedded in optimum cutting temperature compound (Tissue-Tek™ O.C.T. Compound; Sakura Finetek Germany GmbH, Germany) and cut into consecutive coronal cryo-sections of 25 µm thickness in an anterior-posterior direction. These sections were mounted onto microscope slides (SUPERFROST PLUS; Thermo Fisher Scientific, USA). Subsequently, the sections were dried at RT for 1 hour and then incubated with 50 mM Glycine in PBS for 30 minutes, washed, and blocked three times for 10 minutes each with 0.5 % Tween® 20 in PBS (0.5 % PBS-Tw). Next, the sections were incubated with primary antibodies for 3 days at 4 °C. The primary antibodies were diluted in a PBS solution containing 1 % BSA and 0.3 % Triton X-100. After washing the sections three times for 10 minutes each with 0.5 % PBS-Tw, they were incubated for 2 hours at RT with secondary antibodies diluted in PBS with 1 % BSA and 0.3 % Triton X-100. Finally, the slides were washed with PBS three times for 10 minutes each, dried, and coverslipped using FluoroGel mounting medium with 4,6-diamidino-2-phenylindole (DAPI) counterstain (FluoProbes®, Interchim, Montluçon FRANCE). Immunostaining images were acquired using a Nikon Ni-E epifluorescence microscope equipped with a Nikon DS-Qi2 camera. Appropriate filter cubes and identical exposure times were used for all slides within a given experiment.

Silent afferent density, indicated by $EGFP^+/CGRP^+$ fibers, was assessed in specific anatomical regions, including FP (Hoffa's fat pad), LM (lateral meniscus), MM (medial meniscus), LJC (lateral joint capsule), MJC (medial joint capsule), and CL (cruciate ligament). These regions were defined according to previously described landmarks (Obeidat et al. 2019). The quantification was performed using the area fraction tool in NIH ImageJ software (ImageJ 1.53e; Java 1.8.0_172 [64-bit]). In brief, the images were first converted to 8-bit and underwent background subtraction. Subsequently, the image auto local thresholds were set using the Bernsen method. The different immunostaining images (channels) were then merged and processed using the image calculator tool, displaying only the double positive ($EGFP^+/CGRP^+$) signals. The predefined anatomical regions of interest were overlaid onto the images, and the area fraction was determined to represent the labeling density of silent afferents in each anatomical region as a percentage. For each animal, at least three photomicrographs per anatomical region were analyzed and averaged. The labeling density per

anatomical region for all animals was expressed as the mean ± standard error of the mean (SEM). Additionally, representative images of coronal 100 µm knee sections (Cryostat) were acquired and stitched for illustration purposes using a Leica SP8 Confocal microscopy platform equipped with a Lasx 3.5. Laser using detector powers optimized for the combination of antibodies.

2.2.5.3 Cultured DRG neurons and immunohistochemistry

Cultured DRG neurons (see 2.2.6.1 Primary DRG cell culture) for electrophysiological and qPCR experiments were counterstained with Alexa Fluor™ -568 conjugated IB4 (2.5 µg/ml, Isolectin GS-IB4 from Griffonia simplicifolia, Alexa Fluor™ 568 Conjugate, Invitrogen™/Thermo Fisher Scientific, I21412) for 10-15 minutes at RT to identify different nociceptor subpopulations (CHRNA3-EGFP$^+$/FB$^+$ and IB4$^-$/FB$^+$ neurons).

2.2.5.4 Antibodies

Except for immunostainings of cultured DRG neurons, all immunohistochemical procedures were performed on microscope slides. To this end, the following primary antibodies were used: rat anti-GFP (1:3000), rabbit anti-CGRP (1:200), Isolectin GS-IB4 from Griffonia simplicifolia Alexa Fluor™ 568 Conjugate (2.5 µg/ml), Isolectin GS-IB4 from Griffonia simplicifolia Alexa Fluor™ 647 Conjugate (2.5 µg/ml) and rabbit anti-dsRed (1:1000).

Alexa Fluor™ 488 conjugated donkey anti-Rat IgG (1:750) and Alexa Fluor™ 594 conjugated donkey anti-Rabbit IgG (1:750) were used as Alexa Fluor™ conjugated secondary antibodies.

2.2.6 Cell culture

2.2.6.1 Primary DRG cell culture

To establish primary DRG cultures, mice were euthanized by placing them in a CO_2-filled chamber for 2–4 minutes, followed by cervical dislocation. Lumbar L3 and L4

DRG were collected in Ca^{2+} and Mg^{2+}-free ice-cold PBS. The collected DRG were then treated with collagenase IV for 30 minutes (0.5 mg/ml, Sigma-Aldrich, C5138) and with trypsin (0.5 mg/ml, Sigma-Aldrich, T1005) for another 30 minutes at 37 °C. After digestion, the DRG were washed twice with growth medium [DMEM-F12 (Gibco™, Thermo Fisher Scientific) supplemented with L-Glutamine (2 µM, Gibco™, Thermo Fisher Scientific), glucose (8 mg/ml, Carl Roth GmbH & Co. KG, Karlsruhe, Germany), penicillin (200 U/ml)–streptomycin (200 µg/ml) (Gibco™, Thermo Fisher Scientific), 5 % fetal horse serum (Gibco™, Thermo Fisher Scientific)], and then triturated using a pipette with filter tips of decreasing diameter (10x up and down with a 1000µl filter tip, 10x up and down with a 200µl filter tip). The dissociated neurons were plated on a glass coverslip coated with Laminin (GG-12-Laminin coated coverslips, Neuvitro) in a droplet of growth medium. The coverslips were then incubated for 3 hours at 37 °C in a humidified 5 % CO_2 incubator to allow the neurons to adhere before being flooded with fresh growth medium.

Depending on the specific experiment, the neurons were used directly after applying fresh growth medium (see 2.2.7 Reverse transcription and quantitative real-time PCR) or after incubation for 24 hours (see 2.2.9.1 Patch clamp recordings). For the transfection experiments, primary DRG cultures were transfected using the Amaxa™ 4D-Nucleofector™ (Lonza, Switzerland) following the manufacturer's instructions.

2.2.6.2 HEK293 cell maintenance and transfection

To evaluate the mechanosensitivity of TMEM100 and of PIEZO2 in the presence and absence of TMEM100, the respective constructs were (co)-transfected into HEK293 cells using the calcium phosphate method. In brief, the cells were cultured in DMEM (Thermo Fisher) supplemented with 10 % fetal bovine serum (Thermo Fisher), 2 mM L-glutamine (Thermo Fisher), and penicillin-streptomycin (Thermo Fisher, 100 U/mL) at 37 ºC and 5 % CO_2. The day prior to transfection, cells were seeded on glass coverslips treated with poly-L-lysine. For the transfection process, the growth medium was replaced with a transfection medium consisting of DMEM, 10 % calf serum (Thermo Fisher) and 4 mM L-Glutamine. DNA (0.6 µg/coverslip) was diluted in 100 µl of water, and after adding 2.5 M $CaCl_2$ (10 µL per coverslip), the solution was thoroughly mixed. Subsequently, 2x BBS (50 mM HEPES, 280 mM NaCl, 1.5 mM

Na_2HPO_4, adjust to pH 7.0; 100 µL/coverslip) was added and vortexed. Then, the resulting DNA mix was combined with the transfection medium. After an incubation period of 3-4 hours at 37 ºC and 5 % CO_2, the transfection medium/DNA mix was exchanged with the regular HEK293 growth medium. PIEZO2 function was evaluated 48 hours following the transfection.

2.2.6.3 AAV-PHP.S production

Adeno-associated viruses (AAVs) have been widely used as vehicles for gene transfer to the nervous system. Based on the established procedures by Gradinaru and colleagues (Challis et al. 2019) a modified protocol was used to generate AAV-PHP.S viral particles to transduce the peripheral nervous system.

In brief, AAV-293 cells (Agilent, product number: 240073) were seeded on 150 mm dishes and subsequently transfected with the following four plasmids using polyethylenimine (Polysciences, product number: 23966): a pAAV of interest (either AAV-CAG-dsRedExpress2 or AAV-CAG-TMEM100-IRES-dsRedExpress2, both containing AAV2 ITRs), the AAV helper plasmid pAdDeltaF6 (Addgene, product number: 112867), pUCmini-iCAP-PHP.S (Chan et al. 2017; Addgene, product number:103006), and a modified pUCmini-iCAP-PHP.S with a 6xHis tag on the VP3 capsid protein (Zhang et al. 2002). The transfection ratio for the plasmids was 1:2:2:2, respectively. 48 hours and 120 hours after transfection cell culture medium was changed. The supernatant containing viral particles was collected, centrifuged at 1690 g for 10 minutes and subsequently, filtered (0.2 µm) and diluted in PBS. Then, both the cell pellet and filtered medium were stored at 4 °C. At 120 hours after transfection, the pelleted cells and those remaining in the dishes were lysed and incubated at 37 °C for 1 hour in a specific PBS buffer. This PBS buffer contained the following components: 6 mM $MgCl_2$, 0.4 % Triton X-100, 6 µg/ml RNase A (Roche, product number: 10109169001), and 250 U/µl DENARASE (c-LEcta, product number: 20804). Then, the lysed cells were collected and diluted in PBS before being centrifuged at 2300 g for 10 minutes. Subsequently, the supernatant obtained from the cell lysate and the filtered medium were separately incubated with equilibrated Ni-sepharose excel histidine-tagged protein purification resin (Cytiva, product number: 17371202). After incubation at RT for at least 2 hours with gentle mixing, both the filtered medium and cell lysate were carefully loaded through a gravity flow chromatography column with a

30 µm filter (Econo-pac, Bio Rad, product number: 7321010). Then, the beads were washed with 80 ml of washing buffer containing 20 mM imidazole in PBS (pH 7.4) and the viral particles were eluted in 50 ml of elution buffer (500 mM imidazole in PBS, pH 7.4). For buffer exchange and concentration of the viral particles a Vivaspin 20 ultrafiltration unit with a 1,000,000 molecular weight cut-off (Sartorius, Germany) was used. The viral particles were washed and then resuspended in PBS. To determine the viral particle titer, qPCR was performed, using primers that target the WPRE element (Woodchuck Hepatitis Virus (WHV) Posttranscriptional Regulatory Element).

2.2.7 Reverse transcription and quantitative real-time PCR

Reverse transcription and quantitative real-time PCR were performed with manually collected cell samples of distinct nociceptor subpopulations using two experimental approaches. The first approach aimed at comparing the effects of NGF (beta-NGF human, Sigma-Aldrich, product number: SRP3015) on mRNA expression levels of TMEM100 in different nociceptor subclasses. To this end, primary L3-4 DRG neurons from WT mice were cultured under two conditions: without (-) NGF and with (+) NGF (50 ng/ml) for 24 hours before collecting samples of the following nociceptor subpopulations: CHRNA3^{+}, IB4^{-}, IB4^{+} and Aδ-nociceptors. In the second experimental approach, the mRNA expression levels of TMEM100 in knee joint nociceptors were compared between the treated (CFA) and control (saline) groups at the time of peak pain (3 dpi), using CHRNA3-EGFP^{+}/FB^{+} and IB4^{-}/FB^{+} neurons from both the ipsilateral (CFA) and contralateral (saline) sides. To this end, acute primary L3-4 DRG cultures of WT mice were used, which means that cells were collected directly after applying fresh growth medium as soon as sufficient adhesion to coverslips was achieved (~3h of incubation, see 2.2.6.1 Primary DRG cell culture). In both approaches, prior to cell collection, the DRG cultures were counterstained with Alexa Fluor™-568 conjugated IB4 (2.5 µg/ml, Isolectin GS-IB4 from Griffonia simplicifolia, Alexa Fluor™ 568 Conjugate, Invitrogen, I21412) for 10-15 minutes at RT. Counterstaining allowed for correct identification of different nociceptor subpopulations.

The following protocol was used for cell collection, reverse transcription and quantitative real-time PCR. In brief, samples (20 cells per subpopulation and condition) were manually picked using a fire polished pipette with a tip diameter of ~25 µm.

Pipettes were pulled (Flaming-Brown puller, Sutter Instruments, USA) from borosilicate glass capillaries (BF150-86-10, Sutter Instruments, USA) and filled with 2 µl of picking buffer consisting of 1 µL recombinant RNase inhibitor (Takara Bio Europe, product number: 2313A) in 49 µL PBS. After aspirating 20 cells per sample (± NGF: CHRNA3$^+$, IB4$^-$, IB4$^+$, Aδ-nociceptors or CFA/Saline: CHRNA3-EGFP$^+$/FB$^+$, IB4$^-$/FB$^+$), the pipette was immediately shock-frozen in liquid Nitrogen. Subsequently, the cells were expelled into an RNAse-free tube filled with 8 µL of picking buffer and directly stored at -80 °C until further processing. For each gene, a total of 4 to 9 samples were collected, with one sample per subpopulation and condition per mouse. Identification and picking of cell populations were performed with a Zeiss Axio Observer A1 microscope (Carl Zeiss) using a 20x magnification and appropriate filter cubes. Adhering to the provided instructions of the manufacturer, cell lysis and reverse transcription with cDNA synthesis were performed directly on the sample using a thermal cycler (MJ Mini, BIO RAD) and the Power SYBR® Green Cells-to-CT™ Kit (Thermo Fisher Scientific, product number: 4402953). For qPCR reactions, the FastStart Essential DNA Green Master (Roche, product number: 06402712001) was used following the manufacturer's guidelines. Each reaction (with a total reaction volume of 20 µl) contained 4 µl of the synthesized cDNA as template, 10 µl of SYBR Green PCR Master Mix, 4 µl of nuclease-free H_2O, and the primer pair specific for the gene of interest including respective forward (FW) and reverse (RV) primers (1 µl each of a 5 µM dilution, with a final concentration of 250nM) as presented in **Table 14**.

Table | 14 Primer pairs used in qPCR experiments

Product	Primer	Sequence (5' - 3')
GAPDH	FORWARD	GCATGGCCTTCCGTGTTC
	REVERSE	GTAGCCCAAGATGCCCTTCA
TMEM100	FORWARD	GAAAAACCCCAAGAGGGAAG
	REVERSE	ATGGAACCATGGGAATTGAA

qPCR reactions were run in a LightCycler 96 (Roche) using the following thermal cycler profile. Initial preincubation at 95 °C for 10 minutes was followed by 40 PCR

cycles. Each cycle consisted of a denaturing step at 95 °C for 10 seconds, an annealing step at 60 °C for 10 seconds, and an extension step at 72 °C for 10 seconds.

To examine TMEM100 expression in different nociceptor subclasses cultured in the absence and presence of NGF, mean ± SEM expression levels of TMEM100 normalized to the expression levels of the housekeeping gene GAPDH were compared. Additionally, to analyze CFA-induced changes in mRNA expression levels of TMEM100 in CHRNA3-EGFP$^+$/FB$^+$ and IB4$^-$/FB$^+$ neurons, these levels were compared to the levels of contralateral control neurons using the ΔΔCt method.

2.2.8 RNA sequencing

To assess gene expression changes in CHRNA3-EGFP$^+$ upon NGF treatment, RNA sequencing (RNAseq) was performed using CHRNA3-EGFP$^+$ cell samples (20 cells per sample and condition) of 3 WT mice that were processed, cultured (± NGF for 24h) and collected as described above (see 2.2.7 Reverse transcription and quantitative real-time PCR). Cell lysates were processed to reverse transcription according to the SmartSeq2 protocol published by Picelli and colleagues (Picelli et al. 2014) and library preparation was completed with the Nextera DNA Sample Preparation kit (Illumina) following the manufacturer's recommendations. The Illumina HiSeq 2000 sequencer system was used to sequence the prepared libraries. To analyze the data, the sequencing reads were mapped to the GRCm38 mouse reference genome, and differential gene expression analysis was conducted using the BioJupies platform with default parameters. Biojupies is an open access web-based application server for analyses of RNAseq data (Torre et al. 2018). Next generation RNA-sequencing raw data (FASTQ files) have been stored in the Gene Expression Omnibus (GEO) data repository under accession number GSE199580 and are publicly available since the 1st of December 2022.

2.2.9 Electrophysiology

2.2.9.1 Patch clamp recordings

Whole cell patch clamp recordings were conducted on retrogradely FB-labeled sensory neurons innervating the knee (as described in 2.2.3 Retrograde labeling). To differentiate between MIAs and other peptidergic nociceptors, two distinct subpopulations were targeted for recordings: CHRNA3-EGFP$^+$/FB$^+$ neurons and small (< 30 µm) IB4$^-$/FB$^+$ neurons. These two subpopulations comprise the majority of nociceptive knee joint afferents. Cells from both wildtype (WT) and TMEM100 knockout (TMEM100KO) animals were evaluated following CFA and control treatment. To accomplish this, seven days after retrograde tracing of the DRG from both knees (see 2.2.3 Retrograde labeling), a second injection into the left knee was performed using either CFA or Saline. Three days after this second injection, at the time of maximum CFA-induced pain behavior, the animals were euthanized. L3 and L4 DRG from the ipsilateral (CFA/Saline) and contralateral side were collected separately and cultured for 16-24 hours (see 2.2.6.1 Primary DRG cell culture) until they were used for whole cell patch clamp recordings. To this end, the mechano-clamp technique was used as previously described (Lechner and Lewin 2009). In brief, the whole cell patch clamp recordings were performed at RT (20-24 °C) using patch pipettes with a tip resistance of 2-4 MΩ. The patch pipettes were pulled from borosilicate glass capillaries using a Flaming-Brown puller (Sutter Instruments, Novato, CA, USA) and were, then, fire polished using a Microforge CPM-2 (ALA Scientific Instruments, Inc, USA). For the recordings, the patch pipettes were filled with a solution containing 110 mM KCl, 10 mM NaCl, 1 mM $MgCl_2$, 1 mM EGTA (ethylene glycol-bis(β-aminoethyl ether)-N,N,N′,N′-tetraacetic acid), 10 mM HEPES, 2 mM guanosine 5’-triphosphate (GTP), and 2 mM adenosine 5’-triphosphate (ATP), adjusted to pH 7.3 with KOH. The bathing solution contained 140 mM NaCl, 4 mM KCl, 2 mM $CaCl_2$, 1 mM $MgCl_2$, 4 mM glucose, and 10 mM HEPES, adjusted to pH 7.4 with NaOH. All recordings were performed using an EPC-10 amplifier (HEKA, Lambrecht, Germany) in combination with Patchmaster© and Fitmaster© software (HEKA). The auto function of Patchmaster was used to compensate pipette and membrane capacitance. To minimize voltage errors series resistance was compensated by 70 %.

Mechanically activated currents were measured using the whole cell patch clamp configuration. Neurons were clamped to a holding potential of -60 mV and subjected to a series of mechanical stimuli in 0.8 µm increments. These stimuli were applied using a fire-polished glass pipette with a tip diameter of 2-3 µm, positioned at a 45° angle to the surface of the dish. The pipette was moved with a velocity of 3 µm/ms by a piezo-based micromanipulator known as nanomotor© (MM3A, Kleindiek Nanotechnik, Reutlingen, Germany). The resulting whole cell currents were recorded using a sampling frequency of 200 kHz. To analyze the mechanotransduction current inactivation a fitting single exponential function ($C1 + C2 * \exp(-(t - t0) / \tau_{inact})$) was used, where C1 and C2 are constants, t represents time, and τ_{inact} is the inactivation time constant.

2.2.9.2 Ex-vivo skin-nerve preparations

To investigate peripheral sensitization, the mechanosensitivity of C-fiber and Aδ-fiber nociceptors in the tibial nerve was directly measured by recording mechanically evoked action potentials from individual nerve fibers in an ex-vivo skin-nerve preparation. For this purpose, both WT and TMEM100KO mice were sacrificed 3 days after CFA/saline injection by euthanizing them in a CO_2-filled chamber for 2–4 minutes followed by cervical dislocation. Following dissection, the glabrous skin of the hind limb was placed with the corium side up in a heated (32 °C) organ bath chamber perfused with synthetic interstitial fluid (SIF buffer). The SIF buffer consists of 108 mM NaCl, 3.5 mM KCl, 0.7 mM $MgSO_4$, 26 mM $NaHCO_3$, 1.7 mM NaH_2PO_4, 1.5 mM $CaCl_2$, 9.5 mM sodium gluconate, 5.5 mM glucose and 7.5 mM sucrose adjusted to a pH of 7.4. To allow for fiber teasing and single-unit recording the tibial nerve was attached in an adjacent chamber. According to the previously described protocol (Arcourt et al. 2017) single units were isolated using a mechanical search stimulus applied with a glass rod and then classified based on their conduction velocity, von Frey hair thresholds, and adaptation properties to suprathreshold stimuli. To apply mechanical ramp-and-hold stimuli, a cylindrical metal rod with a diameter of 1 mm driven by a nanomotor® (MM3A-LS, Kleindiek Nanotechnik GmbH, Germany) coupled to a force measurement device (FMS-LS, Kleindiek Nanotechnik GmbH, Germany) was used. The mechanical thresholds of single units were determined by applying von Frey filaments (Aesthesio® Precision Tactile Sensory Evaluators) to the most sensitive spot of their receptive fields. The mechanical threshold was defined as the force exerted by the weakest von Frey

filament that elicited an action potential. The raw electrophysiological data were amplified using an AC coupled differential amplifier (Neurolog NL104 AC) and filtered with a notch filter (Neurolog NL125-6). Then, data were converted into a digital signal with a PowerLab SP4 (ADInstruments, New Zealand) and recorded at a sampling frequency of 20 kHz using LabChart 7.1 (ADInstruments, New Zealand).

2.2.9.3 Calcium Imaging

To assess the responsiveness of FB-labelled neurons to the TRPA1 agonist allylisothiocyanate (AITC; Sigma-Aldrich, USA), Ca^{2+}-imaging was performed using Calbryte™ 590 (Calbryte™ 590 AM; AAT Bioquest, USA) as fluorescent indicator for the measurement of intracellular calcium. Briefly, CHRNA3-EGFP^{+}/FB^{+} neurons and small (<30µm) IB4^{-}/FB^{+} neurons from both WT and TMEM100KO mice after control and CFA treatment were collected as previously described (see 2.2.9.1 Patch clamp recordings). The cells were then counterstained with Alexa Fluor™ -647 conjugated IB4 (2.5 µg/ml, Isolectin GS-IB4 from Griffonia simplicifolia, Alexa Fluor™ 647 Conjugate, Invitrogen™/Thermo Fisher Scientific, USA, product number: I32450) for 10-15 min at RT, washed with extracellular buffer (ECB: 140 mM NaCl, 4 mM KCl, 2 mM CaCl2, 1 mM MgCl2, 4 mM glucose, 10 mM HEPES and was adjusted to pH 7.4 with NaOH) and finally incubated with 5 µM of Calbryte™ 590 (5 µM diluted in ECB from a 5 mM stock solution in DMSO) for 30 min at 37 °C. Next, coverslips with loaded cells were washed with ECB, placed into a perfusion chamber and superfused with ECB. To provide a constant laminar flow during superfusion, an 8-channel valve controlled gravity-driven perfusion system (VC3-8xG, ALA Scientific Instruments, USA) and a peristaltic pump were used. Prompt release of ECB and chemical agents into the superfusion chamber was enabled by a manifold system with 8 inlet ports fitted to a single silicon tube bath inlet whose end was positioned at the outer edge of the coverslip without interfering the visual field. For each input line identical tubes were used. This setup provided minimal dead volume and air bubbles in the lines. All calcium imaging experiments were completed at RT (23 ± 1 °C). During the experiment, intracellular calcium changes were monitored and analyzed using fluorescence images. The images were captured at a frequency of 2 Hz using a Hamamatsu ORCO-Flash4.0 camera, which was attached to an inverted Zeiss Axio Observer A1 microscope. To illuminate the samples, a LED light source (CoolLED pE-340fura) was used. The detection and analysis of intracellular calcium changes were carried out with

ZEN 2 pro software (Carl Zeiss Microscopy GmbH). During the imaging process, the following protocol was applied:

1) Baseline (0-30 seconds): baseline measurement with ECB for 30 seconds
2) AITC (31-90 seconds): exposure to AITC (10 µM) for 60 seconds
3) Washout 1 (91-360 seconds): washout with ECB for 270 seconds
4) KCl (361-390 seconds): depolarization with 100 mM KCl for 30 seconds
5) Washout 2 (391-420 seconds): final washout with ECB for 30 seconds

Depolarization of cells using KCl was performed in order to identify viable neurons in contrast to non-neuronal cells or non-functioning neurons. Neuronal viability was determined based on a > 20 % increase in fluorescence intensity compared to the mean intensity recorded 20 seconds before the application of KCl (330-350 seconds).

The analysis process involved the extraction of mean intensity values after background subtraction from two types of neurons: CHRNA3-EGFP$^+$/FB$^+$ neurons and IB4$^-$/FB$^+$ neurons. This was accomplished by manually drawing the regions of interests (ROIs), including a background ROI, using the ZEN 2 pro software (Carl Zeiss Microscopy GmbH). Subsequently, the extracted mean intensity values were transferred into a custom-made Microsoft Excel® template to calculate the proportion of neurons responding to AITC under different conditions (CFA/saline; WT/TMEM100KO). Fluorescence data are represented as $\Delta F/F0$, with $\Delta F = F1 – F0$. F1 denotes the mean intensity of the image, and F0 represents the mean intensity of the baseline fluorescence observed from 0 to 20 seconds. Neurons that exhibited an increase in fluorescence intensity greater than 5 % from the baseline to the application of AITC were categorized as AITC responders. In order to ensure accurate analysis of viable target neurons, cells that did not cross the threshold defined by the KCl application were excluded from the analysis.

2.2.10 Statistical analyses

Unless specified otherwise, all data are presented as means ± SEM. Statistical analyses were conducted using Microsoft® Excel® and Prism 9.0 (Graphpad). The data distribution was assessed systematically using the D'Agostino-Pearson test, and parametric or non-parametric tests were selected accordingly. The display items or corresponding figure legends provide detailed information about the specific statistical tests employed, including the P-values and the number of independent biological replicates. On the graphs, symbols (* or #) indicate the standard P-value ranges: *, $P < 0.05$; **, $P < 0.01$; ***, $P < 0.001$, and ns (not significant), $P > 0.05$.

3. RESULTS

3.1 The transcriptomic signature of MIAs

It has been previously demonstrated that cultured CHRNA3-EGFP$^+$ MIAs gain responsiveness to mechanical stimuli due to the presence of the inflammatory mediator NGF (Prato et al. 2017). Prato and colleagues have illustrated that CHRNA3-EGFP$^+$ MIAs display increased mechanotransduction currents following a 24-hour exposure to NGF Moreover, they have revealed that this NGF-induced mechanosensitivity is mediated by the mechanically gated ion channel PIEZO2 and that this sensitization process necessitates de novo gene transcription of a previously unidentified protein. Thus, in the current study I performed a comparative analysis between the transcriptomes of CHRNA3-EGFP$^+$ neurons cultured without or with NGF (50 ng/ml) for 24 hours in order to pinpoint the proteins necessary for this NGF-triggered acquisition of mechanosensitivity. To achieve this, CHRNA3-EGFP$^+$ neurons were manually selected from DRG cultures with a patch-pipette and then subjected to transcriptome analysis using paired-end RNA sequencing (**Figure 3**).

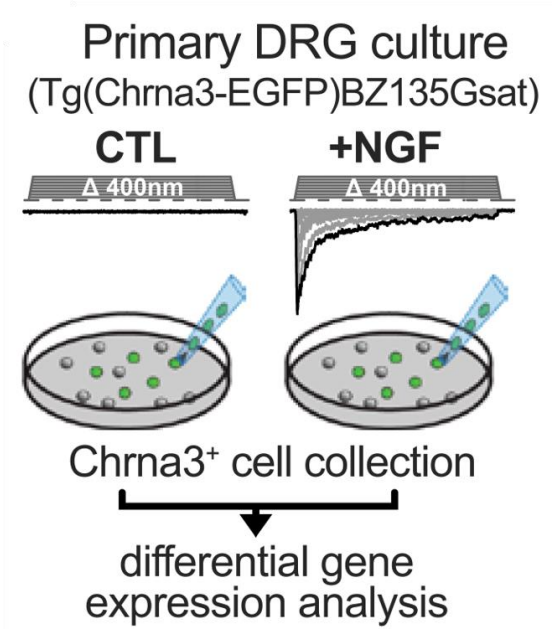

Figure 3 | Experimental setup for RNA sequencing and qPCR analyses
Schematic illustration depicting the experimental design of the RNAseq and qPCR experiments. Primary dorsal root ganglia (DRG) neurons from CHRNA3-EGFP mice (Tg(Chrna3-EGFP)BZ135Gsat) were cultured in the presence (+NGF) and absence (CTL) of nerve growth factor (NGF) for 24 hours.

CHRNA3-EGFP positive neurons (CHRNA3⁺), which developed mechanosensitivity following NGF exposure (top traces) in inflammatory conditions, as well as those from control (CTL) conditions, were aspirated using a patch-pipette. These collected neurons were subsequently processed for RNAseq or qPCR analyses. Adapted from Nees et al. 2023.

The analysis demonstrated that CHRNA3-EGFP⁺ MIAs possess a distinctive transcriptional signature characterized by the co-expression of Ntrk1, Calca, Tac1, TRPV1, Nos1, Ly6e, and Htr3a, while lacking Cyp2j12, Prrx2, and Etv1 (**Figure 4**). Notably, this signature had previously been observed in a subset of peptidergic nociceptors designated as PSPEP2 neurons in a large-scale single-cell RNA sequencing study (Zeisel et al. 2018).

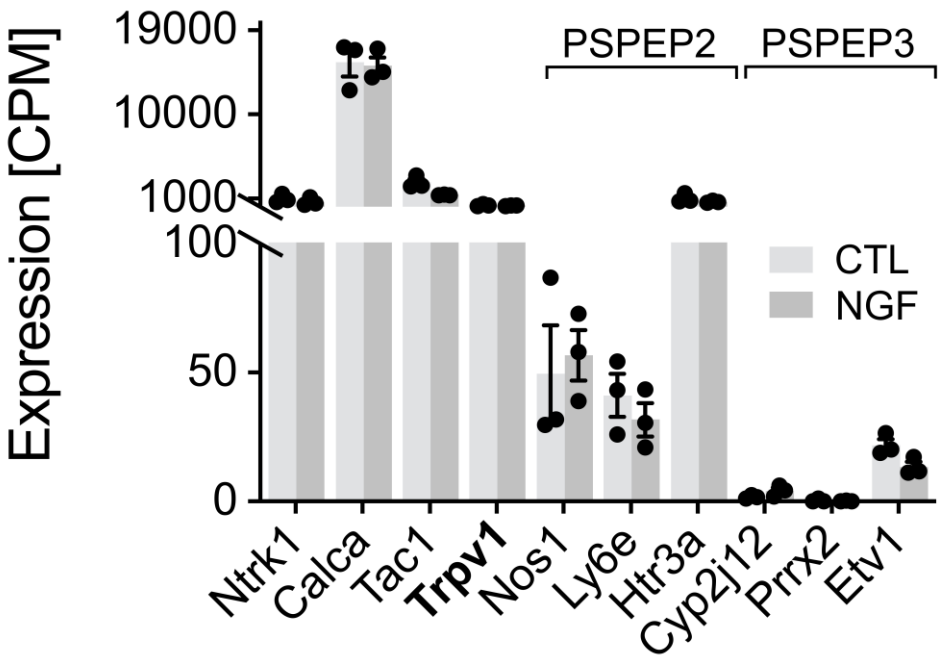

Figure 4 | Transcriptional signature of CHRNA3-EGFP⁺ neurons

Analysis of expression levels (counts per million, CPM) of markers associated with peptidergic nociceptor subclasses in CHRNA3-EGFP-expressing neurons. The transcriptional profile of these neurons is highlighted by the co-expression of Ntrk1, Calca, Tac1, TRPV1, Nos1, Ly6e, and Htr3a. In contrast, they do not express Cyp2j12, Prrx2, and Etv1 (markers of the PSPEP3 type), implying their affiliation with the PSPEP2 subtype based on the Zeisel nomenclature (Zeisel et al. 2018). Treatment with nerve growth factor (NGF) showed no discernible effect on marker expression in comparison to control (CTL) settings. Ntrk1, neurotrophic receptor tyrosine kinase 1; Calca, calcitonin related polypeptide alpha; Tac1, tachykinin precursor 1; Trpv1, transient receptor potential cation channel, subfamily V, member 1; Nos1, nitric oxide synthase 1; Ly6e, lymphocyte antigen 6 family member E; Htr3a, 5-hydroxytryptamine (serotonin) receptor 3A, Cyp2j12, cytochrome P450, family 2, subfamily j, polypeptide 12; Prrx2, paired related homeobox 2; Etv1, ets variant 1. Adapted from Nees et al. 2023.

Importantly, the analysis revealed that the mechanosensitive ion channel PIEZO2, which is crucial for mechanotransduction in CHRNA3-EGFP⁺ neurons (Prato et al. 2017), is not upregulated by NGF. Similarly, there were no NGF-induced expression changes of other ion channels that have been reported to be involved in mediating mechanosensitivity such as PIEZO1, Tmem87a, Tmem120a, Tmc1-3, TRPC3, TRPC6, TRPV4 and TRPA1. Moreover, none of the established PIEZO2 regulators such as Anxa6, Atp2a2, Cdh1, Mtmr2, Nedd4-2, Pcnt, Tmem150c and Stoml3 (Anderson et al. 2018; Huo et al. 2021; Narayanan et al. 2018; Narayanan et al. 2016; Poole et al. 2014; Raouf et al. 2018; Zhang et al. 2017), showed altered expression levels post NGF-exposure (**Figure 5**). These findings suggest that, aside from PIEZO2, neither other recognized mechanotransducers nor PIEZO2 regulators contribute to the NGF-induced onset of mechanosensitivity in CHRNA3-EGFP⁺ neurons.

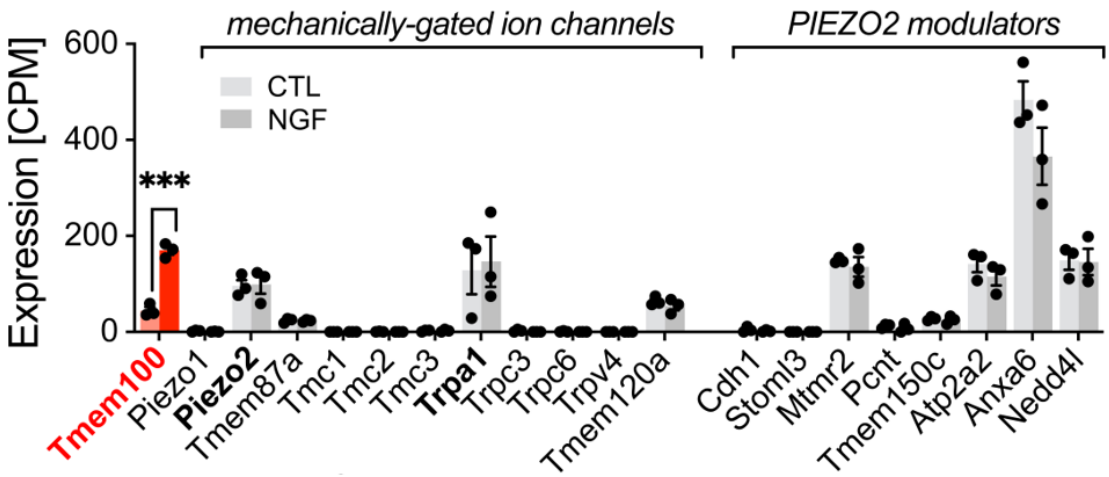

Figure 5 | Expression levels of mechanically-gated ion channels and PIEZO2 modulators
Comparative RNA sequencing analysis of expression levels (counts per million, CPM) for mechanosensitive ion channels and PIEZO2 modulators in CHRNA3-EGFP⁺ neurons. Expression profiles from cultures treated with NGF for 24 hours are juxtaposed with untreated controls (CTL). The statistical significance was determined using a two-sided Student's t-test (***, P = 4.598E-5). Data was compiled from three biologically independent samples, each consisting of 20 cells, and extracted from three separate mice. Adapted from Nees et al. 2023.

Intriguingly, the RNAseq analysis unveiled the upregulation of the transmembrane protein TMEM100 in response to NGF (fold-change=3.805, P=4.12E-5, N=3 samples per condition, as indicated in **Figure 5** and **Figure 6**).

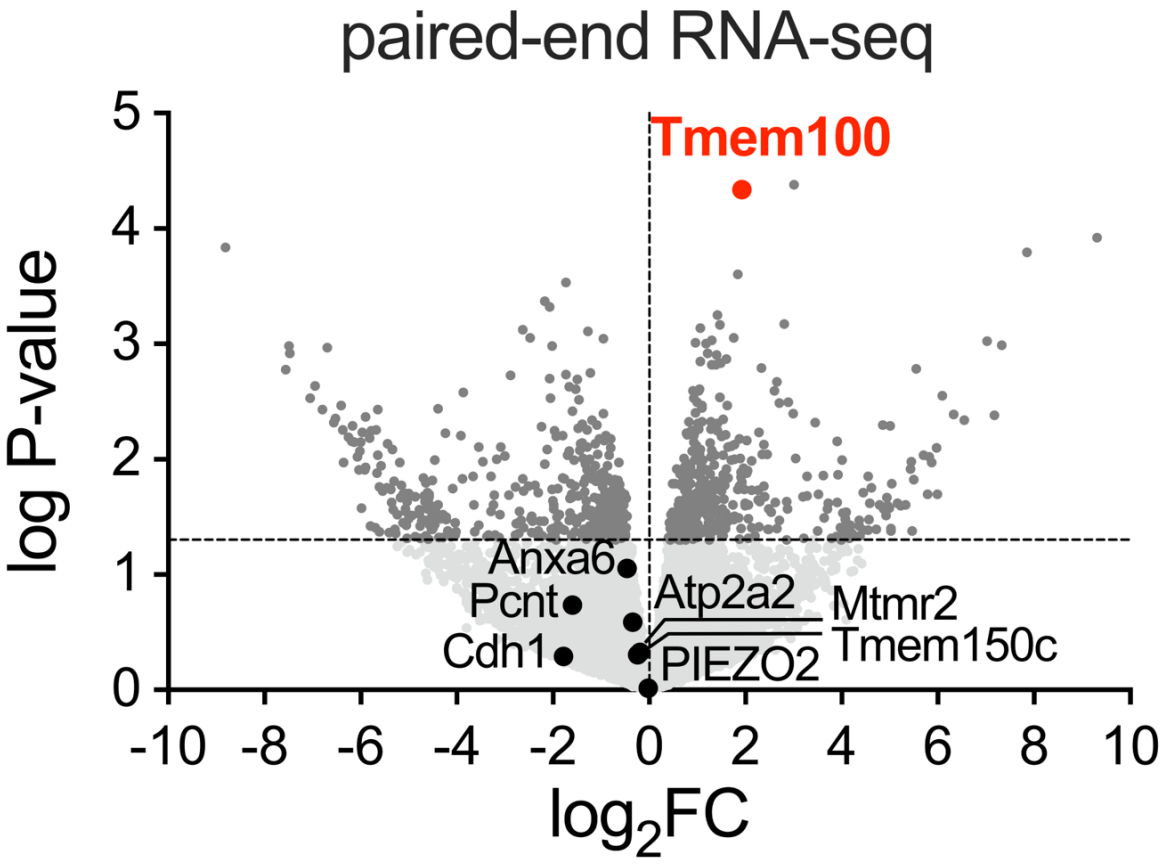

Figure 6 | RNA sequencing analysis: Volcano plot

Volcano plot illustrating differential gene expression after 24-hour NGF treatment, represented by $\log_2$ fold-change ($\log_2$FC) versus log P-value from paired-end RNA sequencing analysis. This analysis encompasses data from three biologically independent samples, with 20 cells per sample, derived from three distinct mice (two-sided Student's t-test). The plot notably underscores the significant upregulation of the transmembrane protein TMEM100 post-NGF administration, exhibiting a fold-change of 3.805 (P = 4.12E-5). Adapted from Nees et al. 2023.

This finding garnered attention since TMEM100 had been previously demonstrated to amplify the activity of TRPA1 (Weng et al. 2015), an ion channel crucial for pain signaling (Talavera et al. 2020). In brief, Weng and colleagues discovered that

TMEM100 establishes a complex with the significant pain channels TRPA1 and TRPV1 in DRG neurons, where TRPA1's activity is restrained by TRPV1. TMEM100 perturbs the interaction between TRPA1 and TRPV1, thereby selectively potentiating TRPA1's activity by relieving its inhibition caused by TRPV1. Interestingly, both TRPA1 and TRPV1 are also significantly expressed in CHRNA3-EGFP$^+$ neurons, irrespective of NGF exposure, as demonstrated in the RNAseq analysis presented in this thesis (see **Figure 4** and **Figure 5**). To verify the heightened levels of TMEM100 expression induced by NGF in cultured CHRNA3-EGFP$^+$ MIAs, and to determine if similar changes in TMEM100 occur in other significant nociceptor subgroups upon NGF stimulation, qPCR experiments were conducted. Significantly, the qPCR outcomes not only validated the NGF-triggered increase in TMEM100 expression within cultured CHRNA3-EGFP$^+$ MIAs but also demonstrated that there were no notable changes in TMEM100 expression across other major nociceptor subpopulations subsequent to NGF treatment (as presented in **Figure 7**).

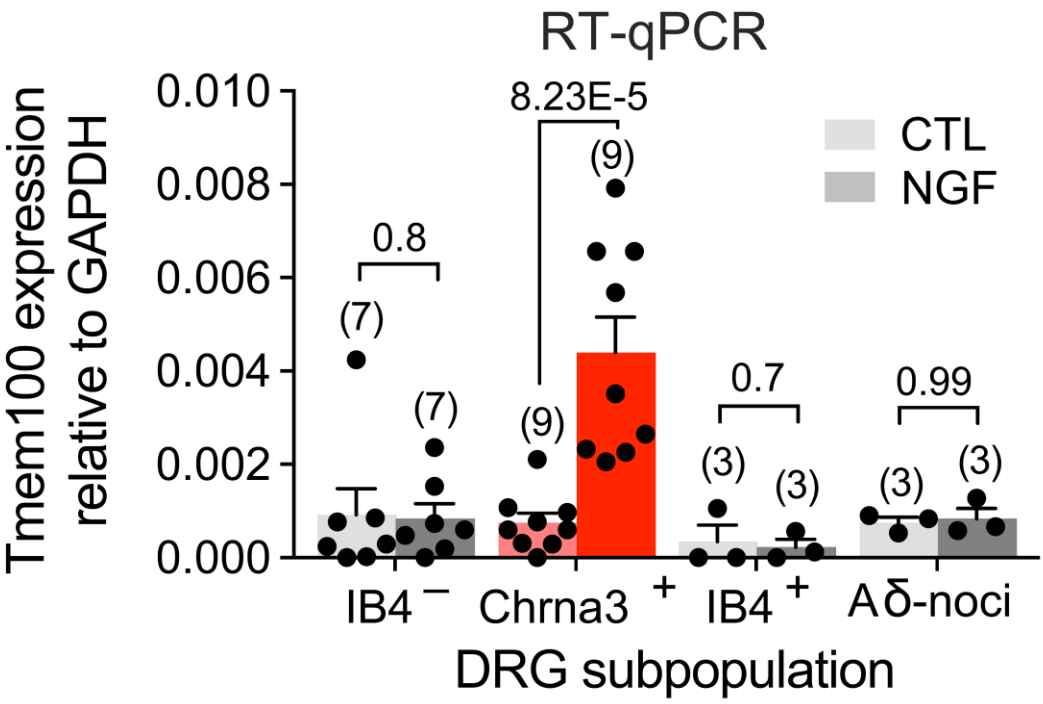

Figure 7 | TMEM100 expression across key nociceptor subpopulations

RT-qPCR results displaying the mean ± SEM expression levels of TMEM100, standardized to the housekeeping gene GAPDH, across major nociceptor subclasses. Cultures were either untreated (CTL) or exposed to nerve growth factor (NGF) for 24 hours. To distinguish between peptidergic C-fiber nociceptors, non-peptidergic C-fiber nociceptors, and Aδ-fiber nociceptors during sample collection,

cultures were derived from Tg(Npy2r-cre)SM19Gsat/Mmucd x B6;129S-Gt(ROSA)26Sortm32(CAG-COP4*H134R/EYFP)Hze/J (Npy2rCre;ChR2-EYFP) mice. In these cultures, Aδ-fiber nociceptors express EYFP. Furthermore, Alex-Fluor-568 conjugated Isolectin B4 (IB4) was used to selectively label non-peptidergic C-fiber nociceptors. Sample counts for each subpopulation are denoted in brackets above the corresponding bars, and individual data points are represented as black dots on the graph. Statistical analysis was conducted using a two-sided Mann-Whitney test, with P-values indicated above the bars. Adapted from Nees et al. 2023.

3.2 TMEM100 induces mechanosensitivity in MIAs

In light of the RNAseq findings suggesting a potential role for TMEM100 in the acquisition of mechanosensitivity in MIAs, CHRNA3-EGFP$^+$ cells from primary DRG cultures were transfected with a plasmid carrying TMEM100-IRES-dsRed-express2. This allowed for the traceable overexpression of TMEM100 in native MIAs (**Figure 8a**). To discern any TMEM100-attributed functional changes, the mechanotransduction currents of these transfected cells were juxtaposed with those of untransfected CHRNA3-EGFP$^+$ neurons. It is crucial to mention that neither group received NGF treatment, ensuring that observed differences stemmed exclusively from TMEM100 expression and not from in-vitro inflammatory conditions. To achieve this, the mechano-clamp technique (Lewis and Grandl 2021) was employed, which is an electrophysiological approach used to record transmembrane currents from cultured DRG neurons. This technique operates in the whole-cell configuration mode of the patch-clamp methodology, while the cell soma is mechanically stimulated using a fire-polished patch-pipette (**Figure 8b**).

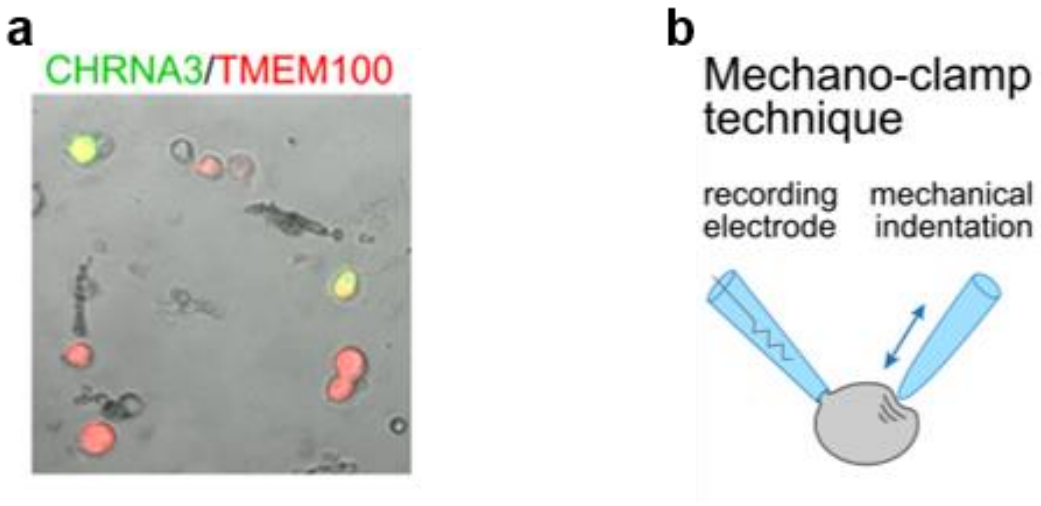

Figure 8 | Mechano-clamp technique in transfected DRG neurons
(**a**) Microscopic view of cultured DRG neurons from CHRNA3-EGFP mice, transfected with the TMEM100-IRES-dsRed-express2 plasmid (red). (**b**) Schematic representation illustrating the mechano-clamp configuration employed in the patch clamp technique. Adapted from Nees et al. 2023.

In line with previous findings (Prato et al. 2017), only a minor fraction of untransfected CHRNA3-EGFP^{+} cells (3 out of 14) displayed a response to mechanical stimulation, eliciting small inward currents (**Figure 9b**). Notably, in contrast, approximately 61 % of CHRNA3-EGFP^{+} neurons (19 out of 31) that were transfected with TMEM100 demonstrated strong mechanotransduction currents (**Figure 9b**), which were markedly larger than the occasional small currents observed in control cells (**Figure 9c**).

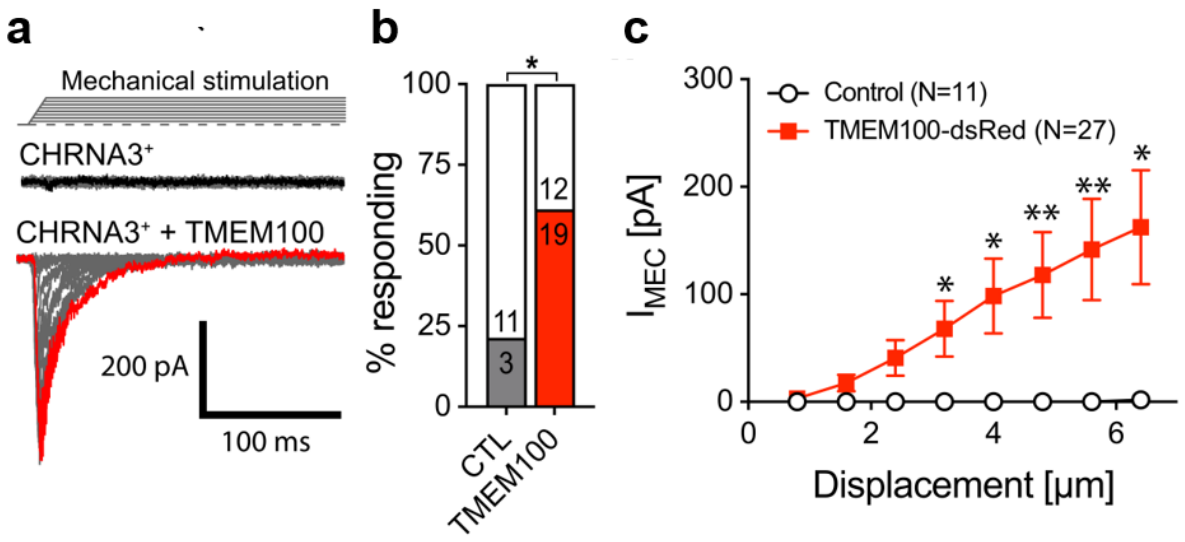

Figure 9 | Influence of TMEM100 on mechanosensitivity in MIAs

(**a**) Representative traces illustrating mechanically-evoked currents in CHRNA3-EGFP⁺ control cells (top) contrasted with those in TMEM100-dsRed transfected CHRNA3-EGFP⁺ cells (bottom). (**b**) Bar graph depicting the percentage of mechanically-responsive cells in both control (CTL) and TMEM100-expressing groups. The comparison of proportions was conducted using Fisher's exact test (*, P=0.023). (**c**) The graph displays the mean ± SEM of peak amplitudes of mechanically-evoked currents, plotted against membrane displacement. Control cells are represented with white circles, while TMEM100 transfected cells are indicated with red squares. Differences in current amplitudes were assessed using multiple Mann-Whitney tests (*, P<0.05; **, P<0.01). The sample sizes (N-numbers) in this section differ from those in (b) due to some recordings terminating prematurely before maximal mechanical stimulation was achieved. pA, picoampere; I_{MEC}, mechanotransduction currents. Adapted from Nees et al. 2023.

To delve deeper into the mechanistic interplay between TMEM100 and PIEZO2, a heterologous expression system was employed. This approach aimed to discern whether TMEM100 inherently exhibits mechanotransduction capabilities or whether it predominantly acts as a modulator of PIEZO2 function. In pursuit of this, HEK293 cells were transfected with either TMEM100 alone, PIEZO2 alone, or a combination of TMEM100 and PIEZO2. The respective constructs were transfected into HEK293 cells using the calcium phosphate method. The mechanosensitivity of the transfected cells was evaluated 48 hours post-transfection utilizing the mechano-clamp technique. Notably, TMEM100 expression in HEK293 cells did not result in any detectable mechanotransduction currents. In contrast, PIEZO2-transfected cells acquire pronounced mechanosensitivity, exhibiting robust mechanotransduction currents.

Importantly, when TMEM100 was co-expressed with PIEZO2 it did not exert any regulatory effect on PIEZO2-mediated currents in these cells as depicted in **Figure 10**.

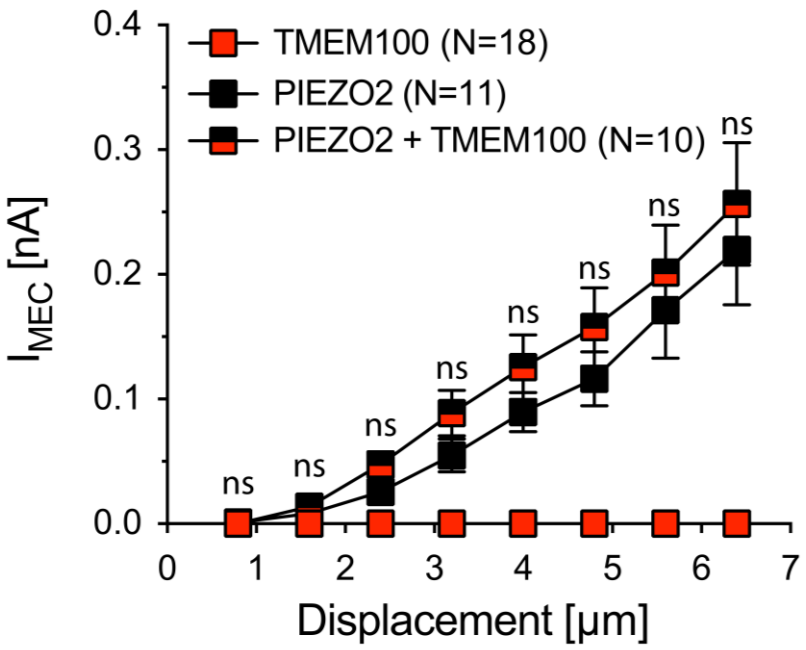

Figure 10 | Mechanosensitivity of TMEM100 and PIEZO2 in HEK293 Cells

To probe the mechanosensitivity of TMEM100 and PIEZO2 – both in conjunction (PIEZO2 + TMEM100) and in the absence of TMEM100 (PIEZO2) – the respective constructs were transfected into HEK293 cells. The graph depicts the mean ± SEM peak amplitudes of mechanically-evoked currents, plotted against membrane displacement (mechano-clamp technique). Symbols used are as follows: TMEM100, red square (N=18); PIEZO2, black square (N=11); combined PIEZO2+TMEM100, black/red square (N=10). Adapted from Nees et al. 2023.

These findings suggest that TMEM100 does not function as a mechanochannel in its own right, nor does it serve as a modulator of PIEZO2. Instead, its unique role seems solely tied to activating PIEZO2 within the specific cellular context of CHRNA3-EGFP^{+} MIAs.

In summary, the in-vitro results demonstrated that NGF selectively upregulates TMEM100 in MIAs, thereby inducing mechanosensitivity. This critical role of TMEM100 is further supported by findings where its overexpression alone can activate MIAs even in the absence of experimental inflammation.

3.3 Behavioral characterization of a mouse model of inflammatory knee pain

Building upon the promising in-vitro results, the next step was to establish a suitable mouse model to validate the in-vitro findings and study silent nociceptors and TMEM100 in vivo. To this end, an inflammatory pain model that involves NGF-upregulation was needed. Thus, I chose the CFA-induced knee joint monoarthritis model for the following reasons. Firstly, silent nociceptors were initially described and are abundantly present in rodent knee joints (Prato et al. 2017; Schaible and Schmidt 1988). In fact, MIAs have been identified as comprising approximately 50 % of all articular nociceptive afferents (Prato et al. 2017; Schaible and Schmidt 1988). Secondly, it is widely accepted that CFA-induced inflammatory pain involves NGF signaling (Denk et al. 2017; Djouhri et al. 2001; Ghilardi et al. 2012; Woolf et al. 1994). The levels of NGF, which trigger TMEM100 upregulation, are markedly elevated in the synovial fluid in rodent models of inflammatory knee joint pain and osteoarthritis patients (Denk et al. 2017; Montagnoli et al. 2017). Thirdly, there is compelling evidence indicating that anti-NGF antibodies have the potential not only to mitigate pain-related behaviors in preclinical models of inflammatory pain but also to alleviate joint pain in individuals with osteoarthritis (Denk et al. 2017; Wise et al. 2021). This suggests that NGF, along with the possibility of MIAs, may have a substantial impact on the onset of knee joint pain.

To begin with, I conducted a immunohistochemical examination to investigate the innervation pattern of silent nociceptors in knee joints. The objective was to confirm the dense innervation previously reported by Prato and colleagues (Prato et al. 2017) and to assess the distribution of silent nociceptors within the knee joint. Consistent with these findings, the analysis revealed that the mouse knee joint is densely innervated by CHRNA3-EGFP^{+} afferents that also express CGRP (**Figure 11a**). It is important to highlight that only those EGFP^{+} fibers co-expressing CGRP qualify as MIAs, whereas CGRP^{-}/EGFP^{+} fibers are sympathetic efferents (Prato et al. 2017). Intriguingly, the highest density of CHRNA3-EGFP^{+} MIAs was observed in the Hoffa's fat pad (0.86 ± 0.29 %), followed by the medial joint capsule (0.3 ± 0.22 %) and lateral meniscus (0.26 ± 0.18 % (**Figure 11c**).

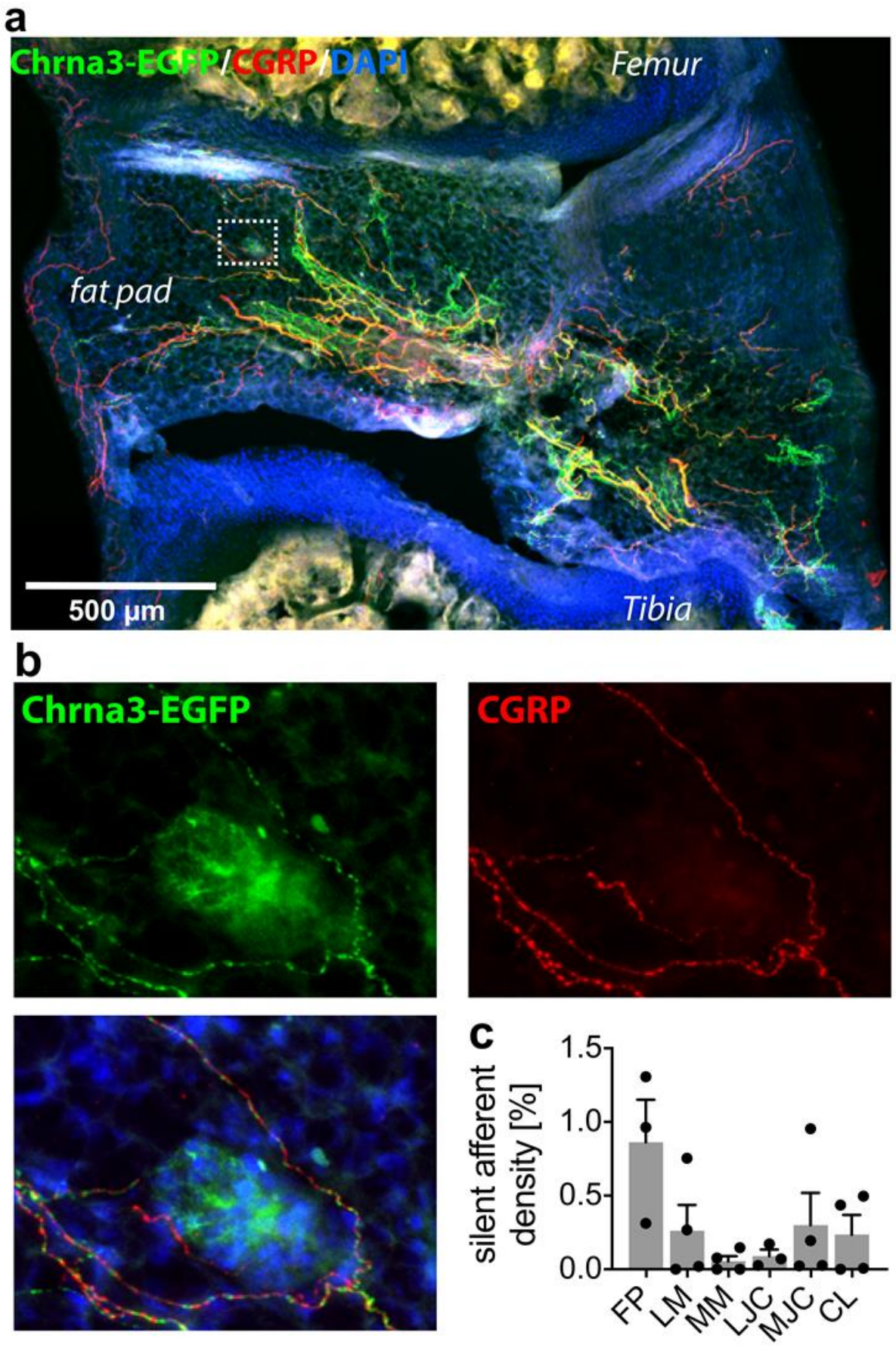
a
Chrna3-EGFP/CGRP/DAPI
Femur
fat pad
500 µm
Tibia
b
Chrna3-EGFP
CGRP
c
silent afferent density [%]
1.5
1.0
0.5
0.0
FP
LM
MM
LJC
MJC
CL

Figure 11 | Immunohistochemical analysis of MIAs innervating the knee joint

(**a**) Representative micrographic image showcasing a coronal knee joint section immunostained for CGRP and EGFP, which amplifies the inherent EGFP signal of CHRNA3^{+} afferents. (**b**) Close-ups of the region marked by the white rectangle in (a), emphasizing co-expression of EGFP and CGRP. (**c**) Bar graph illustrating the quantification of MIA density (EGFP+/CGRP+ fibers) in anatomically defined regions. Bars represent means ± SEM from three different mice. Individual values from each mouse are shown as black dots. FP, Hoffa's fat pad; LM, lateral meniscus; MM, medial meniscus; LJC, lateral joint capsule; MJC, medial joint capsule; CL, cruciate ligament. Adapted from Nees et al. 2023.

To further investigate the role of silent nociceptors and TMEM100 in vivo, I established and characterized a CFA-induced knee joint monoarthritis model to assess its pain behavior. As previously described (Chakrabarti et al. 2018; Krug et al. 2019), intraarticular injections of CFA into the knee joint resulted in significant joint inflammation, which was macroscopically evident through swelling and redness (**Figure 12**). Significant differences in both the anterior-posterior and medio-lateral knee joint diameters were observed in arthritic joints one and five days after CFA injections when compared to knee joints injected with saline (**Figure 12**).

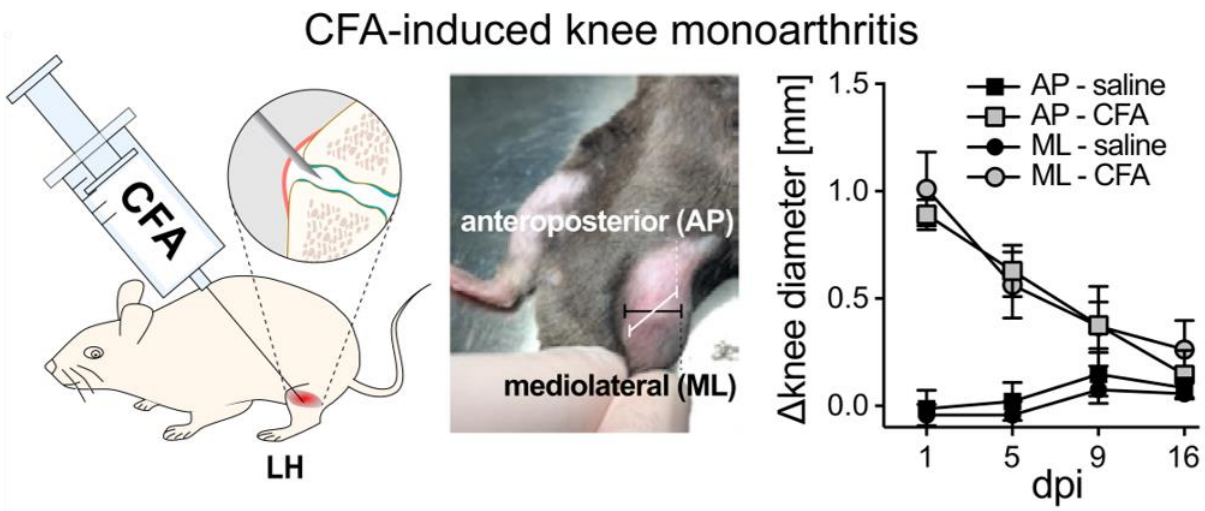

Figure 12 | CFA-induced knee joint monoarthritis

Left: Illustration of the intraarticular injection procedure using Complete Freund's Adjuvant (CFA). **Middle**: Photographic evidence of the inflamed knee, showcasing swelling in both the anteroposterior (AP) and mediolateral (ML) dimensions. **Right**: Timeline (days post-injection, dpi) displaying the progression of inflammation-induced swelling, denoted by alterations in knee diameters relative to baseline measurements. Adapted from Nees et al. 2023.

The subsequent behavioral characterization revealed that CFA-induced knee joint inflammation is associated with severe limping, indicative of primary knee joint pain, as well as mechanical and thermal hypersensitivity in skin regions distant from the knee joint, suggesting secondary hyperalgesia. The assessment of primary knee joint hyperalgesia was conducted using the CatWalk XT gait analysis system **(Figure 13).** The analysis revealed that mice with inflamed knee joints exhibited reduced weight-bearing on the affected leg, as indicated by a decrease in the ratio of the footprint area between the ipsilateral (left) and contralateral (right) hindpaws (before, 1.07 ± 0.03 vs. 3 days post injection (dpi) CFA, 0.57 ± 0.07, N=16, Students paired t-test, P= 2.6E-7), along with a reduction in the swing speed of the inflamed leg (before, 1.041 ± 0.017 vs. 3 dpi CFA, 0.634 ± 0.044, N=16, Students paired t-test, P= 8E-9).

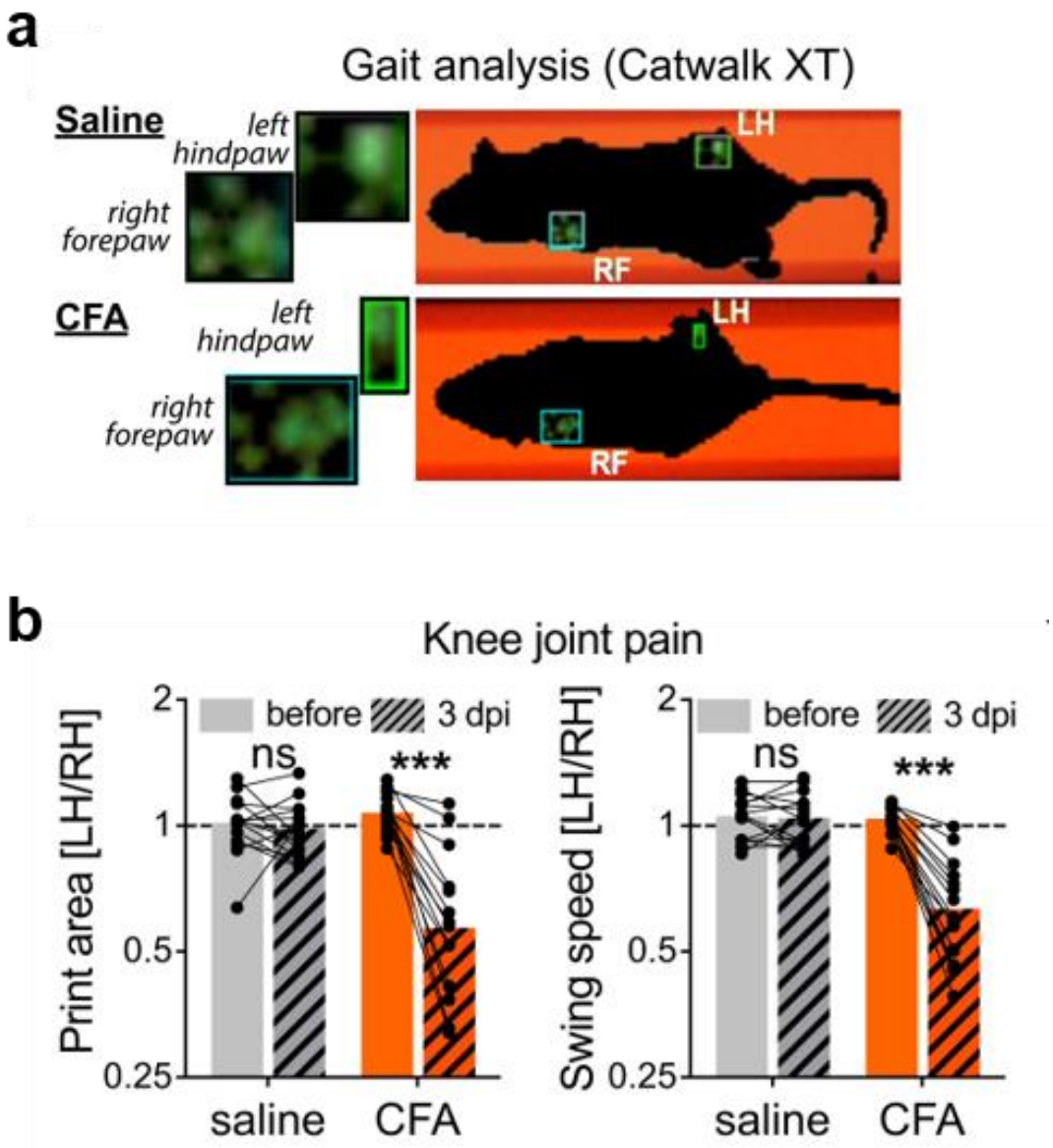

Figure 13 | CFA-induced knee joint monoarthritis: gait analysis

(**a**) Representative frames from CatWalk XT videos displaying saline-treated (top) and CFA-treated (bottom) mice. It is evident that mice treated with CFA exert minimal weight on the left hind paw, resulting in a noticeably smaller footprint. (**b**) Comparative analysis of the footprint area ratio (left/right hind paw; LH/RH) and the leg swing duration ratio (LH/RH). Measurements were taken both prior to treatment (solid bars) and three days post-injection (3 dpi, hatched bars) for saline (gray) and CFA (orange) administrations. Statistical analyses were conducted using a paired Student's t-test (saline N=15, CFA N=16; footprint area for CFA: ***, P = 2.6E-7; swing duration for CFA: ***, P=8E-9). Adapted from Nees et al. 2023.

In light of potential limitations of the CatWalk XT assay in capturing all facets of knee joint pain (see 4.4 Interpretation of the behavioral data), the behavioral assessments were augmented with the LABORAS system (Laboratory Animal Behavior Observation Registration and Analysis System, METRIS b.v). This system is designed to evaluate both overall well-being and pain-related behavioral shifts within a homecage environment. Behavior within the homecage was continuously monitored for 16 hours prior to, and on day 3 following, the administration of both saline and CFA injections. Notably, no statistically significant alterations were detected in behaviors such as grooming, drinking, or immobility, often suggestive of severe pain. However, significant changes were observed in both the total distance traveled and the frequency of rearing. WT mice with CFA-induced knee joint inflammation traveled and reared significantly less compared to those injected with saline (paired Student's t-test; *, P<0.05; saline N=5, CFA N=5) suggesting pain-induced mobility impairments (**Figure 14**).

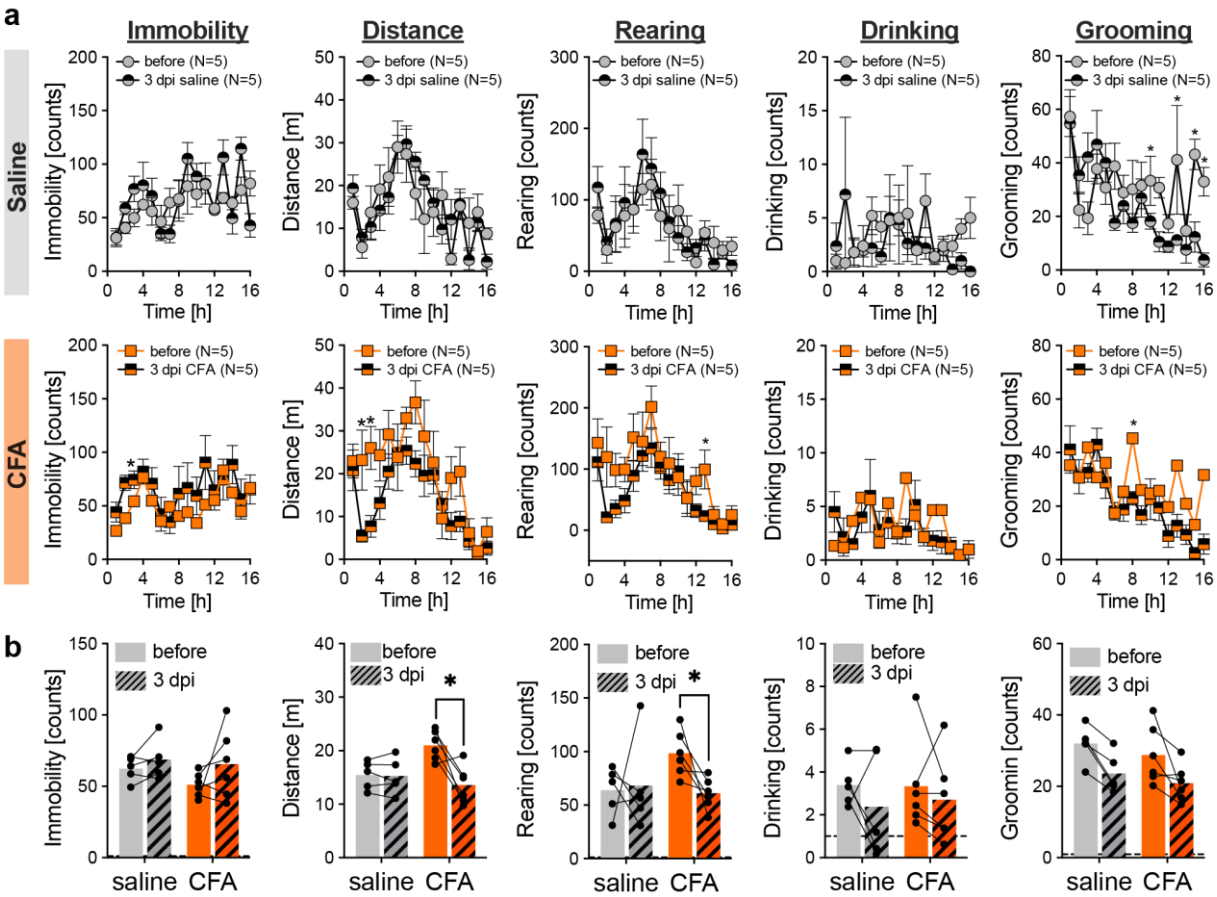

Figure 14 | CFA-induced knee joint monoarthritis: homecage behavior

Animals underwent continuous 16-hour analysis both before and 3 days post-administration of either saline (gray) or CFA (orange). (**a**) Presented data points signify mean ± SEM counts per hour for behaviors: immobility, rearing, drinking, and grooming, along with mean ± SEM distance traveled per hour in meters (m). Upper panels represent the behavior trajectory of the saline group, both before (gray circle) and 3 days post-injection (dpi, gray/black circle). Lower panels depict behavior patterns of the CFA group, pre-injection (orange square) and 3 days post-injection (orange/black square). Behavioral counts at each time point were compared using multiple Mann-Whitney tests (*, P<0.05). N-values are detailed in the graph legends. (**b**) Mean behavioral counts (immobility, rearing, drinking, and grooming) and the distance traveled per test day were compared before (solid bars) and 3 days post-injection (3 dpi, hatched bars) for both saline (gray) and CFA (orange) treated mice using paired Student's t-tests (saline N=5, CFA N=5; *, P<0.05). Adapted from Nees et al. 2023.

Beyond evaluating primary knee joint pain via the CatWalk XT system and gauging overall well-being using the LABORAS platform, I assessed stimulus-evoked pain behaviors. The von Frey and Hargreaves tests were employed to measure mechanical and thermal sensitivity in the ipsilateral hindpaw, respectively, with the aim of uncovering potential signs of secondary hyperalgesia. These tests revealed that CFA-induced monoarthritis significantly diminished the minimal force required to elicit a paw withdrawal reflex in response to punctate mechanical stimuli, as administered to the plantar surface of the hindpaw using von Frey filaments. Specifically, this paw withdrawal threshold decreased from 0.87 ± 0.03 g before CFA injection to 0.15 ± 0.03 g three days post-injection (**Figure 15**). Similarly, the latencies of paw withdrawals induced by heat stimulation of the hindpaw exhibited a significant reduction (before, 6.03 ± 0.28 s vs. 3 dpi CFA 2.31 ± 0.11 s N=16, Student's paired t-test, P=1.8E-9) as indicated in **Figure 15**. It is important to highlight that there is an ongoing rigorous debate regarding whether reflexive paw withdrawal, for example triggered by stimulation with von Frey filaments, represents pain or merely indicates mechanical hypersensitivity in nociceptors (Uhler et al. 2022). Henceforth, a decrease in paw withdrawal thresholds will be described as secondary mechanical hypersensitivity.

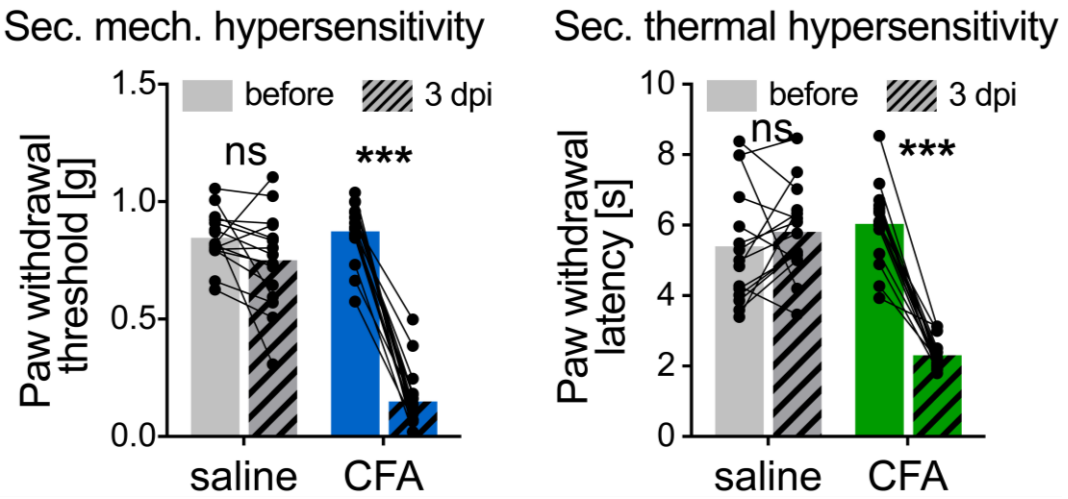

Figure 15 | CFA-induced monoarthritis: secondary hypersensitivity

Left: Comparison of mechanical paw withdrawal thresholds before (solid bars) and three days after (3 dpi, hatched bars) injection with either saline (gray) or CFA (blue). A paired two-sided Student's t-test was used for statistical analysis (saline N = 15, CFA N = 16; CFA, ***, P = 5.18E−12).

Right: Comparison of thermal paw withdrawal latencies before (solid bars) and three days after (3 dpi, hatched bars) injection with either saline (gray) or CFA (blue). A paired two-sided Student's t-test was applied for statistical analysis (saline N = 15, CFA N = 16; CFA, P = 1.8E−9). Adapted from Nees et al. 2023.

In summary, my behavioral analyses in mice with CFA-induced knee joint monoarthritis have successfully validated an inflammatory pain model. Thus, this model has established a foundation for subsequent in-depth in vivo exploration of silent nociceptors. Notably, the animals in this model demonstrate both primary and secondary hypersensitivity, affirming its effectiveness in studying pain mechanisms.

3.4 Knee joint monoarthritis induces TMEM100 expression in knee joint MIAs

To facilitate the investigation of CFA-induced transcriptional and functional alterations in MIAs innervating the knee joint, I subsequently labelled the sensory neurons that contribute to articular afferents via intra-articular knee injection of the retrograde tracer Fast Blue (FB). This approach enabled selective molecular and

electrophysiological assessment of knee joint nociceptors under various conditions. Prior to the start of transcriptional and functional experiments, a characterization of sensory afferents that had undergone back-labeling was carried out to determine and categorize nociceptor subpopulations. This involved the quantification of Fast Blue-positive (FB^+) cells in serial sections of L3 and L4 DRG. On average, approximately 340 DRG neurons were labeled across both L3 and L4 DRGs: 191.5 ± 39.8 cells in the L3 DRG and 150.3 ± 56.7 cells in the L4 DRG (mean ± SEM). These findings are illustrated in **Figure 16**. FB-labeling indicated knee joint innervation by these neurons.

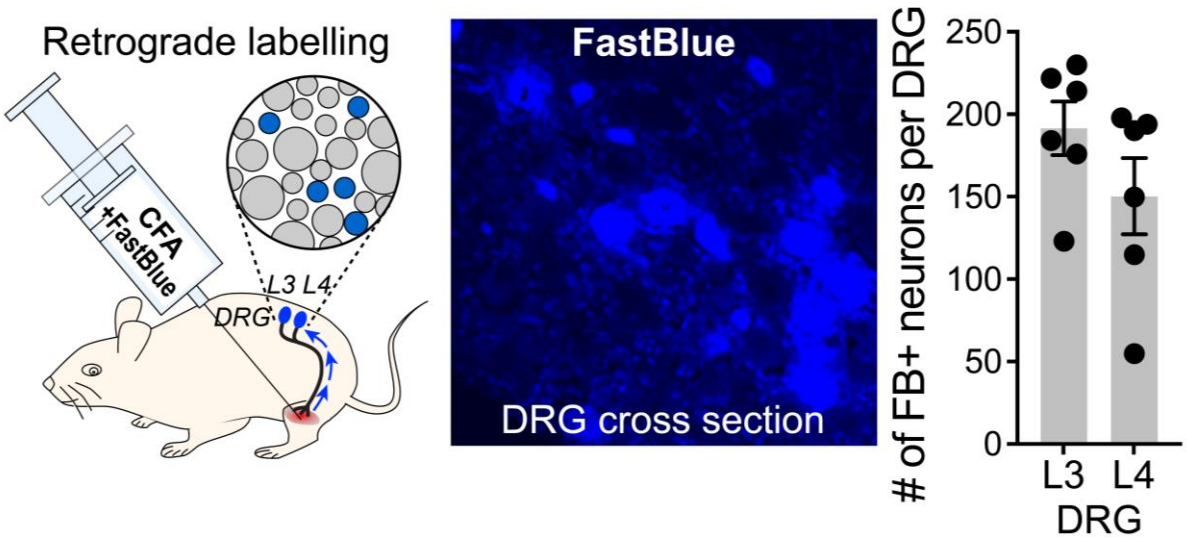

Figure 16 | Sensory afferents innervating the knee joint

Left: Illustration of the experimental approach for retrograde labeling of knee joint afferents with Fast Blue. **Middle**: Representative microscopic image of Fast Blue-positive (FB^+) neurons in a DRG cross section. **Right**: Quantification of the total number of FB^+ neurons in L3 and L4 DRG, based on data from 6 mice. Bar graphs display means ± SEM, with individual mouse DRG data denoted by black dots. Adapted from Nees et al. 2023.

To further differentiate between subsets of primary sensory afferents innervating the knee, DRG cultures from FB-injected mice underwent additional immunolabeling with IB4. The quantification demonstrated that 35.1 % (108/308 FB^+ cells) of the FB^+ cells expressed CHRNA3-$EGFP^+$, while 25.3 % (78/308 FB^+ cells) were characterized as small-diameter (<30 µm) $IB4^-$ peptidergic nociceptors, and 26 % (80/308 FB^+ cells) were identified as large-diameter neurons (**Figure 17**). It is highly probable that these

large-diameter neurons constitute the primary origin of group II articular afferents, responsible for detecting innocuous stimuli. A mere fraction of the retrogradely traced neurons exhibited positivity for IB4 (IB4⁺) staining, amounting to 13.6 % as illustrated in **Figure 17**. This finding serves to underscore that the predominant population of nociceptive afferents originating from the knee joint can be characterized as peptidergic (IB4⁻ and CHRNA3-EGFP⁺). Notably, CHRNA3-EGFP⁺ neurons representing approximately 47 % (108 out of 228 FB⁺ nociceptors) of the entire complement of articular nociceptive afferents.

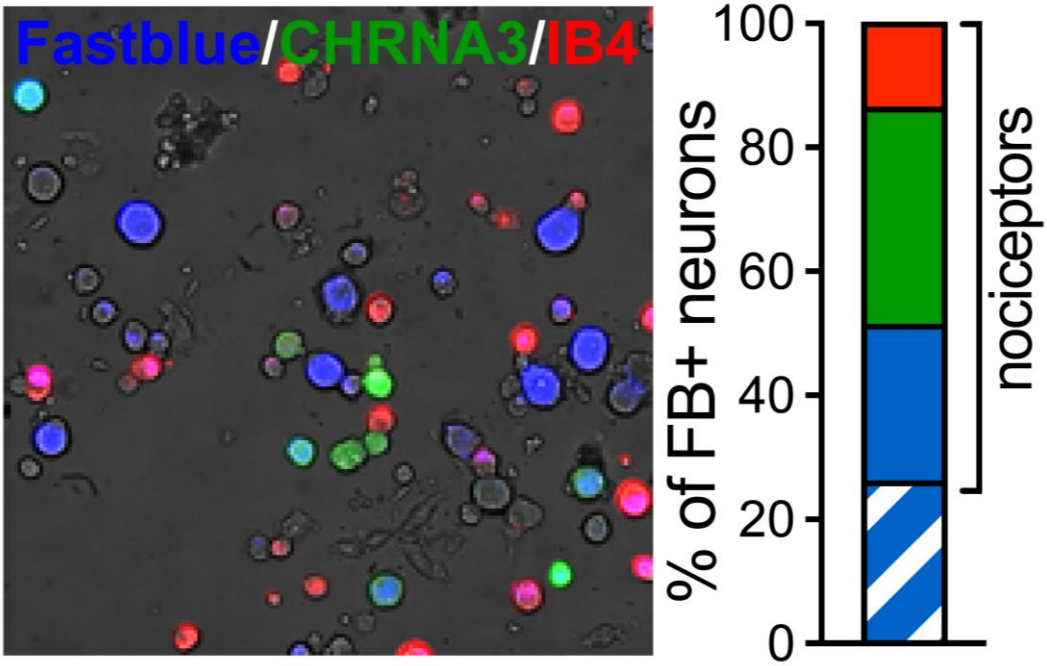

Figure 17 | DRG subpopulations innervating the knee joint

Left: Representative micrograph of a DRG culture from a CHRNA3-EGFP mouse subjected to intraarticular FB injection and IB4 immunolabeling. **Right**: The corresponding bar chart breaks down the different neuronal categories: red represents IB4⁺ cells (indicating non-peptidergic nociceptors), green showcases MIAs, solid blue highlights peptidergic nociceptors (distinguished by being IB4⁻ and smaller than 30 µm), and hatched blue indicates group II articular afferents (those that are IB4⁻ and larger than 30 µm). Adapted from Nees et al. 2023.

Based on these findings, I further analyzed the two primary nociceptor subpopulations innervating the knee joint: MIAs and peptidergic IB4-negative

nociceptors. The aim was to determine whether CFA-induced knee joint inflammation enhances TMEM100 expression within nociceptors that innervate the knee joint. For this purpose, small-diameter (<30 µm) FB⁺ neurons that were IB4-negative (identified as the solid blue subpopulation in **Figure 17**) were isolated, along with those positive for CHRNA3-EGFP (indicated as the green subpopulation in **Figure 17**). These neurons were manually selected from acutely dissociated L3 and L4 DRG neurons from both ipsilateral and contralateral sides after a 3-hour culture, three days following CFA administration. Thereafter, TMEM100 expression levels were assessed using qPCR. The analysis revealed that, akin to the response observed upon *in-vitro* NGF treatment, CFA-induced knee joint inflammation selectively upregulates TMEM100 expression in CHRNA3-EGFP⁺ MIAs, while leaving other C-fiber nociceptors unaffected (as illustrated in **Figure 18**). Interestingly, these elevated TMEM100 expression levels exhibited a transient pattern, returning to baseline values approximately 21 days after CFA injection.

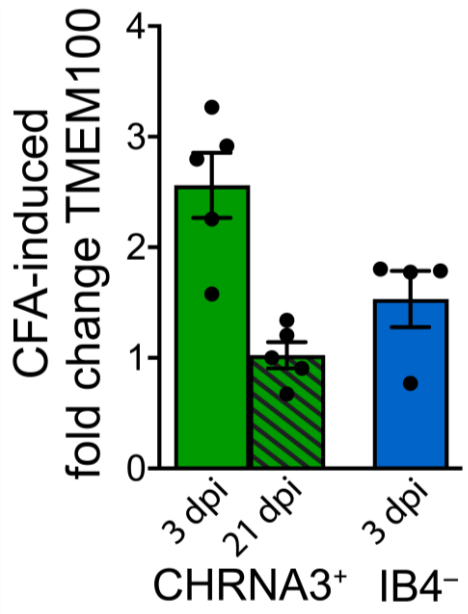

Figure 18 | TMEM100 expression following CFA-induced knee joint monoarthritis
Quantitative analysis of fold changes in TMEM100 expression in retrogradely labeled MIAs (green, FB⁺/CHRNA3-EGFP⁺/IB4⁻, <30 µm) and peptidergic nociceptors (blue, FB⁺/ CHRNA3-EGFP⁻/ IB4⁻, <30 µm). Expression levels in the ipsilateral DRG post-CFA injection were contrasted with those in the contralateral DRG at 3 and 21 days post-injection (dpi) for the MIA group, and at 3 dpi for the peptidergic nociceptors. Quantification was conducted using qPCR with the ΔΔCt method for comparative analysis. CFA, Complete Freund's Adjuvant; CHRNA3, cholinergic receptor nicotinic alpha 3 subunit; DRG, dorsal root ganglia; IB4, Isolectin B4; MIA, mechanically insensitive afferent. Adapted from Nees et al. 2023.

3.5 Knee joint monoarthritis induces mechanosensitivity in knee joint MIAs

Following these observations, the focus shifted to discerning whether the selective upregulation of TMEM100 in MIAs during knee joint inflammation leads to functional changes and subsequent MIA activation. To address this, I assessed the mechanosensitivity of FB-labeled DRG neurons in the context of CFA-induced knee joint monoarthritis, using the previously established mechano-clamp technique. In line with prior findings (Prato et al. 2017), CHRNA3-EGFP$^+$/FB$^+$ neurons originating from animals subjected to knee joint saline injection exhibited no detectable currents in response to mechanical stimulation of the plasma membrane (as illustrated in **Figure 19**).

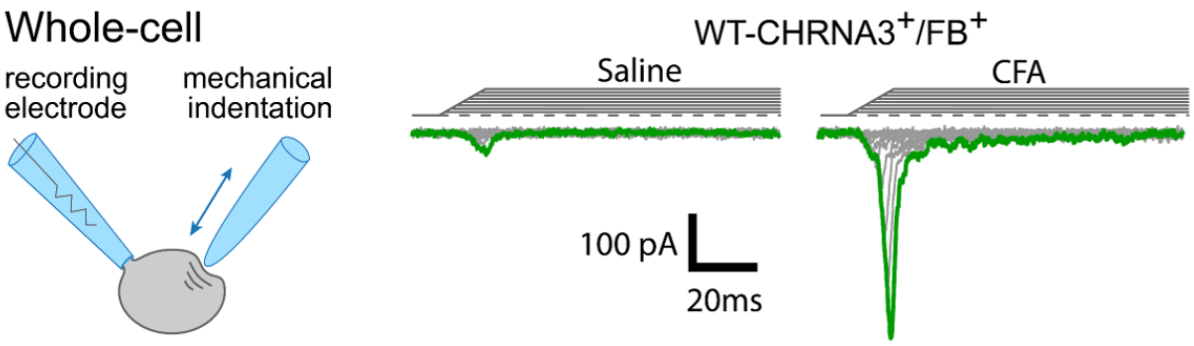

Figure 19 | Mechanically-evoked currents in knee joint MIAs from WT mice
Left: Schematic illustration of the mechano-clamp configuration used in the patch clamp technique. Right: Representative traces showing mechanically-evoked currents in retrogradely traced (FB$^+$) knee joint-innervating MIAs (CHRNA3$^+$) from wildtype (WT) mice, taken 3 days post saline or CFA injections. CFA, Complete Freund's Adjuvant; CHRNA3, cholinergic receptor nicotinic alpha 3 subunit; FB, Fast Blue; pA, picoampere; MIA, mechanically insensitive afferent; ms, millisecond. Adapted from Nees et al. 2023.

Conversely, 3 days subsequent to intraarticular CFA administration at the time of maximum pain, FB-labeled CHRNA3-EGFP$^+$ neurons exhibited robust mechanotransduction currents, significantly surpassing the small inward currents occasionally detected in control subjects (see **Figure 19** and **Figure 20**).

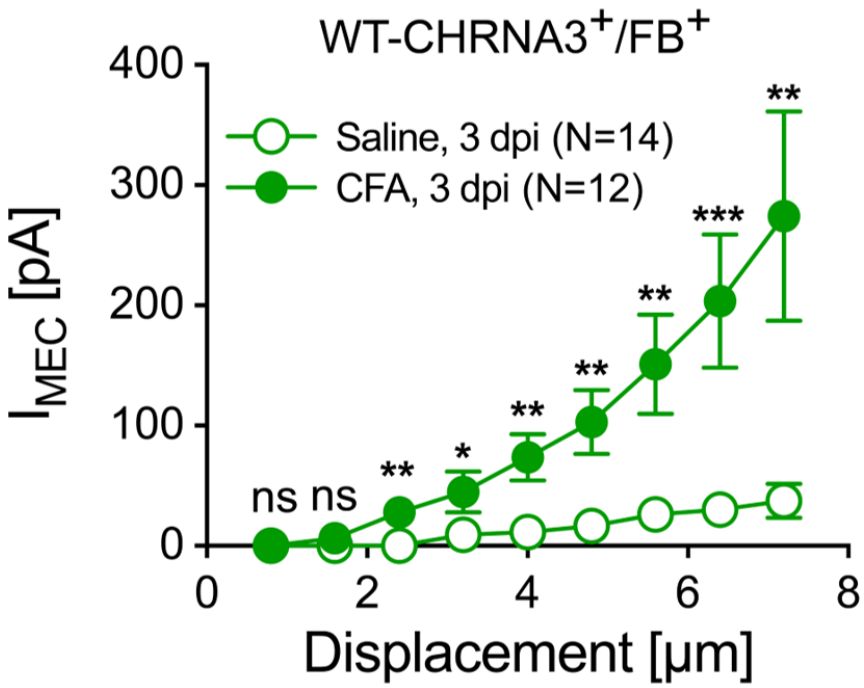

Figure 20 | Acquisition of mechanosensitivity in knee joint MIAs post CFA treatment
The graph delineates the peak amplitudes of mechanically-evoked currents in relation to membrane displacement in retrogradely traced (FB^+) MIAs from wildtype (WT) mice treated with saline (represented by open symbols) or CFA (represented by solid symbols). Comparisons of current amplitudes were conducted 3 days post-injection (dpi) using the Mann-Whitney test (*, P<0.05; **, P<0.01; ***, P<0.001; ns, P>0.05). Sample sizes (N-numbers) are specified in the graph legends. CFA, Complete Freund's Adjuvant; CHRNA3, cholinergic receptor nicotinic alpha 3 subunit; FB, Fast Blue; I_{MEC}, mechanotransduction currents; MIA, mechanically insensitive afferent; pA, picoampere; µm, micrometer. Adapted from Nees et al. 2023.

Intriguingly, in small-diameter $IB4^-$ nociceptors of CFA-treated wildtype mice, the amplitudes of mechanotransduction currents remained unaltered when compared to saline treated counterparts (**Figure 21**).

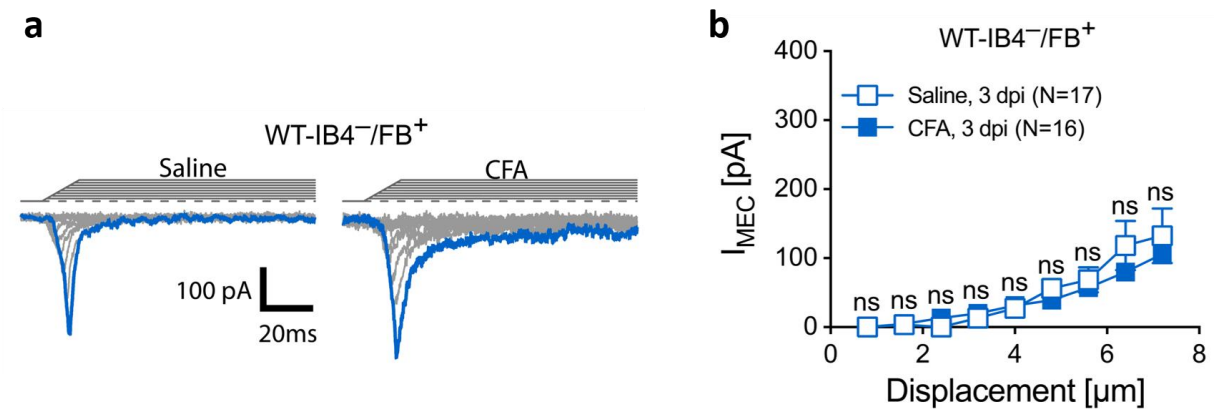

Figure 21 | Mechanosensitivity of IB4⁻ knee joint nociceptors after CFA treatment

(**a**) Representative traces showing mechanically-evoked currents in retrogradely traced (FB⁺) knee joint-innervating peptidergic (IB4⁻) nociceptors from wildtype (WT) mice, taken 3 days post CFA or saline injections. (**b**) Peak amplitudes of mechanically-evoked currents in relation to membrane displacement in retrogradely traced (FB⁺) peptidergic (IB4⁻) nociceptors from WT mice treated with saline (represented by open symbols) or CFA (represented by solid symbols). Comparisons of current amplitudes were conducted 3 days post-injection (dpi) using the Mann-Whitney test (ns, P>0.05). Sample sizes (N-numbers) are specified in the graph legends. CFA, Complete Freund's Adjuvant; FB, Fast Blue; IB4, Isolectin B4; I_{MEC}, mechanotransduction currents; ms, millisecond; ns; not significant; pA, picoampere; µm, micrometer. Adapted from Nees et al. 2023.

Interestingly, in the peptidergic IB4⁻ nociceptor subpopulation, a subtle but statistically significant elevation was noted in the inactivation time constants of mechanically-evoked currents after CFA treatment. In contrast, in the MIA subpopulation, the inactivation time constants remained unaffected by CFA treatment (**Figure 22**).

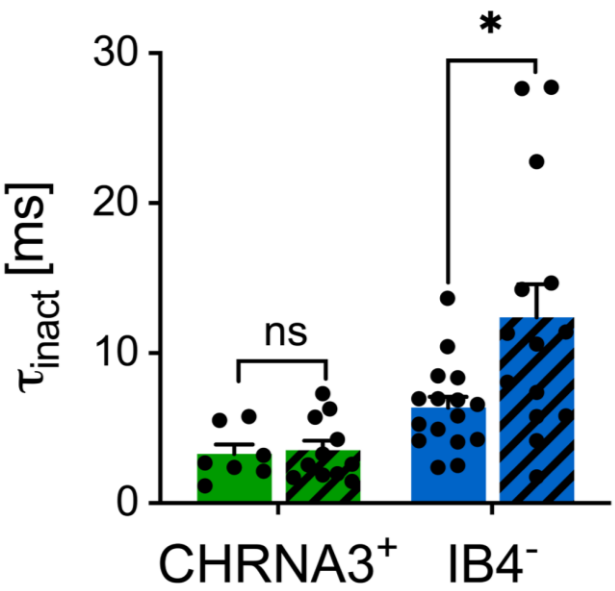

Figure 22 | Analysis of inactivation time constants in mechanically evoked currents
Comparative analysis of inactivation time constants (τ_{inact}) for mechanically evoked currents, quantified through a single exponential fit. Mechanically insensitive afferents (MIAs) are indicated in green (CHRNA3$^+$) and peptidergic nociceptors in blue (IB4$^-$). Solid bars represent the control responses to saline treatment, while hatched bars illustrate responses after CFA injections. Each bar denotes the mean ± SEM, with individual data points represented by black dots. Statistical significance was determined using a two-sided T-test (ns, P > 0.5; *, P < 0.05). The number of independent experiments is as follows: N = 7 for CHRNA3$^+$ saline (green solid), N = 11 for CHRNA3$^+$ CFA (green hatched), N = 16 for IB4$^-$ saline (blue solid), and N = 14 for IB4$^-$ CFA (blue hatched).
CFA, Complete Freund's Adjuvant; CHRNA3, cholinergic receptor nicotinic alpha 3 subunit; FB, Fast Blue; Isolectin B4; ms, millisecond. Adapted from Nees et al. 2023.

3.6 Knee joint monoarthritis potentiates TRPA1 activity in knee joint MIAs

As TMEM100 has been previously demonstrated to amplify the activity of TRPA1 channels in TMEM100-dependet manner (Weng et al. 2015), I examined the responsiveness of FB-labeled neurons to the TRPA1 agonist AITC using Calbryte-590 Ca^{2+}-imaging. The proportion of CHRNA3-EGFP$^+$/FB$^+$ knee joint MIAs responsive to AITC in mice treated with saline was 8 % (4 out of 50 cells). Remarkably, upon CFA treatment, the proportion of responsive CHRNA3-EGFP$^+$/FB$^+$ knee joint MIAs significantly increased, reaching 41 % (23 out of 56 cells) as illustrated in **Figure 23a**.

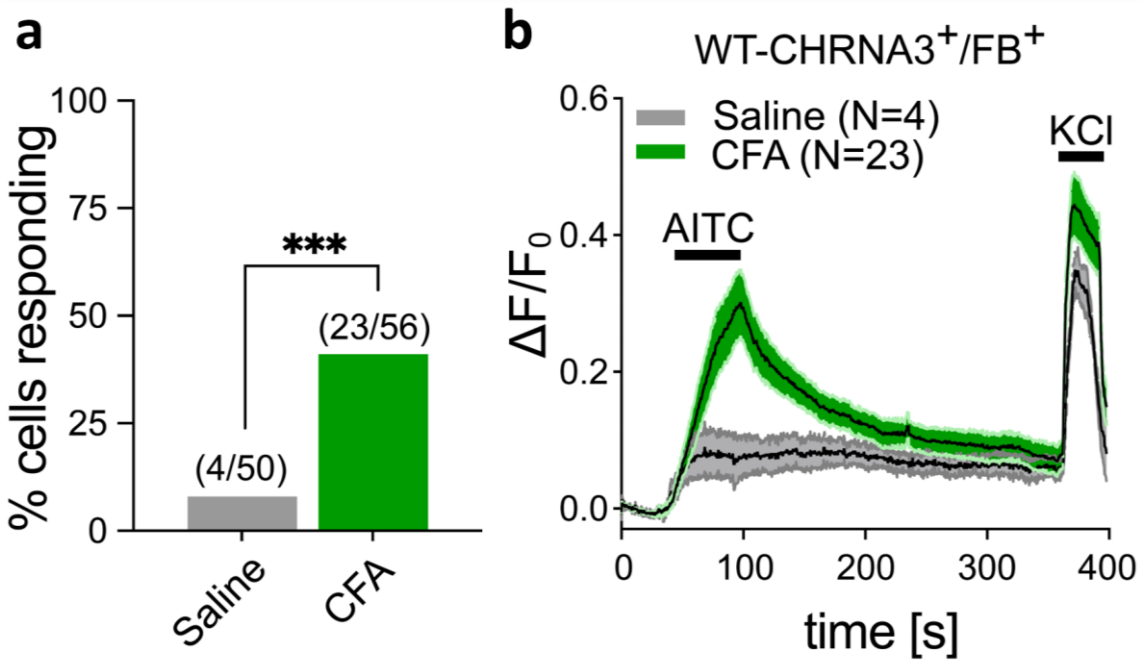

Figure 23 | Calcium imaging analysis of knee innervating MIAs in WT mice

(**a**) Bar graphs represent the percentage of knee-innervating MIAs (CHRNA3$^+$) from wildtype (WT) mice that responded to a 10 µM AITC treatment three days post-saline (gray) or CFA (green) injections, as determined by Calbryte-590 Ca^{2+} imaging. Two-sided Fisher's exact test was used to compare these proportions (ns, no significant; ***, P=1.02E-4). (**b**) Time course changes in intracellular Ca^{2+} concentrations, captured via Calbryte-590 Ca^{2+} imaging, highlight retrogradely labelled (FB$^+$) MIAs from both saline and CFA-treated mice upon exposure to 10 µM AITC and 100 mM KCl. The graph legends provide the sample sizes (N-numbers). AITC, allylisothiocyanate; CFA, Complete Freund's Adjuvant; CHRNA3, cholinergic receptor nicotinic alpha 3 subunit; FB, Fast Blue; KCl, potassium chloride; MIA, mechanically insensitive afferent; s, second. Adapted from Nees et al. 2023.

In contrast, the proportion of AITC-sensitive small-diameter IB4$^-$/FB$^+$ neurons, presumed to be peptidergic polymodal C-fiber nociceptors, remained unchanged following CFA treatment (as shown in **Figure 24**). Specifically, only 4 out of 36 IB4$^-$/FB$^+$ cells (11 %) responded to AITC in the context of CFA-induced knee joint inflammation, which did not differ from the proportion of AITC responders observed in the saline-treated control animals (4 out of 30 cells, 13 %). This finding aligns with the observation that CFA-induced knee joint inflammation does not modify TMEM100 expression within this nociceptor subpopulation.

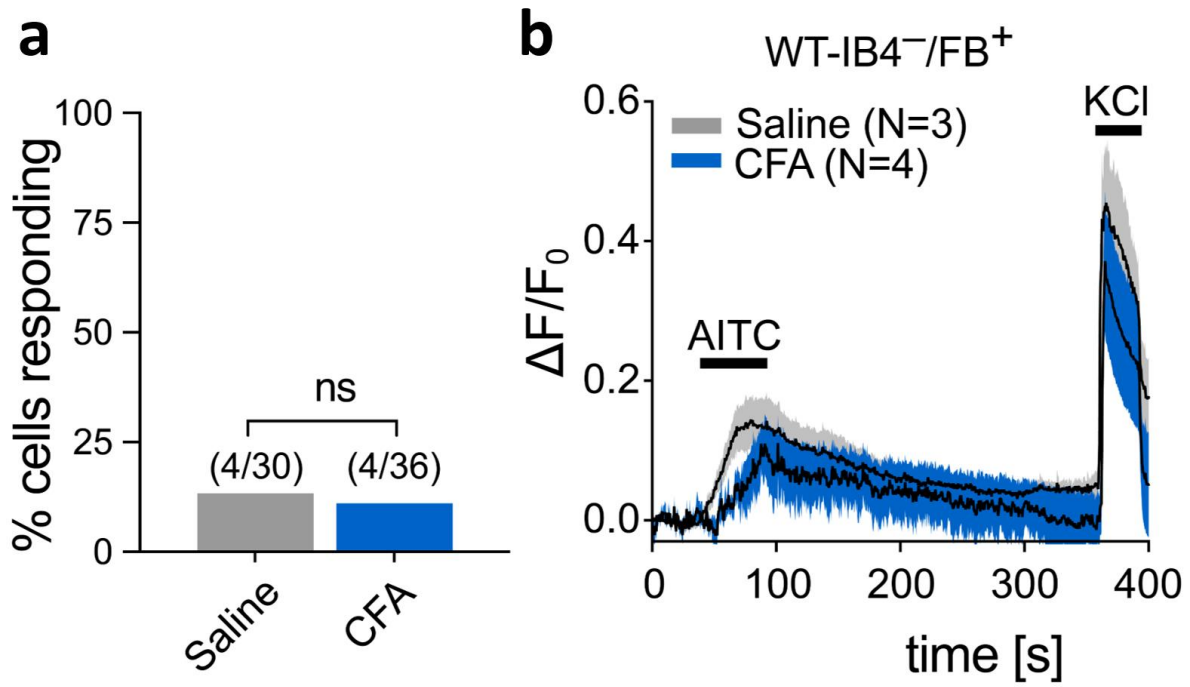

Figure 24 | Calcium imaging analysis of knee innervating IB4⁻ nociceptors in WT mice
(**a**) Bar graphs represent the percentage of knee-innervating peptidergic IB4 negative (IB4⁻) nociceptors from wildtype (WT) mice that responded to a 10 µM AITC treatment three days post-saline (gray) or CFA (blue) injections, as determined by Calbryte-590 Ca^{2+} imaging. Two-sided Fisher's exact test was used to compare these proportions (ns, no significant). (**b**) Time course changes in intracellular Ca^{2+} concentrations, captured via Calbryte-590 Ca^{2+} imaging, highlight retrogradely labelled (FB^{+}) IB4⁻ peptidergic nociceptors from both saline and CFA-treated mice upon exposure to 10 µM AITC and 100 mM KCl. The graph legends provide the sample sizes (N-numbers). AITC, allylisothiocyanate; CFA, Complete Freund's Adjuvant; FB, Fast Blue; IB4, Isolectin B4; KCl, potassium chloride; s, second. Adapted from Nees et al. 2023.

Additionally, a notable increase in the average response amplitude of CHRNA3-$EGFP^{+}$ neurons was observed (**Figure 23b**). However, due to the limited number of responsive cells in the saline-treated group (n=4), the interpretability and significance of this effect may be constrained.

Cumulatively, the data reveals that the intraarticular injection of CFA leads to knee joint pain and secondary hypersensitivity in the ipsilateral hind paw. These nociceptive responses coincide with an increase in TMEM100 expression, potentiation of TRPA1 activity, and, significantly, the development of mechanosensitivity in CHRNA3-$EGFP^{+}$ neurons.

3.7 Pain behavior in TMEM100KO mice with knee joint monoarthritis

Next, I aimed to elucidate the potential causal connection between the observed pain phenotype in CFA-induced knee monoarthritis (as outlined in 3.3 Behavioral characterization of a mouse model of inflammatory knee pain) and the sensitization of CHRNA3-EGFP$^+$ nociceptors. Specifically, I sought to determine whether this sensitization is triggered by the upregulation of TMEM100. To address this, conditional TMEM100 knockout mice, hereafter referred to as TMEM100KO mice, were generated through a crossbreeding strategy involving mice harboring a conditional TMEM100 allele (Moon et al. 2010) with SNS-Cre mice. The latter strain is characterized by Cre-recombinase expression driven by the voltage-gated sodium channel $Na_v1.8$ promoter (Agarwal et al. 2004), thereby encompassing all nociceptors, including CHRNA3-EGFP$^+$ neurons (Schaefer et al. 2018).

Initially, primary knee joint pain was evaluated through CatWalk XT gait analysis over a period of 21 days. This analysis included male wildtype (WT) mice that received intraarticular saline injections, as well as male WT and TMEM100KO mice subjected to CFA injections. Male WT mice administered with CFA exhibited discernibly altered gait, indicative of knee joint pain, during the initial seven days post-CFA injection. In contrast to saline-treated WT animals, WT mice with CFA-induced knee joint monoarthritis displayed a significant reduction in weight-bearing on the affected leg. This was evident from the decreased ratios of stand time, footprint area, and leg swing speed observed between the ipsilateral (left) and contralateral (right) hindpaws. Gait alterations indicating knee joint pain peaked on the third day post-injection (3 dpi) and remained significantly noticeable for at least one week following the administration of CFA. Surprisingly, CFA-treated TMEM100KO mice also exhibited knee joint pain displaying altered gait patterns. This behavior significantly differed from that of saline-treated WT mice but closely resembled the gait observed in CFA-treated WT mice. Statistically, there was no difference observed in the gait analysis between CFA-treated WT and TMEM100KO animals (**Figure 25**).

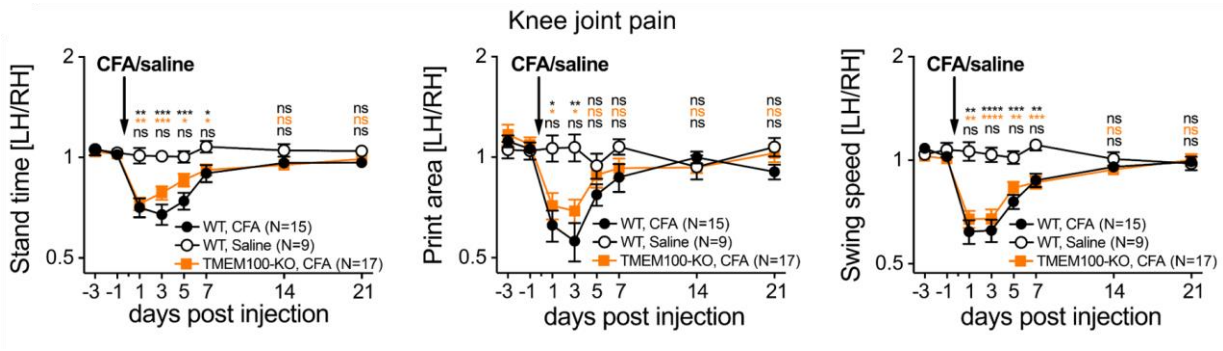

Figure 25 | Gait analysis in TMEM100KO mice with CFA-induced knee joint monoarthritis
Temporal changes in stand time (**left**), footprint area (**middle**), and leg swing speed (**right**) were compared among saline-injected WT mice (white circles), CFA-injected WT mice (black circles), and CFA-injected TMEM100KO mice (orange squares). Gait parameters for both left (LH) and right hind paws (RH) are expressed as a ratio (LH/RH). Each symbol denotes the mean ± SEM. Ratios at distinct time points were statistically contrasted using a mixed-model ANOVA, with the ensuing P-values from Tukey's multiple comparisons outlined above the white circles: top, WT-saline vs. WT-CFA; middle, WT-saline vs. TMEM100KO-CFA; bottom, WT-CFA vs. TMEM100KO-CFA (*, $P < 0.05$; **, $P < 0.01$; ***, $P < 0.001$; ns, $P > 0.05$). Sample sizes (N-numbers) are specified in the graph legends. CFA, Complete Freund's Adjuvant; ns, not significant; TMEM100KO, TMEM100 knockout; WT, wildtype. Adapted from Nees et al. 2023.

Notably, however, CFA-induced secondary mechanical hypersensitivity in the ipsilateral hind paw was markedly attenuated in TMEM100KO mice. Specifically, the von Frey paw withdrawal thresholds exhibited only transient reductions from day 3 to day 5, returning to baseline values by day 7 in TMEM100KO mice. In contrast, CFA-treated WT mice displayed persistent secondary mechanical hypersensitivity that extended throughout the examination period, lasting until day 21 (as illustrated in **Figure 26**).

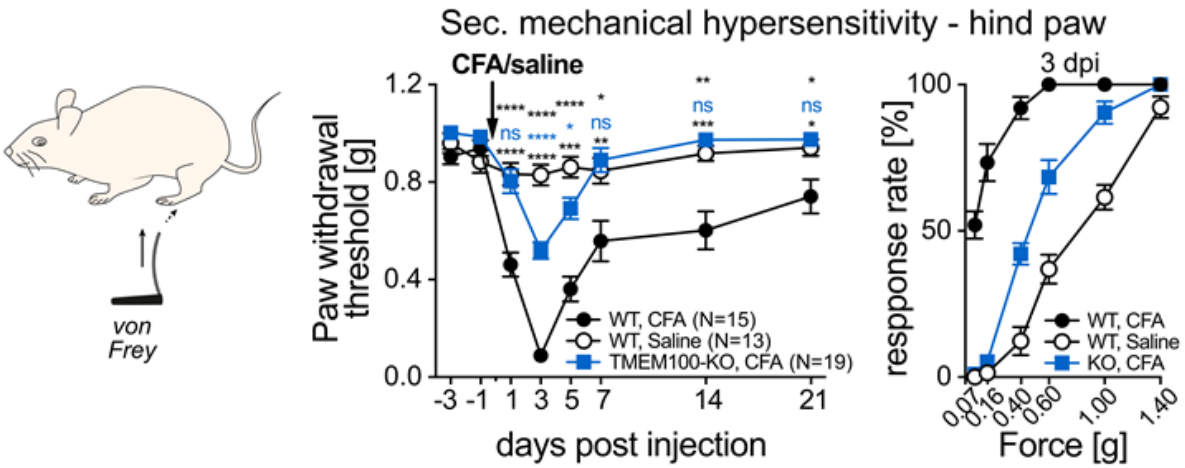

Figure 26 | Mechanical sensitivity in TMEM100KO mice with knee joint monoarthritis

Left: Illustration of the experimental approach for measuring secondary mechanical hypersensitivity in the ipsilateral hindpaw using von Frey filaments. **Middle**: Time courses depicting changes in mechanical paw withdrawal thresholds over days post-injection (dpi) for: Saline-injected WT mice (white circles), CFA-injected WT mice (black circles), and CFA-injected TMEM100KO mice (blue squares). Each symbol denotes the mean ± SEM. Paw withdrawal thresholds were compared using a mixed model ANOVA followed by Tukey's multiple comparisons test. P-values from multiple comparisons are outlined above the white circles: top, WT-saline vs. WT-CFA; middle, WT-saline vs. TMEM100KO-CFA; bottom, WT-CFA vs. TMEM100KO-CFA (*, $P < 0.05$; **, $P < 0.01$; ***, $P < 0.001$; ns, $P > 0.05$). Sample sizes (N-numbers) are specified in the graph legends. **Right**: Responsiveness (in percentages, %) of the three mouse groups to all tested von Frey filaments, measured three days after saline/CFA injection (3 dpi). Each symbol denotes the mean ± SEM. Response rates were compared mixed model ANOVA followed by Tukey's multiple comparisons test. P-values of multiple comparisons are as follows: WT-saline vs. WT-CFA, $P_{0.07g}$ = 7.5E-08, $P_{0.16g}$ = 2.8E-08, $P_{0.4g}$ = 8.7E-12, $P_{0.6g}$ = 7.5E-08, P_{1g} = 2.6E-06, $P_{1.4g}$ = 1.2E-01; WT-saline vs. TMEM100KO-CFA, $P_{0.07g}$ = 5.9E-01, $P_{0.16g}$ = 3.3E-01, $P_{0.4g}$ = 1.5E-04, $P_{0.6g}$ = 7.8E-04, P_{1g} = 6.8E-05, $P_{1.4g}$ = 1.2E-01; WT-CFA vs. TMEM100KO-CFA, $P_{0.07g}$ = 5.2E-08, $P_{0.16g}$ = 3.6E-08, $P_{0.4g}$ = 3.9E-10, $P_{0.6g}$ = 9.9E-05, P_{1g} = 6.1E-02, $P_{1.4g}$ = not determined). Sample sizes (N-numbers) are specified in the graph legends of the middle panel. CFA, Complete Freund's Adjuvant; ns, not significant; TMEM100KO, TMEM100 knockout; WT, wildtype. Adapted from Nees et al. 2023.

Interestingly, while the lack of TMEM100 led to a significant reduction in secondary mechanical hypersensitivity during CFA-induced knee joint inflammation (**Figure 26**), it did not affect secondary thermal hypersensitivity in TMEM100KO mice. Both WT and TMEM100KO mice displayed notable secondary thermal hypersensitivity following CFA injections, especially when contrasted with saline-injected WT mice. Crucially, post-CFA injection, the intensity and time course of thermal hypersensitivity was

statistically indistinguishable between WT and TMEM100KO mice, underscoring that TMEM100's absence had no impact on CFA-induced secondary thermal hypersensitivity (**Figure 27**).

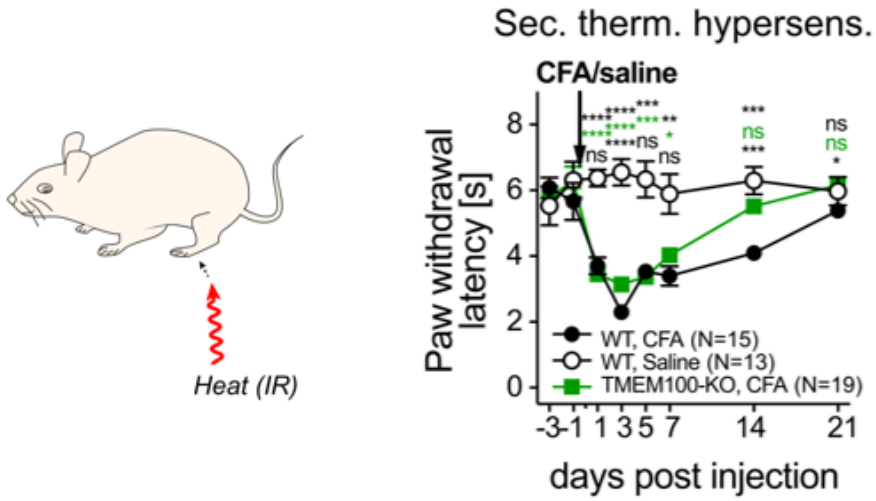

Figure 27 | Thermal sensitivity in TMEM100KO mice with knee joint monoarthritis
Left: Illustration of the experimental approach for measuring secondary thermal hypersensitivity in the ipsilateral hindpaw using a radiant infrared (IR) heat source. **Right**: Time course illustrating changes in thermal paw withdrawal latencies in seconds (s) over days post-injection (dpi) for: Saline-injected WT mice (white circles), CFA-injected WT mice (black circles), and CFA-injected TMEM100KO mice (green squares). Each symbol denotes the mean ± SEM. Paw withdrawal latencies were compared using a mixed model ANOVA followed by Tukey's multiple comparisons test. P-values from multiple comparisons are outlined above the white circles: top, WT-saline vs. WT-CFA; middle, WT-saline vs. TMEM100KO-CFA; bottom, WT-CFA vs. TMEM100KO-CFA (*, $P < 0.05$; **, $P < 0.01$; ***, $P < 0.001$; ns, $P > 0.05$). Sample sizes (N-numbers) are specified in the graph legends. CFA, Complete Freund's Adjuvant; ns, not significant; TMEM100KO, TMEM100 knockout; WT, wildtype. Adapted from Nees et al. 2023.

Given the emerging body of literature highlighting sex-based disparities in pain sensitivity, I replicated the behavioral experiments using female TMEM100KO mice. Intriguingly, their pain phenotype mirrored that of male mice in both primary and secondary hypersensitivity. This underscores a sex-independent function of TMEM100 in inflammatory pain. Like their male counterparts, female mice displayed significant

gait impairments post-CFA injection. These impairments manifested as reductions in print area, stand time, and swing speed of the affected leg (**Figure 28**).

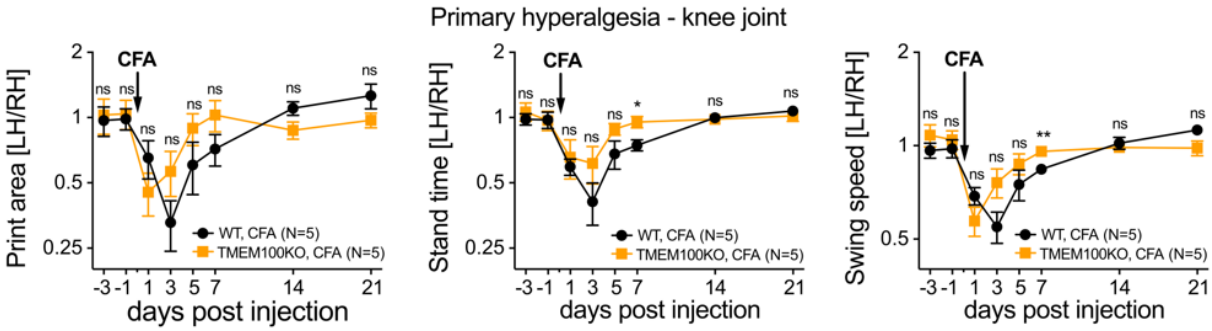

Figure 28 | Gait analysis in female TMEM100KO mice with knee joint monoarthritis
Temporal changes in stand time (**left**), footprint area (**middle**), and leg swing speed (**right**) were compared among female CFA-injected WT mice (black circles), and female CFA-injected TMEM100KO mice (orange squares). Gait parameters for both left (LH) and right hind paws (RH) are expressed as a ratio (LH/RH). Each symbol denotes the mean ± SEM. Ratios at distinct time points were statistically contrasted using Multiple Mann-Whitney test, with the ensuing P-values outlined above the orange squares: WT-CFA vs. TMEM100KO-CFA (*, $P < 0.05$; **, $P < 0.01$; ns, $P > 0.05$). Sample sizes (N-numbers) are specified in the graph legends. CFA, Complete Freund's Adjuvant; ns, not significant; TMEM100KO, TMEM100 knockout; WT, wildtype. Adapted from Nees et al. 2023.

However, consistent with observations in male mice, TMEM100 ablation notably diminished secondary mechanical hypersensitivity post-CFA injection, evident as early as 1dpi. Similar to the behavioral pattern in male mice, the TMEM100KO model exhibited no significant impact on thermal hypersensitivity after CFA administration when compared to CFA-treated WT mice (**Figure 29**).

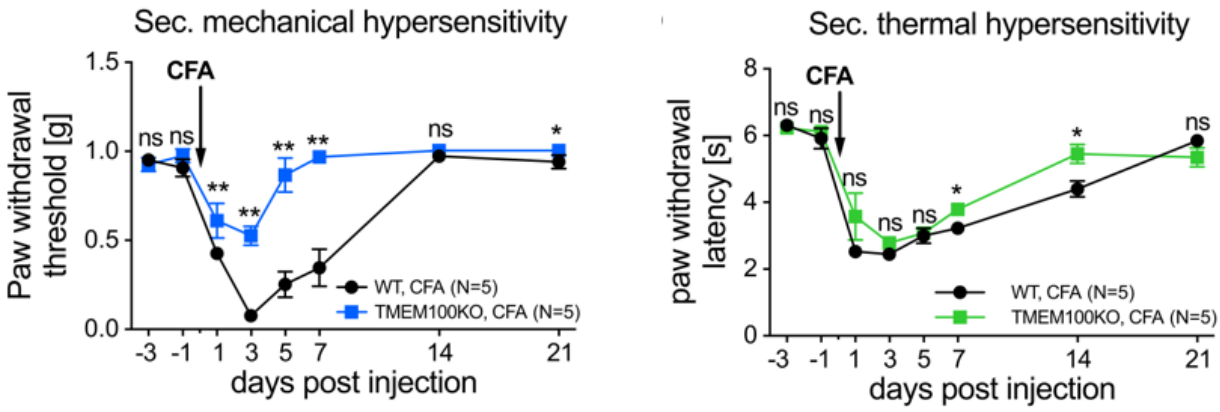

Figure 29 | Mechanical and thermal sensitivity in female mice with knee joint monoarthritis
Left: Temporal changes of mechanical paw withdrawal thresholds in CFA-injected female WT mice (black circles) versus CFA-injected female TMEM100KO mice (blue squares). **Right**: Time courses of thermal paw withdrawal latencies in CFA-injected female WT mice (black circles) compared to CFA-injected female TMEM100KO mice (green squares). Symbols represent means ± SEM. Comparative analysis at different time points was performed using Multiple Mann-Whitney test. The significance between WT-CFA and TMEM100KO-CFA is denoted as follows: ns ($P > 0.05$), * ($P < 0.05$), ** ($P < 0.01$). Sample sizes (N-numbers) are detailed in the graph legends. CFA, Complete Freund's Adjuvant; ns, not significant; TMEM100KO, TMEM100 knockout; WT, wildtype. Adapted from Nees et al. 2023.

Therefore, regardless of genotype, TMEM100KO did not affect primary knee joint pain or thermal hypersensitivity but significantly mitigated mechanical hypersensitivity in the CFA-induced monoarthritis model.

3.8 Mechanosensitivity of knee joint MIAs in TMEM100KO mice

In light of the compelling *in-vitro* and *in-vivo* results obtained thus far, which strongly indicate that TMEM100 may play a role in the manifestation of inflammatory pain signs, the subsequent experiments aimed to evaluate the involvement of TMEM100 in the onset of mechanosensitivity and the enhancement of TRPA1 activity in CHRNA3-EGFP$^+$ knee joint afferents during CFA-induced monoarthritis. To achieve this goal, I performed patch-clamp recordings on retrogradely traced (FB$^+$) nociceptors innervating the knee joint in TMEM100KO mice following either CFA or saline treatment. This encompassed both CHRNA3-EGFP$^+$ MIAs and IB4$^-$ nociceptors.

Strikingly, the mechano-clamp experiments demonstrated that articular CHRNA3-EGFP⁺ MIAs from TMEM100KO mice did not exhibit an acquisition of mechanosensitivity during CFA-induced inflammation. Just like the CHRNA3-EGFP⁺ MIAs from TMEM100KO animals that received saline injections, the knee joint MIAs in CFA-treated TMEM100KO mice occasionally displayed small inward currents. However, they did not exhibit pronounced mechanotransduction currents (**Figure 30**). This contrasts with the robust mechanotransduction currents observed in WT animals with CFA-induced knee joint monoarthritis (**Figure 20**). Furthermore, the mechanosensitivity of FB⁺/IB4⁻ neurons in TMEM100KO mice remained unchanged. Regardless of CFA treatment, the knee joint-innervating IB4⁻ nociceptors exhibited comparable mechanotransduction currents. Last but not least, in both CHRNA3-EGFP⁺ MIAs and IB4⁻ nociceptors of TMEM100KO mice, the inactivation time constants did not exhibit significant variations following CFA treatment when compared to saline control injections (**Figure 30**).

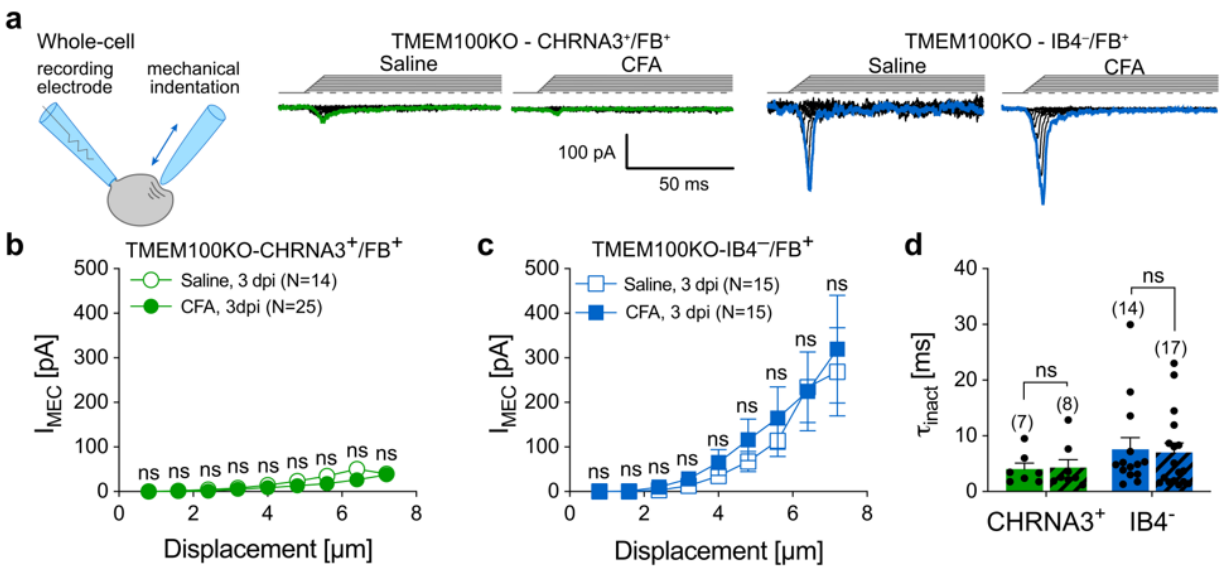

Figure 30 | Mechanosensitivity of knee joint nociceptors from TMEM100KO mice

(**a**) Illustration of the mechano-clamp configuration used in the patch clamp technique (left) alongside representative traces of mechanically-evoked currents in retrogradely-traced (FB⁺) knee joint innervating MIAs (CHRNA3⁺, green; middle) and peptidergic IB4⁻ nociceptors (blue; right) from TMEM100KO mice at 3 days post-injection (dpi) of either saline or CFA. (**b-c**) Peak amplitudes of mechanically-evoked currents against membrane displacement in (**b**) MIAs (green) and (**c**) peptidergic IB4⁻ nociceptors (blue) from both saline (open symbols) and CFA-treated (filled symbols) TMEM100KO mice. Statistical analyses were performed using the Mann-Whitney test (ns, P>0.05). (**d**) Comparison

of the inactivation time constants (τ_{inac}) of the mechanically-evoked currents determined using a single exponential fit. The MIAs are represented in green (CHRNA3$^+$), and the peptidergic nociceptors are shown in blue (IB4$^-$). Responses following saline treatments are depicted by solid bars, whereas those post-CFA injections are shown using hatched bars. Each bar provides the mean ± SEM, with individual values denoted by black dots. A two-sided unpaired t-test was employed for statistical analyses (ns, P>0.5). N-numbers of independent experiments (numbers in brackets) are shown above the bars. CFA, Complete Freund's Adjuvant; CHRNA3, cholinergic receptor nicotinic alpha 3 subunit; FB, Fast Blue; I_{MEC}, mechanotransduction currents; Isolectin B4; ms, millisecond; ns, not significant; pA; picoampere; TMEM100KO, TMEM100 knockout, µm, micrometer. Adapted from Nees et al. 2023.

Moreover, to investigate the previously suggested role of TMEM100 in the disinhibition of TRPA1 channels (Weng et al. 2015), Calbryte-590 Ca^{2+} imaging was employed. In accordance with the findings reported by Weng and colleagues, neither the proportion of AITC-sensitive CHRNA3-EGFP$^+$ knee joint afferents nor the magnitude of their responses exhibited any changes following CFA treatment in TMEM100KO mice (**Figure 31**). Approximately 19 % (11 out of 58 cells) and 20 % (14 out of 71 cells) of the articular CHRNA3-EGFP$^+$ MIAs from TMEM100KO mice responded to AITC after saline and CFA treatment, respectively.

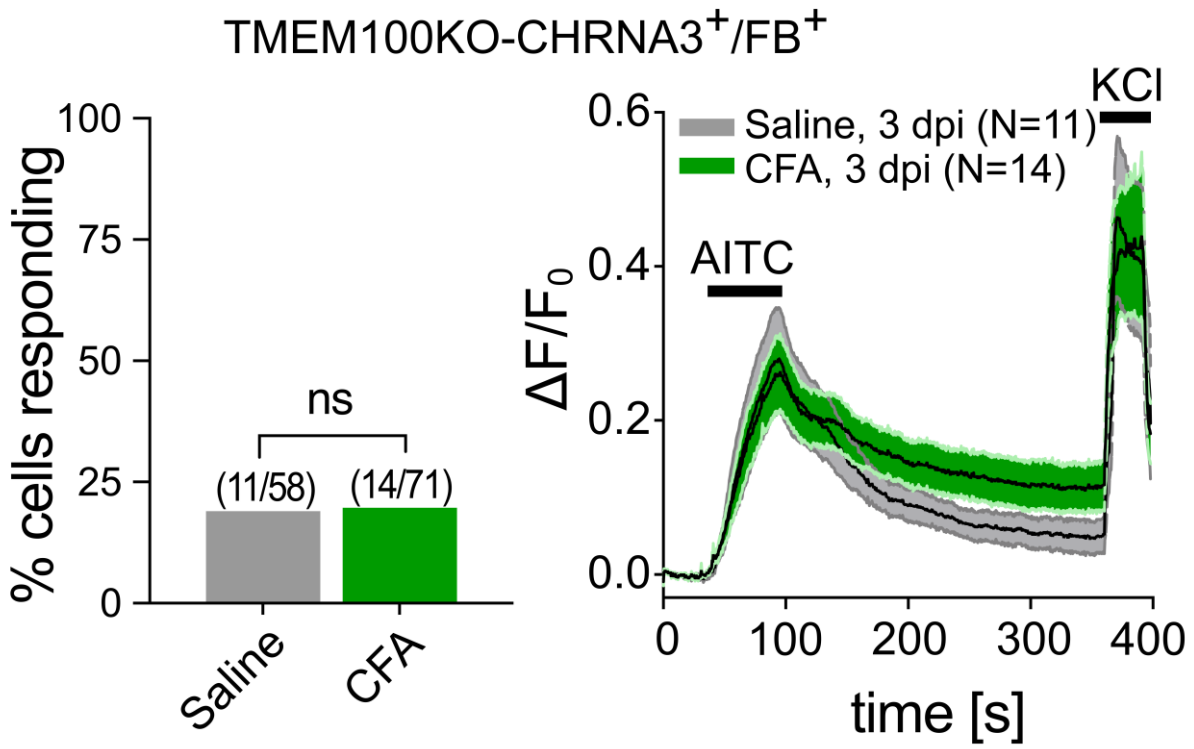

Figure 31 | Calcium imaging analysis of knee innervating MIAs in TMEM100KO mice

Left: Bar graphs represent the percentage (%) of knee-innervating MIAs (CHRNA3$^+$) from TMEM100 knockout (TMEM100KO) mice that responded to a 10 µM AITC treatment post saline (gray) or CFA (green) injections, as determined by Calbryte-590 Ca^{2+} imaging. Two-sided Fisher's exact test was used to compare these proportions (ns, not significant) Numbers in brackets above the bars indicate the number of responders and number of tested cells. **Right**: Time course changes in intracellular Ca^{2+} concentrations, captured via Calbryte-590 Ca^{2+} imaging, highlight retrogradely labelled (FB$^+$) MIAs from both saline (gray) and CFA-treated (green) TMEM100KO mice upon exposure to 10 µM AITC and 100 mM KCl. The graph legends provide the sample sizes (N-numbers). AITC, allylisothiocyanate; CFA, Complete Freund's Adjuvant; CHRNA3, cholinergic receptor nicotinic alpha 3 subunit; dpi, days post injection; FB, Fast Blue; KCl, potassium chloride; s, second. Adapted from Nees et al. 2023.

Likewise, the AITC responses of articular small-diameter IB4$^-$ nociceptors in TMEM100KO mice remained unaltered (**Figure 32**). Regardless of CFA treatment, the magnitude of responses to AITC in the small-diameter FB$^+$ IB4$^-$ nociceptors remained consistent. Additionally, the proportion of AITC-sensitive articular IB4$^-$ nociceptors did not show a statistically significant difference between saline and CFA-treated TMEM100KO mice.

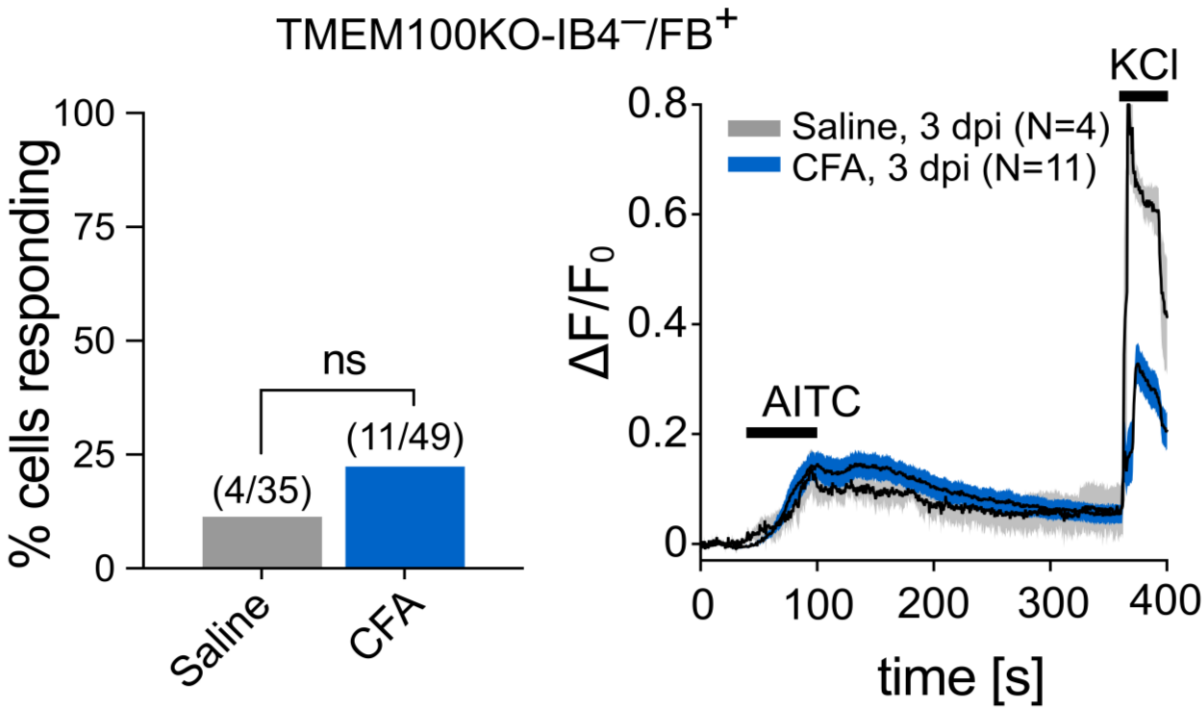

Figure 32 | Calcium imaging analysis of articular IB4⁻ nociceptors in TMEM100KO mice

Left: Bar graphs represent the percentage (%) of knee-innervating peptidergic IB4 negative (IB4⁻) nociceptors from TMEM100 knockout (TMEM100KO) mice that responded to a 10 µM AITC treatment 3 days post injections (dpi) of saline (gray) or CFA (blue), as determined by Calbryte-590 Ca^{2+} imaging. Two-sided Fisher's exact test was used to compare these proportions (ns, not significant). Numbers in brackets above the bars indicate the number of responders and number of tested cells. **Right**: Time course changes in intracellular Ca^{2+} concentrations, captured via Calbryte-590 Ca^{2+} imaging, highlight retrogradely labelled (FB⁺) IB4⁻ peptidergic nociceptors from both saline and CFA-treated TMEM100KO mice upon exposure to 10 µM AITC and 100 mM KCl. The graph legends provide the sample sizes (N-numbers). AITC, allylisothiocyanate; CFA, Complete Freund's Adjuvant; FB, Fast Blue; IB4, Isolectin B4; KCl, potassium chloride; s, second. Adapted from Nees et al. 2023

Therefore, the presented dataset signifies that CFA treatment specifically upregulates TMEM100 within CHRNA3-EGFP⁺ MIAs (as illustrated in **Figure 18**), subsequently prompting the acquisition of mechanosensitivity and the potentiation of TRPA1 (as depicted in **Figure 20** and **Figure 23**). These observations, coupled with the fact that the decrease of paw withdrawal thresholds was significantly attenuated in TMEM100KO mice during CFA-induced knee inflammation, while knee joint pain remained unaltered (see **Figure 25** and **Figure 26**), collectively suggest that the activation of articular MIAs due to TMEM100-induced un-silencing instigates the development of secondary mechanical hypersensitivity.

3.9 Sensitization of cutaneous C-fiber nociceptors in knee joint inflammation

In the context of pain processing, it is firmly established that central sensitization, denoting the amplification of synaptic transmission within spinal cord pain processing circuits, plays a substantial role in the development of secondary mechanical hypersensitivity (Eitner et al. 2017; Sandkühler 2009). Given the pronounced reduction in paw withdrawal thresholds during CFA-induced knee joint monoarthritis (as illustrated in **Figure 26**), it is pertinent to ask if sensitization of cutaneous nociceptors also plays a part in this process. To investigate this, the mechanosensitivity of C-fiber and Aδ-fiber nociceptors in the tibial nerve – which innervates the plantar surface of the hindpaw – was directly assessed. This was accomplished by recording mechanically induced action potentials from individual nerve fibers in an ex-vivo skin-nerve preparation from mice subjected to intraarticular knee joint CFA administration. At the beginning of each single unit recording, the conduction velocity (CV) of the fiber under examination was determined (see **Figure 33**) to classify it as either a C-fiber (CV < 1 m/s) or an Aδ-fiber (CV 1-10 m/s). Additionally, the mechanical activation threshold was ascertained using von Frey filaments, the same tool used to gauge paw withdrawal thresholds in behavioral tests.

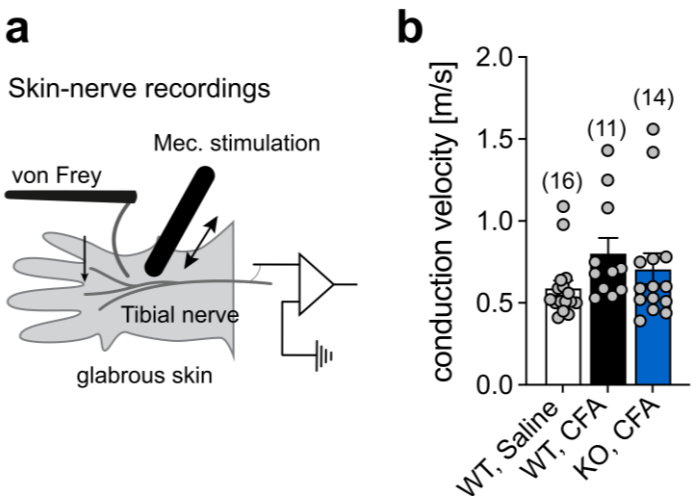

Figure 33 | Skin-nerve recordings of cutaneous nociceptors in the tibial nerve

(**a**) Schematic representation of the experimental setup. (**b**) Scatter dot plots illustrating conduction velocities (in m/s) of the afferent fibers from wildtype (WT) and TMEM100 knockout (KO) animals, 3 days post-injection with either saline or Complete Freund's Adjuvant (CFA) into the knee joint. Sample sizes (N-numbers) are indicated above the bars in brackets. Bars indicate mean ± SEM. Adapted from Nees et al. 2023.

In WT mice with CFA-induced knee joint monoarthritis, the recordings revealed that about 40 % of cutaneous C-fiber nociceptors responded to von Frey filaments weighing 0.16 g or less. Furthermore, almost all C-fibers (90 %) showed sensitivity to von Frey filaments of 0.4 g or less. In stark contrast, none of the cutaneous C-fiber nociceptors from saline-treated WT mice (control) reacted to von Frey stimuli ≤ 0.16 g, with only around 17 % activated by the 0.4 g filament. Similarly, the percentage of cutaneous Aδ-fiber nociceptors that exhibited responses to von Frey stimuli with ≤ 0.16g was notably higher in CFA-treated WT mice, although this disparity was less prominent than in the case of C-fibers. Of paramount significance, the responsiveness of cutaneous C-fiber and Aδ-fiber nociceptors in TMEM100KO mice remained unchanged following intra-articular CFA injection when compared to saline injections (see **Figure 34**).

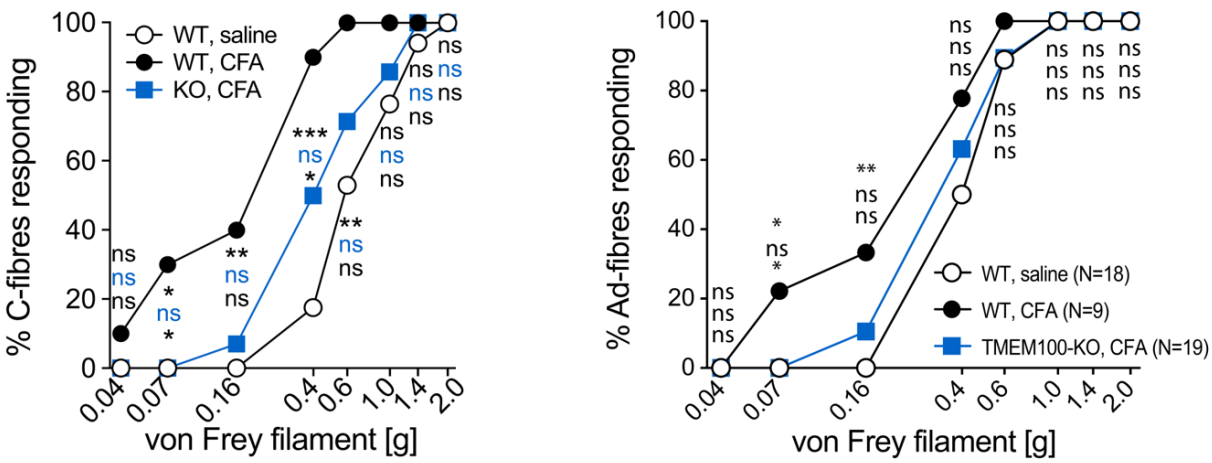

Figure 34 | Skin-nerve recordings of cutaneous nociceptors: response proportions
Comparison of response proportions (%) for C-fiber (**left**) and Aδ-fiber (**right**) nociceptors from WT and TMEM100 knockout (KO) animals, 3 days after injection with either saline or CFA into the knee joint, upon mechanical stimulation using specified von Frey filaments. Response proportions were determined from all C-fibers (left; same N-numbers as Figure 33b) and all Aδ-fibers (right; N-numbers provided in graph legends) gathered from 3 distinct mice per group. Pairwise comparisons were conducted using the two-sided Chi-square test. P-values (ns, P>0.05; *P<0.05; **P<0.01; ***P<0.001) are displayed adjacent to graph symbols and pertain to: WT-saline vs. WT-CFA (top, black), WT-saline vs. TMEM100KO-CFA (middle, blue), and WT-CFA vs. TMEM100KO (bottom, black). CFA, Complete Freund's Adjuvant; ns, not significant, WT, wildtype. Adapted from Nees et al. 2023.

In addition to the assessment of von Frey thresholds, the impact of CFA-treatment on the supra-threshold firing patterns exhibited by cutaneous C- and Aδ-fiber nociceptors was investigated. To accomplish this objective, a sequence of ramp-and-hold mechanical stimuli, progressively increasing in magnitude, was administered to the receptive fields through the utilization of a piezoelectric micromanipulator. These experimental endeavors revealed a noteworthy observation: cutaneous C-fibers derived from CFA-treated mice exhibited a significantly augmented occurrence of action potentials in response to suprathreshold mechanical stimuli, as depicted in **Figure 35a**.

Aδ-fiber nociceptors similarly displayed a propensity toward elevated firing rates; however, this increase attained statistical significance solely in the context of the most robustly applied stimulus, as delineated in **Figure 35b**. Remarkably, in TMEM100KO mice, both the mechanical activation thresholds and firing rates exhibited by C-fiber nociceptors and Aδ-fiber nociceptors after CFA treatment were found to be indiscernible when compared to their counterparts in saline-treated WT control mice.

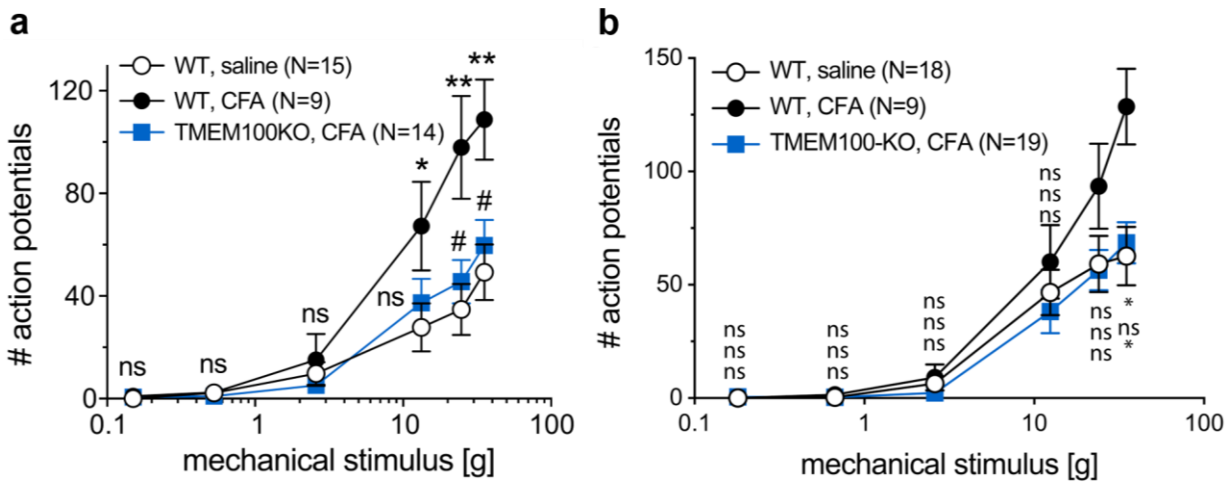

Figure 35 | Skin-nerve recordings of cutaneous nociceptors: action potentials The firing rates (quantified as the number of action potentials) of cutaneous (**a**) C-fiber and (**b**) Aδ-fiber nociceptors are compared in response to a sequence of ramp-and-hold stimuli with incrementally increasing amplitudes. These stimuli applied specific forces to the receptive fields 3 days post-injection of saline or Complete Freund's Adjuvant (CFA) into the knee joint of either wildtype (WT) or TMEM100 knockout (KO) mice. Symbols represent the mean ± SEM of the action potentials, with the associated P-values and sample sizes (N-numbers) detailed adjacent to the symbols within the graph. For (**a**): WT-saline vs. WT-CFA distinctions are *P<0.05 and **P<0.01; whereas WT-CFA vs. TMEM100KO-CFA is denoted by #P<0.05. For (**b**): comparisons are designated as ns (not significant, P>0.05) and * (P<0.05), referencing, from top to bottom, WT-saline vs. WT-CFA, WT-saline vs. TMEM100-KO CFA, and WT-CFA vs. TMEM100-KO CFA, respectively. Adapted from Nees et al. 2023.

Example traces of mechanically-evoked action potentials recorded from single C-fiber nociceptors from the tibial nerve of WT an TMEM100KO mice 3 days post saline and CFA knee joint injections are shown in **Figure 36**.

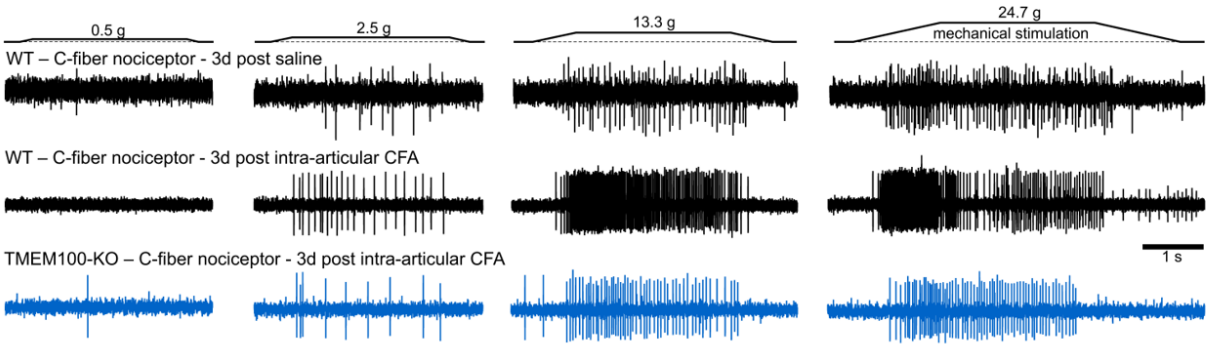

Figure 36 | Skin-nerve recordings from C-fibers: example traces of action potentials Illustrated are representative traces of mechanically-evoked action potentials sourced from individual C-fiber nociceptors within the tibial nerve of wildtype (WT) mice. These recordings were taken 3 days following intraarticular injections of saline (top) and Complete Freund's Adjuvant (CFA) (middle) into the knee joint. Additionally, recordings from TMEM100 knockout (KO) mice 3 days post-CFA injection are depicted (bottom). Adapted from Nees et al. 2023.

Example traces of mechanically-evoked action potentials recorded from single Aδ-fiber nociceptors from the tibial nerve of WT an TMEM100KO mice 3 days post saline and CFA knee joint injections are shown in **Figure 37**.

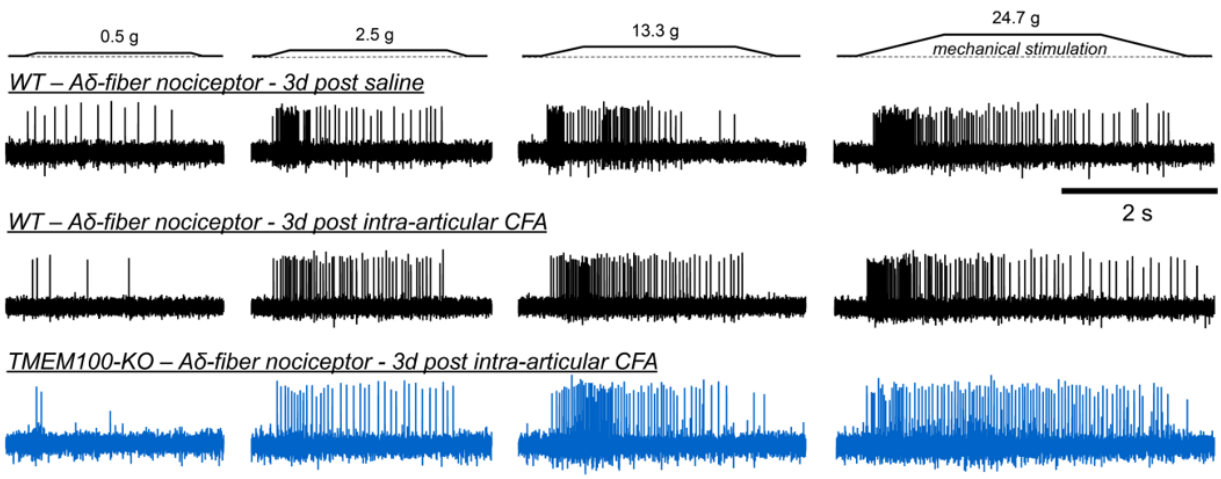

Figure 37 | Skin-nerve recordings from Adelta-fibers: example traces of action potentials
Illustrated are representative traces of mechanically-evoked action potentials sourced from individual Aδ-fiber nociceptors within the tibial nerve of wildtype (WT) mice. These recordings were taken 3 days following intraarticular injections of saline (top) and Complete Freund's Adjuvant (CFA) (middle) into the knee joint. Additionally, recordings from TMEM100 knockout (KO) mice 3 days post-CFA injection are depicted (bottom). Adapted from Nees et al. 2023.

In summary, these findings demonstrate that the knee joint inflammation induced by CFA has the effect of altering the mechanosensitivity of a substantial subset of cutaneous C-fiber nociceptors, rendering them responsive to innocuous mechanical stimuli. This alteration in mechanosensitivity is further associated with a leftward shift in paw withdrawal thresholds within the same group of mice. Consequently, it implies that the sensitization of both cutaneous C-fiber and Aδ-fiber nociceptors plays a contributory role in the development of secondary mechanical hypersensitivity in the hindpaw resulting from knee joint inflammation.

3.10 Overexpression of TMEM100 in knee joint afferents

The noteworthy observation that the prevention of long-lasting secondary mechanical hypersensitivity is achieved by inhibiting the un-silencing of MIAs through TMEM100 knockout suggests a potential pivotal role of MIAs in inducing secondary mechanical hypersensitivity. To rigorously examine this hypothesis, it became necessary to activate MIAs without provoking an inflammatory response. Consequently, a selective overexpression of TMEM100 within knee joint afferents was pursued through intra-articular injection of an AAV-PHP.S-TMEM100-Ires-dsRed viral

vector (30 µl, titer: 1.5E+11 viral genomes; as depicted in **Figure 38**). After a period of four days post virus injection to facilitate viral expression, a total of 339 ± 7 neurons within the ipsilateral L3 and L4 DRG exhibited prominent dsRed fluorescence. Notably, the concurrent presence of dsRed fluorescence signals, due to the coupling of TMEM100 and dsRed via an IRES cassette, serves as an indicator of TMEM100 overexpression.

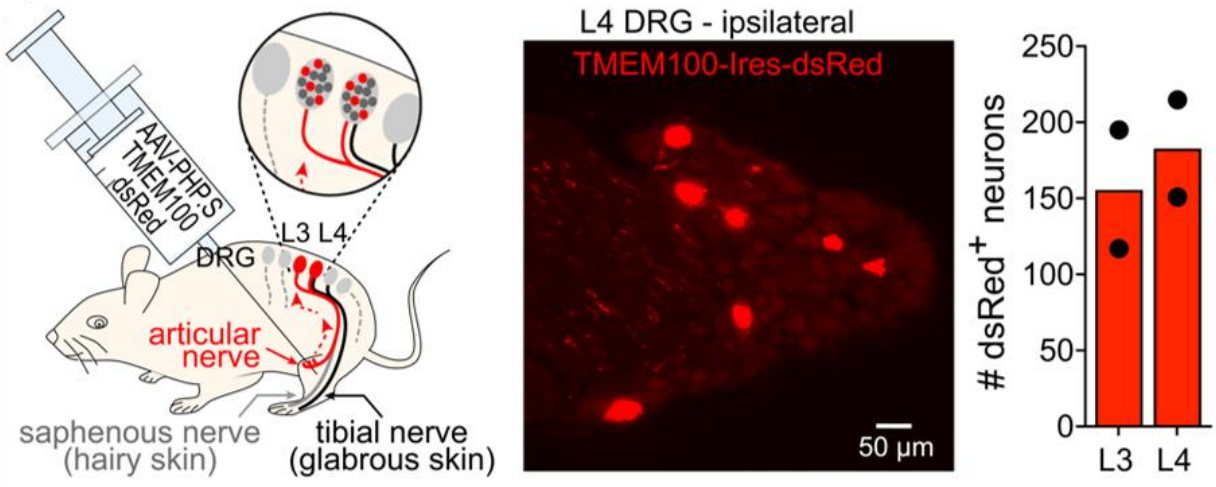

Figure 38 | TMEM100 Overexpression in mouse knee joint afferents mediated by AAV-PHP.S
Left: Schematic illustration of the experimental setup, depicting intra-articular injection of AAV-PHP.S vectors into the mouse knee joint. **Middle**: Representative micrograph of a dorsal root ganglion (DRG) section from a mouse following intra-articular injection with AAV-PHP.S-TMEM100-IRES-dsRed. **Right**: Bar graph showing the quantification of the mean ± SEM of dsRed⁺ neurons in L3 and L4 DRG, with individual data points from two mice represented by black dots. Adapted from Nees et al. 2023.

It is noteworthy that an abundance of nerve fibers within the saphenous nerve, proximal to the knee, including the medial articular nerve, displayed dsRed expression. The medial articular nerve plays a pivotal role in innervating the knee joint and is historically recognized as the nerve in which silent nociceptors were initially described (Schaible and Schmidt 1988). Conversely, within the tibial nerve distal to the knee joint, which primarily harbors cutaneous afferents responsible for innervating the plantar surface of the hind paw, only scarce dsRed⁺ fibers were discernible. Therefore, the intraarticular administration of AAV-PHP.S-TMEM100-Ires-dsRed results in the

selective overexpression of TMEM100 within knee joint afferents while not affecting afferent neurons responsible for innervating the plantar surface of the hind paw.

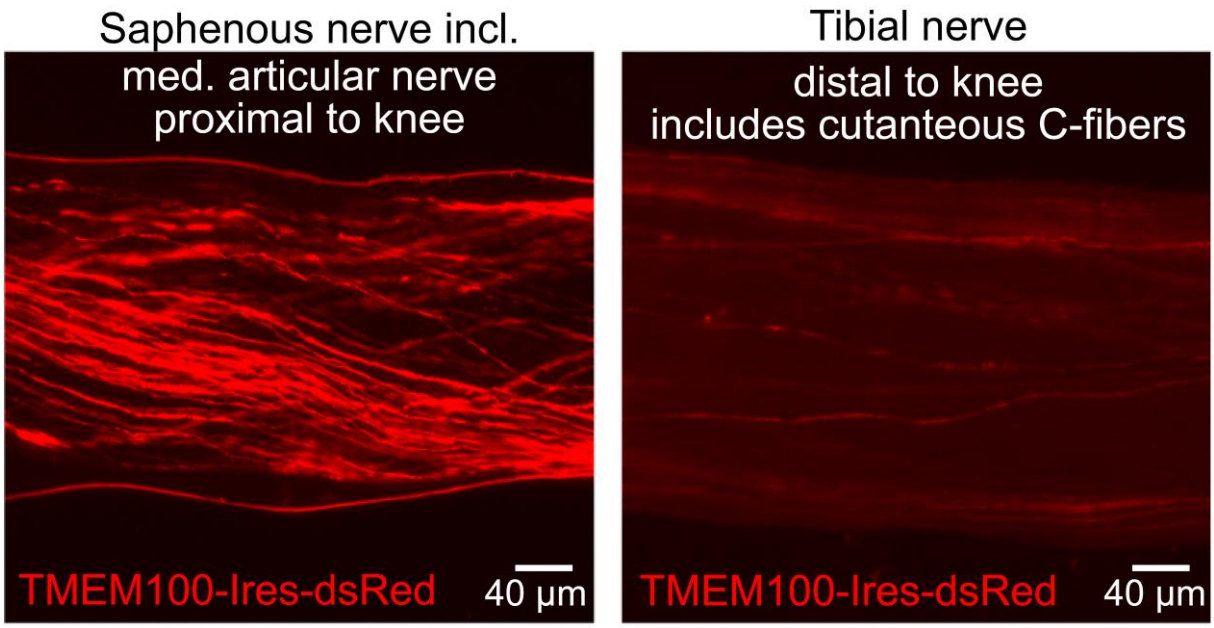

Figure 39 | Selective TMEM100 overexpression in knee joint afferents
Representative micrographs of nerve sections following intraarticular knee joint injection with AAV-PHP.S-TMEM100-IRES-dsRed. **Left**: the saphenous nerve, including the medial articular nerve proximal to the knee joint, shows pronounced dsRed fluorescence across numerous nerve fibers, denoting significant TMEM100 overexpression. **Right**: In contrast, the tibial nerve distal to the knee joint displays sparse dsRed-positive fibers, reflecting minimal to negligible gene expression in cutaneous fibers innervating the hindpaw. Adapted from Nees et al. 2023.

In order to evaluate whether the targeted overexpression of TMEM100 in neurons innervating the knee joint, in the absence of inducing knee joint inflammation, results in behavioral alterations, a comprehensive assessment of pain-related behavior was conducted. This assessment encompassed a battery of behavioral tests, including gait analysis, the von Frey test, and monitoring of homecage behavior. Interestingly, the behavioral characterization revealed that mice overexpressing TMEM100 exhibited a normal gait pattern in the CatWalk XT analysis, with no discernible alterations in stand time or swing speed of the leg when compared to mice that had received an injection of a control virus (AAV-PHP.S-dsRed).

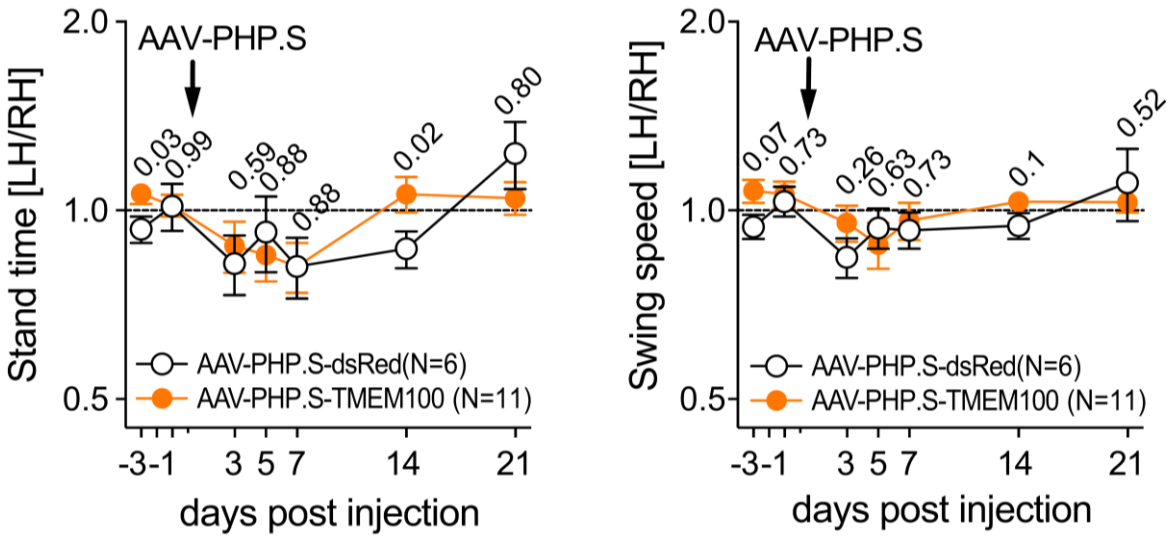

Figure 40 | Gait analysis after AAV-PHP.S injections into mouse knee joints

Assessment of gait dynamics in wildtype mice post intraarticular injection with either AAV-PHP.S-dsRed control virus (white circles) or AAV-PHP.S-TMEM100-IRES-dsRed (orange circles). Stand time (**left**) and swing speed ratios (**right**) for both left (LH) and right hind limbs (RH) are depicted as ratios (LH/RH). Symbols represent the mean ± SEM. Statistical comparisons were performed using multiple two-sided Mann-Whitney tests, with P-values and sample sizes (N) detailed adjacent to the symbols and in the legend of the graph. Adapted from Nees et al. 2023.

Strikingly, it is noteworthy that these TMEM100-overexpressing mice exhibited a pronounced onset of mechanical hypersensitivity in the ipsilateral hind paw five days following AAV injection. This hypersensitivity persisted until the conclusion of the observation period at 21 dpi, as illustrated in **Figure 41**. Specifically, the mechanical paw withdrawal thresholds decreased from an initial value of 0.92 ± 0.066 g at baseline prior to AAV-injections (-1 dpi) to 0.373 ± 0.035 g at 14 dpi. It is important to underscore that mice that received an injection of a control virus lacking TMEM100 (AAV-PHP.S-dsRed) did not manifest any indications of mechanical hypersensitivity.

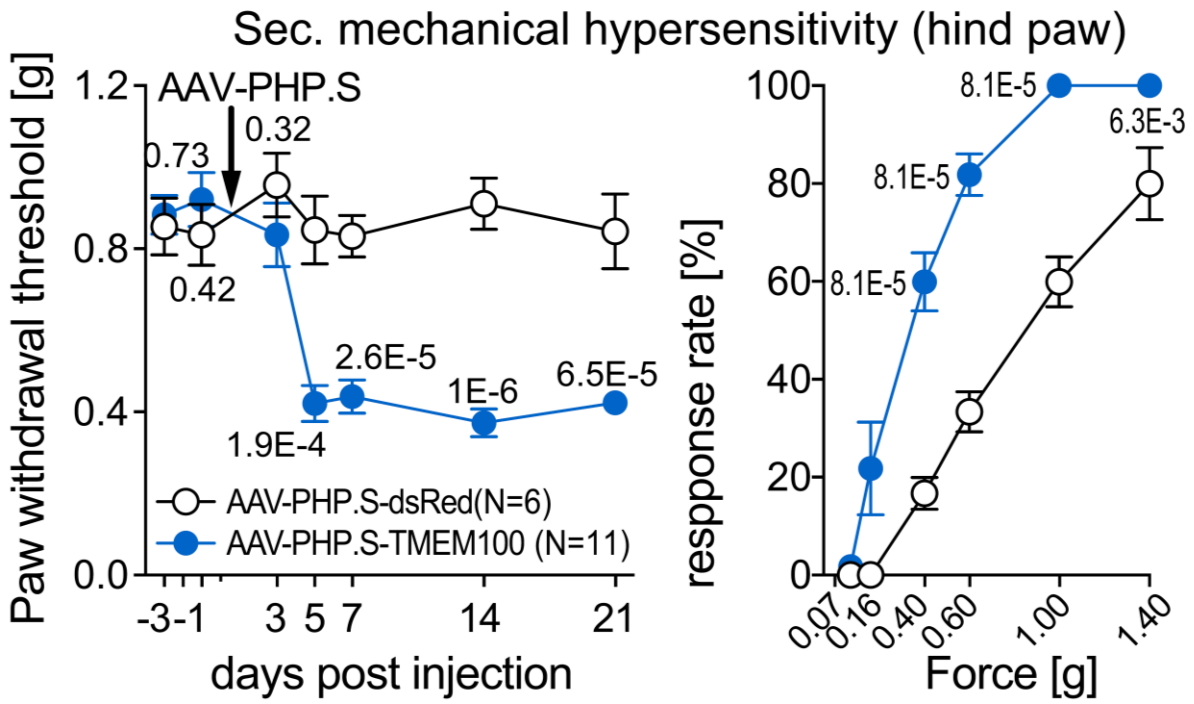

Figure 41 | Mechanical sensitivity after AAV-PHP.S injections into mouse knee joints
Evaluation of mechanical hindpaw sensitivity in the wildtype mice from Figure 40 following intraarticular injections of AAV-PHP.S constructs. **Left**: Dynamics of mechanical paw withdrawal threshold (mean ± SEM) over time post-injection with either AAV-PHP.S-dsRed control virus (white circles) or AAV-PHP.S-TMEM100-IRES-dsRed (blue circles). **Right**: Percentage of responses to mechanical stimuli using von Frey filaments at 14 days post-injection (dpi), represented as the percentage of paw withdrawals upon five consecutive stimulations (% response rate) for each treatment group. Statistical significance was assessed using two-sided Mann-Whitney tests, with P-values annotated beside the symbols; the number of animals tested is consistent across both panels and specified in the figure legend of the left panel. Adapted from Nees et al. 2023.

Additional behaviors potentially associated with pain were assessed using the LABORAS system. However, significant differences between TMEM100-overexpressing mice and the control group were not detected. The administration of AAV injections, both with and without TMEM100, did not result in any notable changes in the distance traveled or the frequencies of drinking, grooming, and rearing behaviors. This observation held true when comparing the control group to the TMEM100-overexpression group, as well as when examining data within each group before and after the AAV injection at 18 dpi (**Figure 42**).

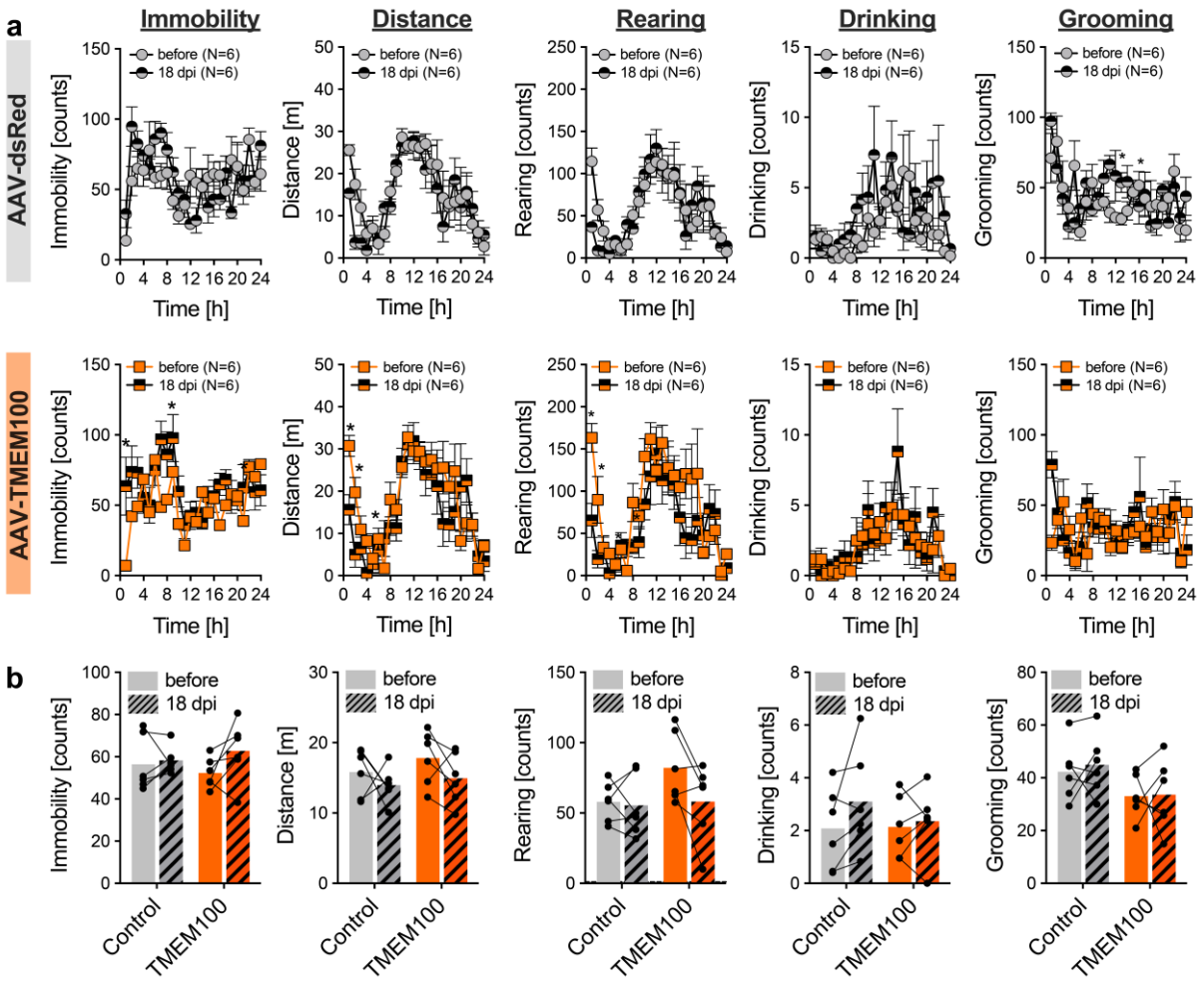

Figure 42 | Homecage behavior of WT mice after AAV-PHP.S knee joint injection

This figure illustrates the homecage activities of WT mice before and 18 days following intraarticular injection of AAV-PHP.S constructs. (**a**) The graph depicts the hourly mean ± SEM counts for behaviors such as immobility, rearing, drinking, grooming, and distance traveled in meters (m), monitored over a 24-hour cycle. Top panels compare control group behaviors pre-injection (gray circles) and 18 days post-injection (dpi; gray/black circles) with AAV-PHP.S-dsRed control virus. Bottom panels contrast behaviors of the treatment group pre-injection (orange squares) and 18 dpi with AAV-PHP.S-TMEM100-IRES-dsRed (orange/black squares). Behavioral changes were statistically evaluated at each time point using two-sided Mann-Whitney tests (*, P<0.05). The sample sizes (N) are indicated in the figure legends. (**b**) Bar graphs summarize daily averages for immobility, rearing, drinking, grooming, and traveled distance pre-injection (solid bars) and at 18 dpi (hatched bars) for both AAV-PHP.S-dsRed control (gray) and AAV-PHP.S-TMEM100-IRES-dsRed (orange) injections. Two-sided paired Student's t-tests were conducted (control N=6, treatment N=6), showing no significant differences. Adapted from Nees et al. 2023.

To investigate whether there exists an electrophysiological correlation with the mechanical hypersensitivity observed in the plantar surface of the hindpaw of mice

overexpressing TMEM100 in knee joint afferents, single-unit action potential recordings from a tibial nerve glabrous skin preparation were conducted. **Figure 43** depicts representative traces of mechanically-evoked action potentials from cutaneous C-fiber nociceptors in the tibial nerve for both the AAV-PHP.s-dsRed and AAV-PHP.s-TMEM100 groups.

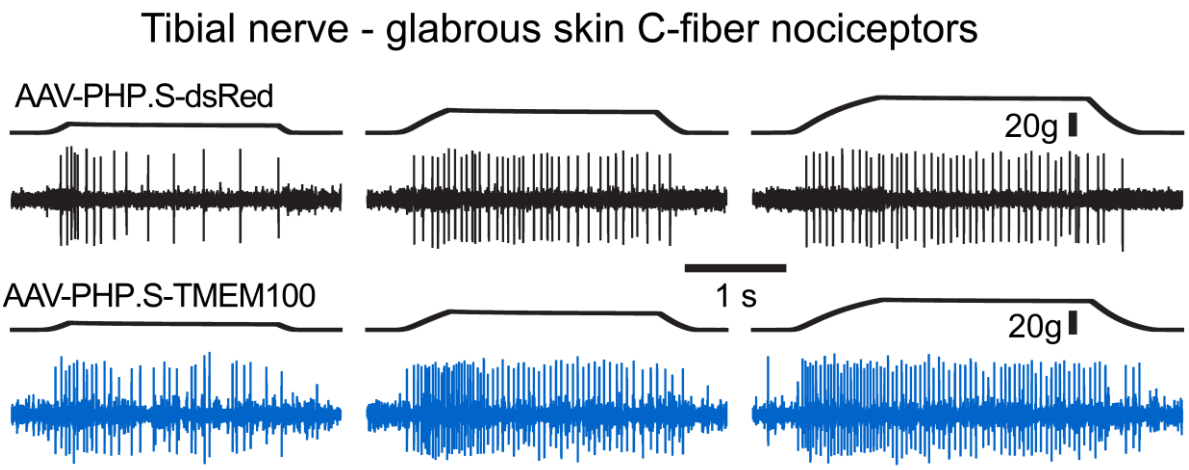

Figure 43 | Example traces of cutaneous C-fiber nociceptors after AAV-PHP.S injections
Representative traces show mechanically-evoked action potentials from cutaneous C-fiber nociceptors in the tibial nerve following AAV-PHP.S injections into knee joints of wildtype mice. Control mice (top trace, AAV-PHP.S-dsRed) are compared with mice overexpressing TMEM100 in articular afferents (bottom trace, AAV-PHP.S-TMEM100-Ires-dsRed). Adapted from Nees et al. 2023.

Remarkably, the recordings demonstrated that cutaneous C-fiber nociceptors generated approximately twice the number of action potentials in response to supra-threshold stimuli in TMEM100 overexpressing mice compared to those administered with a control virus injection. Additionally, these nociceptors showed significantly lower von Frey thresholds when TMEM100 was overexpressed in knee joint afferents (**Figure 44**).

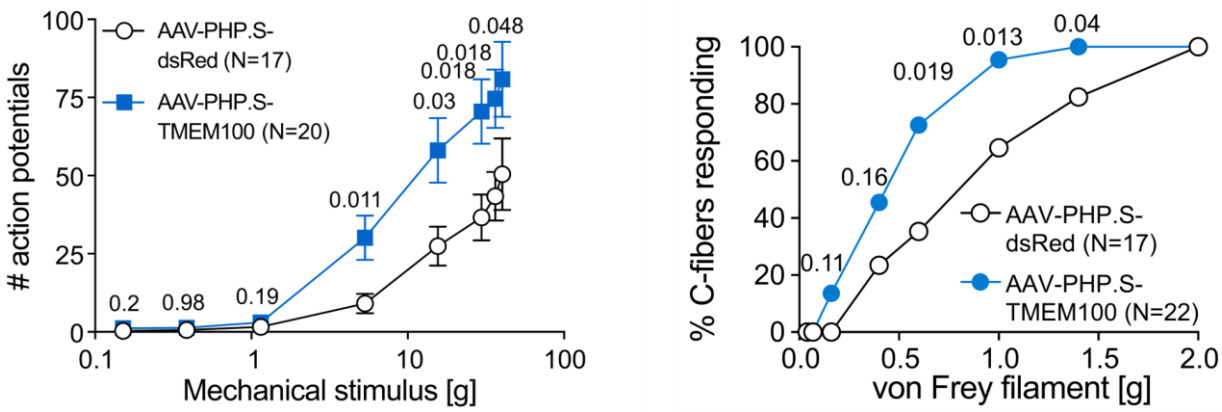

Figure 44 | Sensitization of cutaneous C-fiber nociceptors after TMEM100 overexpression
Left: The chart compares firing rates of cutaneous C-fiber nociceptors triggered by ramp-and-hold stimuli exerting specific forces on receptive fields in mice following knee joint injections with either AAV-PHP.S-dsRed control virus (white circles) or AAV-PHP.S-TMEM100-IRES-dsRed (blue circles). Symbols represent the mean ± SEM of action potential counts, with multiple two-sided Mann-Whitney tests used for analysis (exact P-values and N-numbers are indicated next to the symbols). **Right**: This panel shows the comparison of the percentage of C-fiber nociceptors that react to mechanical stimulation using designated von Frey filaments. Proportional comparisons were conducted with two-sided Chi-square tests, and exact P-values and N-numbers are provided alongside the symbols. Adapted from Nees et al. 2023.

Furthermore, akin to the effects observed with CFA treatment, the overexpression of TMEM100 within articular afferents was found to reduce the mechanical activation thresholds of cutaneous Aδ-fiber nociceptors while concurrently augmenting the action potential firing rate in response to suprathreshold stimuli (see **Figure 45**)

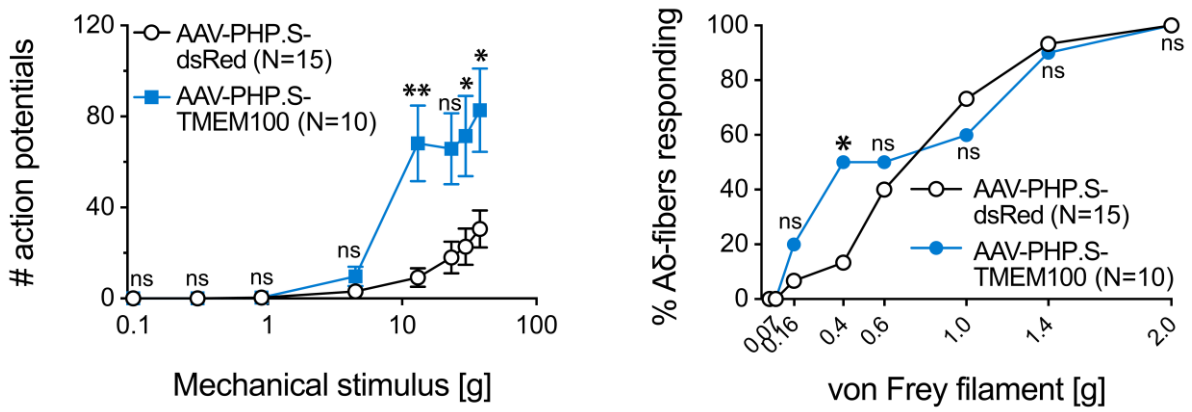

Figure 45 | Sensitization of cutaneous Ad-fiber nociceptors after TMEM100 overexpression
Left: Firing rates of Aδ-fiber nociceptors evoked by a series of ramp-and-hold stimuli with increasing amplitudes that exerted the indicated force to the receptive fields are compared post knee joint injection with either the control AAV-PHP.S-dsRed virus (white circles) or the AAV-PHP.S-TMEM100-IRES-dsRed (blue circles). Symbols represent the mean ± SEM numbers of action potentials, which were compared using multiple two-sided Mann-Whitney tests. P-values (ns, P>0.05; *, P<0.05) and N-numbers are annotated in the graph. **Right**: this graph compares the percentages (%) of Aδ-fiber nociceptors that react to mechanical stimulation via the specified von Frey filaments. Proportions were analyzed pairwise with two-sided Chi-square tests, and P-values (ns, P>0.05; *, P<0.05) along with sample sizes (N) are provided on the graph. Ns, not significant. Adapted from Nees et al. 2023.

In brief, the data presented herein illustrates that overexpression of TMEM100 alone, resulting in the activation of formerly quiescent MIAs, has the capability to initiate mechanical hypersensitivity in remote skin areas. This observation is further substantiated by the specific upregulation of TMEM100 in MIAs during the course of inflammation induced by CFA. Additionally, the exclusive abrogation of long-lasting secondary mechanical hypersensitivity following the knockout of TMEM100 strongly implicates sensory input from these unsilenced MIAs as the principal instigator in the initiation of secondary mechanical hypersensitivity, as illustrated in **Figure 46**.

4. DISCUSSION

The unique characteristics of MIAs have generated conjecture concerning their significant involvement in inflammatory pain since their initial documentation over three decades ago (Gold and Gebhart 2010; Michaelis et al. 1996; Schaible and Schmidt 1988). Nevertheless, neither the molecular mechanism governing their sensitization nor their precise physiological role in pain transmission has been comprehensively elucidated thus far.

Recent in-vitro investigations have unveiled that the inflammatory mediator NGF possesses the capacity to activate MIAs, with the mechanically-gated ion channel PIEZO2 serving as the mediator of NGF-induced mechanosensitivity in MIAs. Additionally, it has been experimentally demonstrated that the entire process, specifically the acquisition of mechanosensitivity in MIAs induced by NGF, necessitates de-novo gene transcription of a previously undefined protein (Prato et al. 2017).

The evidence presented in this thesis substantiates that TMEM100 experiences specific upregulation in CHRNA3-EGFP$^+$ MIAs during both in-vitro and in-vivo inflammatory conditions. Furthermore, my findings underscore that overexpression of TMEM100 alone is sufficient to activate MIAs, while the genetic deletion of TMEM100 impedes the activation of MIAs in a murine model of knee joint monoarthritis induced by CFA. Importantly, the data from this thesis suggests that the primary role of MIAs in pain signaling is to initiate secondary mechanical hypersensitivity.

Consequently, aligning with the objectives of this thesis, my results provide compelling evidence to address the hitherto unresolved questions regarding the physiological role and molecular mechanism of MIA activation. Specifically, this work has identified TMEM100 as an indispensable protein for the activation of MIAs, which is likely the previously undefined protein in question, and has shed light on the physiological role of MIAs, which appears to involve triggering the induction of secondary mechanical hypersensitivity. Therefore, the results of this thesis offer profound insights into MIAs and contribute to a more comprehensive understanding and elucidation of this distinctive nociceptor subpopulation.

4.1 The molecular mechanism of un-silencing MIAs

The results of this thesis unequivocally demonstrate the pivotal role of TMEM100 in the molecular cascade leading to the sensitization of MIAs. Transfection of CHRNA3-EGFP$^+$ cells, derived from primary DRG cultures, with a TMEM100 plasmid induced mechanosensitivity in otherwise mechanically insensitive afferents. Furthermore, in TMEM100KO mice, CFA-induced knee joint inflammation failed to sensitize MIAs, accompanied by a significant reduction in secondary mechanical hypersensitivity. Conversely, AAV-mediated overexpression of TMEM100 in primary sensory afferents innervating the knee joint led to the development of substantial secondary mechanical hypersensitivity, without inducing knee joint inflammation or primary joint pain. Additionally, the upregulation of TMEM100 during inflammation was specifically confined to the CHRNA3-EGFP$^+$ subpopulation of nociceptors and was not observed in other major nociceptor subsets, including IB4$^-$ C-fiber nociceptors. These nociceptors constitute a significant proportion of knee joint innervation, distinct from MIAs. Collectively, these data strongly indicate that TMEM100 is both necessary and sufficient to activate MIAs, both in vitro and in vivo.

To appreciate the significance of TMEM100's role in MIA activation, it is noteworthy that the expression of PIEZO2 remains unaltered during the inflammation-associated process of MIA un-silencing. PIEZO2 is the mechanically-gated ion channel that is responsible for mediating mechanosensitivity in sensitized MIAs. Prato and colleagues have reported that more than 90 % of CHRNA3-EGFP$^+$ neurons within knee joint innervating DRG express PIEZO2. Consequently, they convincingly demonstrated that NGF-induced mechanosensitivity in MIAs is mediated by PIEZO2, as pharmacological blockade of PIEZO2 currents hampers mechanotransduction currents in CHRNA3-EGFP$^+$ MIAs. Additionally, siRNA-mediated PIEZO2 knockdown impedes the acquisition of mechanosensitivity in this specific nociceptor subpopulation. (Prato et al. 2017). Interestingly, they have also shown that PIEZO2 exhibits high expression levels in CHRNA3-EGFP$^+$ MIAs, while none of the other candidate mechanotransduction genes are expressed at significant levels. More importantly, NGF exposure does not induce any changes in either PIEZO2 mRNA levels or the expression levels of other putative mechanotransduction genes present in MIAs. This observation is corroborated by the RNAseq analysis presented in this thesis. In this analysis, PIEZO2, along with virtually all ion channels known to be mechanically-gated, including TRPA1, does not

exhibit expression changes upon exposure to NGF. These findings suggest that the acquisition of mechanosensitivity in MIAs is mediated by functional changes in PIEZO2 channels, which are modulated independently of increasing PIEZO2 gene expression. Given that CHRNA3-EGFP$^+$ MIAs exhibit high PIEZO2 expression levels, even in situations where they lack mechanosensitivity, and considering that PIEZO2 operates normally without reliance on an auxiliary subunit, it was hypothesized that PIEZO2 is somehow maintained in a 'silent' state within these neurons under physiological conditions. Consequently, an examination of the RNAseq data was conducted to identify potential regulators of PIEZO2 that might impact its functional state during inflammation. This screening effort unveiled that CHRNA3-EGFP$^+$ MIAs express four known PIEZO2 modulators with inhibitory properties: Annexin A6 (Anxa6) (Raouf et al. 2018), MTMR2 (Narayanan et al. 2018), Nedd4-2 (Huo et al. 2021), and SERCA2 (Atp2a2) (Zhang et al. 2017). However, it is noteworthy that none of these PIEZO2 inhibitors demonstrated a down-regulation in response to NGF treatment, which could potentially result in disinhibition. Moreover, all four of these modulators have been reported to exhibit ubiquitous expression in sensory neurons (Zeisel et al. 2018). Consequently, it seems highly improbable that any of the known PIEZO2 inhibitors expressed in MIAs are involved in maintaining PIEZO2 in a quiescent state. Instead, the data imply that PIEZO2 is primed for activation through the upregulation of TMEM100 via an as-yet-undisclosed interaction. Therefore, while the data presented identify TMEM100 as a critical protein, both necessary and sufficient for the activation of MIAs, the exact mechanism by which it maintains PIEZO2 in an inactive state within CHRNA3-EGFP$^+$ MIAs is still unclear. This gap in our understanding underscores the urgent need for further research in this area.

4.2 TMEM100 and its role in pain signaling

Tmem100 is a protein-coding gene that exhibits a high degree of conservation across vertebrate species, including zebrafish, xenopus, chicken, and mammals such as mice and humans. It encodes a 134-amino acid, two-transmembrane protein bearing the same name. Importantly, TMEM100 positions its N and C termini on the intracellular facet of the plasma membrane, facilitating interactions with other proteins.

TMEM100 was initially documented as a transcript within the mouse genome (Kawai et al. 2001). The expression of TMEM100 has been reported in various tissues, extending beyond the DRG. These tissues include embryonic vasculature, enteric nerves, lung, prostate, and kidney tissues in both humans and mice (Eisenman et al. 2013; Georgas et al. 2009; Moon et al. 2010; Somekawa et al. 2012; van der Heul-Nieuwenhuijsen et al. 2006). TMEM100 has been implicated in several biological processes, including vascular morphogenesis, angiogenesis, lung and renal development, lung cancer cell invasiveness, and colorectal and prostate cancer. Nevertheless, the functional role of TMEM100 and the signaling pathways through which it operates remain largely uncharacterized. (Georgas et al. 2009; Hong et al. 2022; Karolak et al. 2022; Moon et al. 2010; Ye et al. 2023; Zheng et al. 2022). The involvement of TMEM100 in pain signaling has been the subject of only a handful of studies to date. The prevailing body of literature, albeit limited, indicates that TMEM100 expression in nociceptive neurons is influenced by the specific pain pathology. Noteworthily, inflammatory pain conditions seem to elevate TMEM100 expression, while neuropathic pain is linked to a decrease in TMEM100 expression within DRG neurons (Chung et al. 2016; Weng et al. 2015; Yu et al. 2019). Specifically, TMEM100 is predominantly found in $CGRP^+$ peptidergic neurons of dorsal root and trigeminal ganglia in both mice and rats. Its expression notably surges during inflammatory conditions such as CFA-induced inflammation of the masseter muscle or hindpaw (Chung et al. 2016; Yu et al. 2019). In contrast, neuropathic pain mouse models, encompassing chronic constriction injury, tibial nerve injury, spared nerve injury, and spinal nerve ligation, showed a marked decline in TMEM100 expression in the affected DRG (Yu et al. 2019). Given its variable expression based on the pain pathology, TMEM100 has been put forth as a potential modulator of pain signaling. However, the intricacies of its regulatory mechanisms remain largely uncharted. In neuropathic pain models, where a decline in TMEM100 expression coincides with the onset of painful neuropathies, the restoration of TMEM100 expression via AAV led to diminished pain behavior. This restoration was also paired with an inhibition of inflammatory cell activation and mediators. For instance, reinstating TMEM100 expression in neuropathic pain-affected mice attenuated the activation of glial cells, including microglia and astrocytes, and inflammatory mediators such as TNF-α, IL-6, and IL-1β. These observations bolster the idea that TMEM100 modulates neuropathic pain conditions by suppressing the expression of specific cellular and molecular

inflammatory factors (Cui et al. 2023). Corroborating this, associations between TMEM100 and the inflammatory mediator IL-6 were identified in a rat model of lumbar discogenic pain (Guo et al. 2023). In summation, while existing literature emphasizes TMEM100's significant regulatory role in pain signaling, a comprehensive understanding of the mechanisms by which TMEM100 influences pain transmission remains to be uncovered. Weng and colleagues spearheaded, to our knowledge, the seminal study illuminating the mechanistic interplay between TMEM100 and pain-transducing channels in nociceptors. Their findings revealed that TMEM100 is manifested in peptidergic sensory neurons. Intriguingly, a substantial fraction of these neurons concurrently express two pivotal ion channels - TRPA1 and TRPV1 - renowned for their roles in pain signaling. Within these neurons, TMEM100 seems to function as a transmembrane adaptor protein, orchestrating both the functional dynamics and direct interplay between TRPA1 and TRPV1 (Weng et al. 2015). Weyer and Stucky have previously underscored the importance of the interactions between TRPA1 and TRPV1 in determining their functional activity. Targeting the mutual interaction between these proteins could represent a promising strategy for influencing their activity (Weyer and Stucky 2015). Although some studies have explored the signaling pathway interactions between TRPA1 and TRPV1 (Akopian 2011), recent research emphasizes a direct physical interaction between them, notably through heteromer formation. These heteromers bestow unique properties onto native sensory neurons (Fischer et al. 2014; Salas et al. 2009; Staruschenko et al. 2010). Consequently, targeting the genesis of TRPA1-TRPV1 heteromers or their interrelations in these complexes emerges as a novel approach in mitigating TRP-mediated pain (Weyer and Stucky). Weng et al.'s research reveals that without TMEM100, TRPV1 tightly binds with TRPA1, significantly inhibiting TRPA1's response to its agonist, mustard oil, while leaving TRPV1's response to capsaicin unaffected. When TMEM100 is present, the interaction between TRPA1 and TRPV1 weakens, lessening the inhibition of TRPA1 and enhancing its responsiveness to chemical agonists. This study emphasizes that a specific KRR motif in the C terminus of TMEM100 is crucial for regulating this interaction. Altering just these three amino acids intensifies the inhibition of TRPA1 by TRPV1, indicating that modifications to this small segment in TMEM100's C terminus introduce a new method of TRPA1 inhibition (Weng et al. 2015). Consistent with in-vitro findings, mice with a sensory neuron-specific TMEM100 knockout display notable decreases in mechanical pain behavior post CFA-

induced inflammation and following TRPA1-linked nociception due to mustard oil injections. However, the pain behavior dependent on TRPV1, triggered by capsaicin injections, remains unchanged. Moreover, administering a cell-permeable peptide derived from the mutated C terminus of TMEM100 has been observed to mitigate pain behaviors to some extent (Weng et al. 2015). Taken together, Weng and colleagues presented robust evidence indicating that TMEM100 significantly influences pain signaling by augmenting TRPA1 activity in a TRPV1-dependent fashion. Coupled with abundant data underscoring TRPA1's role in refining the mechanosensitivity of sensory afferents, these findings fueled my interest in TMEM100. This interest was further piqued upon observing the RNAseq results, which showcased notable NGF-induced TMEM100 upregulation selectively in the MIA subpopulation. Indeed, studies have demonstrated that both pharmacological inhibition and genetic deletion of TRPA1 lead to a partial suppression of mechanotransduction currents in cultured DRG neurons, alongside a reduction in the firing rate of cutaneous C-fiber nociceptor (Brierley et al. 2011; Garrison and Stucky 2014; Kerstein et al. 2009; Vilceanu and Stucky 2010). Specifically, using an ex-vivo skin nerve preparation, mechanical firing in C-fiber nociceptors is notably impeded when TRPA1 is pharmacologically blocked with a selective antagonist (Kerstein et al. 2009). Furthermore, TRPA1 seems pivotal for typical behavioral and afferent reactions to mechanical stimuli. It is also implicated in the onset of CFA-induced mechanical hypersensitivity in an age-dependent manner. Strikingly, aged TRPA1-deficient mice (24 months old) did not exhibit mechanical sensitization of nociceptors or heightened mechanical sensitivity. In contrast, young TRPA1-deficient mice (3 months old) manifested a delayed yet pronounced mechanical hypersensitivity. This was coupled with a significant increase in mechanical responses in C-fibers post-CFA injection into the plantar hindpaw (Garrison and Stucky 2014). Consistent with these observations, the absence of TRPA1 markedly decreased the amplitudes of intermediately adapting mechanically activated currents in small-diameter neurons from short-term DRG cultures. Conversely, overexpressing TRPA1 augmented the amplitude in this specific neuronal subgroup. These results reinforce the notion that TRPA1 plays a pivotal role in regular nociceptor mechanosensation. Furthermore, they imply that TRPA1 can modulate neuronal mechanosensitivity based on its level of activation or expression (Brierley et al. 2011). A subsequent study, utilizing both genetic and pharmacological methodologies, further supports the idea that TRPA1 modulates mechanically activated currents in small-diameter neurons

derived from adult DRG. Notably, these neurons were identified as being IB4-negative (Vilceanu and Stucky 2010). Collectively, the data strongly suggest TRPA1's role in adjusting the mechanosensitivity of sensory afferents. Yet, according to contemporary studies, TRPA1 does not respond directly to mechanical indentation of the cell membrane. Instead, it is believed to be primarily gated by intracellular calcium via an EF-hand motif (Zurborg et al. 2007). This leads to the hypothesis that TRPA1 may enhance PIEZO2-facilitated Ca^{2+} influx, thus elevating mechanosensitivity in sensory neurons. Echoing the findings of Weng and colleagues, this dissertation presents data illustrating that inflammation in the knee joint, induced by CFA, bolsters TRPA1 activity, contingent upon TMEM100. These insights not only corroborate but also build on the work of Weng et al. (Weng et al. 2015), showing that TMEM100 upregulation, particularly in the context of CFA-induced knee monoarthritis and following in-vitro NGF treatments, is specific to CHRNA3-EGFP^{+} neurons. This selective upregulation boosts TRPA1 activity exclusively in MIAs, bypassing other nociceptor subpopulations. In sum, the comprehensive analysis from this dissertation posits TMEM100 as a versatile protein. It seems to prime mechanosensitivity in MIAs by possibly engaging PIEZO2 via a yet-to-be-deciphered mechanism and further magnifies PIEZO2-related mechanosensitivity by liberating TRPA1 from TRPV1-induced suppression.

Importantly, the genetic deletion of TMEM100 did not impact basal mechanosensitivity or thermal sensitivity, corroborating the observations made by Weng and colleagues (Weng et al. 2015). Given that undesirable thermoregulatory effects and diminished normal noxious sensations were primary concerns leading to the failure of TRPA1 and TRPV1 inhibitors in clinical trials (Kaneko and Szallasi 2014), these findings underscore the potential of TMEM100 as an efficacious therapeutic target for mitigating mechanical pain.

It is worth noting that various findings from the calcium imaging experiments, which were conducted to assess TRPA1 activity in MIAs in relation to TMEM100 presence and CFA-induced sensitization, deserve particular attention. Firstly, MIAs derived from saline-administered TMEM100KO mice already show amplified AITC-induced responses in comparison to those from saline-treated WT counterparts. Interestingly, the fraction of CHRNA3-EGFP^{+} neurons responsive to AITC significantly escalates post-CFA treatment in WT mice, but this trend is absent in TMEM100KO mice. When comparing CFA-treated WT mice, they have a notably higher percentage of AITC-

responders than any other groups or genotypes. Furthermore, the ratios of AITC-responding neurons among CFA-treated TMEM100KO mice, saline-injected TMEM100KO mice, and saline-administered WT mice remain statistically indistinguishable. As a result, the surge in the percentage of AITC-sensitive neurons (observed as an increase from 8 % in saline-treated WT mice to 41 % in CFA-treated WT mice) appears to exert a more pronounced effect on pain sensitivity than the minor enhancement in the response intensity of individual neurons.

4.3 The physiological role of MIAs in pain signaling

The unique characteristics of MIAs have intrigued researchers for over three decades since their initial discovery, leading many to speculate about their significant role in inflammatory pain. A prevailing hypothesis suggests that the activation of MIAs during inflammation markedly elevates nociceptive signaling to the spinal cord. This heightened input is believed to bolster central pain processing, resulting in amplified pain sensation at the affected area. However, diverging from this prevailing view, findings from this thesis crucially reveal that MIAs primarily serve to trigger the induction of secondary mechanical hypersensitivity.

Pain hypersensitivity typically presents as primary hypersensitivity, characterized as either hyperalgesia or allodynia. Primary hypersensitivity, by definition, is limited to the site of inflammation. It is postulated to be a consequence of peripheral sensitization, specifically the direct sensitization of nerve endings in the inflamed tissue. As the underlying cause of pain is addressed, this primary hypersensitivity typically diminishes. However, beyond this, many patients experience secondary pain hypersensitivity which extends outside the initial inflammation or injury area, encompassing both mechanical and thermal sensations. Notably, even after the primary pain source has abated, this secondary hypersensitivity often remains. Clinical studies suggest a correlation between the extent and severity of this secondary pain hypersensitivity and the risk of evolving into chronic pain (Richebé et al. 2018). Secondary pain hypersensitivity has been observed in several painful disorders in humans as well as in rodent models of pain including experimental arthritis (Eitner et al. 2017; Sandkühler 2009). Contrary to primary pain hypersensitivity, secondary pain

hypersensitivity is widely recognized not to originate from the sensitization of nociceptive nerve endings, but is instead thought to mainly stem from central sensitization. Central sensitization involves changes in the sensory information processing within the central nervous system, spanning both spinal and supraspinal levels, leading nociceptive neurons to become hyperexcitable. Such alterations amplify nociceptive processing. Notably, the induction of secondary pain hypersensitivity – a hallmark of central sensitization – necessitates activity from peripheral nociceptive fibers. However, its maintenance is independent of ongoing afferent input. In fact, applying an anesthetic block to the injured site can preemptively halt its onset, but it cannot reverse pre-established secondary hyperalgesia (Sandkühler 2009). Indeed, patients with end-stage osteoarthritis present signs of central sensitization with widespread pain expanding beyond the arthritic joint and reduced pressure pain threshold in both subcutaneous and cutaneous structures along the entire leg (Eitner et al. 2017; Schaible 2012; Suokas et al. 2012). For instance, a meta-analysis highlighted that through quantitative sensory testing of pressure pain thresholds, individuals with osteoarthritis could be effectively differentiated from healthy controls. Specifically, patients with osteoarthritis exhibited significantly lower pressure pain thresholds at distant sites, suggestive of central sensitization (Suokas et al. 2012). Accordingly, various animal models of osteoarthritis, including the monosodium iodoacetate, medial meniscal destabilization, and transection of the medial collateral ligament models, further bolster the notion that secondary pain hypersensitivity can develop during the progression of osteoarthritis-associated joint inflammation (Bove et al. 2006; Malfait et al. 2010; Sagar et al. 2011). However, the precise mechanisms underlying this central sensitization in osteoarthritis remain largely uncharted. Current research points to an increase in spinal neuropeptides like substance P and CGRP. Additionally, there are heightened levels of inflammatory mediators and excitatory neurotransmitters, such as bradykinin and glutamate, respectively, which contribute to spinal hyperexcitability (Eitner et al. 2017; Im et al. 2010; Puttfarcken et al. 2010). Another contributing factor appears to be a diminished inhibitory input to the spinal pain processing network from descending pathways, as implicated in osteoarthritis-associated central sensitization (Rahman et al. 2009; Vanegas and Schaible 2004). Yet, the specific peripheral input that triggers central sensitization and consequently results in secondary mechanical hypersensitivity remains to be identified.

The findings presented in this thesis shed light on the intricate relationships between the un-silencing of articular MIAs and the development of secondary mechanical hypersensitivity in distant skin regions. When TMEM100 is knocked out, thereby blocking the un-silencing of articular MIAs, it was observed that long-lasting secondary mechanical hypersensitivity in remote skin regions is inhibited. Notably, this does not impact pain in the direct region of CFA-induced inflammation. Furthermore, without the presence of inflammation or injury, TMEM100 overexpression-induced un-silencing of knee joint MIAs results in mechanical hypersensitivity in the paw. However, it does not precipitate pain hypersensitivity in the knee joint itself. Skin-nerve recordings provide further depth, showcasing that the sensitization of cutaneous C-fiber nociceptors, together with the previously discussed central sensitization, plays a role in fostering secondary mechanical hypersensitivity. Given that merely the un-silencing of knee joint MIAs via selective TMEM100 overexpression can instigate the sensitization of cutaneous afferents which project to distant skin regions, a hypothesis emerges. It posits that this sensitization is orchestrated by an unidentified mechanism, possibly a central one – such as interactions at the DRG or the spinal cord level (as theorized in **Figure 46**)

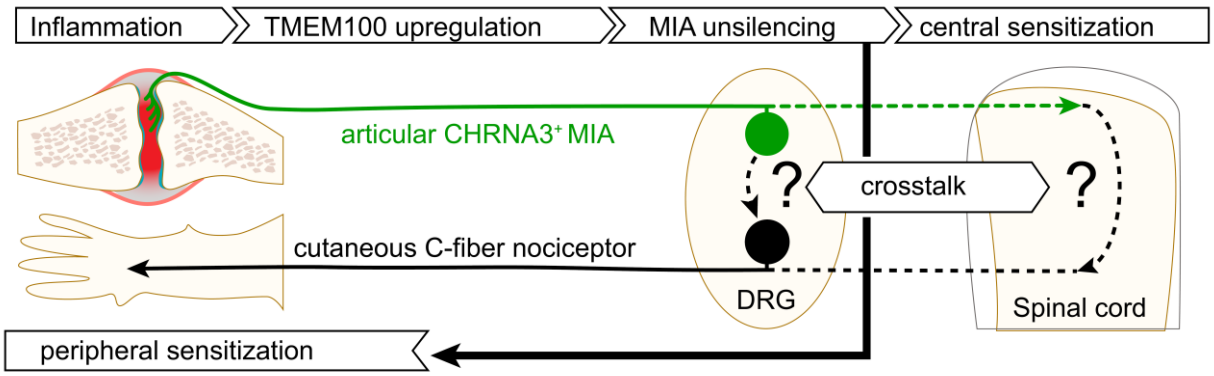

Figure 46 | Theoretical framework for MIA-induced secondary hypersensitivity

The schematic illustrates the proposed mechanisms by which activated mechanically insensitive afferents (MIA) trigger the onset of secondary hypersensitivity. Adapted from (Nees et al. 2023).

4.4 Interpretation of the behavioral data

It is crucial to highlight a key distinction from the study by Weng et al., which investigated pain responses over an acute timeframe of up to two days and documented only a partial reduction in primary mechanical hyperalgesia. In contrast, the present findings extend the observation period to three weeks post-injury. These data indicate a full reversal of secondary mechanical hypersensitivity just one week following CFA-induced knee joint inflammation. Consequently, this underscores the potential of targeting TMEM100 as a potent approach to manage secondary mechanical hypersensitivity. Furthermore, it suggests the promise of averting the onset of chronic pain syndromes by mitigating the activation of MIAs during inflammatory responses. It is noteworthy that elevated TMEM100 expression levels in MIAs from WT mice manifest solely during the acute inflammation phase (3 dpi) and are absent in the subacute phase (21 dpi). This suggests that, from a clinical standpoint, interventions targeting TMEM100 and hence MIAs are most beneficial when administered promptly after injury.

The observations indicating that TMEM100KO mice do not exhibit prolonged secondary mechanical hypersensitivity, combined with the fact that selective overexpression of TMEM100 in knee joint afferents triggers secondary hypersensitivity in the paw, unequivocally support the notion that CHRNA3-EGFP^{+} MIAs play a pivotal role in inflammation-induced knee joint pain. It is imperative to emphasize the nuance in terminology: the descriptor "secondary" should not be misconstrued as implying a lesser significance or intensity of pain relative to primary hypersensitivity. Instead, "secondary" delineates pain hypersensitivity manifesting outside the immediate zone of injury or inflammation. As highlighted earlier (see 4.3 The physiological role of MIAs in pain signaling), primary hypersensitivity is predominantly governed by peripheral mechanisms. This means it typically subsides concurrently with the resolving inflammation. In contrast, secondary hypersensitivity is rooted in neural plasticity within the spinal cord. It often lingers long after the initiating event, be it inflammation or injury, has abated. This protracted persistence is suspected to catalyze the progression from acute to chronic pain. To underscore this point, notable research has elucidated a robust correlation between the magnitude of secondary hyperalgesia and the propensity to develop chronic post-surgical pain (Richebé et al. 2018). Hence, delving

into the mechanisms triggering prolonged secondary mechanical hypersensitivity, which is the focus of this research, holds profound clinical implications.

Building on the previous discussion about TMEM100's role, it is pertinent to address potential limitations in this study (Nees et al. 2023). The interpretation of the behavioral data presupposes that the CatWalk XT gait analysis system predominantly measures primary knee joint pain. There may be contentions suggesting that pain localized to the paw can influence gait. Conversely, modifications in gait might not exclusively signify joint pain but could also be influenced by structural joint damage. However, two pivotal observations mitigate these concerns. Firstly, overexpression of TMEM100 significantly decreases paw withdrawal thresholds without influencing the CatWalk XT gait outcome. Secondly, the temporal progression of alterations in gait metrics and paw withdrawal thresholds is not synchronous. These points render it implausible that secondary mechanical hypersensitivity in the paw skews the CatWalk XT assay results. Additionally, the prospect of structural joint damage influencing our results appears remote, given that the deviations in gait and stride metrics are ephemeral and revert to baseline within a short span.

The results from the AAV-mediated TMEM100 overexpression experiments also warrant a nuanced interpretation. When administered intra-articularly, AAV-PHP.S affects all sensory afferent subclasses within the knee joint. Consequently, the manifested secondary mechanical hypersensitivity might, in theory, arise from TMEM100 overexpression in knee joint afferents beyond just CHRNA3-EGFP^{+} MIAs. It might even be attributable to non-neuronal cells, such as microglia and astrocytes, which have previously been identified as TMEM100 expressers (Cui et al. 2023). The current data set does not entirely negate this possibility. However, several observations counter this interpretation. First, if TMEM100 overexpression indeed sensitized non-MIA articular neurons, one would expect to detect primary knee joint pain in the CatWalk XT gait analysis alongside the noted secondary mechanical hypersensitivity. Such primary pain was conspicuously absent. Further strengthening this stance, TMEM100 expression was found to be singularly upregulated in MIAs during CFA-induced monoarthritis, and not within other major nociceptor subclasses innervating the knee joint. Moreover, TMEM100-deficient mice displayed functional shortcomings exclusively within MIAs and not in other articular nociceptors. These mice also specifically lost secondary mechanical hypersensitivity while retaining knee joint pain.

Collectively, these findings robustly underscore the pivotal role of MIAs in the genesis of secondary mechanical hypersensitivity.

4.5 Conclusion and future directions

In sum, the findings from my thesis provide a mechanistic model of inflammatory knee joint pain (Nees et al. 2023), suggesting that polymodal nociceptors are major contributors to primary hyperalgesia, while MIAs play a pivotal role in instigating secondary mechanical hypersensitivity. My investigations reveal that inflammation-induced upregulation of TMEM100 activates MIAs. This activation, through an as-yet unidentified central mechanism, results in sensitization of cutaneous nociceptors, leading to secondary mechanical hypersensitivity in skin areas distant from the inflammation site. While I have not directly probed whether MIA activation also incites central sensitization – a known factor in secondary mechanical hypersensitivity – the substantial reduction in paw withdrawal thresholds relative to the diminished mechanical activation thresholds of individual cutaneous C- and Aδ-fiber nociceptors suggests an alteration in the central processing of nociceptor input. This change implies that even subthreshold nociceptor stimuli might produce pain responses.

Further exploration is warranted to decipher the possible interactions at the level of the DRG or in the spinal cord that trigger secondary hypersensitivity downstream of inflammation-induced MIA activation. Such interactions are suspected to initiate both the sensitization of cutaneous C-fiber nociceptors as well as the sensitization of neural circuits in the dorsal horn that process sensory input from cutaneous sensory afferents. Accordingly, future studies could involve electrophysiological recordings from spinal cord slices to identify specific pain processing circuits that are engaged following MIA activation and that may mediate peripheral sensitization. Moreover, transcriptomics of retrogradely labeled cutaneous afferents from mice with and without CFA-induced knee joint inflammation, could be performed to gain detailed insights into the molecular mechanisms underlying the sensitization of cutaneous C-fiber and A-fiber nociceptors.

The distinction made in this work – that primary and secondary pain hypersensitivities are mediated by distinct primary sensory afferent subclasses – is

pivotal. Especially considering that MIAs represent nearly half of all nociceptors in visceral and deep somatic tissues, this study forms a cornerstone for subsequent research focusing on the roles of different afferent subtypes in various clinically significant pain manifestations. A deeper dive into the role of CHRNA3-EGFP^{+} MIAs in inflammatory and neuropathic pain might benefit from an approach centered on sensory neuron-specific ablation. However, generating a new transgenic mouse model was beyond the scope of this thesis. In conclusion, my research lays a foundational groundwork, pointing toward innovative strategies to mitigate the transition from acute to chronic pain, be it post-injury, following inflammation, or after surgical procedures

5. REFERENCES

Abraira, V. E. and Ginty, D. D. (2013). **The sensory neurons of touch**. Neuron *79 (4)*, 618-639, doi: 10.1016/j.neuron.2013.07.051.

Agarwal, N., Offermanns, S. and Kuner, R. (2004). **Conditional gene deletion in primary nociceptive neurons of trigeminal ganglia and dorsal root ganglia**. Genesis *38 (3)*, 122-129, doi: 10.1002/gene.20010.

Akopian, A. N. (2011). **Regulation of nociceptive transmission at the periphery via TRPA1-TRPV1 interactions**. Curr Pharm Biotechnol *12 (1)*, 89-94, doi: 10.2174/138920111793937952.

Anderson, E. O., Schneider, E. R., Matson, J. D., Gracheva, E. O. and Bagriantsev, S. N. (2018). **TMEM150C/Tentonin3 Is a Regulator of Mechano-gated Ion Channels**. Cell Rep *23 (3)*, 701-708, doi: 10.1016/j.celrep.2018.03.094.

Andreev, N. Y., Dimitrieva, N., Koltzenburg, M. and McMahon, S. B. (1995). **Peripheral administration of nerve growth factor in the adult rat produces a thermal hyperalgesia that requires the presence of sympathetic post-ganglionic neurones**. Pain *63 (1)*, 109-115, doi: 10.1016/0304-3959(95)00024-m.

Arcourt, A., Gorham, L., Dhandapani, R., Prato, V., Taberner, F. J., Wende, H., Gangadharan, V., Birchmeier, C., Heppenstall, P. A. and Lechner, S. G. (2017). **Touch Receptor-Derived Sensory Information Alleviates Acute Pain Signaling and Fine-Tunes Nociceptive Reflex Coordination**. Neuron *93 (1)*, 179-193, doi: 10.1016/j.neuron.2016.11.027.

Ashraf, S., Bouhana, K. S., Pheneger, J., Andrews, S. W. and Walsh, D. A. (2016). **Selective inhibition of tropomyosin-receptor-kinase A (TrkA) reduces pain and joint damage in two rat models of inflammatory arthritis**. Arthritis Res Ther *18 (1)*, 97, doi: 10.1186/s13075-016-0996-z.

Averill, S., McMahon, S. B., Clary, D. O., Reichardt, L. F. and Priestley, J. V. (1995). **Immunocytochemical localization of trkA receptors in chemically**

identified subgroups of adult rat sensory neurons. Eur J Neurosci *7 (7)*, 1484-1494, doi: 10.1111/j.1460-9568.1995.tb01143.x.

Bandell, M., Story, G. M., Hwang, S. W., Viswanath, V., Eid, S. R., Petrus, M. J., Earley, T. J. and Patapoutian, A. (2004). **Noxious cold ion channel TRPA1 is activated by pungent compounds and bradykinin**. Neuron *41 (6)*, 849-857, doi: 10.1016/s0896-6273(04)00150-3.

Barber, L. A. and Vasko, M. R. (1996). **Activation of protein kinase C augments peptide release from rat sensory neurons**. J Neurochem *67 (1)*, 72-80, doi: 10.1046/j.1471-4159.1996.67010072.x.

Barouch, R., Kazimirsky, G., Appel, E. and Brodie, C. (2001). **Nerve growth factor regulates TNF-alpha production in mouse macrophages via MAP kinase activation**. J Leukoc Biol *69 (6)*, 1019-1026.

Basbaum, A. I., Bautista, D. M., Scherrer, G. and Julius, D. (2009). **Cellular and Molecular Mechanisms of Pain**. Cell *139 (2)*, 267-284, doi: https://doi.org/10.1016/j.cell.2009.09.028.

Bautista, D. M., Jordt, S. E., Nikai, T., Tsuruda, P. R., Read, A. J., Poblete, J., Yamoah, E. N., Basbaum, A. I. and Julius, D. (2006). **TRPA1 mediates the inflammatory actions of environmental irritants and proalgesic agents**. Cell *124 (6)*, 1269-1282, doi: 10.1016/j.cell.2006.02.023.

Bautista, D. M., Siemens, J., Glazer, J. M., Tsuruda, P. R., Basbaum, A. I., Stucky, C. L., Jordt, S. E. and Julius, D. (2007). **The menthol receptor TRPM8 is the principal detector of environmental cold**. Nature *448 (7150)*, 204-208, doi: 10.1038/nature05910.

Bautista, D. M., Sigal, Y. M., Milstein, A. D., Garrison, J. L., Zorn, J. A., Tsuruda, P. R., Nicoll, R. A. and Julius, D. (2008). **Pungent agents from Szechuan peppers excite sensory neurons by inhibiting two-pore potassium channels**. Nat Neurosci *11 (7)*, 772-779, doi: 10.1038/nn.2143.

Bennett, D. L., Michael, G. J., Ramachandran, N., Munson, J. B., Averill, S., Yan, Q., McMahon, S. B. and Priestley, J. V. (1998). **A distinct subgroup of small DRG cells express GDNF receptor components and GDNF is protective for these neurons after nerve injury**. J Neurosci *18 (8)*, 3059-3072, doi: 10.1523/jneurosci.18-08-03059.1998.

Bessou, P. and Perl, E. R. (1969). **Response of cutaneous sensory units with unmyelinated fibers to noxious stimuli**. J Neurophysiol *32 (6)*, 1025-1043, doi: 10.1152/jn.1969.32.6.1025.

Bhave, G. and Gereau, R. W. t. (2004). **Posttranslational mechanisms of peripheral sensitization**. J Neurobiol *61 (1)*, 88-106, doi: 10.1002/neu.20083.

Birder, L. A. and Perl, E. R. (1994). **Cutaneous sensory receptors**. J Clin Neurophysiol *11 (6)*, 534-552, doi: 10.1097/00004691-199411000-00002.

Bove, S. E., Laemont, K. D., Brooker, R. M., Osborn, M. N., Sanchez, B. M., Guzman, R. E., Hook, K. E., Juneau, P. L., Connor, J. R. and Kilgore, K. S. (2006). **Surgically induced osteoarthritis in the rat results in the development of both osteoarthritis-like joint pain and secondary hyperalgesia**. Osteoarthritis Cartilage *14 (10)*, 1041-1048, doi: 10.1016/j.joca.2006.05.001.

Braz, J., Solorzano, C., Wang, X. and Basbaum, A. I. (2014). **Transmitting pain and itch messages: a contemporary view of the spinal cord circuits that generate gate control**. Neuron *82 (3)*, 522-536, doi: 10.1016/j.neuron.2014.01.018.

Brenneis, C., Kistner, K., Puopolo, M., Segal, D., Roberson, D., Sisignano, M., Labocha, S., Ferreirós, N., Strominger, A., Cobos, E. J., Ghasemlou, N., Geisslinger, G., Reeh, P. W., Bean, B. P. and Woolf, C. J. (2013). **Phenotyping the function of TRPV1-expressing sensory neurons by targeted axonal silencing**. J Neurosci *33 (1)*, 315-326, doi: 10.1523/jneurosci.2804-12.2013.

Brierley, S. M., Castro, J., Harrington, A. M., Hughes, P. A., Page, A. J., Rychkov, G. Y. and Blackshaw, L. A. (2011). **TRPA1 contributes to specific mechanically activated currents and sensory neuron mechanical hypersensitivity**. J Physiol *589 (Pt 14)*, 3575-3593, doi: 10.1113/jphysiol.2011.206789.

Cain, D. M., Khasabov, S. G. and Simone, D. A. (2001). **Response properties of mechanoreceptors and nociceptors in mouse glabrous skin: an in vivo study**. J Neurophysiol *85 (4)*, 1561-1574, doi: 10.1152/jn.2001.85.4.1561.

Caterina, M. J., Leffler, A., Malmberg, A. B., Martin, W. J., Trafton, J., Petersen-Zeitz, K. R., Koltzenburg, M., Basbaum, A. I. and Julius, D. (2000). **Impaired nociception and pain sensation in mice lacking the capsaicin receptor**. Science *288 (5464)*, 306-313, doi: 10.1126/science.288.5464.306.

Caterina, M. J., Schumacher, M. A., Tominaga, M., Rosen, T. A., Levine, J. D. and Julius, D. (1997). **The capsaicin receptor: a heat-activated ion channel in the pain pathway**. Nature *389 (6653)*, 816-824, doi: 10.1038/39807.

Catterall, W. A. (2000). **Structure and regulation of voltage-gated Ca2+ channels**. Annu Rev Cell Dev Biol *16*, 521-555, doi: 10.1146/annurev.cellbio.16.1.521.

Cavanaugh, D. J., Lee, H., Lo, L., Shields, S. D., Zylka, M. J., Basbaum, A. I. and Anderson, D. J. (2009). **Distinct subsets of unmyelinated primary sensory fibers mediate behavioral responses to noxious thermal and mechanical stimuli**. Proc Natl Acad Sci U S A *106 (22)*, 9075-9080, doi: 10.1073/pnas.0901507106.

Cesare, P., Dekker, L. V., Sardini, A., Parker, P. J. and McNaughton, P. A. (1999). **Specific involvement of PKC-epsilon in sensitization of the neuronal response to painful heat**. Neuron *23 (3)*, 617-624, doi: 10.1016/s0896-6273(00)80813-2.

Chakrabarti, S., Pattison, L. A., Singhal, K., Hockley, J. R. F., Callejo, G. and Smith, E. S. J. (2018). **Acute inflammation sensitizes knee-innervating sensory neurons and decreases mouse digging behavior in a TRPV1-dependent manner**. Neuropharmacology *143*, 49-62, doi: 10.1016/j.neuropharm.2018.09.014.

Chalfie, M. (2009). **Neurosensory mechanotransduction**. Nat Rev Mol Cell Biol *10 (1)*, 44-52, doi: 10.1038/nrm2595.

Challis, R. C., Ravindra Kumar, S., Chan, K. Y., Challis, C., Beadle, K., Jang, M. J., Kim, H. M., Rajendran, P. S., Tompkins, J. D., Shivkumar, K., Deverman, B. E. and Gradinaru, V. (2019). **Systemic AAV vectors for widespread and targeted gene delivery in rodents**. Nat Protoc *14 (2)*, 379-414, doi: 10.1038/s41596-018-0097-3.

Chan, K. Y., Jang, M. J., Yoo, B. B., Greenbaum, A., Ravi, N., Wu, W. L., Sánchez-Guardado, L., Lois, C., Mazmanian, S. K., Deverman, B. E. and Gradinaru, V. (2017). **Engineered AAVs for efficient noninvasive gene delivery to the central and peripheral nervous systems**. Nat Neurosci *20 (8)*, 1172-1179, doi: 10.1038/nn.4593.

Chang, D. S., Hsu, E., Hottinger, D. G. and Cohen, S. P. (2016). **Anti-nerve growth factor in pain management: current evidence**. J Pain Res *9*, 373-383, doi: 10.2147/jpr.S89061.

Chartier, S. R., Mitchell, S. A., Majuta, L. A. and Mantyh, P. W. (2017). **Immunohistochemical localization of nerve growth factor, tropomyosin receptor kinase A, and p75 in the bone and articular cartilage of the mouse femur**. Mol Pain *13*, 1744806917745465, doi: 10.1177/1744806917745465.

Cho, H., Shin, J., Shin, C. Y., Lee, S. Y. and Oh, U. (2002). **Mechanosensitive ion channels in cultured sensory neurons of neonatal rats**. J Neurosci *22 (4)*, 1238-1247, doi: 10.1523/jneurosci.22-04-01238.2002.

Chung, M. K., Park, J., Asgar, J. and Ro, J. Y. (2016). **Transcriptome analysis of trigeminal ganglia following masseter muscle inflammation in rats**. Mol Pain *12*, doi: 10.1177/1744806916668526.

Coste, B., Mathur, J., Schmidt, M., Earley, T. J., Ranade, S., Petrus, M. J., Dubin, A. E. and Patapoutian, A. (2010). **Piezo1 and Piezo2 are essential components of distinct mechanically activated cation channels**. Science *330 (6000)*, 55-60, doi: 10.1126/science.1193270.

Cui, H., Guo, Z., Guo, Z., Fan, Z., Shen, N., Qi, X., Ma, Y., Zhu, Y., Wu, X., Chen, B. and Xiang, H. (2023). **TMEM100 Regulates Neuropathic Pain by Reducing the Expression of Inflammatory Factors**. Mediators Inflamm *2023*, 9151967, doi: 10.1155/2023/9151967.

Davidson, G., Murphy, S., Polke, J., Laura, M., Salih, M., Muntoni, F., Blake, J., Brandner, S., Davies, N., Horvath, R., Price, S., Donaghy, M., Roberts, M., Foulds, N., Ramdharry, G., Soler, D., Lunn, M., Manji, H., Davis, M., Houlden, H. and Reilly, M. (2012). **Frequency of mutations in the genes associated with hereditary sensory and autonomic neuropathy in a UK cohort**. J Neurol *259 (8)*, 1673-1685, doi: 10.1007/s00415-011-6397-y.

Davis, B. M., Lewin, G. R., Mendell, L. M., Jones, M. E. and Albers, K. M. (1993). **Altered expression of nerve growth factor in the skin of transgenic mice leads to changes in response to mechanical stimuli**. Neuroscience *56 (4)*, 789-792, doi: 10.1016/0306-4522(93)90127-2.

Davis, J. B., Gray, J., Gunthorpe, M. J., Hatcher, J. P., Davey, P. T., Overend, P., Harries, M. H., Latcham, J., Clapham, C., Atkinson, K., Hughes, S. A., Rance, K., Grau, E., Harper, A. J., Pugh, P. L., Rogers, D. C., Bingham, S., Randall, A. and Sheardown, S. A. (2000). **Vanilloid receptor-1 is essential for inflammatory thermal hyperalgesia**. Nature *405 (6783)*, 183-187, doi: 10.1038/35012076.

Delmas, P. and Coste, B. (2013). **Mechano-gated ion channels in sensory systems**. Cell *155 (2)*, 278-284, doi: 10.1016/j.cell.2013.09.026.

Denk, F., Bennett, D. L. and McMahon, S. B. (2017). **Nerve Growth Factor and Pain Mechanisms**. Annu Rev Neurosci *40*, 307-325, doi: 10.1146/annurev-neuro-072116-031121.

Dhaka, A., Murray, A. N., Mathur, J., Earley, T. J., Petrus, M. J. and Patapoutian, A. (2007). **TRPM8 is required for cold sensation in mice**. Neuron *54 (3)*, 371-378, doi: 10.1016/j.neuron.2007.02.024.

Di Castro, A., Drew, L. J., Wood, J. N. and Cesare, P. (2006). **Modulation of sensory neuron mechanotransduction by PKC- and nerve growth factor-**

dependent pathways. Proc Natl Acad Sci U S A *103 (12)*, 4699-4704, doi: 10.1073/pnas.0508005103.

Djouhri, L., Dawbarn, D., Robertson, A., Newton, R. and Lawson, S. N. (2001). **Time course and nerve growth factor dependence of inflammation-induced alterations in electrophysiological membrane properties in nociceptive primary afferent neurons**. J Neurosci *21 (22)*, 8722-8733, doi: 10.1523/jneurosci.21-22-08722.2001.

Djouhri, L. and Lawson, S. N. (2004). **Abeta-fiber nociceptive primary afferent neurons: a review of incidence and properties in relation to other afferent A-fiber neurons in mammals**. Brain Res Brain Res Rev *46 (2)*, 131-145, doi: 10.1016/j.brainresrev.2004.07.015.

Dobler, T., Springauf, A., Tovornik, S., Weber, M., Schmitt, A., Sedlmeier, R., Wischmeyer, E. and Döring, F. (2007). **TRESK two-pore-domain K+ channels constitute a significant component of background potassium currents in murine dorsal root ganglion neurones**. J Physiol *585 (Pt 3)*, 867-879, doi: 10.1113/jphysiol.2007.145649.

Doerner, J. F., Gisselmann, G., Hatt, H. and Wetzel, C. H. (2007). **Transient receptor potential channel A1 is directly gated by calcium ions**. J Biol Chem *282 (18)*, 13180-13189, doi: 10.1074/jbc.M607849200.

Dong, X., Han, S., Zylka, M. J., Simon, M. I. and Anderson, D. J. (2001). **A diverse family of GPCRs expressed in specific subsets of nociceptive sensory neurons**. Cell *106 (5)*, 619-632, doi: 10.1016/s0092-8674(01)00483-4.

Drake, R. A., Leith, J. L., Almahasneh, F., Martindale, J., Wilson, A. W., Lumb, B. and Donaldson, L. F. (2016). **Periaqueductal Grey EP3 Receptors Facilitate Spinal Nociception in Arthritic Secondary Hypersensitivity**. J Neurosci *36 (35)*, 9026-9040, doi: 10.1523/jneurosci.4393-15.2016.

Drew, L. J., Rohrer, D. K., Price, M. P., Blaver, K. E., Cockayne, D. A., Cesare, P. and Wood, J. N. (2004). **Acid-sensing ion channels ASIC2 and ASIC3 do not contribute to mechanically activated currents in mammalian sensory neurones**. J Physiol *556 (Pt 3)*, 691-710, doi: 10.1113/jphysiol.2003.058693.

Drew, L. J., Wood, J. N. and Cesare, P. (2002). **Distinct mechanosensitive properties of capsaicin-sensitive and -insensitive sensory neurons**. J Neurosci *22 (12)*, Rc228, doi: 10.1523/JNEUROSCI.22-12-j0001.2002.

Dubin, A. E., Murthy, S., Lewis, A. H., Brosse, L., Cahalan, S. M., Grandl, J., Coste, B. and Patapoutian, A. (2017). **Endogenous Piezo1 Can Confound Mechanically Activated Channel Identification and Characterization**. Neuron *94 (2)*, 266-270.e263, doi: 10.1016/j.neuron.2017.03.039.

Dubin, A. E. and Patapoutian, A. (2010). **Nociceptors: the sensors of the pain pathway**. J Clin Invest *120 (11)*, 3760-3772, doi: 10.1172/jci42843.

Dubin, A. E., Schmidt, M., Mathur, J., Petrus, M. J., Xiao, B., Coste, B. and Patapoutian, A. (2012). **Inflammatory signals enhance piezo2-mediated mechanosensitive currents**. Cell Rep *2 (3)*, 511-517, doi: 10.1016/j.celrep.2012.07.014.

Dyck, P. J., Peroutka, S., Rask, C., Burton, E., Baker, M. K., Lehman, K. A., Gillen, D. A., Hokanson, J. L. and O'Brien, P. C. (1997). **Intradermal recombinant human nerve growth factor induces pressure allodynia and lowered heat-pain threshold in humans**. Neurology *48 (2)*, 501-505, doi: 10.1212/wnl.48.2.501.

Einarsdottir, E., Carlsson, A., Minde, J., Toolanen, G., Svensson, O., Solders, G., Holmgren, G., Holmberg, D. and Holmberg, M. (2004). **A mutation in the nerve growth factor beta gene (NGFB) causes loss of pain perception**. Hum Mol Genet *13 (8)*, 799-805, doi: 10.1093/hmg/ddh096.

Eisenman, S. T., Gibbons, S. J., Singh, R. D., Bernard, C. E., Wu, J., Sarr, M. G., Kendrick, M. L., Larson, D. W., Dozois, E. J., Shen, K. R. and Farrugia, G. (2013). **Distribution of TMEM100 in the mouse and human gastrointestinal tract--a novel marker of enteric nerves**. Neuroscience *240*, 117-128, doi: 10.1016/j.neuroscience.2013.02.034.

Eitner, A., Hofmann, G. O. and Schaible, H. G. (2017). **Mechanisms of Osteoarthritic Pain. Studies in Humans and Experimental Models**. Front Mol Neurosci *10*, 349, doi: 10.3389/fnmol.2017.00349.

England, S., Bevan, S. and Docherty, R. J. (1996). **PGE2 modulates the tetrodotoxin-resistant sodium current in neonatal rat dorsal root ganglion neurones via the cyclic AMP-protein kinase A cascade**. J Physiol *495 (Pt 2) (Pt 2)*, 429-440, doi: 10.1113/jphysiol.1996.sp021604.

Evans, A. R., Vasko, M. R. and Nicol, G. D. (1999). **The cAMP transduction cascade mediates the PGE2-induced inhibition of potassium currents in rat sensory neurones**. J Physiol *516 (Pt 1) (Pt 1)*, 163-178, doi: 10.1111/j.1469-7793.1999.163aa.x.

Feng, B. and Gebhart, G. F. (2011). **Characterization of silent afferents in the pelvic and splanchnic innervations of the mouse colorectum**. Am J Physiol Gastrointest Liver Physiol *300 (1)*, G170-180, doi: 10.1152/ajpgi.00406.2010.

Fischer, M. J., Balasuriya, D., Jeggle, P., Goetze, T. A., McNaughton, P. A., Reeh, P. W. and Edwardson, J. M. (2014). **Direct evidence for functional TRPV1/TRPA1 heteromers**. Pflugers Arch *466 (12)*, 2229-2241, doi: 10.1007/s00424-014-1497-z.

Fjell, J., Cummins, T. R., Davis, B. M., Albers, K. M., Fried, K., Waxman, S. G. and Black, J. A. (1999). **Sodium channel expression in NGF-overexpressing transgenic mice**. J Neurosci Res *57 (1)*, 39-47, doi: 10.1002/(sici)1097-4547(19990701)57:1<39::Aid-jnr5>3.0.Co;2-m.

Fleischer, E., Handwerker, H. O. and Joukhadar, S. (1983). **Unmyelinated nociceptive units in two skin areas of the rat**. Brain Res *267 (1)*, 81-92, doi: 10.1016/0006-8993(83)91041-7.

Fujimoto, S., Uratsuji, H., Saeki, H., Kagami, S., Tsunemi, Y., Komine, M. and Tamaki, K. (2008). **CCR4 and CCR10 are expressed on epidermal keratinocytes and are involved in cutaneous immune reaction**. Cytokine *44 (1)*, 172-178, doi: 10.1016/j.cyto.2008.07.472.

Garrison, S. R. and Stucky, C. L. (2014). **Contribution of transient receptor potential ankyrin 1 to chronic pain in aged mice with complete Freund's adjuvant-induced arthritis**. Arthritis Rheumatol *66 (9)*, 2380-2390, doi: 10.1002/art.38724.

Gaskin, D. J. and Richard, P. (2012). **The economic costs of pain in the United States**. J Pain *13 (8)*, 715-724, doi: 10.1016/j.jpain.2012.03.009.

GBD (2017). **Global, regional, and national incidence, prevalence, and years lived with disability for 328 diseases and injuries for 195 countries, 1990-2016: a systematic analysis for the Global Burden of Disease Study 2016**. Lancet *390 (10100)*, 1211-1259, doi: 10.1016/s0140-6736(17)32154-2.

Gebhart, G. F. (1999). **Peripheral contributions to visceral hyperalgesia**. Can J Gastroenterol *13 Suppl A*, 37a-41a, doi: 10.1155/1999/730765.

Gebhart, G. F. and Schmidt, R. F. (2013). **Primary and Secondary Hyperalgesia**. In: Encyclopedia of Pain, eds. Gebhart, G. F. and Schmidt, R. F., Springer Berlin Heidelberg, Berlin, Heidelberg, pp. 3174-3174.

Georgas, K., Rumballe, B., Valerius, M. T., Chiu, H. S., Thiagarajan, R. D., Lesieur, E., Aronow, B. J., Brunskill, E. W., Combes, A. N., Tang, D., Taylor, D., Grimmond, S. M., Potter, S. S., McMahon, A. P. and Little, M. H. (2009). **Analysis of early nephron patterning reveals a role for distal RV proliferation in fusion to the ureteric tip via a cap mesenchyme-derived connecting segment**. Dev Biol *332 (2)*, 273-286, doi: 10.1016/j.ydbio.2009.05.578.

Ghilardi, J. R., Freeman, K. T., Jimenez-Andrade, J. M., Coughlin, K. A., Kaczmarska, M. J., Castaneda-Corral, G., Bloom, A. P., Kuskowski, M. A. and Mantyh, P. W. (2012). **Neuroplasticity of sensory and sympathetic nerve fibers in a mouse model of a painful arthritic joint**. Arthritis Rheum *64 (7)*, 2223-2232, doi: 10.1002/art.34385.

Gold, M. S. and Gebhart, G. F. (2010). **Nociceptor sensitization in pain pathogenesis**. Nat Med *16 (11)*, 1248-1257, doi: 10.1038/nm.2235.

Goldberg, D. S. and McGee, S. J. (2011). **Pain as a global public health priority**. BMC Public Health *11*, 770, doi: 10.1186/1471-2458-11-770.

Golden, J. P., Hoshi, M., Nassar, M. A., Enomoto, H., Wood, J. N., Milbrandt, J., Gereau, R. W. t., Johnson, E. M., Jr. and Jain, S. (2010). **RET signaling is required for survival and normal function of nonpeptidergic nociceptors**. J Neurosci *30 (11)*, 3983-3994, doi: 10.1523/jneurosci.5930-09.2010.

Guo, Z., Ma, Y., Wang, Y., Xiang, H., Yang, S. Y., Guo, Z., Wang, R., Chen, W., Xing, D., Chen, B., Tao, H. and Wu, X. (2023). **The Role of IL-6 and TMEM100 in Lumbar Discogenic Pain and the Mechanism of the Glycine-Serine-Threonine Metabolic Axis: A Metabolomic and Molecular Biology Study**. J Pain Res *16*, 437-461, doi: 10.2147/jpr.S400871.

Häbler, H. J., Jänig, W. and Koltzenburg, M. (1990). **Activation of unmyelinated afferent fibres by mechanical stimuli and inflammation of the urinary bladder in the cat**. The Journal of Physiology *425 (1)*, 545-562, doi: https://doi.org/10.1113/jphysiol.1990.sp018117.

Handwerker, H. O., Anton, F. and Reeh, P. W. (1987). **Discharge patterns of afferent cutaneous nerve fibers from the rat's tail during prolonged noxious mechanical stimulation**. Exp Brain Res *65 (3)*, 493-504, doi: 10.1007/bf00235972.

Handwerker, H. O., Kilo, S. and Reeh, P. W. (1991). **Unresponsive afferent nerve fibres in the sural nerve of the rat**. J Physiol *435*, 229-242, doi: 10.1113/jphysiol.1991.sp018507.

Hao, J. and Delmas, P. (2010). **Multiple desensitization mechanisms of mechanotransducer channels shape firing of mechanosensory neurons**. J Neurosci *30 (40)*, 13384-13395, doi: 10.1523/jneurosci.2926-10.2010.

Hargreaves, K., Dubner, R., Brown, F., Flores, C. and Joris, J. (1988). **A new and sensitive method for measuring thermal nociception in cutaneous hyperalgesia**. Pain *32 (1)*, 77-88, doi: 10.1016/0304-3959(88)90026-7.

Hiltunen, J. O., Laurikainen, A., Väkevä, A., Meri, S. and Saarma, M. (2001). **Nerve growth factor and brain-derived neurotrophic factor mRNAs are regulated in distinct cell populations of rat heart after ischaemia and reperfusion**. J Pathol *194 (2)*, 247-253, doi: 10.1002/path.878.

Hirth, M., Rukwied, R., Gromann, A., Turnquist, B., Weinkauf, B., Francke, K., Albrecht, P., Rice, F., Hägglöf, B., Ringkamp, M., Engelhardt, M., Schultz, C., Schmelz, M. and Obreja, O. (2013). **Nerve growth factor induces sensitization of nociceptors without evidence for increased intraepidermal nerve fiber density**. Pain *154 (11)*, 2500-2511, doi: 10.1016/j.pain.2013.07.036.

Hong, G. S., Lee, B., Wee, J., Chun, H., Kim, H., Jung, J., Cha, J. Y., Riew, T. R., Kim, G. H., Kim, I. B. and Oh, U. (2016). **Tentonin 3/TMEM150c Confers Distinct Mechanosensitive Currents in Dorsal-Root Ganglion Neurons with Proprioceptive Function**. Neuron *91 (1)*, 107-118, doi: 10.1016/j.neuron.2016.05.029.

Hong, Y., Si, J., Xiao, B., Xiong, Y., Dai, C., Yang, Y., Li, S. and Ma, Y. (2022). **circ_0000567/miR-421/TMEM100 Axis Promotes the Migration and Invasion of Lung Adenocarcinoma and Is Associated with Prognosis**. J Cancer *13 (5)*, 1540-1552, doi: 10.7150/jca.60124.

Horigome, K., Pryor, J. C., Bullock, E. D. and Johnson, E. M., Jr. (1993). **Mediator release from mast cells by nerve growth factor. Neurotrophin specificity and receptor mediation**. J Biol Chem *268 (20)*, 14881-14887.

Hsieh, M. T., Donaldson, L. F. and Lumb, B. M. (2015). **Differential contributions of A- and C-nociceptors to primary and secondary inflammatory hypersensitivity in the rat**. Pain *156 (6)*, 1074-1083, doi: 10.1097/j.pain.0000000000000151.

Hu, J. and Lewin, G. R. (2006). **Mechanosensitive currents in the neurites of cultured mouse sensory neurones**. J Physiol *577 (Pt 3)*, 815-828, doi: 10.1113/jphysiol.2006.117648.

Huo, L., Gao, Y., Zhang, D., Wang, S., Han, Y., Men, H., Yang, Z., Qin, X., Wang, R., Kong, D., Bai, H., Zhang, H., Zhang, W. and Jia, Z. (2021). **Piezo2 channel in nodose ganglia neurons is essential in controlling hypertension in a pathway regulated directly by Nedd4-2**. Pharmacol Res *164*, 105391, doi: 10.1016/j.phrs.2020.105391.

IASP (2023). **Terminology**. URL: https://www.iasp-pain.org/resources/terminology/ [as of06.11.2023].

Iggo, A. (1960). **Cutaneous mechanoreceptors with afferent C fibres**. J Physiol *152 (2)*, 337-353, doi: 10.1113/jphysiol.1960.sp006491.

Im, H. J., Kim, J. S., Li, X., Kotwal, N., Sumner, D. R., van Wijnen, A. J., Davis, F. J., Yan, D., Levine, B., Henry, J. L., Desevré, J. and Kroin, J. S. (2010). **Alteration of sensory neurons and spinal response to an experimental osteoarthritis pain model**. Arthritis Rheum *62 (10)*, 2995-3005, doi: 10.1002/art.27608.

Ishikawa, G., Koya, Y., Tanaka, H. and Nagakura, Y. (2015). **Long-term analgesic effect of a single dose of anti-NGF antibody on pain during motion without notable suppression of joint edema and lesion in a rat model of osteoarthritis**. Osteoarthritis Cartilage *23 (6)*, 925-932, doi: 10.1016/j.joca.2015.02.002.

Iwakura, N., Ohtori, S., Orita, S., Yamashita, M., Takahashi, K. and Kuniyoshi, K. (2010). **Role of low-affinity nerve growth factor receptor inhibitory antibody in reducing pain behavior and calcitonin gene-related Peptide expression in a rat model of wrist joint inflammatory pain**. J Hand Surg Am *35 (2)*, 267-273, doi: 10.1016/j.jhsa.2009.10.030.

Ji, R. R., Samad, T. A., Jin, S. X., Schmoll, R. and Woolf, C. J. (2002). **p38 MAPK activation by NGF in primary sensory neurons after inflammation increases TRPV1 levels and maintains heat hyperalgesia**. Neuron *36 (1)*, 57-68, doi: 10.1016/s0896-6273(02)00908-x.

Jimenez-Andrade, J. M., Ghilardi, J. R., Castañeda-Corral, G., Kuskowski, M. A. and Mantyh, P. W. (2011). **Preventive or late administration of anti-NGF therapy**

attenuates tumor-induced nerve sprouting, neuroma formation, and cancer pain. Pain *152 (11)*, 2564-2574, doi: 10.1016/j.pain.2011.07.020.

Jimenez-Andrade, J. M. and Mantyh, P. W. (2012). **Sensory and sympathetic nerve fibers undergo sprouting and neuroma formation in the painful arthritic joint of geriatric mice**. Arthritis Res Ther *14 (3)*, R101, doi: 10.1186/ar3826.

Jordt, S. E., Bautista, D. M., Chuang, H. H., McKemy, D. D., Zygmunt, P. M., Högestätt, E. D., Meng, I. D. and Julius, D. (2004). **Mustard oils and cannabinoids excite sensory nerve fibres through the TRP channel ANKTM1**. Nature *427 (6971)*, 260-265, doi: 10.1038/nature02282.

Kaneko, Y. and Szallasi, A. (2014). **Transient receptor potential (TRP) channels: a clinical perspective**. Br J Pharmacol *171 (10)*, 2474-2507, doi: 10.1111/bph.12414.

Karolak, J. A., Deutsch, G., Gambin, T., Szafranski, P., Popek, E. and Stankiewicz, P. (2022). **Transcriptome and Immunohistochemical Analyses in TBX4- and FGF10-Deficient Lungs Imply TMEM100 as a Mediator of Human Lung Development**. Am J Respir Cell Mol Biol *66 (6)*, 694-697, doi: 10.1165/rcmb.2021-0470LE.

Kawai, J., Shinagawa, A., Shibata, K., Yoshino, M., Itoh, M., Ishii, Y., Arakawa, T., Hara, A., Fukunishi, Y., Konno, H., Adachi, J., Fukuda, S., Aizawa, K., Izawa, M., Nishi, K., Kiyosawa, H., Kondo, S., Yamanaka, I., Saito, T., Okazaki, Y., Gojobori, T., Bono, H., Kasukawa, T., Saito, R., Kadota, K., Matsuda, H., Ashburner, M., Batalov, S., Casavant, T., Fleischmann, W., Gaasterland, T., Gissi, C., King, B., Kochiwa, H., Kuehl, P., Lewis, S., Matsuo, Y., Nikaido, I., Pesole, G., Quackenbush, J., Schriml, L. M., Staubli, F., Suzuki, R., Tomita, M., Wagner, L., Washio, T., Sakai, K., Okido, T., Furuno, M., Aono, H., Baldarelli, R., Barsh, G., Blake, J., Boffelli, D., Bojunga, N., Carninci, P., de Bonaldo, M. F., Brownstein, M. J., Bult, C., Fletcher, C., Fujita, M., Gariboldi, M., Gustincich, S., Hill, D., Hofmann, M., Hume, D. A., Kamiya, M., Lee, N. H., Lyons, P., Marchionni, L., Mashima, J., Mazzarelli, J., Mombaerts, P., Nordone, P., Ring, B., Ringwald, M., Rodriguez, I., Sakamoto, N., Sasaki, H., Sato, K., Schönbach, C., Seya, T., Shibata, Y., Storch, K. F., Suzuki, H., Toyo-oka, K., Wang, K. H., Weitz, C., Whittaker, C., Wilming, L., Wynshaw-Boris, A., Yoshida, K., Hasegawa, Y., Kawaji, H., Kohtsuki, S. and Hayashizaki, Y. (2001). **Functional annotation of a full-length mouse cDNA collection**. Nature *409 (6821)*, 685-690, doi: 10.1038/35055500.

Kerstein, P. C., del Camino, D., Moran, M. M. and Stucky, C. L. (2009). **Pharmacological blockade of TRPA1 inhibits mechanical firing in nociceptors**. Mol Pain *5*, 19, doi: 10.1186/1744-8069-5-19.

Kidd, B. L. and Urban, L. A. (2001). **Mechanisms of inflammatory pain**. BJA: British Journal of Anaesthesia *87 (1)*, 3-11, doi: 10.1093/bja/87.1.3.

Kissin, I. (2010). **The development of new analgesics over the past 50 years: a lack of real breakthrough drugs**. Anesth Analg *110 (3)*, 780-789, doi: 10.1213/ANE.0b013e3181cde882.

Knowlton, W. M., Palkar, R., Lippoldt, E. K., McCoy, D. D., Baluch, F., Chen, J. and McKemy, D. D. (2013). **A sensory-labeled line for cold: TRPM8-expressing sensory neurons define the cellular basis for cold, cold pain, and cooling-mediated analgesia**. J Neurosci *33 (7)*, 2837-2848, doi: 10.1523/jneurosci.1943-12.2013.

Koewler, N. J., Freeman, K. T., Buus, R. J., Herrera, M. B., Jimenez-Andrade, J. M., Ghilardi, J. R., Peters, C. M., Sullivan, L. J., Kuskowski, M. A., Lewis, J. L. and Mantyh, P. W. (2007). **Effects of a monoclonal antibody raised against nerve growth factor on skeletal pain and bone healing after fracture of the C57BL/6J mouse femur**. J Bone Miner Res *22 (11)*, 1732-1742, doi: 10.1359/jbmr.070711.

Kress, M., Koltzenburg, M., Reeh, P. W. and Handwerker, H. O. (1992). **Responsiveness and functional attributes of electrically localized terminals of cutaneous C-fibers in vivo and in vitro**. J Neurophysiol *68 (2)*, 581-595, doi: 10.1152/jn.1992.68.2.581.

Krug, H. E., Dorman, C., Blanshan, N., Frizelle, S. and Mahowald, M. (2019). **Spontaneous and Evoked Measures of Pain in Murine Models of Monoarticular Knee Pain**. J Vis Exp *(144)*, doi: 10.3791/59024.

Kupari, J., Usoskin, D., Parisien, M., Lou, D., Hu, Y., Fatt, M., Lönnerberg, P., Spångberg, M., Eriksson, B., Barkas, N., Kharchenko, P. V., Loré, K., Khoury,

S., Diatchenko, L. and Ernfors, P. (2021). **Single cell transcriptomics of primate sensory neurons identifies cell types associated with chronic pain**. Nature Communications *12 (1)*, 1510, doi: 10.1038/s41467-021-21725-z.

Kwan, K. Y., Allchorne, A. J., Vollrath, M. A., Christensen, A. P., Zhang, D. S., Woolf, C. J. and Corey, D. P. (2006). **TRPA1 contributes to cold, mechanical, and chemical nociception but is not essential for hair-cell transduction**. Neuron *50 (2)*, 277-289, doi: 10.1016/j.neuron.2006.03.042.

Kwan, K. Y., Glazer, J. M., Corey, D. P., Rice, F. L. and Stucky, C. L. (2009). **TRPA1 modulates mechanotransduction in cutaneous sensory neurons**. J Neurosci *29 (15)*, 4808-4819, doi: 10.1523/jneurosci.5380-08.2009.

LaBranche, T. P., Bendele, A. M., Omura, B. C., Gropp, K. E., Hurst, S. I., Bagi, C. M., Cummings, T. R., Grantham, L. E., 2nd, Shelton, D. L. and Zorbas, M. A. (2017). **Nerve growth factor inhibition with tanezumab influences weight-bearing and subsequent cartilage damage in the rat medial meniscal tear model**. Ann Rheum Dis *76 (1)*, 295-302, doi: 10.1136/annrheumdis-2015-208913.

Latremoliere, A. and Woolf, C. J. (2009). **Central sensitization: a generator of pain hypersensitivity by central neural plasticity**. J Pain *10 (9)*, 895-926, doi: 10.1016/j.jpain.2009.06.012.

Lechner, S. G. (2017). **An update on the spinal and peripheral pathways of pain signalling**. e-Neuroforum *23 (3)*, 131-136, doi: doi:10.1515/nf-2017-A020.

Lechner, S. G. and Lewin, G. R. (2009). **Peripheral sensitisation of nociceptors via G-protein-dependent potentiation of mechanotransduction currents**. J Physiol *587 (Pt 14)*, 3493-3503, doi: 10.1113/jphysiol.2009.175059.

Lee, Y. J., Zachrisson, O., Tonge, D. A. and McNaughton, P. A. (2002). **Upregulation of bradykinin B2 receptor expression by neurotrophic factors and nerve injury in mouse sensory neurons**. Mol Cell Neurosci *19 (2)*, 186-200, doi: 10.1006/mcne.2001.1073.

Lennertz, R. C., Kossyreva, E. A., Smith, A. K. and Stucky, C. L. (2012). **TRPA1 mediates mechanical sensitization in nociceptors during inflammation**. PLoS One *7 (8)*, e43597, doi: 10.1371/journal.pone.0043597.

Lesser, S. S. and Lo, D. C. (1995). **Regulation of voltage-gated ion channels by NGF and ciliary neurotrophic factor in SK-N-SH neuroblastoma cells**. J Neurosci *15 (1 Pt 1)*, 253-261, doi: 10.1523/jneurosci.15-01-00253.1995.

Levi-Montalcini, R. and Hamburger, V. (1951). **Selective growth stimulating effects of mouse sarcoma on the sensory and sympathetic nervous system of the chick embryo**. J Exp Zool *116 (2)*, 321-361, doi: 10.1002/jez.1401160206.

Lewin, G. R., Lechner, S. G. and Smith, E. S. (2014). **Nerve growth factor and nociception: from experimental embryology to new analgesic therapy**. Handb Exp Pharmacol *220*, 251-282, doi: 10.1007/978-3-642-45106-5_10.

Lewin, G. R. and Mendell, L. M. (1994). **Regulation of cutaneous C-fiber heat nociceptors by nerve growth factor in the developing rat**. J Neurophysiol *71 (3)*, 941-949, doi: 10.1152/jn.1994.71.3.941.

Lewin, G. R. and Moshourab, R. (2004). **Mechanosensation and pain**. J Neurobiol *61 (1)*, 30-44, doi: 10.1002/neu.20078.

Lewin, G. R., Ritter, A. M. and Mendell, L. M. (1993). **Nerve growth factor-induced hyperalgesia in the neonatal and adult rat**. J Neurosci *13 (5)*, 2136-2148, doi: 10.1523/jneurosci.13-05-02136.1993.

Lewin, G. R., Rueff, A. and Mendell, L. M. (1994). **Peripheral and central mechanisms of NGF-induced hyperalgesia**. Eur J Neurosci *6 (12)*, 1903-1912, doi: 10.1111/j.1460-9568.1994.tb00581.x.

Lewis, A. H. and Grandl, J. (2021). **Stretch and poke stimulation for characterizing mechanically activated ion channels**. Methods Enzymol *654*, 225-253, doi: 10.1016/bs.mie.2020.12.024.

Li, C. L., Li, K. C., Wu, D., Chen, Y., Luo, H., Zhao, J. R., Wang, S. S., Sun, M. M., Lu, Y. J., Zhong, Y. Q., Hu, X. Y., Hou, R., Zhou, B. B., Bao, L., Xiao, H. S. and Zhang, X. (2016). **Somatosensory neuron types identified by high-coverage single-cell RNA-sequencing and functional heterogeneity**. Cell Res *26 (8)*, 967, doi: 10.1038/cr.2016.90.

Lin, C. L., Heron, P., Hamann, S. R. and Smith, G. M. (2014). **Functional distinction between NGF-mediated plasticity and regeneration of nociceptive axons within the spinal cord**. Neuroscience *272*, 76-87, doi: 10.1016/j.neuroscience.2014.04.053.

Lumpkin, E. A. and Caterina, M. J. (2007). **Mechanisms of sensory transduction in the skin**. Nature *445 (7130)*, 858-865, doi: 10.1038/nature05662.

Lynn, B. and Carpenter, S. E. (1982). **Primary afferent units from the hairy skin of the rat hind limb**. Brain Res *238 (1)*, 29-43, doi: 10.1016/0006-8993(82)90768-5.

Ma, Q. (2010). **Labeled lines meet and talk: population coding of somatic sensations**. J Clin Invest *120 (11)*, 3773-3778, doi: 10.1172/jci43426.

MacDonald, D. I., Luiz, A. P., Iseppon, F., Millet, Q., Emery, E. C. and Wood, J. N. (2021). **Silent cold-sensing neurons contribute to cold allodynia in neuropathic pain**. Brain *144 (6)*, 1711-1726, doi: 10.1093/brain/awab086.

Macpherson, L. J., Dubin, A. E., Evans, M. J., Marr, F., Schultz, P. G., Cravatt, B. F. and Patapoutian, A. (2007). **Noxious compounds activate TRPA1 ion channels through covalent modification of cysteines**. Nature *445 (7127)*, 541-545, doi: 10.1038/nature05544.

Malfait, A. M., Ritchie, J., Gil, A. S., Austin, J. S., Hartke, J., Qin, W., Tortorella, M. D. and Mogil, J. S. (2010). **ADAMTS-5 deficient mice do not develop mechanical allodynia associated with osteoarthritis following medial meniscal destabilization**. Osteoarthritis Cartilage *18 (4)*, 572-580, doi: 10.1016/j.joca.2009.11.013.

Mamet, J., Baron, A., Lazdunski, M. and Voilley, N. (2002). **Proinflammatory mediators, stimulators of sensory neuron excitability via the expression of acid-sensing ion channels**. J Neurosci *22 (24)*, 10662-10670, doi: 10.1523/jneurosci.22-24-10662.2002.

Mantyh, P. W., Koltzenburg, M., Mendell, L. M., Tive, L. and Shelton, D. L. (2011). **Antagonism of nerve growth factor-TrkA signaling and the relief of pain**. Anesthesiology *115 (1)*, 189-204, doi: 10.1097/ALN.0b013e31821b1ac5.

Mantyh, W. G., Jimenez-Andrade, J. M., Stake, J. I., Bloom, A. P., Kaczmarska, M. J., Taylor, R. N., Freeman, K. T., Ghilardi, J. R., Kuskowski, M. A. and Mantyh, P. W. (2010). **Blockade of nerve sprouting and neuroma formation markedly attenuates the development of late stage cancer pain**. Neuroscience *171 (2)*, 588-598, doi: 10.1016/j.neuroscience.2010.08.056.

Marshall, J. S., Gomi, K., Blennerhassett, M. G. and Bienenstock, J. (1999). **Nerve growth factor modifies the expression of inflammatory cytokines by mast cells via a prostanoid-dependent mechanism**. J Immunol *162 (7)*, 4271-4276.

Martindale, J. C., Wilson, A. W., Reeve, A. J., Chessell, I. P. and Headley, P. M. (2007). **Chronic secondary hypersensitivity of dorsal horn neurones following inflammation of the knee joint**. Pain *133 (1-3)*, 79-86, doi: 10.1016/j.pain.2007.03.006.

McCarter, G. C., Reichling, D. B. and Levine, J. D. (1999). **Mechanical transduction by rat dorsal root ganglion neurons in vitro**. Neurosci Lett *273 (3)*, 179-182, doi: 10.1016/s0304-3940(99)00665-5.

McCoy, E. S., Taylor-Blake, B., Street, S. E., Pribisko, A. L., Zheng, J. and Zylka, M. J. (2013). **Peptidergic CGRPα primary sensory neurons encode heat and itch and tonically suppress sensitivity to cold**. Neuron *78 (1)*, 138-151, doi: 10.1016/j.neuron.2013.01.030.

McMahon, S. B. and Koltzenburg, M. (1990). **Novel classes of nociceptors: beyond Sherrington**. Trends Neurosci *13 (6)*, 199-201, doi: 10.1016/0166-2236(90)90159-8.

McNamara, C. R., Mandel-Brehm, J., Bautista, D. M., Siemens, J., Deranian, K. L., Zhao, M., Hayward, N. J., Chong, J. A., Julius, D., Moran, M. M. and Fanger, C. M. (2007). **TRPA1 mediates formalin-induced pain**. Proc Natl Acad Sci U S A *104 (33)*, 13525-13530, doi: 10.1073/pnas.0705924104.

Meyer, R. A., Davis, K. D., Cohen, R. H., Treede, R. D. and Campbell, J. N. (1991). **Mechanically insensitive afferents (MIAs) in cutaneous nerves of monkey**. Brain Res *561 (2)*, 252-261, doi: 10.1016/0006-8993(91)91601-v.

Michael, G. J., Averill, S., Nitkunan, A., Rattray, M., Bennett, D. L., Yan, Q. and Priestley, J. V. (1997). **Nerve growth factor treatment increases brain-derived neurotrophic factor selectively in TrkA-expressing dorsal root ganglion cells and in their central terminations within the spinal cord**. J Neurosci *17 (21)*, 8476-8490, doi: 10.1523/jneurosci.17-21-08476.1997.

Michaelis, M., Häbler, H.-J. and Jänig, W. (1996). **SILENT AFFERENTS: A SEPARATE CLASS OF PRIMARY AFFERENTS?** Clinical and Experimental Pharmacology and Physiology *23 (2)*, 99-105, doi: https://doi.org/10.1111/j.1440-1681.1996.tb02579.x.

Miller, R. E., Block, J. A. and Malfait, A. M. (2017). **Nerve growth factor blockade for the management of osteoarthritis pain: what can we learn from clinical trials and preclinical models?** Curr Opin Rheumatol *29 (1)*, 110-118, doi: 10.1097/bor.0000000000000354.

Miller, R. E., Tran, P. B., Ishihara, S., Syx, D., Ren, D., Miller, R. J., Valdes, A. M. and Malfait, A. M. (2020). **Microarray analyses of the dorsal root ganglia support a role for innate neuro-immune pathways in persistent pain in experimental osteoarthritis**. Osteoarthritis Cartilage *28 (5)*, 581-592, doi: 10.1016/j.joca.2020.01.008.

Mills, S. E. E., Nicolson, K. P. and Smith, B. H. (2019). **Chronic pain: a review of its epidemiology and associated factors in population-based studies**. Br J Anaesth *123 (2)*, e273-e283, doi: 10.1016/j.bja.2019.03.023.

Mishra, S. K. and Hoon, M. A. (2010). **Ablation of TrpV1 neurons reveals their selective role in thermal pain sensation**. Mol Cell Neurosci *43 (1)*, 157-163, doi: 10.1016/j.mcn.2009.10.006.

Miyagi, M., Ishikawa, T., Kamoda, H., Suzuki, M., Inoue, G., Sakuma, Y., Oikawa, Y., Orita, S., Uchida, K., Takahashi, K., Takaso, M. and Ohtori, S. (2017). **Efficacy of nerve growth factor antibody in a knee osteoarthritis pain model in mice**. BMC Musculoskelet Disord *18 (1)*, 428, doi: 10.1186/s12891-017-1792-x.

Molliver, D. C., Wright, D. E., Leitner, M. L., Parsadanian, A. S., Doster, K., Wen, D., Yan, Q. and Snider, W. D. (1997). **IB4-Binding DRG Neurons Switch from NGF to GDNF Dependence in Early Postnatal Life**. Neuron *19 (4)*, 849-861, doi: https://doi.org/10.1016/S0896-6273(00)80966-6.

Montagnoli, C., Tiribuzi, R., Crispoltoni, L., Pistilli, A., Stabile, A. M., Manfreda, F., Placella, G., Rende, M. and Cerulli, G. G. (2017). **β-NGF and β-NGF receptor upregulation in blood and synovial fluid in osteoarthritis**. Biol Chem *398 (9)*, 1045-1054, doi: 10.1515/hsz-2016-0280.

Moon, E. H., Kim, M. J., Ko, K. S., Kim, Y. S., Seo, J., Oh, S. P. and Lee, Y. J. (2010). **Generation of mice with a conditional and reporter allele for Tmem100**. Genesis *48 (11)*, 673-678, doi: 10.1002/dvg.20674.

Narayanan, P., Hütte, M., Kudryasheva, G., Taberner, F. J., Lechner, S. G., Rehfeldt, F., Gomez-Varela, D. and Schmidt, M. (2018). **Myotubularin related protein-2 and its phospholipid substrate PIP(2) control Piezo2-mediated mechanotransduction in peripheral sensory neurons**. Elife *7*, doi: 10.7554/eLife.32346.

Narayanan, P., Sondermann, J., Rouwette, T., Karaca, S., Urlaub, H., Mitkovski, M., Gomez-Varela, D. and Schmidt, M. (2016). **Native Piezo2 Interactomics Identifies Pericentrin as a Novel Regulator of Piezo2 in Somatosensory**

Neurons. J Proteome Res *15 (8)*, 2676-2687, doi: 10.1021/acs.jproteome.6b00235.

Nees, T. A., Tappe-Theodor, A., Sliwinski, C., Motsch, M., Rupp, R., Kuner, R., Weidner, N. and Blesch, A. (2016). **Early-onset treadmill training reduces mechanical allodynia and modulates calcitonin gene-related peptide fiber density in lamina III/IV in a mouse model of spinal cord contusion injury**. Pain *157 (3)*, 687-697, doi: 10.1097/j.pain.0000000000000422.

Nees, T. A., Wang, N., Adamek, P., Zeitzschel, N., Verkest, C., La Porta, C., Schaefer, I., Virnich, J., Balkaya, S., Prato, V., Morelli, C., Begay, V., Lee, Y. J., Tappe-Theodor, A., Lewin, G. R., Heppenstall, P. A., Taberner, F. J. and Lechner, S. G. (2023). **Role of TMEM100 in mechanically insensitive nociceptor un-silencing**. Nat Commun *14 (1)*, 1899, doi: 10.1038/s41467-023-37602-w.

Noël, J., Zimmermann, K., Busserolles, J., Deval, E., Alloui, A., Diochot, S., Guy, N., Borsotto, M., Reeh, P., Eschalier, A. and Lazdunski, M. (2009). **The mechano-activated K+ channels TRAAK and TREK-1 control both warm and cold perception**. Embo j *28 (9)*, 1308-1318, doi: 10.1038/emboj.2009.57.

Nwosu, L. N., Mapp, P. I., Chapman, V. and Walsh, D. A. (2016). **Blocking the tropomyosin receptor kinase A (TrkA) receptor inhibits pain behaviour in two rat models of osteoarthritis**. Ann Rheum Dis *75 (6)*, 1246-1254, doi: 10.1136/annrheumdis-2014-207203.

Obeidat, A. M., Miller, R. E., Miller, R. J. and Malfait, A. M. (2019). **The nociceptive innervation of the normal and osteoarthritic mouse knee**. Osteoarthritis Cartilage *27 (11)*, 1669-1679, doi: 10.1016/j.joca.2019.07.012.

Obreja, O., Ringkamp, M., Turnquist, B., Hirth, M., Forsch, E., Rukwied, R., Petersen, M. and Schmelz, M. (2011). **Nerve growth factor selectively decreases activity-dependent conduction slowing in mechano-insensitive C-nociceptors**. Pain *152 (9)*, 2138-2146, doi: 10.1016/j.pain.2011.05.021.

Orita, S., Ishikawa, T., Miyagi, M., Ochiai, N., Inoue, G., Eguchi, Y., Kamoda, H., Arai, G., Toyone, T., Aoki, Y., Kubo, T., Takahashi, K. and Ohtori, S. (2011). **Pain-related sensory innervation in monoiodoacetate-induced osteoarthritis in**

rat knees that gradually develops neuronal injury in addition to inflammatory pain. BMC Musculoskelet Disord *12*, 134, doi: 10.1186/1471-2474-12-134.

Osikowicz, M., Longo, G., Allard, S., Cuello, A. C. and Ribeiro-da-Silva, A. (2013). **Inhibition of endogenous NGF degradation induces mechanical allodynia and thermal hyperalgesia in rats**. Mol Pain *9*, 37, doi: 10.1186/1744-8069-9-37.

Page, A. J., Brierley, S. M., Martin, C. M., Martinez-Salgado, C., Wemmie, J. A., Brennan, T. J., Symonds, E., Omari, T., Lewin, G. R., Welsh, M. J. and Blackshaw, L. A. (2004). **The ion channel ASIC1 contributes to visceral but not cutaneous mechanoreceptor function**. Gastroenterology *127 (6)*, 1739-1747, doi: 10.1053/j.gastro.2004.08.061.

Park, K. A., Fehrenbacher, J. C., Thompson, E. L., Duarte, D. B., Hingtgen, C. M. and Vasko, M. R. (2010). **Signaling pathways that mediate nerve growth factor-induced increase in expression and release of calcitonin gene-related peptide from sensory neurons**. Neuroscience *171 (3)*, 910-923, doi: 10.1016/j.neuroscience.2010.09.027.

Patapoutian, A., Tate, S. and Woolf, C. J. (2009). **Transient receptor potential channels: targeting pain at the source**. Nat Rev Drug Discov *8 (1)*, 55-68, doi: 10.1038/nrd2757.

Peirs, C. and Seal, R. P. (2016). **Neural circuits for pain: Recent advances and current views**. Science *354 (6312)*, 578-584, doi: 10.1126/science.aaf8933.

Perl, E. R. (1968). **Myelinated afferent fibres innervating the primate skin and their response to noxious stimuli**. J Physiol *197 (3)*, 593-615, doi: 10.1113/jphysiol.1968.sp008576.

Petrus, M., Peier, A. M., Bandell, M., Hwang, S. W., Huynh, T., Olney, N., Jegla, T. and Patapoutian, A. (2007). **A role of TRPA1 in mechanical hyperalgesia is revealed by pharmacological inhibition**. Mol Pain *3*, 40, doi: 10.1186/1744-8069-3-40.

Picelli, S., Faridani, O. R., Björklund, A. K., Winberg, G., Sagasser, S. and Sandberg, R. (2014). **Full-length RNA-seq from single cells using Smart-seq2**. Nat Protoc *9 (1)*, 171-181, doi: 10.1038/nprot.2014.006.

Poole, K., Herget, R., Lapatsina, L., Ngo, H. D. and Lewin, G. R. (2014). **Tuning Piezo ion channels to detect molecular-scale movements relevant for fine touch**. Nat Commun *5*, 3520, doi: 10.1038/ncomms4520.

Prato, V., Taberner, F. J., Hockley, J. R. F., Callejo, G., Arcourt, A., Tazir, B., Hammer, L., Schad, P., Heppenstall, P. A., Smith, E. S. and Lechner, S. G. (2017). **Functional and Molecular Characterization of Mechanoinsensitive "Silent" Nociceptors**. Cell Rep *21 (11)*, 3102-3115, doi: 10.1016/j.celrep.2017.11.066.

Prescott, S. A., Ma, Q. and De Koninck, Y. (2014). **Normal and abnormal coding of somatosensory stimuli causing pain**. Nat Neurosci *17 (2)*, 183-191, doi: 10.1038/nn.3629.

Price, M. P., Lewin, G. R., McIlwrath, S. L., Cheng, C., Xie, J., Heppenstall, P. A., Stucky, C. L., Mannsfeldt, A. G., Brennan, T. J., Drummond, H. A., Qiao, J., Benson, C. J., Tarr, D. E., Hrstka, R. F., Yang, B., Williamson, R. A. and Welsh, M. J. (2000). **The mammalian sodium channel BNC1 is required for normal touch sensation**. Nature *407 (6807)*, 1007-1011, doi: 10.1038/35039512.

Puttfarcken, P. S., Han, P., Joshi, S. K., Neelands, T. R., Gauvin, D. M., Baker, S. J., Lewis, G. R., Bianchi, B. R., Mikusa, J. P., Koenig, J. R., Perner, R. J., Kort, M. E., Honore, P., Faltynek, C. R., Kym, P. R. and Reilly, R. M. (2010). **A-995662 [(R)-8-(4-methyl-5-(4-(trifluoromethyl)phenyl)oxazol-2-ylamino)-1,2,3,4-tetrahydronaphthalen-2-ol], a novel, selective TRPV1 receptor antagonist, reduces spinal release of glutamate and CGRP in a rat knee joint pain model**. Pain *150 (2)*, 319-326, doi: 10.1016/j.pain.2010.05.015.

Quick, K., Zhao, J., Eijkelkamp, N., Linley, J. E., Rugiero, F., Cox, J. J., Raouf, R., Gringhuis, M., Sexton, J. E., Abramowitz, J., Taylor, R., Forge, A., Ashmore, J., Kirkwood, N., Kros, C. J., Richardson, G. P., Freichel, M., Flockerzi, V., Birnbaumer, L. and Wood, J. N. (2012). **TRPC3 and TRPC6 are essential for normal mechanotransduction in subsets of sensory neurons and cochlear hair cells**. Open Biol *2 (5)*, 120068, doi: 10.1098/rsob.120068.

Rahman, W., Bauer, C. S., Bannister, K., Vonsy, J. L., Dolphin, A. C. and Dickenson, A. H. (2009). **Descending serotonergic facilitation and the antinociceptive effects of pregabalin in a rat model of osteoarthritic pain**. Mol Pain *5*, 45, doi: 10.1186/1744-8069-5-45.

Raja, S. N., Carr, D. B., Cohen, M., Finnerup, N. B., Flor, H., Gibson, S., Keefe, F. J., Mogil, J. S., Ringkamp, M., Sluka, K. A., Song, X.-J., Stevens, B., Sullivan, M. D., Tutelman, P. R., Ushida, T. and Vader, K. (2020). **The revised International Association for the Study of Pain definition of pain: concepts, challenges, and compromises**. PAIN *161 (9)*, 1976-1982, doi: 10.1097/j.pain.0000000000001939.

Ramsey, I. S., Delling, M. and Clapham, D. E. (2006). **An introduction to TRP channels**. Annu Rev Physiol *68*, 619-647, doi: 10.1146/annurev.physiol.68.040204.100431.

Ranade, S. S., Woo, S. H., Dubin, A. E., Moshourab, R. A., Wetzel, C., Petrus, M., Mathur, J., Bégay, V., Coste, B., Mainquist, J., Wilson, A. J., Francisco, A. G., Reddy, K., Qiu, Z., Wood, J. N., Lewin, G. R. and Patapoutian, A. (2014). **Piezo2 is the major transducer of mechanical forces for touch sensation in mice**. Nature *516 (7529)*, 121-125, doi: 10.1038/nature13980.

Raouf, R., Lolignier, S., Sexton, J. E., Millet, Q., Santana-Varela, S., Biller, A., Fuller, A. M., Pereira, V., Choudhary, J. S., Collins, M. O., Moss, S. E., Lewis, R., Tordo, J., Henckaerts, E., Linden, M. and Wood, J. N. (2018). **Inhibition of somatosensory mechanotransduction by annexin A6**. Sci Signal *11 (535)*, doi: 10.1126/scisignal.aao2060.

Rau, K. K., McIlwrath, S. L., Wang, H., Lawson, J. J., Jankowski, M. P., Zylka, M. J., Anderson, D. J. and Koerber, H. R. (2009). **Mrgprd enhances excitability in specific populations of cutaneous murine polymodal nociceptors**. J Neurosci *29 (26)*, 8612-8619, doi: 10.1523/jneurosci.1057-09.2009.

Renthal, W., Tochitsky, I., Yang, L., Cheng, Y. C., Li, E., Kawaguchi, R., Geschwind, D. H. and Woolf, C. J. (2020). **Transcriptional Reprogramming of Distinct Peripheral Sensory Neuron Subtypes after Axonal Injury**. Neuron *108 (1)*, 128-144.e129, doi: 10.1016/j.neuron.2020.07.026.

Richebé, P., Capdevila, X. and Rivat, C. (2018). **Persistent Postsurgical Pain: Pathophysiology and Preventative Pharmacologic Considerations**. Anesthesiology *129 (3)*, 590-607, doi: 10.1097/aln.0000000000002238.

Romero, M. I., Rangappa, N., Li, L., Lightfoot, E., Garry, M. G. and Smith, G. M. (2000). **Extensive sprouting of sensory afferents and hyperalgesia induced by conditional expression of nerve growth factor in the adult spinal cord**. J Neurosci *20 (12)*, 4435-4445, doi: 10.1523/jneurosci.20-12-04435.2000.

Rostock, C., Schrenk-Siemens, K., Pohle, J. and Siemens, J. (2018). **Human vs. Mouse Nociceptors - Similarities and Differences**. Neuroscience *387*, 13-27, doi: 10.1016/j.neuroscience.2017.11.047.

Rugiero, F., Drew, L. J. and Wood, J. N. (2010). **Kinetic properties of mechanically activated currents in spinal sensory neurons**. J Physiol *588 (Pt 2)*, 301-314, doi: 10.1113/jphysiol.2009.182360.

Rukwied, R., Mayer, A., Kluschina, O., Obreja, O., Schley, M. and Schmelz, M. (2010). **NGF induces non-inflammatory localized and lasting mechanical and thermal hypersensitivity in human skin**. Pain *148 (3)*, 407-413, doi: 10.1016/j.pain.2009.11.022.

Sagar, D. R., Burston, J. J., Hathway, G. J., Woodhams, S. G., Pearson, R. G., Bennett, A. J., Kendall, D. A., Scammell, B. E. and Chapman, V. (2011). **The contribution of spinal glial cells to chronic pain behaviour in the monosodium iodoacetate model of osteoarthritic pain**. Mol Pain *7*, 88, doi: 10.1186/1744-8069-7-88.

Salas, M. M., Hargreaves, K. M. and Akopian, A. N. (2009). **TRPA1-mediated responses in trigeminal sensory neurons: interaction between TRPA1 and TRPV1**. Eur J Neurosci *29 (8)*, 1568-1578, doi: 10.1111/j.1460-9568.2009.06702.x.

Sandkühler, J. (2009). **Models and mechanisms of hyperalgesia and allodynia**. Physiol Rev *89 (2)*, 707-758, doi: 10.1152/physrev.00025.2008.

Sauerstein, K., Liebelt, J., Namer, B., Schmidt, R., Rukwied, R. and Schmelz, M. (2018). **Low-Frequency Stimulation of Silent Nociceptors Induces Secondary Mechanical Hyperalgesia in Human Skin**. Neuroscience *387*, 4-12, doi: 10.1016/j.neuroscience.2018.03.006.

Schaefer, I., Prato, V., Arcourt, A., Taberner, F. J. and Lechner, S. G. (2018). **Differential modulation of voltage-gated sodium channels by nerve growth factor in three major subsets of TrkA-expressing nociceptors**. Mol Pain *14*, 1744806918814640, doi: 10.1177/1744806918814640.

Schaible, H. G. (2012). **Mechanisms of chronic pain in osteoarthritis**. Curr Rheumatol Rep *14 (6)*, 549-556, doi: 10.1007/s11926-012-0279-x.

Schaible, H. G. and Schmidt, R. F. (1988). **Time course of mechanosensitivity changes in articular afferents during a developing experimental arthritis**. J Neurophysiol *60 (6)*, 2180-2195, doi: 10.1152/jn.1988.60.6.2180.

Schmelz, M., Mantyh, P., Malfait, A.-M., Farrar, J., Yaksh, T., Tive, L. and Viktrup, L. (2019). **Nerve growth factor antibody for the treatment of osteoarthritis pain and chronic low-back pain: mechanism of action in the context of efficacy and safety**. PAIN *160 (10)*, 2210-2220, doi: 10.1097/j.pain.0000000000001625.

Schmidt, R., Schmelz, M., Forster, C., Ringkamp, M., Torebjörk, E. and Handwerker, H. (1995). **Novel classes of responsive and unresponsive C nociceptors in human skin**. J Neurosci *15 (1 Pt 1)*, 333-341, doi: 10.1523/jneurosci.15-01-00333.1995.

Sengupta, J. N. and Gebhart, G. F. (1994a). **Characterization of mechanosensitive pelvic nerve afferent fibers innervating the colon of the rat**. J Neurophysiol *71 (6)*, 2046-2060, doi: 10.1152/jn.1994.71.6.2046.

Sengupta, J. N. and Gebhart, G. F. (1994b). **Mechanosensitive properties of pelvic nerve afferent fibers innervating the urinary bladder of the rat**. J Neurophysiol *72 (5)*, 2420-2430, doi: 10.1152/jn.1994.72.5.2420.

Sevcik, M. A., Ghilardi, J. R., Peters, C. M., Lindsay, T. H., Halvorson, K. G., Jonas, B. M., Kubota, K., Kuskowski, M. A., Boustany, L., Shelton, D. L. and Mantyh, P. W. (2005). **Anti-NGF therapy profoundly reduces bone cancer pain and the accompanying increase in markers of peripheral and central sensitization**. Pain *115 (1-2)*, 128-141, doi: 10.1016/j.pain.2005.02.022.

Shelton, D. L., Zeller, J., Ho, W. H., Pons, J. and Rosenthal, A. (2005). **Nerve growth factor mediates hyperalgesia and cachexia in auto-immune arthritis**. Pain *116 (1-2)*, 8-16, doi: 10.1016/j.pain.2005.03.039.

Shi, C., Das, V., Li, X., Kc, R., Qiu, S., I, O. S., Ripper, R. L., Kroin, J. S., Mwale, F., Wallace, A. A., Zhu, B., Zhao, L., van Wijnen, A. J., Ji, M., Lu, J., Votta-Velis, G., Yuan, W. and Im, H. J. (2018). **Development of an in vivo mouse model of discogenic low back pain**. J Cell Physiol *233 (10)*, 6589-6602, doi: 10.1002/jcp.26280.

Skoff, A. M. and Adler, J. E. (2006). **Nerve growth factor regulates substance P in adult sensory neurons through both TrkA and p75 receptors**. Exp Neurol *197 (2)*, 430-436, doi: 10.1016/j.expneurol.2005.10.006.

Snider, W. D. and McMahon, S. B. (1998). **Tackling pain at the source: new ideas about nociceptors**. Neuron *20 (4)*, 629-632, doi: 10.1016/s0896-6273(00)81003-x.

Somekawa, S., Imagawa, K., Hayashi, H., Sakabe, M., Ioka, T., Sato, G. E., Inada, K., Iwamoto, T., Mori, T., Uemura, S., Nakagawa, O. and Saito, Y. (2012). **Tmem100, an ALK1 receptor signaling-dependent gene essential for arterial endothelium differentiation and vascular morphogenesis**. Proc Natl Acad Sci U S A *109 (30)*, 12064-12069, doi: 10.1073/pnas.1207210109.

Staruschenko, A., Jeske, N. A. and Akopian, A. N. (2010). **Contribution of TRPV1-TRPA1 interaction to the single channel properties of the TRPA1 channel**. J Biol Chem *285 (20)*, 15167-15177, doi: 10.1074/jbc.M110.106153.

Suokas, A. K., Walsh, D. A., McWilliams, D. F., Condon, L., Moreton, B., Wylde, V., Arendt-Nielsen, L. and Zhang, W. (2012). **Quantitative sensory testing in painful osteoarthritis: a systematic review and meta-analysis**. Osteoarthritis Cartilage *20 (10)*, 1075-1085, doi: 10.1016/j.joca.2012.06.009.

Svensson, P., Cairns, B. E., Wang, K. and Arendt-Nielsen, L. (2003). **Injection of nerve growth factor into human masseter muscle evokes long-lasting mechanical allodynia and hyperalgesia**. Pain *104 (1-2)*, 241-247, doi: 10.1016/s0304-3959(03)00012-5.

Talavera, K., Startek, J. B., Alvarez-Collazo, J., Boonen, B., Alpizar, Y. A., Sanchez, A., Naert, R. and Nilius, B. (2020). **Mammalian Transient Receptor Potential TRPA1 Channels: From Structure to Disease**. Physiol Rev *100 (2)*, 725-803, doi: 10.1152/physrev.00005.2019.

Todd, A. J. (2010). **Neuronal circuitry for pain processing in the dorsal horn**. Nat Rev Neurosci *11 (12)*, 823-836, doi: 10.1038/nrn2947.

Todorovic, S. M., Jevtovic-Todorovic, V., Meyenburg, A., Mennerick, S., Perez-Reyes, E., Romano, C., Olney, J. W. and Zorumski, C. F. (2001). **Redox modulation of T-type calcium channels in rat peripheral nociceptors**. Neuron *31 (1)*, 75-85, doi: 10.1016/s0896-6273(01)00338-5.

Torre, D., Lachmann, A. and Ma'ayan, A. (2018). **BioJupies: Automated Generation of Interactive Notebooks for RNA-Seq Data Analysis in the Cloud**. Cell Syst *7 (5)*, 556-561.e553, doi: 10.1016/j.cels.2018.10.007.

Treede, R. D., Rief, W., Barke, A., Aziz, Q., Bennett, M. I., Benoliel, R., Cohen, M., Evers, S., Finnerup, N. B., First, M. B., Giamberardino, M. A., Kaasa, S., Kosek, E., Lavand'homme, P., Nicholas, M., Perrot, S., Scholz, J., Schug, S., Smith, B. H., Svensson, P., Vlaeyen, J. W. S. and Wang, S. J. (2015). **A classification of chronic pain for ICD-11**. Pain *156 (6)*, 1003-1007, doi: 10.1097/j.pain.0000000000000160.

Tuthill, J. C. and Azim, E. (2018). **Proprioception**. Current Biology *28 (5)*, R194-R203, doi: https://doi.org/10.1016/j.cub.2018.01.064.

Uhler, M., Schonhoff, M., Nees, T. A., Wonerow, T., Nuppnau, J., Mantwill, F., Kretzer, J. P. and Schroeder, S. (2022). **Rheological Behavior of Different Calf Sera before, during and after Biomechanical Testing**. Lubricants *10 (9)*, 224.

Usoskin, D., Furlan, A., Islam, S., Abdo, H., Lönnerberg, P., Lou, D., Hjerling-Leffler, J., Haeggström, J., Kharchenko, O., Kharchenko, P. V., Linnarsson, S. and Ernfors, P. (2015). **Unbiased classification of sensory neuron types by large-scale single-cell RNA sequencing**. Nature Neuroscience *18 (1)*, 145-153, doi: 10.1038/nn.3881.

van der Heul-Nieuwenhuijsen, L., Hendriksen, P. J., van der Kwast, T. H. and Jenster, G. (2006). **Gene expression profiling of the human prostate zones**. BJU Int *98 (4)*, 886-897, doi: 10.1111/j.1464-410X.2006.06427.x.

Vanegas, H. and Schaible, H. G. (2004). **Descending control of persistent pain: inhibitory or facilitatory?** Brain Res Brain Res Rev *46 (3)*, 295-309, doi: 10.1016/j.brainresrev.2004.07.004.

Vasko, M. R. (2009). **Inflammatory Pain**. In: Encyclopedia of Neuroscience, eds. Binder, M. D., Hirokawa, N. and Windhorst, U., Springer Berlin Heidelberg, Berlin, Heidelberg, pp. 1952-1955.

Verkest, C., Schaefer, I., Nees, T. A., Wang, N., Jegelka, J. M., Taberner, F. J. and Lechner, S. G. (2022). **Intrinsically disordered intracellular domains control key features of the mechanically-gated ion channel PIEZO2**. Nat Commun *13 (1)*, 1365, doi: 10.1038/s41467-022-28974-6.

Vilceanu, D. and Stucky, C. L. (2010). **TRPA1 mediates mechanical currents in the plasma membrane of mouse sensory neurons**. PLoS One *5 (8)*, e12177, doi: 10.1371/journal.pone.0012177.

Waldmann, R. and Lazdunski, M. (1998). **H(+)-gated cation channels: neuronal acid sensors in the NaC/DEG family of ion channels**. Curr Opin Neurobiol *8 (3)*, 418-424, doi: 10.1016/s0959-4388(98)80070-6.

Weidner, C., Schmelz, M., Schmidt, R., Hansson, B., Handwerker, H. O. and Torebjörk, H. E. (1999). **Functional attributes discriminating mechano-insensitive and mechano-responsive C nociceptors in human skin**. J Neurosci *19 (22)*, 10184-10190, doi: 10.1523/jneurosci.19-22-10184.1999.

Weng, H. J., Patel, K. N., Jeske, N. A., Bierbower, S. M., Zou, W., Tiwari, V., Zheng, Q., Tang, Z., Mo, G. C., Wang, Y., Geng, Y., Zhang, J., Guan, Y., Akopian, A. N. and Dong, X. (2015). **Tmem100 Is a Regulator of TRPA1-TRPV1 Complex and Contributes to Persistent Pain**. Neuron *85 (4)*, 833-846, doi: 10.1016/j.neuron.2014.12.065.

Weyer, A. D., O'Hara, C. L. and Stucky, C. L. (2015). **Amplified Mechanically Gated Currents in Distinct Subsets of Myelinated Sensory Neurons following In Vivo Inflammation of Skin and Muscle**. J Neurosci *35 (25)*, 9456-9462, doi: 10.1523/jneurosci.0549-15.2015.

Weyer, A. D. and Stucky, C. L. (2015). **Loosening pain's grip by tightening TRPV1-TRPA1 interactions**. Neuron *85 (4)*, 661-663, doi: 10.1016/j.neuron.2015.02.004.

Wise, B. L., Seidel, M. F. and Lane, N. E. (2021). **The evolution of nerve growth factor inhibition in clinical medicine**. Nat Rev Rheumatol *17 (1)*, 34-46, doi: 10.1038/s41584-020-00528-4.

Woo, S. H., Lukacs, V., de Nooij, J. C., Zaytseva, D., Criddle, C. R., Francisco, A., Jessell, T. M., Wilkinson, K. A. and Patapoutian, A. (2015). **Piezo2 is the principal mechanotransduction channel for proprioception**. Nat Neurosci *18 (12)*, 1756-1762, doi: 10.1038/nn.4162.

Woolf, C. J. (1983). **Evidence for a central component of post-injury pain hypersensitivity**. Nature *306 (5944)*, 686-688, doi: 10.1038/306686a0.

Woolf, C. J. (2011). **Central sensitization: implications for the diagnosis and treatment of pain**. Pain *152 (3 Suppl)*, S2-s15, doi: 10.1016/j.pain.2010.09.030.

Woolf, C. J. and Ma, Q. (2007). **Nociceptors--noxious stimulus detectors**. Neuron *55 (3)*, 353-364, doi: 10.1016/j.neuron.2007.07.016.

Woolf, C. J., Ma, Q. P., Allchorne, A. and Poole, S. (1996). **Peripheral cell types contributing to the hyperalgesic action of nerve growth factor in inflammation**. J Neurosci *16 (8)*, 2716-2723, doi: 10.1523/jneurosci.16-08-02716.1996.

Woolf, C. J., Safieh-Garabedian, B., Ma, Q. P., Crilly, P. and Winter, J. (1994). **Nerve growth factor contributes to the generation of inflammatory sensory hypersensitivity**. Neuroscience *62 (2)*, 327-331, doi: 10.1016/0306-4522(94)90366-2.

Xu, L., Nwosu, L. N., Burston, J. J., Millns, P. J., Sagar, D. R., Mapp, P. I., Meesawatsom, P., Li, L., Bennett, A. J., Walsh, D. A. and Chapman, V. (2016). **The anti-NGF antibody muMab 911 both prevents and reverses pain behaviour and subchondral osteoclast numbers in a rat model of osteoarthritis pain**. Osteoarthritis Cartilage *24 (9)*, 1587-1595, doi: 10.1016/j.joca.2016.05.015.

Ye, Z., Xia, Y., Li, L., Li, B., Chen, W., Han, S., Zhou, X., Chen, L., Yu, W., Ruan, Y. and Cheng, F. (2023). **Effect of transmembrane protein 100 on prostate cancer progression by regulating SCNN1D through the FAK/PI3K/AKT pathway**. Transl Oncol *27*, 101578, doi: 10.1016/j.tranon.2022.101578.

Yu, H., Shin, S. M., Wang, F., Xu, H., Xiang, H., Cai, Y., Itson-Zoske, B. and Hogan, Q. H. (2019). **Transmembrane protein 100 is expressed in neurons and glia of dorsal root ganglia and is reduced after painful nerve injury**. Pain Rep *4 (1)*, e703, doi: 10.1097/pr9.0000000000000703.

Zeisel, A., Hochgerner, H., Lönnerberg, P., Johnsson, A., Memic, F., van der Zwan, J., Häring, M., Braun, E., Borm, L. E., La Manno, G., Codeluppi, S., Furlan, A., Lee, K., Skene, N., Harris, K. D., Hjerling-Leffler, J., Arenas, E., Ernfors, P., Marklund, U. and Linnarsson, S. (2018). **Molecular Architecture of the Mouse Nervous System**. Cell *174 (4)*, 999-1014.e1022, doi: 10.1016/j.cell.2018.06.021.

Zhang, H. G., Xie, J., Dmitriev, I., Kashentseva, E., Curiel, D. T., Hsu, H. C. and Mountz, J. D. (2002). **Addition of six-His-tagged peptide to the C terminus of adeno-associated virus VP3 does not affect viral tropism or production**. J Virol *76 (23)*, 12023-12031, doi: 10.1128/jvi.76.23.12023-12031.2002.

Zhang, T., Chi, S., Jiang, F., Zhao, Q. and Xiao, B. (2017). **A protein interaction mechanism for suppressing the mechanosensitive Piezo channels**. Nat Commun *8 (1)*, 1797, doi: 10.1038/s41467-017-01712-z.

Zheng, Y., Liu, P., Bai, L., Trimmer, J. S., Bean, B. P. and Ginty, D. D. (2019). **Deep Sequencing of Somatosensory Neurons Reveals Molecular Determinants of Intrinsic Physiological Properties**. Neuron *103 (4)*, 598-616.e597, doi: 10.1016/j.neuron.2019.05.039.

Zheng, Y., Zhao, Y., Jiang, J., Zou, B. and Dong, L. (2022). **Transmembrane Protein 100 Inhibits the Progression of Colorectal Cancer by Promoting the Ubiquitin/Proteasome Degradation of HIF-1α**. Front Oncol *12*, 899385, doi: 10.3389/fonc.2022.899385.

Zimmer, Z., Fraser, K., Grol-Prokopczyk, H. and Zajacova, A. (2022). **A global study of pain prevalence across 52 countries: examining the role of country-level contextual factors**. Pain *163 (9)*, 1740-1750, doi: 10.1097/j.pain.0000000000002557.

Zurborg, S., Yurgionas, B., Jira, J. A., Caspani, O. and Heppenstall, P. A. (2007). **Direct activation of the ion channel TRPA1 by Ca2+**. Nat Neurosci *10 (3)*, 277-279, doi: 10.1038/nn1843.

6. PUBLICATIONS

The course of my Ph.D. studies has culminated in the contribution to three publications.

6.1 First-author publication

The majority of experiments and findings detailed in this thesis were disseminated through the following original research article, which represents the centerpiece of my Ph.D. endeavor.

Nees, T. A., Wang, N., Adamek, P., Zeitzschel, N., Verkest, C., La Porta, C., Schaefer, I., Virnich, J., Balkaya, S., Prato, V., Morelli, C., Begay, V., Lee, Y. J., Tappe-Theodor, A., Lewin, G. R., Heppenstall, P. A., Taberner, F. J. and Lechner, S. G. (2023). **Role of TMEM100 in mechanically insensitive nociceptor unsilencing**. Nat Commun *14 (1)*, 1899, doi: 10.1038/s41467-023-37602-w.

6.2 Co-Author publications

Additionally, I have contributed to two other publications by assisting with experiments and data analysis. These works, while not directly related to the central questions of my Ph.D. project, reflect the collaborative spirit and interdisciplinary engagement of my academic pursuits.

Verkest, C., Schaefer, I., **Nees, T. A.**, Wang, N., Jegelka, J. M., Taberner, F. J. and Lechner, S. G. (2022). **Intrinsically disordered intracellular domains control key features of the mechanically-gated ion channel PIEZO2**. Nat Commun *13 (1)*, 1365, doi: 10.1038/s41467-022-28974-6.

Gangadharan, V., Zheng, H., Taberner, F. J., Landry, J., **Nees, T. A.**, Pistolic, J., Agarwal, N., Männich, D., Benes, V., Helmstaedter, M., Ommer, B., Lechner, S. G., Kuner, T. and Kuner, R. (2022). **Neuropathic pain caused by miswiring and abnormal end organ targeting**. Nature *606 (7912)*, 137-145, doi: 10.1038/s41586-022-04777-z.

ACKNOWLEDGMENT

First and foremost, I extend my sincerest gratitude to my supervisor, **Prof. Dr. Stefan G. Lechner**, for his exceptional support throughout the course of my thesis project. His invaluable advice during countless scientific discussions, combined with his remarkable talent and empathetic approach to tackling and solving problems, have been instrumental to my research. He has not only been a tremendous mentor to me personally but also a visionary leader within our group. I thank him wholeheartedly for his dedication to fostering my academic development and for the unwavering encouragement of my career aspirations.

I am deeply grateful to my thesis advisory committee, which includes **Prof. Dr. Marc Freichel** and **Prof. Dr. Babak Moradi**. Their constructive criticism and encouraging guidance throughout this process have been invaluable.
Special thanks are due to Prof. Dr. Marc Freichel for his trust and generosity in granting me access to his calcium imaging setup and for the opportunity to engage in teaching activities, all of which have been valuable learning experiences.
My sincerest gratitude extends to Prof. Dr. Moradi. Amid his substantial clinical responsibilities, he has found the time to significantly support my research and career development. His dedication to both clinical practice and academic mentorship is truly inspiring

I wish to thank **Prof. Dr. Rohini Kuner** for providing resources and environment conducive to rigorous scholarly research.

I owe a debt of gratitude to **Paul V. Naser** for his unwavering support and companionship throughout this academic endeavor. His tireless dedication and remarkable ability to assist and sustain me have been truly invaluable. Without his contributions, this work may not have come to fruition.

Profound gratitude is extended to **Dr. Na Wang**, **Dr. Clément Verkest**, **Dr. Francisco J. Taberner**, **Irina Schäfer**, **Anke Niemann** from the Lechner group, **Dr. Carmen La Porta**, **Nicolas Mandel**, **Priv.-Doz. Anke Tappe-Theodor** from the Kuner group, and **Barbara Kurpiers**, **Claudia Pitzer** from the Interdisciplinary Behavioral Core for their experimental support, technical assistance, and contribution to an excellent working environment.

I express my deep gratitude to the **Heidelberg Biosciences International Graduate School** for the opportunity to pursue my Ph.D. studies. I am very thankful for the comprehensive academic and extracurricular support.

I extend my heartfelt gratitude to my beloved parents, **Jutta Nees** and **Dr. rer. nat. Friedbert W. Nees**, for their unwavering support and encouragement throughout this project. The strength and resolve I have maintained are a direct reflection of your enduring faith in me.

Last but not least, my sincerest appreciation goes to my beloved wife, **Dr. Lisa K. Nees**, who has been an indispensable pillar throughout my Ph.D. studies. From the bottom of my heart, thank you for your remarkable emotional support and the invaluable pep talks that have lifted my spirits during challenging times. Your incredible patience and understanding of the long hours spent on my work have not gone unnoticed. This accomplishment would not have been possible without you.